ENGINEERING HYDROGEL CHEMISTRIES AND STRUCTURES FOR BIOMEDICAL APPLICATIONS

ENGINEERING HYDROGEL CHEMISTRIES AND STRUCTURES FOR BIOMEDICAL APPLICATIONS

By FEI XU, B.Eng., M.ASc.

A Thesis Submitted to the School of Graduate Studies in Partial Fulfillment of the Requirements for the Degree Doctor of Philosophy

McMaster University

DOCTOR OF PHILOSOPHY (2018) McMaster University

Department of Chemical Engineering Hamilton, Ontario

TITLE: Engineering Hydrogel Chemistries and Structures for Biomedical Applications

AUTHOR: Fei Xu
B.Eng., Materials Science and Engineering,
Beijing University of Chemical Technology
M.ASc. Honours, Materials Science and Engineering,
Beijing University of Chemical Technology

SUPERVISORS: Professor Todd R. Hoare
Professor Heather Sheardown

PAGES: xxii, pp 247

Lay Abstract

Biomaterials, materials that are used in contact with the human body, have become increasingly important in our daily life due to their medical applications in drug delivery, cell transplantation, and tissue regeneration. Among the various types of biomaterials reported, hydrogels (water-swollen networks of long-chain molecules) have attracted particular interest given the fact that their chemistry, mechanics, and biological properties are similar to those of native tissues. However, the effective translation of hydrogels into the clinic has faced multiple challenges, including how to administer the gel non-invasively (i.e. non-surgically), how to control the release rates of drugs from hydrogels in predictable and tunable ways, and how to better mimic the complex fibrous structures that are present in native tissues to "trick" cells into behaving as if they are in a native environment. In this thesis, I developed potential solutions to these challenges. First, using a set of polymers that can spontaneously gel upon mixing (enabling easy injection of a hydrogel directly into a patient), I used an automated robotics system to prepare a wide range of different hydrogels for drug release applications. By exploiting the various hydrogel properties that can be achieved upon mixing different types of polymers, the duration and dose of drug release from such hydrogels can be controlled. Second, using these same spontaneously gelling polymers, I developed a new strategy to fabricate degradable hydrogel nanofibers directly in a single step. By adding cells during the nanofiber formation process, "ready-to-use" cell-loaded tissue patches were prepared that can be safely stored for a long period of time under freezing but enable cell growth and tissue regeneration upon re-thawing. Overall, by developing new ways to make hydrogels with highly customizable compositions and/or shapes, hydrogels can be designed faster and more precisely for solving current and emerging challenges in medicine.

Abstract

Hydrogels have been widely applied for drug delivery and tissue engineering given their highly relevant physiochemical and biological properties such as hydrophilicity, biomimetic mechanics, low protein absorption, and non-toxicity. However, the practical and effective use of hydrogels in such applications demands the development of methods to (1) rapidly identify hydrogel compositions that can exhibit a desired set of properties and (2) fabricate hydrogels with the internal morphology, degradability, and mechanics required to match the needs of the application. In this thesis, new strategies for high-throughput hydrogel synthesis and characterization techniques and reactive electrospinning of reactive pre-polymers directly into hydrogel nanofibers have been developed and applied for drug delivery and tissue engineering applications, using hydrazide and aldehyde-functionalized precursor polymers as the basis for investigations. To optimize injectable hydrogels for protein delivery, high throughput robotics were used to mix 14 different types of precursor polymers functionalized with hydrazide or aldehyde groups to create 126 hydrogels within 30 mins. Coupled with the development of corresponding high-throughput screening strategies for measuring key hydrogel physicochemical and pharmacokinetic properties (e.g. swelling, degradation, mechanics, transparency, and protein release), correlations were identified between hydrogel composition and protein release. To better mimic the nanofibrous nature of native extracellular matrix, a reactive electrospinning method was developed to co-extrude hydrazide and aldehyde-functionalized polymers based on poly(oligoethylene glycol methacrylate) (POEGMA) into well-defined nanofibrous hydrogels with fast swelling responses. Reactive electrospinning of thermoresponsive POEGMA precursors resulted in fast reversible temperature-responsive macroporous nanofibrous hydrogels that could be reversibly thermally cycled and act as highly effective substrates for cell growth and triggered delamination. The inclusion of cells within the precursor polymers enables the direct development of cell-loaded scaffolds that maintain very high cell viability even when dried, facilitate effective cell proliferation, and can be stored in liquid nitrogen for a long period without any added cryoprotectants while preserving high cell viability, representing a

"ready-to-use" tissue patch for the clinic. Finally, the morphologies of electrospun scaffolds can also be tuned from microbeads to nanofibers by controlling concentration of POEGMA in the system, enabling precise nanostructural control over the resulting scaffolds. Overall, this work provides new insight into the design of hydrogels with more biologically-relevant properties for clinical applications.

Acknowledgement

Here, I would like to express my earnest appreciation to these lovely people who have helped me in the past five and half years. I can't image how my life would be without you stand with me. And this work would not be completed as expected without the continued support and inclusion from all of you.

First and foremost, my sincere thanks go to my supervisor Prof. Todd Hoare. Without his professional guidance, I would not be shaped to who I am today. His brilliance, devotion and passion have absolutely enriched my understanding and interest in academia, which will continue to motivate me in my future. His timely advice, meticulous attitude and scientific approach have granted me, not only the scientific knowledge, but also the pathway to discover the world in a rational and precise manner. I sincerely appreciate the freedom and the bright response that I acquired from Dr. Hoare in the past five years. Needless to say, it has been a great honor being in Dr. Hoare's lab.

I would also like to thank my co-supervisor Prof. Heather Sheardown. I appreciate the chance that Dr. Sheardown has provided me to be part of her group. Her enormous patience and supreme work ethic unconsciously influenced me to become a mature and well-trained engineer. The most important thing I learnt from Dr. Sheardown is that I should respect what I'm doing and should be delightful to be a PhD student. That's why I have had tremendous memorable moments in the past five years. I devoutly appreciate your scholarly suggestion and entirely support. It was my good fortune to have both of you as my supervisors during my PhD study.

My appreciation turns to my committee member Dr. Jose Moran-Mirabal for his ingenious advice and scientific support. His suggestions and comments always enlighten me. I would also like to thank Dr. Harald Stöver for his generosity for offering me access to confocal microscopy. I would like to extend thanks to NSERC for funding my projects.

I am grateful to my friends for composing the best part of my life in Canada. I would like to thank Dr. Jianfeng Zhang who initiated me into science world back to my undergrad. I would like to thank Dr. Niels Smeet who gave me the best training of POEGMA in Dr Hoare's lab. I would like to thank my best summer student Monika Budi Hartono who was one of the most intelligent people that I have known. The time working with Monika was the best part in my research and I believe you have found your destination of peace. Special thanks go to Angus Lam, Ian Gough, Syndey Bell and Chiyan Zhang for their assistance in my projects. My lovely lab mates including Hoare lab and Sheardown lab deserve my deep acknowledgement for creating such a wonderful place to work. My appreciation goes to some of my lovely friends Dr. Yujie Zhu, Kayla Liu and Mengchen Liao for the enjoyable time in Hamilton.

My deepest appreciation goes to my lovely parents Chengsen Xu and Jiafang Jiang for your love and support. You always give me the most freedom to choose what I want to do and where I am going. Thank you for your encouragement, trust and kindness even most of time you might not understand what I am doing but I never get a "no" answer from you. Wherever I am, your place is always my cozy harbor. I love you and thank you for being together with me all the time.

Finally, but most importantly, I would like to express my most heartfelt appreciation to my husband Chenlong Xie, who has supported me over the past six years with love, patience and understanding. Thank you for moving across the country and starting a new life with me together. Thank you for being who you are and letting me be who I am. No matter what happen in our future, I will be always with you and cherish our love and friendship.

Table of Contents

List of Figures and Tables

.

Chapter 5

Chapter 6

List of all Abbreviations and Symbols

AA	acrylic acid
ADH	adipic acid dihydrazide
AIBMe	2,2-azobisisobutryic acid dimethyl ester
AP	alkaline phosphatase
BCS	bovine calf serum
CFSE	carboxyfluorescein diacetate succinimidyl ester
CLSM	confocal laser scanning microscopy
CMC	sodium carboxymethyl cellulose
CPRG	chlorophenol red β-galactopyranoside
DAPI	4′,6-diamidino-2-phenylindole
DIW	distilled deionized water
DSC	differential scanning calorimetry
DMAEMA	N,N-dimethylaminoethyl methacrylate
DMEM	Dulbecco's Modified Eagle's Medium
DMEMAm	*N*-(2,2-dimethoxyethyl) methacrylamide
ECM	extracellular matrix
EDC	*N*'-ethyl-*N*-(3-dimethylaminopropyl)-carbodiimide
EO	ethylene oxide
FBS	fetal bovine serum
GPC	gel permeation chromatography
FITC	fluorescein isothiocyanate
HCl	hydrogen chloride
LCST	lower critical solution temperature
MACC	monochloroacetic acid
$M(EO)_2MA$	di(ethylene glycol) methyl ether methacrylate
MEHQ	methyl ether hydroquinone
MWCO	molecular weight cut-off

NaOH	sodium hydroxide
$OEGMA_{475}$	oligo (ethylene glycol) methyl ether methacrylate
PBS	phosphate buffered saline
PEG	poly (ethylene glycol)
PEO	poly(ethylene oxide)
POA	aldehyde-functionalized POEGMA
POEGMA	poly(oligoethylene glycol methacrylate)
POH	Hydrazide-functionalized POEGMA
PS	penicillin-streptomycin
SEM	scanning electron microscopy
TGA	thioglycolic acid
UCST	upper critical solution temperature
β-gal	β-galactosidase
$W_{initial}$	weight before swelling
$W_{swollen}$	weight after swelling
V_{intial}	volume before swelling
V_{final}	volume after swelling
c_e	entanglement concentration
c^*	chain overlap concentration
M_e	entanglement molecular weight
ϕ	solute volume fraction
M_w	polymer molecular weight.
$(n_e)_{soln}$	solution entanglement number
T	temperature

Declaration of Academic Achievement

Fei Xu, Brandon Corbett, Sydney Bell, Chiyan Zhang, Monika Budi Hartono, and Todd Hoare. "High-throughput synthesis, analysis, and optimization of injectable hydrogels for protein delivery", to be submitted.

Fei Xu, Ian Gough, Heather Sheardown and Todd Hoare. "Single Step, All-Aqueous Electrospinning of Nanostructured Degradable Macroporous Hydrogel Networks With Controllable Internal Morphologies", to be submitted.

Fei Xu, Angus Lam, Heather Sheardown and Todd Hoare. "Fast thermo-responsive POEGMA-based nanofibrous hydrogel for controlling cell interactions", to be submitted.

Fei Xu, Megan Dodd, Heather Sheardown, and Todd Hoare. "Single-Step Reactive Electrospinning of Cell-Loaded Nanofibrous Scaffolds as Ready-to-Use Tissue Patches". *Biomacromolecules*. 2018.

Fei Xu, Heather Sheardown, and Todd Hoare. "Reactive Electrospinning of Degradable Poly(oligoethylene glycol methacrylate)-Based Nanofibrous Hydrogel Networks". *Chem. Comm*., 2016, 52, 1451. (IF: 6.32)

Ali Affar, **Fei Xu (co-author)**, and Todd Hoare. "Poly(ethylene glycol) (PEG) and synthetic PEG derivatives for tissue engineering and cell delivery" *Material Matters*, in press.

Kevin J. De France, **Fei Xu (co-author)**, and Todd Hoare. "Structured Macroporous Hydrogels: Progress, Challenges, and Opportunities". *Adv. Healthcare Mater*., 2018, 7, 1700927. (back cover, IF: 5.11)

Daryl Sivakumaran, Emilia Bakaic, Scott B. Campbell, **Fei Xu**, Eva Mueller, Todd Hoare. "Fabricating Degradable Thermoresponsive Hydrogels on Multiple Length Scales Via Reactive Extrusion, Microfluidics, Self-Assembly, and Electrospinning". *JoVE Video Journal.* 2018, 134, 54502.

Jianfeng Zhang, Ben Muirhead, Megan Dodd, Lina Liu, **Fei Xu**, Nicole Mangiacotte, Todd Hoare, and Heather Sheardown. "An Injectable Hydrogel Prepared Using a PEG/Vitamin E Copolymer Facilitating Aqueous-Driven Gelation". *Biomacromolecules*, 2016, 17, 3648. (IF: 5.25)

Xudong Deng, Mengsu Chen, Qiang Fu, Niels M. B. Smeets, **Fei Xu**, Zhuyuan Zhang, Carlos D. M. Filipe, and Todd Hoare. "A Highly Sensitive Immunosorbent Assay Based on Biotinylated Graphene Oxide and the Quartz Crystal Microbalance". *ACS Appl. Mater. Interfaces,* 2016, 3, 1893. (IF: 7.50)

Chapter 1

Introduction and Objectives

1.1 Hydrogels

Hydrogels are soft three dimensional polymeric networks that have been widely used in biomedical engineering due to their inherently high water contents and typical cell compatibility.[1] The chemical, physical and biological properties of hydrogels, coupled with the flexibility of these properties depending on hydrogel composition, make hydrogels relevant in multiple applications (Figure 1.1),[2] depending on the crosslinking method, degradability, mechanical properties, cytocompatibility, and topology best suited for that application.

Hydrogels can be prepared using either natural and synthetic polymers, each of which has pros and cons in biomedical applications. For example, natural polymers show high cell compatibility but often poor mechanical properties and more challenging chemical modification whereas synthetic polymers offer desirable tunable chemical and mechanical properties but lack inherent degradability and cytocompatibility.[3]

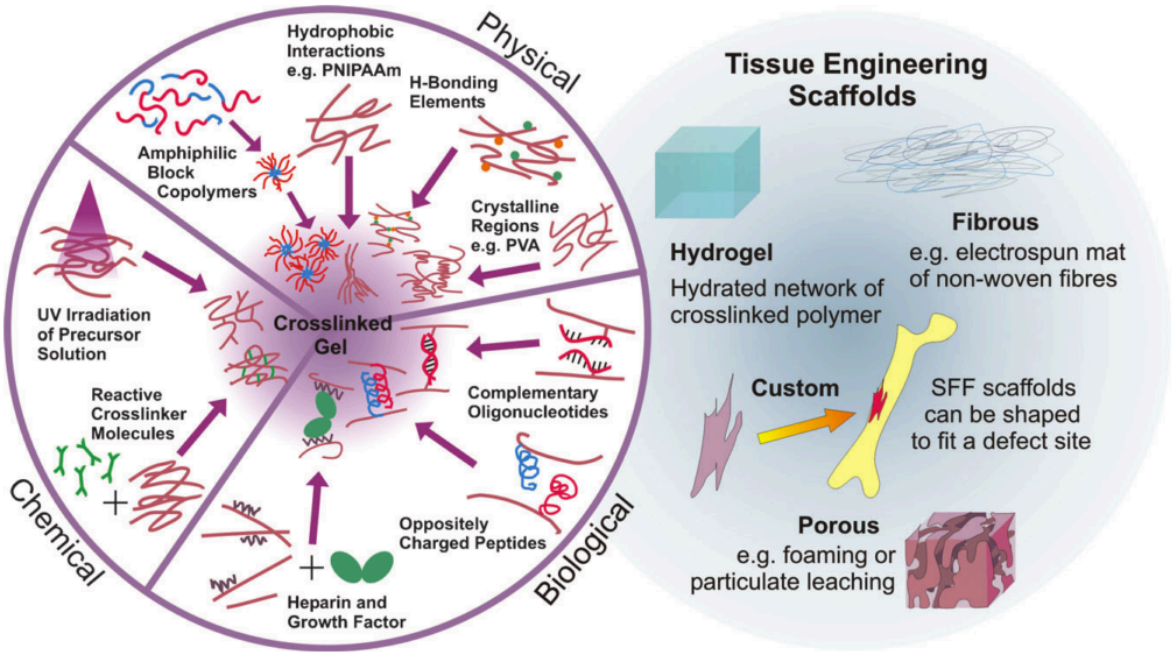

Figure 1.1 Scheme of hydrogel design for tissue engineering.[2] (reproduced with permission from Royal Society of Chemistry)

1.1.1 Natural polymers

Natural polymers are most often used materials for tissue engineering given their similar properties to the natural extracellular matrix (ECM) and thus often high cell compatibility. They can be classified in two broad categories based on chemical structures of backbone: polysaccharides and proteins.[4] Polysaccharide-based hydrogels prepared using components such as hyaluronic acid (HA)[5], chitosan[6], alginate[7] and cellulose[8] have attracted significant attention given their tunable chemical properties and excellent biological properties. Polysaccharides such as HA that have similar structures as the glucosaminoglycans (GAGs) that play an important role in regulating cells in ECM[9] offer particular interest in the context of biomedical products.[5] Methacrylate-functionalized HA is most widely used to prepare HA-based hydrogels via free radical photopolymerization upon the addition of a photoinitiator.[10] Other carbohydrates offer other desirable properties.Chitosan is derived from crustacean shells and has a net cationic charge at neutral pH that makes it attractive in many cell/tissue adhesion and drug delivery applications (although presenting challenges

with solubility at neutral pH).[11,12]. Alginate is an anionic hydrophilic biopolymer derived from brown algae[13] that has been widely used in food additives, drug delivery, tissue engineering, and wound dressings, although its poor inherent cell adhesion and non-physiological degradation properties need to be considered when using it in vivo.[13] Cellulose derivatives such as methyl cellulose, carboxymethyl cellulose and hydroxypropyl cellulose have also been studied for drug delivery and tissue engineering,[4] with emerging recent interest in the investigation of nanocellulose to enhance the often weaker mechanical properties of carbohydrate-based hydrogels.[14,15]

Among proteins used in biomedical applications, collagen is by far the most popular given its dominant presence in native ECM, excellent cell compatibility, and its potential to be naturally degraded by proteases.[4,16] However, to achieve adequate mechanical properties for most collagen-based scaffolds, cytotoxic crosslinkers such as glutaraldehyde[17] and carbodiimide[18,19] are most commonly required. Gelatin, a hydrolysis product of collagen, is often used instead of collagen for preparing scaffolds due to its simpler structure, lower immunogenicity, and improved ease of handling and functionalization.[20,21] Methacrylated gelatin (GelMA) has been particularly widely applied in tissue engineering applications given the improved inherent cell adhesive nature of gelatin relative to most other natural polymers. As examples, Khademhosseini's lab developed cell-laden GelMA hydrogels with controlled microarchitectures on the low to 100 μm size range by photocrosslinking.[22] By incorporating gellan gum methacrylate (GGMA) into GelMA hydrogel using a two-step polymercrosslinking strategy, the mechanical properties of the hydrogels were improved due to the double-network formation.[23] Lin et al. reported the use of photopolymerized GelMA as a cell carrier, preserving high cell viability within the matrix following polymerization under UV light for 15-30s.[24] Lai et al. synthesized copolymer hydrogels based on GelMA and carboxybetaine methacrylate (CBMA) that effectively induced angiogenesis to an extent controlled by the concentration of CBMA.[25]

1.1.2 Synthetic polymers

Compared to natural polymers, synthetic polymers display more diverse chemical, physical and mechanical properties given that they can be modified and functionalized by various synthetic chemistry techniques. However, the lack of cell compatibility and/or potential for cell adhesion of most synthetic polymers remains a challenge, although one that can be managed either by blending/co-gelling a natural polymer with adhesive cues or grafting functional tags (e.g. cell adhesive peptides) to direct cell responses.[2]

The most often used synthetic polymer for biomedical applications is poly (ethylene glycol) (PEG), a highly hydrophilic and non-toxic polymer applied in a range of both biomedical and personal care applications such as cell encapsulation, wound healing, tissue regeneration, drug delivery and targeted diagnostics.[26–29] The hydroxyl end groups coupled with the ether linkages between the repeat units provides excellent water binding capacity and water solubility, leading to the highly protein-repellent nature of PEG that has made it particularly attractive in a biomedical context. On the other hand, the high water content and limited scope for crosslinking (as only the chain ends are crosslinkable) typically results in PEG hydrogels being mechanically soft and poor for supporting cell adhesion. The inherent challenges of modifying hydroxyl end groups are also a consideration that limits the biological properties of PEG. As an alternative, poly(ethylene glycol) diacrylate (PEGDA) can be used to prepare PEG-based hydrogel via UV photocrosslinking; however, the non-reversible reaction of double bond results in such gels being non-degradable, limiting their potential biomedical use.[30,31] The crosslinking strategy can also be chosen to create smart/responsive scaffolds that can be manipulated to mimic natural ECM. For example, Anseth's group prepared a well-patterned and controlled degradable PEG hydrogel by using a four-arm PEG tetra-azide that was functionalized with polypeptide to form enzymatically degradable crosslinks in the hydrogel.[32,33]

Block copolymers of PEG with hydrophobic degradable synthetic polymers such as poly-(caprolactone) (PCL), poly (lactic acid) (PLA), poly (lactic-co-glycolic acid) (PLGA) or poly (glycolic acid) (PGA) have also been widely used to form PEG-based hydrogels via

physical interactions (i.e. hydrophobic interactions between the PCL/PLA/PGA blocks). PEG-PCL-PEG triblock copolymer has been successfully applied for bone tissue engineering due to its cytocompatibility and tunable mechanical properties.[34,35] Poly (amidoamine)-poly (ethylene glycol)-poly (amidoamine) (PAA-PEG-PAA) triblock polymer offered dual (pH and temperature)-responsive properties, strong bioadhesion, and controlled release of drugs, including transient assembly/disassembly as a function of pH.[36] Poly (β-amino ester urethane) (PAEU)/PEG multiblock copolymer hydrogels successfully sustained the release of doxorubicin for more than one month.[37] However, the physical nature of the crosslinking interaction makes the lifetime of these gels challenging to control in the highly diluting *in vivo* environment in which other competing hydrophobic interactions are present.[38,39]

1.2 Methods of hydrogel preparation

For the use of hydrogels as matrices for controlled drug release and cell delivery, it is required that the gels have a good compatibility and (for most applications) controllable degradability under physiological conditions. To meet these goals, a large variety of crosslinking methods have been developed to create hydrogel networks that can be most broadly categorized as either physical or chemical.[40]

1.2.1 Physical crosslinking

Recently, physically crosslinked hydrogels have has attracted increasing attention since gelation can occur without reactive crosslinking agents that may cause toxicity. Crosslinked networks can be formed by a variety of physical interactions such as ionic interactions, hydrogen bond formation, crystallization, or host-guest interactions.[40] Divalent cation-mediated crosslinking of alginate is likely the most common of these strategies in biomedical techniques, with the swelling, mechanical stability, and permeability of the resulting gel controllable based on the cation used for hydrogel formation and the alginate molecular weight and concentration.[13,41] Poly (vinyl alcohol) (PVA) hydrogels are

commonly formed via crystallization following freeze-thaw cycling processes.[40,42] Multiple types of hydrophobically-assembled hydrogels have been reported based on hydrophobic side chain grafted polymers and/or amphiphilic block polymers that can self-assemble in water,[43–45] including the block copolymer PEG-based hydrogels previously reviewed. The self-assembling hydrophobes may include thermoresponsive polymers that switch from hydrophilic to more hydrophobic as the temperature is either increased (for lower critical solution temperature (LCST) polymers like PNIPAM or decreased (for upper critical solution temperature (UCST) polymers like polyacrylamide (PAAm)-based copolymers).[46–49] Combination hydrogels have also been reported exploiting more than one physical interaction. For example, Hu et al. developed a dual physically crosslinked polyacrylamide/PAA hydrogel by both ionic interactions and hydrogen bonding using clay nanosheets and iron ions (Fe^{3+}).[50] The mechanical property of gels was improved due to the double network formation, while the reversible nature of the physical crosslinks could be leveraged for self-healing. However, controlling degradation rates in physically crosslinked gels is typically challenging since physical interactions are subject to competitive interactions with chemicals in the body (e.g. other charged or hydrophobic species) and/or sensitive to dilution effects in the body.

1.2.2 Chemical crosslinking

Covalent crosslinks can be formed either through the use of multi-functional monomers (3 or more reactive functional groups in step-growth polymerization or 2 or more reactive functional groups in chain-growth polymerization) or via chemical reaction of functional groups tethered to polymers.[40] One of the originally exploited hydrogel chemistries involves radical polymerization is poly(2-hydroxyethyl methacrylate) (pHEMA) crosslinked with ethylene glycol dimethacrylate (EGDMA) or tetraethylene glycol dimethacrylate (TEGDMA) in the presence of initiator or crosslinker.[40,51] UV-induced photopolymerization is particularly widely used as an initiation strategy since heating is not required for gelation to occur.[10,52] Though the crosslinking density can be simply adjusted by changing the crosslinker content, incomplete conversions of monomers, crosslinkers, or initiator can limit the use of this approach for biomedical applications

unless the hydrogel is thoroughly washed prior to use. In addition, the carbon-carbon backbone formed as a result of free radical polymerization is not degradable, limiting the scope of applications *in vivo*. Various degradable crosslinkers, including thiolated matrix metalloproteinase (MMP) degradable peptides[53], disulfides[54], or anhydrides[55], have been used to help to address this problem, by which the network can degrade over time or upon the application of a stimulus. As another example, Anseth's lab has created a photodegradable PEG-based hydrogels crosslinked using a synthesized photolabile macromer whose degradation can be induced spatiotemporally by light,[56] allowing precise external control over drug release and cell activities.[33,57,58]

Alternately, crosslinked networks can be formed by a range of addition or condensation reactions.[40] If the reactive functional groups for such reactions are tethered to reactive pre-polymers, *in situ* crosslinked hydrogels can be prepared without any post treatment or small molecules, minimizing any potential cytotoxic contribution. In this context, a variety of *in situ*-gelling hydrogel chemistries (beyond the hydrazone chemistry already described[59,60]) have been developed. Liu et al. prepared a dextran-based hydrogels by crosslinking glycidyl methacrylated dextran (Dex-GMA) and dithiothreitol (DTT) via thiol-Michael additions under physiological conditions, with the low toxicity of the precursor polymers useful for direct cell encapsulation.[61] Wei et al. prepared a thermosensitive hydrogel through crosslinking of maleimide and furan functional groups via Diels-Alder chemistry in water, demonstrating that gelation can be controlled by temperature.[62] Grover et al. developed a hydrogel system that could be delivered via a catheter by crosslinking 4-armed ketone-PEG with 4-armed aminooxy-PEG/or oxidized polysaccharide polymer (hyaluronic acid and alginate) *in situ* using oxime chemistry.[63]

1.3 Injectable hydrogels for biomedical applications

The exploitation of the various *in situ* physical and chemical gelation strategies described above allow for the design of injectable hydrogels for a range of biomedical applications including drug/cell delivery and tissue engineering (Figure 1.2),[59,64,65] avoiding the risks

and financial/time burdens of surgical procedures. *In situ* gelling or shear-thinning hydrogels have been developed as delivery vehicles due to their flowable in catheter or syringe needle and can form gels from minutes to hours, which allow to apply for local injection in the body.[47,66] Relative to bulk hydrogels, the injectability avoids surgical implantation; relative to shear-thinning hydrogels that are injectable due to transient disruption of crosslinking rather than gelation induced only upon injection, *in situ*-gelling hydrogels avoid the typically higher yield stresses upon injection and reduce the shear stress on cells upon injection, promoting high cell viability. Examples of the implementation of injectable hydrogels in drug delivery, cell delivery, and tissue engineering are highlighted in the following sections.

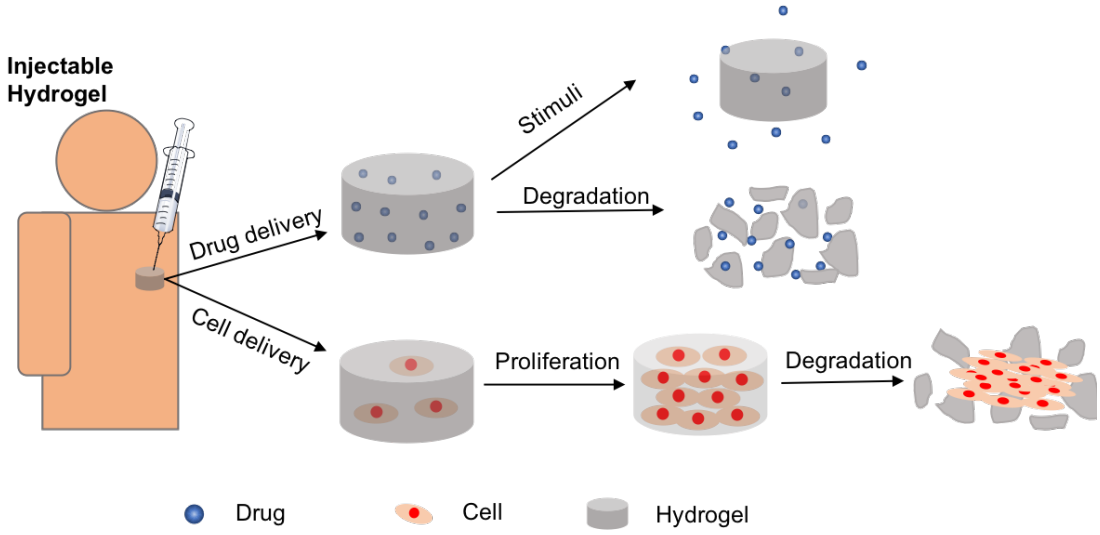

Figure 1.2 Scheme of injectable hydrogel for drug delivery and tissue engineering.

1.3.1 Drug delivery

Injectable hydrogels offer particular benefits in drug delivery given that (1) they facilitate nearly complete encapsulation of an added drug and/or drug carrier, unlike traditional bulk hydrogels that are typically loaded via diffusion; (2) they can deliver a drug with a defined dose directly at the site of interest; and (3) the degradation time can be engineered to match the required release rate of the drug. Drugs can be encapsulated in hydrogel through either

simple physical interactions or covalent bonding.[67] The potential of injectable hydrogels to entrap drug-loaded nanoparticles or even drug crystals can also be leveraged to deliver different types of drugs and/or different dosings of those drugs than otherwise possible. For example, our lab created an injectable nanocomposite hydrogel based on hydrazone chemistry that encapsulated poly (N-isopropylacrylamide)-based microgels in a carbohydrate bulk hydrogel to elongate the period of small molecule drug release up to 60 days,[68] significantly longer than typically possible with a single phase hydrogel. Ishii et al.[69] developed an injectable gel from cationic polyamine-PEG-polyamine copolymer that showed a sol-gel phase transition induced by temperature. The ionic interaction between drugs and gel prevented the initial burst release *in vitro* while also increasing retention of protein at the local injection site. Altunbas et al.[70] prepared an injectable hydrogel vehicle formed by self-assembling peptide fibrils containing loaded curcumin that showed a sustained drug concentration *in vitro* for two weeks.

"Smart" injectable hydrogels that can remotely induce changes in drug release kinetics and/or degradation times have recently attracted broad interest given their potential to spatiotemporally control drug dosings via either external or internal environmental signals. The porosity of hydrogel allows drugs to be encapsulated and released externally mediated mechanisms to cleave chemical bonds[71] (for example, light-induced triggering) or environmental stimuli using triggers such as temperature[72,73], pH[74] or magnetic field[75]. For example, Compall et al.[76] developed an injectable PNIPAM-dextran hydrogel scaffold containing thermoresponsive microgels and superparamagnetic iron oxide nanoparticles (SPIONs), which can trigger drug release by both temperature and magnetic pulse while also prolonging drug release over several days. Joshi et al.[77] reported a hydrogel platform that controlled local drug release based on the concentration of enzyme during arthritis flares. Sridhar et al.[78] reported a 4-armed PEG-based photoresponsive hydrogel that could be degraded by UV light exposure to enable on-demand protein release.

1.3.2 Cell delivery

Cell-based therapy is a developing technique that delivers living cells to specific injured site where cells can secrete therapeutic biomolecules or regenerate damaged tissues.[41,79,80] Since direct cell injection may result in dilution by body fluid, rapid removal of the cells via phagocytic mechanisms, and/or unexpected interaction with host cells, biomaterials have been used as a cargo to encapsulate cells and deliver them to the target location.[41] Therefore, it is required that these biomaterials should be cell compatible, degradable at an appropriate rate for releasing the cells for therapeutic benefit, adequately stiff to support cell activity, and maintain cell viability before/after injection.[41] Injectable hydrogels are ideal in this context to minimize the invasiveness of cell delivery while still providing the ECM-like microenvironment required to maintain cell viability. As examples, Bakaic et al.[81] developed injectable, peptide-free POEGMA-based hydrogels containing tunable charged groups to encapsulate ARPE-19 human retinal epithelia cells in 3D matrices, while Ballios et al.[82] created a degradable hydrogel based on hyaluronan and methylcellulose to deliver retinal stem-progenitor cells in the sub-retinal space for the treatment of retinal degenerative diseases.

1.3.3 Tissue engineering

Tissue engineering is a complex and interdisciplinary field that combines material science and cell biology to develop biomaterial-based scaffolds useful to deliver and subsequently develop cells into functional replacements for damaged tissue. Injectable hydrogels offer obvious advantages for tissue engineering in that their mechanical properties can be designed to match those of soft tissues and that they generally present high cell compatibility.[83,84] 3D porous hydrogels are increasingly used since its high porosity and inherent interconnectivity that permit cell adhesion and diffusion of nutrient and gases,[85,86] although developing well-controlled porous scaffolds that are also injectable remains a significant challenge. As an alternative, increasing attention is being paid to dynamic injectable cell scaffolds that can be remodeled by cells as they grow. Lu et al. [87] developed an injectable and self-healing hydrogel composed of chondroitin sulfate multiple aldehyde (CSMA) and N-succinyl-chitosan (SC) that had demonstrated potential to deliver cells and

degrade *in vivo*. Yesilyurt et al.[88] functionalized 4-armed PEG-NH_2 with 4-carboxy-phenylboronic acid or D-glucolactone in presence of trimethylamine to yield PEG-PBA and PEG-diol; the resulting self-healing PEG-based hydrogels based on the reversible interaction between PEG-PBA and *cis*-diols showed strongly pH-dependent and tunable mechanical properties useful for 3D cell encapsulation.[88]

1.4 POEGMA hydrogels

More recently, different PEG derivatives have been studied to prepare hydrogels in an attempt to overcome some of the drawbacks of the use of PEG-based hydrogels in drug delivery and tissue engineering. Branched PEG methacrylate polymers such as poly (oligo ethylene glycol methacrylate) (POEGMA) have attracted particular attention. POEGMA offers similar key properties as PEG but, due to the free radical instead of step growth mechanism of polymerization, significantly more possibilities in terms of controlling polymer chemistry and molecular weight.[59] Our lab has reported injectable POEGMA hydrogels that can be crosslinked *in situ* at room temperature via hydrazone chemistry without any post-treatment, using hydrazide functionalized POEGMA (POH) and aldehyde functionalized POEGMA (POA) as precursors. (Figure 1.3)[59] These POEGMA hydrogels have been demonstrated to exhibit low toxicity, low protein adsorption, tunable degradation, and minimal acute or chronic inflammation;[89] furthermore, the low molecular weight of these POEGMA precursors (~20 kDa) coupled with the hydrolytic lability of the hydrazone crosslinking strategy offers the potential for eventual degradation and clearance from the body.[90] Moreover, POEGMA-based hydrogels can also be engineered to exhibit thermosensitive properties by reducing the length of the PEG side-chains, with the temperature at which the phase transition occurs tunable based on the ratio of oligo (ethylene glycol) methacrylate ($OEGMA_{475}$) monomer and diethylene glycol methacrylate ($M(EO)_2MA$) monomer.[90] Relative to conventional thermoresponsive hydrogels (typically based on poly(N-isopropylacrylamide[91,92] or other N-alkylacrylamide derivatives[93]), POEGMA offers the clear advantages of less toxic starting materials and degradable side-products (PEG and poly(methacrylic acid), both of which are generally regarded as safe in

various biomedical and food applications[59,94,95]). We have implemented POEGMA in combination with several comonomers to customize hydrogels for various biomedical applications (Figure 1.3).

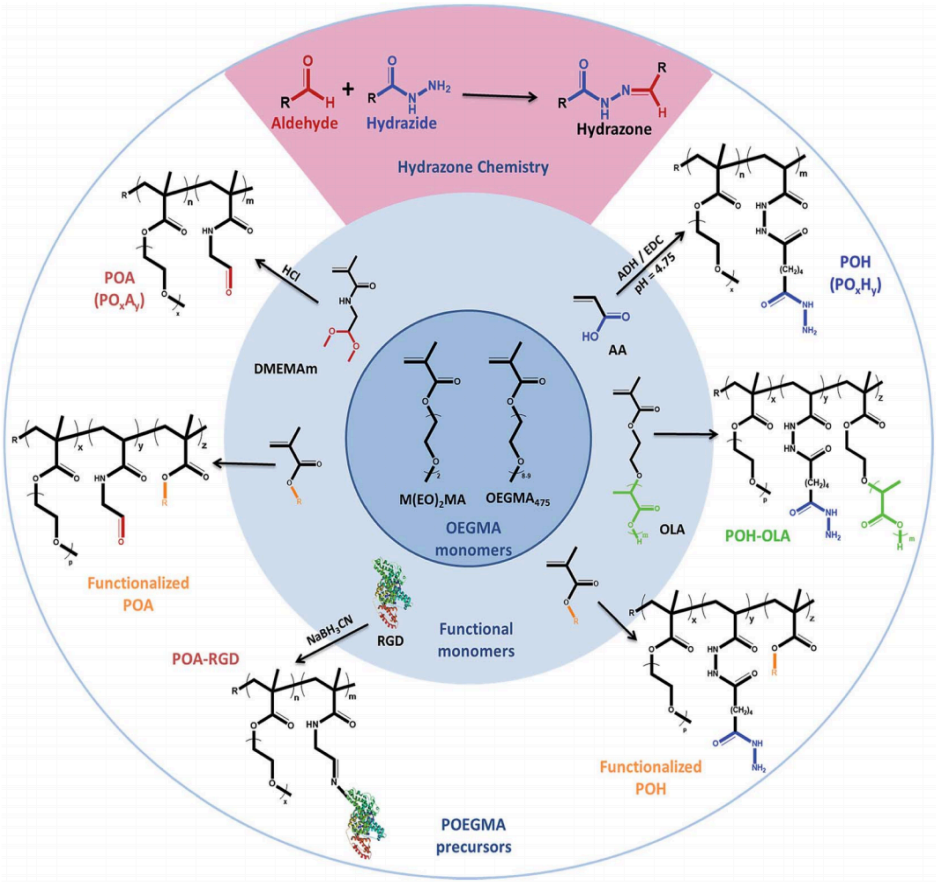

Figure 1.3 Scheme of preparation of hydrazide and aldehyde functionalized poly (oligo ethylene glycol methacrylate) (POEGMA) hydrogel precursors.[59] (reproduced with permission from Royal Society of Chemistry)

The combination of the fast-gelling hydrazone chemistry with the mixing-induced mechanism of gelation also yields significant potential for using *in situ*-gelling precursor polymers to design hydrogels with well-defined internal morphologies based on the geometry in which the materials are mixed. For instance, Chau et al.[96] used a freeze-casting/chemical crosslinking method to prepare well-defined cellulose nanocrystal (CNCs)-POEGMA hydrogels in which the anisotropic columnar, lamellar, or fibrous

structures formed via freeze casting were locked in place via the chemical hydrazone crosslinking. Deng et al.[97] developed a paper-based biosensor using a POEGMA-based hydrogel to decrease nonspecific protein adsorption by dip-coating the hydrogel on cellulose paper, a covalent gelation version of polyelectrolyte layer-by-layer deposition. Mateen et al.[98] reported a printable hydrogel system based on surface printed POEGMA hydrogels which can be used as high-throughput drug screening platform.

1.5 Structured hydrogels

Hydrogels containing well-defined micro- or nanostructures have been increasingly studied in recent decades since these structures permit more opportunities for cell adhesion and migration.[99] Conventional techniques such as templating[100–102], freeze drying[103,104], gas foaming[105] have been developed to import macro or micro porous structure in hydrogels; these strategies as well as other methods for making macroporous structured hydrogels will be discussed in more detail in Chapter 2. For controlled porous structured hydrogels, 3D printing is in many ways an ideal fabrication technique given the control it can offer over the directionality and length scale of features. However, even the best current 3D printing methods for hydrogels offer resolutions only on the tens of micron length scale.[106,107] In contrast, native ECM contains thousands of micro- and nanofibrous structures that play essential roles in promoting cell adhesion, cell proliferation, and various other cell signalling events within the scaffold.[99] Compared to microporous/microfibrous structures, nanofibrous scaffolds thus provide a more biomimetic environment for cells to grow into native tissues (see Figure 1.4). Furthermore, by controlling the thickness and the porosity of a nanofibrous scaffold, effective control over drug release from the network can be achieved.[108,109]

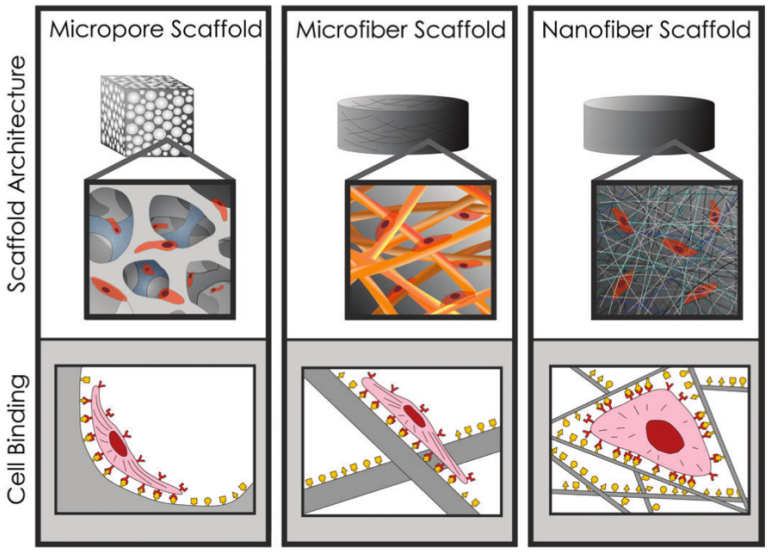

Figure 1.4 Schematic diagram showing how scaffold architecture affects cell binding and spreading.[99] (reproduced with permission from Science)

1.6 Electrospinning

Electrospinning has gained major attention and interest since the 1990s as a simple and versatile method to prepare nanofibrous scaffolds that also have high porosity between fibers.[110–112] In brief, there are three main components that are required for electrospinning: a polymer solution, a high voltage supply, and a counter electrode as a collector (Figure 1.5).[113] The applied high voltage can overcome the surface tension of the polymer solution to form a jet from the drop at front of electrospinning needle named a Taylor cone.[114] Provided there is sufficient polymer entanglement to allow for stretching of the fibers by the electric potential without causing the jet to break up into droplets (an alternate process called electrospraying), nanofibrous polymer solutions can be stretched from the instable jet and fall on counter electrode for collection as solid fibers (i.e. the solvent evaporates during the jetting and whipping process between the needle and the collector).

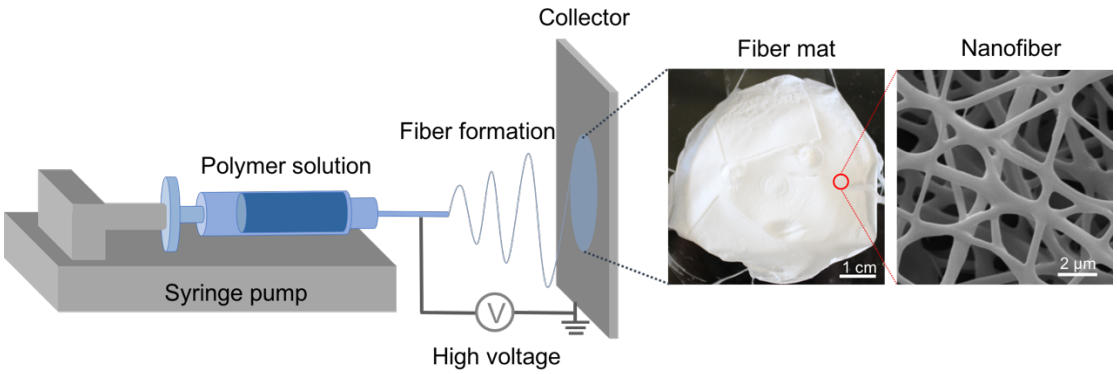

Figure 1.5 Scheme of electrospinning setup.

Parameters such as polymer concentration, molecular weight, viscosity, solvent volatility, feed rate, falling distance, and environmental humidity play an important role on fiber formation.[115–118] Some of these parameters can be independently controlled during the electrospinning process (e.g. voltage, falling distance), whereas others (e.g. polymer molecular weight, concentration and viscosity) are highly correlated in that they all determine whether or not chain entanglements are achieved. Broadly speaking, polymer chain overlaps result in physical interlocking of polymer chains (termed entanglements); increasing the molecular weight and/or the concentration of a polymer in solution both increase the probability of entanglements being observed. As the frequency of chain entanglements is decreased, a transition from fibers to beads is observed consistent with the lower stability of the stretched fibers emerging from the Taylor cone. [119–121] As such, high molecular weight polymers like poly(vinyl alcohol) (PVA)[116], polycaprolactone (PCL)[122] or poly(ethylene oxide) (PEO)[123] have been used directly for electrospinning or as an electrospinning aid to improve the spinnability of other types of polymers.

Various modifications of basic electrospinning method have been reported that can alter the structure and/or the orientation of the resulting nanofibers. Nanofibers with specific morphologies such as core-shell, porous or hollow fibers have been reported by using a coaxial needle to simultaneously electrospin two polymer solutions loaded separately in the inner and outer layer of the needle, respectively.[124] For example, Yu et al.[125] prepared a

functional trilayer ethyl cellulose nanofibers containing loaded drugs using a triaxial electrospinning strategy in which each of the three layers contained the same electrospun precursor solution but varying concentrations of drug. The drug gradient from the inner layer to outer layer enabled zero-order release from the scaffold for the first 20 h. [125] Alternately, core-shell structures can be induced by phase separation between a mixture of polymers upon drying. For example, Zhang et al.[126] created core-shell structured PEO/chitosan nanofibers induced by phase separation using a single electrospinning setup. Collecting the fibers using a rotating drum, with or without defined collection gaps, can result in aligned fiber scaffolds that could be used for tissue engineering of aligned tissues like bone or muscle.[122,127,128] Kishan et al.[129] prepared a gradient aligned electrospun scaffold to mimic native tendon-bone interface using a rotating drum as collector.

The fabrication of hydrogel nanofibers using electrospinning is significantly more challenging than conventional "hard" polymeric nanofibers given that the operating solvent is typically water (harder to evaporate on the timescale of electrospinning) and a mechanism must be provided to crosslink the fibers either during the spinning process or after spinning and before the exposure of the fibers to water (to avoid simple re-dissolution of the water soluble polymers required for hydrogel formation). Various strategies have been reported to fabricate hydrogel nanofibers. For example, Baker et al.[130] created electropsun dextran methacrylate fibers by irradiating the electrospun matrix with UV light during electrospinning that exhibited tunable mechanical properties (from soft to stiff) that can affect cell spreading and proliferation. Ji et al.[110] reported crosslinked hydrogel nanofibers by electrospinning polyethylene glycol diacrylate (PEGDA) and thiolated hyaluronic acid (HA) using a dual syringe system, enabling crosslinking via Michael addition chemistry upon mixing the two precursor polymers. [110] However, all these strategies have drawbacks in that (1) crosslinking occurs via C-C bonding, making the resulting networks difficult or impossible to degrade; (2) crosslinking requires external energy (e.g. UV irradiation, heating) which poses challenges with cell toxicity; and (3) crosslinking typically requires an extra processing step to create a stable nanofibrous network.

1.7 Objectives

To extend the successful applications of *in situ*-gelling hydrogels in a variety of drug delivery and tissue engineering applications, this thesis is focused on leveraging the *in situ* gelling hydrogel preparation strategy to design highly tunable hydrogels for drug delivery and tissue engineering applications. In particular, by leveraging our capacity to mix various *in situ* gelling polymer precursors in various sequences and at various geometries, the potential for designing optimized hydrogels for protein delivery as well as structured hydrogel scaffolds (based on a new reactive electrospinning strategy developed in this thesis) for tissue engineering and controlled release applications is demonstrated.

Chapter 2 reviews the most recent work on methods for fabricating structured hydrogels and the applications of each method. A wide variety of hydrogels is included in this review, with the pros and cons of various materials and structuring methods specifically highlighted. This chapter is reprinted as it appears in Advanced Healthcare Materials, with permission from the John Wiley and Sons © 2017.

Chapter 3 describes the fabrication of bulk hydrogels with tunable compositions using a high-throughput robotics screening approach. A mix of natural/synthetic, thermoresponsive/non-responsive, and charged/uncharged polymers are fabricated by simple controlled mixing of different precursor polymers and analyzed using high-throughput techniques developed in this work to assess hydrogel swelling, degradation, drug release kinetics, and transparency. Latent variable statistical methods will be used in conjunction with the high throughput data to identify hydrogel compositions best suited for long-term protein delivery applications.

Chapter 4 focus on the preparation of hydrogel nanofibers using a new reactive electrospinning method developed by loading a double barrel syringe with *in situ*-gelling POEGMA precursor polymers as the electrospinning solution. The swelling, degradation,

morphology, and mechanical stability of the resulting nanofibrous hydrogels were assessed. We show that our single and one-step reactive electrospinning process can be used to create degradable nanofibrous hydrogels without any post treatment, offering potential for biomedical applications. This chapter is reprinted as it appears in Chemical communications, with permission from the Royal Society of Chemistry © 2016.

Chapter 5 investigates the use of thermoresponsive nanofibrous hydrogels prepared by reactive electrospinning of short side-chain POEGMA precursor polymers and the utility of these materials in the context of cell adhesion and delamination applications. We show the potential of thermoresponsive POEGMA-based nanofibrous hydrogels used as scaffolds for cell engineering in which the dynamic manipulation of cell-scaffold interactions is desirable.

Chapter 6 shows the development of "ready-to-use" cellularized nanofibrous hydrogel scaffolds prepared by reactive electrospinning of POEGMA polymers in the presence of cells. The method is demonstrated to maintain remarkably high cell viabilities (despite the high voltage processing and the scaffolds being macroscopically dry) and the potential for cell proliferation upon subsequent culturing, with 4-5-fold increases in cell number observed over 18 day incubation periods. This capacity for cell proliferation is maintained even following long-term storage of the scaffolds in liquid nitrogen without adding any additional cryoprotectants. We anticipate this method has significant potential to facilitate the production of storable, transportable, and functional thin tissue patches in the clinic. This chapter is reprinted as it appears in Biomacromolecules, with permission from the American Chemical Society © 2018.

Chapter 7 further develops this reactive electrospinning strategy to develop hydrogel scaffolds with different morphologies that can be controlled by varying the concentrations of the polymer precursor solutions. The structure can be tuned from "pure beads" to "bead-on-fiber" to "pure fibers". The experiments focus on how the morphology of the nanofibers affects the physiochemical properties of each scaffold and the application of these

structured hydrogels. We show that nano-/macrostructured hydrogel scaffolds with controlled morphology can alter the mechanical and cell proliferation properties of the hydrogels produced, enabling the application of these hydrogels for cell delivery or tissue engineering applications.

Chapter 8 briefly describes the conclusions of the thesis as well as suggestions for future work to extend the results and knowledge gained from this thesis work.

1.8 References

(1) Drury, J. L.; Mooney, D. J. Hydrogels for Tissue Engineering: Scaffold Design Variables and Applications. *Biomaterials* **2003**, *24* (24), 4337–4351.

(2) Place, E. S.; George, J. H.; Williams, C. K.; Stevens, M. M. Synthetic Polymer Scaffolds for Tissue Engineering. *Chem. Soc. Rev.* **2009**, *38* (4), 1139–1151.

(3) Patterson, J.; Martino, M. M.; Hubbell, J. A. Biomimetic Materials in Tissue Engineering. *Mater. Today* **2010**, *13* (1–2), 14–22.

(4) Van Vlierberghe, S.; Dubruel, P.; Schacht, E. Biopolymer-Based Hydrogels As Scaffolds for Tissue Engineering Applications: A Review. *Biomacromolecules* **2011**, *12* (5), 1387–1408.

(5) Burdick, J. A.; Prestwich, G. D. Hyaluronic Acid Hydrogels for Biomedical Applications. *Adv. Mater.* **2011**, *23* (12), 41–56.

(6) Tan, H.; Chu, C. R.; Payne, K. A.; Marra, K. G. Injectable in Situ Forming Biodegradable Chitosan-Hyaluronic Acid Based Hydrogels for Cartilage Tissue Engineering. *Biomaterials* **2009**, *30* (13), 2499–2506.

(7) Sergeeva, A.; Feoktistova, N.; Prokopovic, V.; Gorin, D.; Volodkin, D. Design of Porous Alginate Hydrogels by Sacrificial CaCO3 Templates: Pore Formation Mechanism. *Adv. Mater. Interfaces* **2015**, *2* (18), 1–10.

(8) Chang, C.; Lue, A.; Zhang, L. Effects of Crosslinking Methods on Structure and Properties of Cellulose/PVA Hydrogels. *Macromol. Chem. Phys.* **2008**, *209* (12), 1266–1273.

(9) Coombe, D. R. Biological Implications of Glycosaminoglycan Interactions with Haemopoietic Cytokines. *Immunol Cell Biol* **2008**, *86* (7), 598–607.

(10) Park, Y. D.; Tirelli, N.; Hubbell, J. A. Photopolymerized Hyaluronic Acid-Based Hydrogels and Interpenetrating Networks. *Biomaterials* **2003**, *24* (6), 893–900.

(11) Suh, J. F.; Matthew, H. W. T. Application of Chitosan-Based Polysaccharide Biomaterials in Cartilage Tissue Engineering : A Review. **2000**, *21*.

(12) Ravi Kumar, M. N. V. A Review of Chitin and Chitosan Applications. *React.*

Funct. Polym. **2000**, *46* (1), 1–27.

(13) Augst, A. D.; Kong, H. J.; Mooney, D. J. Alginate Hydrogels as Biomaterials. *Macromol. Biosci.* **2006**, *6* (8), 623–633.

(14) De France, K. J.; Hoare, T.; Cranston, E. D. Review of Hydrogels and Aerogels Containing Nanocellulose. *Chem. Mater.* **2017**, acs.chemmater.7b00531.

(15) De France, K. J.; Chan, K. J. W.; Cranston, E. D.; Hoare, T. Enhanced Mechanical Properties in Cellulose Nanocrystal–Poly(Oligoethylene Glycol Methacrylate) Injectable Nanocomposite Hydrogels through Control of Physical and Chemical Cross-Linking. *Biomacromolecules* **2016**, *17* (2), 649–660.

(16) Glowacki, J.; Mizuno, S. Collagen Scaffolds for Tissue Engineering. *Biopolymers* **2008**, *89* (5), 338–344.

(17) Ma, L.; Gao, C.; Mao, Z.; Zhou, J.; Shen, J.; Hu, X.; Han, C. Collagen/Chitosan Porous Scaffolds with Improved Biostability for Skin Tissue Engineering. *Biomaterials* **2003**, *24* (26), 4833–4841.

(18) Park, S.-N.; Park, J.-C.; Kim, H. O.; Song, M. J.; Suh, H. Characterization of Porous Collagen/Hyaluronic Acid Scaffold Modified by 1-Ethyl-3-(3-Dimethylaminopropyl)Carbodiimide Cross-Linking. *Biomaterials* **2002**, *23* (4), 1205–1212.

(19) Song, E.; Yeon Kim, S.; Chun, T.; Byun, H.-J.; Lee, Y. M. Collagen Scaffolds Derived from a Marine Source and Their Biocompatibility. *Biomaterials* **2006**, *27* (15), 2951–2961.

(20) Zhu, J.; Marchant, R. E. Design Properties of Hydrogel Tissue-Engineering Scaffolds. *Expert Rev. Med. Devices* **2011**, *8* (5), 607–626.

(21) Lee, J. B.; Wang, X.; Faley, S.; Baer, B.; Balikov, D. A.; Sung, H.-J.; Bellan, L. M. Development of 3D Microvascular Networks Within Gelatin Hydrogels Using Thermoresponsive Sacrificial Microfibers. *Adv. Healthc. Mater.* **2016**, *5* (7), 781–785.

(22) Nichol, J. W.; Koshy, S. T.; Bae, H.; Hwang, C. M.; Yamanlar, S.; Khademhosseini, A. Cell-Laden Microengineered Gelatin Methacrylate Hydrogels. *Biomaterials* **2010**, *31* (21), 5536–5544.

(23) Shin, H.; Olsen, B. D.; Khademhosseini, A. The Mechanical Properties and Cytotoxicity of Cell-Laden Double-Network Hydrogels Based on Photocrosslinkable Gelatin and Gellan Gum Biomacromolecules. *Biomaterials* **2012**, *33* (11), 3143–3152.

(24) Lin, R.-Z.; Chen, Y.-C.; Moreno-Luna, R.; Khademhosseini, A.; Melero-Martin, J. M. Transdermal Regulation of Vascular Network Bioengineering Using a Photopolymerizable Methacrylated Gelatin Hydrogel. *Biomaterials* **2013**, *34* (28), 6785–6796.

(25) Lai, T. C.; Yu, J.; Tsai, W. B. Gelatin Methacrylate/Carboxybetaine Methacrylate Hydrogels with Tunable Crosslinking for Controlled Drug Release. *J. Mater. Chem. B* **2016**, *4* (13), 2304–2313.

(26) Burdick, J. A.; Anseth, K. S. Photoencapsulation of Osteoblasts in Injectable RGD-Modified PEG Hydrogels for Bone Tissue Engineering. *Biomaterials* **2002**, *23* (22), 4315–4323.

(27) Hutanu, D. Recent Applications of Polyethylene Glycols (PEGs) and PEG Derivatives. *Mod. Chem. Appl.* **2014**, *02* (02), 2–7.

(28) Phelps, E. A.; Enemchukwu, N. O.; Fiore, V. F.; Sy, J. C.; Murthy, N.; Sulchek, T. A.; Barker, T. H.; García, A. J. Maleimide Cross-Linked Bioactive PEG Hydrogel Exhibits Improved Reaction Kinetics and Cross-Linking for Cell Encapsulation and In Situ Delivery. *Adv. Mater.* **2012**, *24* (1), 64–70.

(29) Veronese, F. M.; Pasut, G. PEGylation, Successful Approach to Drug Delivery. *Drug Discov. Today* **2005**, *10* (21), 1451–1458.

(30) Bryant, S. J.; Anseth, K. S. The Effects of Scaffold Thickness on Tissue Engineered Cartilage in Photocrosslinked Poly(Ethylene Oxide) Hydrogels. *Biomaterials* **2001**, *22* (6), 619–626.

(31) Mellott, M. B.; Searcy, K.; Pishko, M. V. Release of Protein from Highly Cross-Linked Hydrogels of Poly(Ethylene Glycol) Diacrylate Fabricated by UV Polymerization. *Biomaterials* **2001**, *22* (9), 929–941.

(32) DeForest, C. A.; Polizzotti, B. D.; Anseth, K. S. Sequential Click Reactions for Synthesizing and Patterning Three-Dimensional Cell Microenvironments. *Nat Mater* **2009**, *8* (8), 659–664.

(33) DeForest, C. A.; Anseth, K. S. Photoreversible Patterning of Biomolecules within Click-Based Hydrogels. *Angew. Chemie* **2012**, *124* (8), 1852–1855.

(34) Ni, P.; Ding, Q.; Fan, M.; Liao, J.; Qian, Z.; Luo, J.; Li, X.; Luo, F.; Yang, Z.; Wei, Y. Injectable Thermosensitive PEG–PCL–PEG Hydrogel/Acellular Bone Matrix Composite for Bone Regeneration in Cranial Defects. *Biomaterials* **2014**, *35* (1), 236–248.

(35) Fu, S.; Ni, P.; Wang, B.; Chu, B.; Zheng, L.; Luo, F.; Luo, J.; Qian, Z. Injectable and Thermo-Sensitive PEG-PCL-PEG Copolymer/Collagen/n-HA Hydrogel Composite for Guided Bone Regeneration. *Biomaterials* **2012**, *33* (19), 4801–4809.

(36) Nguyen, M. K.; Park, D. K.; Lee, D. S. Injectable Poly(Amidoamine)-Poly(Ethylene Glycol)-Poly(Amidoamine) Triblock Copolymer Hydrogel with Dual Sensitivities: PH and Temperature. *Biomacromolecules* **2009**, *10* (4), 728–731.

(37) Huynh, C. T.; Nguyen, M. K.; Kim, J. H.; Kang, S. W.; Kim, B. S.; Lee, D. S.

Sustained Delivery of Doxorubicin Using Biodegradable PH/Temperature-Sensitive Poly(Ethylene Glycol)-Poly([Small Beta]-Amino Ester Urethane) Multiblock Copolymer Hydrogels. *Soft Matter* **2011**, *7* (10), 4974–4982.

(38) Kim, S.; Shi, Y.; Kim, J. Y.; Park, K.; Cheng, J.-X. Overcoming the Barriers in Micellar Drug Delivery: Loading Efficiency, in Vivo Stability, and Micelle–Cell Interaction. *Expert Opin. Drug Deliv.* **2010**, *7* (1), 49–62.

(39) Walkey, C. D.; Chan, W. C. W. Understanding and Controlling the Interaction of Nanomaterials with Proteins in a Physiological Environment. *Chem. Soc. Rev.* **2012**, *41* (7), 2780–2799.

(40) Hennink, W. E.; van Nostrum, C. F. Novel Crosslinking Methods to Design Hydrogels. *Adv. Drug Deliv. Rev.* **2002**, *54* (1), 13–36.

(41) Bidarra, S. J.; Barrias, C. C.; Granja, P. L. Injectable Alginate Hydrogels for Cell Delivery in Tissue Engineering. *Acta Biomater.* **2014**, *10* (4), 1646–1662.

(42) Takamura, A.; Ishii, F.; Hidaka, H. Drug Release from Poly(Vinyl Alcohol) Gel Prepared by Freeze-Thaw Procedure. *J. Control. Release* **1992**, *20* (1), 21–27.

(43) Youngjong, K.; Andrew, T. T. Core/Shell Gold Nanoparticles by Self-Assembly and Crosslinking of Micellar, Block-Copolymer Shells. *Angew. Chemie* **2004**, *117* (3), 413–416.

(44) L., A. M.; Afsaneh, L.; S., K. G. Amphiphilic Block Copolymers for Drug Delivery. *J. Pharm. Sci.* **2003**, *92* (7), 1343–1355.

(45) Mai, Y.; Eisenberg, A. Self-Assembly of Block Copolymers. *Chem. Soc. Rev.* **2012**, *41* (18), 5969–5985.

(46) Zhang, S. Fabrication of Novel Biomaterials through Molecular Self-Assembly. *Nat. Biotechnol.* **2003**, *21*, 1171.

(47) Zhang, Y. S.; Khademhosseini, A. Advances in Engineering Hydrogels. *Science (80-.).* **2017**, *356* (6337).

(48) Ward, M. A.; Georgiou, T. K. Thermoresponsive Polymers for Biomedical Applications. *Polymers* . 2011.

(49) Asadujjaman, A.; Espinosa de Oliveira, T.; Mukherji, D.; Bertin, A. Polyacrylamide “Revisited”: UCST-Type Reversible Thermoresponsive Properties in Aqueous Alcoholic Solutions. *Soft Matter* **2018**, *14* (8), 1336–1343.

(50) Hu, Y.; Du, Z.; Deng, X.; Wang, T.; Yang, Z.; Zhou, W.; Wang, C. Dual Physically Cross-Linked Hydrogels with High Stretchability, Toughness, and Good Self-Recoverability. *Macromolecules* **2016**, *49* (15), 5660–5668.

(51) Langer, R. S.; Peppas, N. A. Present and Future Applications of Biomaterials in Controlled Drug Delivery Systems. *Biomaterials* **1981**, *2* (4), 201–214.

(52) Ifkovits, J. L.; Burdick, J. a. Review: Photopolymerizable and Degradable Biomaterials for Tissue Engineering Applications. *Tissue Eng.* **2007**, *13* (10),

2369–2385.

(53) Skaalure, S. C.; Milligan, I. L.; Bryant, S. J.; Carles-Carner, M.; Saleh, L. S. The Effects of Hydroxyapatite Nanoparticles Embedded in a MMP-Sensitive Photoclickable PEG Hydrogel on Encapsulated MC3T3-E1 Pre- Osteoblasts The Effects of Hydroxyapatite Nanoparticles Embedded in a MMP- Sensitive Photoclickable PEG Hydrogel on Encapsula. *Biomed. Mater* **2018**, *13*.

(54) M., A.; M., P. F.; A., D.; Yu., G. I.; B., M. Poly(Hydroxyethyl Methacrylate)-Based Macroporous Hydrogels with Disulfide Cross-Linker. *Macromol. Chem. Phys.* **2008**, *209* (6), 577–584.

(55) Kristi S., A.; Deborah J., Q. Polymerizations of Multifunctional Anhydride Monomers to Form Highly Crosslinked Degradable Networks. *Macromol. Rapid Commun.* **2001**, *22* (8), 564–572.

(56) Kloxin, A. M.; Kasko, A. M.; Salinas, C. N.; Anseth, K. S. Photodegradable Hydrogels for Dynamic Tuning of Physical and Chemical Properties. *Science (80-.).* **2009**, *324* (5923), 59–63.

(57) Caldwell, A. S.; Campbell, G. T.; Shekiro, K. M. T.; Anseth, K. S. Clickable Microgel Scaffolds as Platforms for 3D Cell Encapsulation. *Adv. Healthc. Mater.* **2017**, *6* (15), 1700254–n/a.

(58) Brown, T. E.; Anseth, K. S. Spatiotemporal Hydrogel Biomaterials for Regenerative Medicine. *Chem. Soc. Rev.* **2017**, *46* (21), 6532–6552.

(59) Bakaic, E.; Smeets, N. M. B.; Hoare, T. Injectable Hydrogels Based on Poly(Ethylene Glycol) and Derivatives as Functional Biomaterials. *RSC Adv.* **2015**, *5* (45), 35469–35486.

(60) Patenaude, M.; Smeets, N. M. B.; Hoare, T. Designing Injectable, Covalently Cross-Linked Hydrogels for Biomedical Applications. *Macromol. Rapid Commun.* **2014**, *35* (6), 598–617.

(61) Liu, Z. Q.; Wei, Z.; Zhu, X. L.; Huang, G. Y.; Xu, F.; Yang, J. H.; Osada, Y.; Zrínyi, M.; Li, J. H.; Chen, Y. M. Dextran-Based Hydrogel Formed by Thiol-Michael Addition Reaction for 3D Cell Encapsulation. *Colloids Surfaces B Biointerfaces* **2015**, *128*, 140–148.

(62) Wei, H.-L.; Yang, Z.; Zheng, L.-M.; Shen, Y.-M. Thermosensitive Hydrogels Synthesized by Fast Diels–Alder Reaction in Water. *Polymer (Guildf).* **2009**, *50* (13), 2836–2840.

(63) N., G. G.; L., B. R.; L., C. K. Oxime Cross-Linked Injectable Hydrogels for Catheter Delivery. *Adv. Mater.* **2013**, *25* (21), 2937–2942.

(64) Kretlow, J. D.; Young, S.; Klouda, L.; Wong, M.; Mikos, A. G. Injectable Biomaterials for Regenerating Complex Craniofacial Tissues. *Adv. Mater.* **2009**, *21* (32–33), 3368–3393.

(65) Staruch, R. M.; Glass, G. E.; Rickard, R.; Hettiaratchy, S. P.; Butler, P. Injectable Pore Forming Hydrogel Scaffolds for Complex Wound Tissue Engineering: Designing and Controlling Their Porosity and Mechanical Properties. *Tissue Eng. Part B Rev.* **2017**, *23* (2), 183–198.

(66) Highley, C. B.; Rodell, C. B.; Burdick, J. A. Direct 3D Printing of Shear-Thinning Hydrogels into Self-Healing Hydrogels. *Adv. Mater.* **2015**, *27* (34), 5075–5079.

(67) Hoare, T. R.; Kohane, D. S. Hydrogels in Drug Delivery: Progress and Challenges. *Polymer (Guildf).* **2008**, *49* (8), 1993–2007.

(68) Sivakumaran, D.; Maitland, D.; Hoare, T. Injectable Microgel-Hydrogel Composites for Prolonged Small-Molecule Drug Delivery. *Biomacromolecules* **2011**, *12* (11), 4112–4120.

(69) Ishii, S.; Kaneko, J.; Nagasaki, Y. Development of a Long-Acting, Protein-Loaded, Redox-Active, Injectable Gel Formed by a Polyion Complex for Local Protein Therapeutics. *Biomaterials* **2016**, *84*, 210–218.

(70) Altunbas, A.; Lee, S. J.; Rajasekaran, S. A.; Schneider, J. P.; Pochan, D. J. Encapsulation of Curcumin in Self-Assembling Peptide Hydrogels as Injectable Drug Delivery Vehicles. *Biomaterials* **2011**, *32* (25), 5906–5914.

(71) Wang, K.; Luo, G.-F.; Liu, Y.; Li, C.; Cheng, S.-X.; Zhuo, R.-X.; Zhang, X.-Z. Redox-Sensitive Shell Cross-Linked PEG-Polypeptide Hybrid Micelles for Controlled Drug Release. *Polym. Chem.* **2012**, *3* (4), 1084–1090.

(72) López-Noriega, A.; Hastings, C. L.; Ozbakir, B.; O'Donnell, K. E.; O'Brien, F. J.; Storm, G.; Hennink, W. E.; Duffy, G. P.; Ruiz-Hernández, E. Hyperthermia-Induced Drug Delivery from Thermosensitive Liposomes Encapsulated in an Injectable Hydrogel for Local Chemotherapy. *Adv. Healthc. Mater.* **2014**, *3* (6), 854–859.

(73) Loh, X. J.; Peh, P.; Liao, S.; Sng, C.; Li, J. Controlled Drug Release from Biodegradable Thermoresponsive Physical Hydrogel Nanofibers. *J. Control. Release* **2010**, *143* (2), 175–182.

(74) Schmaljohann, D. Thermo- and PH-Responsive Polymers in Drug Delivery. *Adv. Drug Deliv. Rev.* **2006**, *58* (15), 1655–1670.

(75) Hoare, T.; Santamaria, J.; Goya, G. F.; Irusta, S.; Lin, D.; Lau, S.; Padera, R.; Langer, R.; Kohane, D. S. A Magnetically Triggered Composite Membrane for On-Demand Drug Delivery. *Nano Lett.* **2009**, *9* (10), 3651–3657.

(76) Campbell, S.; Maitland, D.; Hoare, T. Enhanced Pulsatile Drug Release from Injectable Magnetic Hydrogels with Embedded Thermosensitive Microgels. *ACS Macro Lett.* **2015**, *4* (3), 312–316.

(77) Joshi, N.; Yan, J.; Levy, S.; Bhagchandani, S.; Slaughter, K. V; Sherman, N. E.; Amirault, J.; Wang, Y.; Riegel, L.; He, X.; et al. Towards an Arthritis Flare-

Responsive Drug Delivery System. *Nat. Commun.* **2018**, *9* (1), 1275.

(78) Sridhar, B. V; Janczy, J. R.; Hatlevik, Ø.; Wolfson, G.; Anseth, K. S.; Tibbitt, M. W. Thermal Stabilization of Biologics with Photoresponsive Hydrogels. *Biomacromolecules* **2018**, *19* (3), 740–747.

(79) Seliktar, D. Designing Cell-Compatible Hydrogels for Biomedical Applications. *Science (80-.).* **2012**, *336* (6085), 1124 LP-1128.

(80) Wang, C.; Varshney, R. R.; Wang, D.-A. Therapeutic Cell Delivery and Fate Control in Hydrogels and Hydrogel Hybrids. *Adv. Drug Deliv. Rev.* **2010**, *62* (7), 699–710.

(81) Bakaic, E.; Smeets, N. M. B.; Badv, M.; Dodd, M.; Barrigar, O.; Siebers, E.; Lawlor, M.; Sheardown, H.; Hoare, T. Injectable and Degradable Poly(Oligoethylene Glycol Methacrylate) Hydrogels with Tunable Charge Densities as Adhesive Peptide-Free Cell Scaffolds. *ACS Biomater. Sci. Eng.* **2017**.

(82) Ballios, B. G.; Cooke, M. J.; van der Kooy, D.; Shoichet, M. S. A Hydrogel-Based Stem Cell Delivery System to Treat Retinal Degenerative Diseases. *Biomaterials* **2010**, *31* (9), 2555–2564.

(83) Magin, C. M.; Alge, D. L.; Anseth, K. S. Bio-Inspired 3D Microenvironments: A New Dimension in Tissue Engineering. *Biomed. Mater.* **2016**, *11* (2), 022001.

(84) Place, E. S.; Evans, N. D.; Stevens, M. M. Complexity in Biomaterials for Tissue Engineering. *Nat. Mater.* **2009**, *8* (6), 457–470.

(85) Baker, B. M.; Chen, C. S. Deconstructing the Third Dimension - How 3D Culture Microenvironments Alter Cellular Cues. *J. Cell Sci.* **2012**, *125* (13), 3015–3024.

(86) Hollister, S. J. Porous Scaffold Design for Tissue Engineering. *Nat. Mater.* **2005**, *4* (July), 518–524.

(87) Lü, S.; Gao, C.; Xu, X.; Bai, X.; Duan, H.; Gao, N.; Feng, C.; Xiong, Y.; Liu, M. Injectable and Self-Healing Carbohydrate-Based Hydrogel for Cell Encapsulation. *ACS Appl. Mater. Interfaces* **2015**, *7* (23), 13029–13037.

(88) Volkan, Y.; J., W. M.; A., A. E.; Colin, G.; Robert, L.; G., A. D. Injectable Self-Healing Glucose-Responsive Hydrogels with PH-Regulated Mechanical Properties. *Adv. Mater.* **2015**, *28* (1), 86–91.

(89) Smeets, N. M. B.; Bakaic, E.; Patenaude, M.; Hoare, T. Injectable and Tunable Poly(Ethylene Glycol) Analogue Hydrogels Based on Poly(Oligoethylene Glycol Methacrylate). *Chem. Commun.* **2014**, *50* (25), 3306–3309.

(90) Bakaic, E.; Smeets, N. M. B.; Dorrington, H.; Hoare, T. "Off-the-Shelf" Thermoresponsive Hydrogel Design: Tuning Hydrogel Properties by Mixing Precursor Polymers with Different Lower-Critical Solution Temperatures. *RSC Adv.* **2015**, *5* (42), 33364–33376.

(91) Lutz, J.-F.; Akdemir, Ö.; Hoth, A. Point by Point Comparison of Two

Thermosensitive Polymers Exhibiting a Similar LCST: Is the Age of Poly(NIPAM) Over? *J. Am. Chem. Soc.* **2006**, *128* (40), 13046–13047.

(92) Patenaude, M.; Hoare, T. Injectable, Degradable Thermoresponsive Poly(N-Isopropylacrylamide) Hydrogels. *ACS Macro Lett.* **2012**, *1* (3), 409–413.

(93) Avoce, D.; Liu, H. Y.; Zhu, X. X. N-Alkylacrylamide Copolymers with (Meth)Acrylamide Derivatives of Cholic Acid: Synthesis and Thermosensitivity. *Polymer (Guildf).* **2003**, *44* (4), 1081–1087.

(94) Caló, E.; Khutoryanskiy, V. V. Biomedical Applications of Hydrogels: A Review of Patents and Commercial Products. *Eur. Polym. J.* **2015**, *65*, 252–267.

(95) D'souza, A. A.; Shegokar, R. Polyethylene Glycol (PEG): A Versatile Polymer for Pharmaceutical Applications. *Expert Opin. Drug Deliv.* **2016**, *13* (9), 1257–1275.

(96) Chau, M.; De France, K. J.; Kopera, B.; Machado, V. R.; Rosenfeldt, S.; Reyes, L.; Chan, K. J. W.; Förster, S.; Cranston, E. D.; Hoare, T.; et al. Composite Hydrogels with Tunable Anisotropic Morphologies and Mechanical Properties. *Chem. Mater.* **2016**, *28* (10), 3406–3415.

(97) Deng, X.; Smeets, N. M. B.; Sicard, C.; Wang, J.; Brennan, J. D.; Filipe, C. D. M.; Hoare, T. Poly(Oligoethylene Glycol Methacrylate) Dip-Coating: Turning Cellulose Paper into a Protein-Repellent Platform for Biosensors. *J. Am. Chem. Soc.* **2014**, *136* (37), 12852–12855.

(98) Mateen, R.; Ali, M. M.; Hoare, T. A Printable Hydrogel Microarray for Drug Screening Avoids False Positives Associated with Promiscuous Aggregating Inhibitors. *Nat. Commun.* **2018**, *9* (1), 602.

(99) Stevens, M. M.; George, J. H. Exploring and Engineering the Cell Surface Interface. *Science* **2005**, *310* (November), 1135–1138.

(100) Kang, H.-W.; Tabata, Y.; Ikada, Y. Fabrication of Porous Gelatin Scaffolds for Tissue Engineering. *Biomaterials* **1999**, *20* (14), 1339–1344.

(101) Barbetta, A.; Gumiero, A.; Pecci, R.; Bedini, R.; Dentini, M. Gas-in-Liquid Foam Templating as a Method for the Production of Highly Porous Scaffolds. *Biomacromolecules* **2009**, *10* (12), 3188–3192.

(102) Gitli, T.; Silverstein, M. S. Bicontinuous Hydrogel–Hydrophobic Polymer Systems through Emulsion Templated Simultaneous Polymerizations. *Soft Matter* **2008**, *4* (12), 2475.

(103) Ricciardi, R.; Auriemma, F.; De Rosa, C. Structure and Properties of Poly(Vinyl Alcohol) Hydrogels Obtained by Freeze/Thaw Techniques. *Macromol. Symp.* **2005**, *222*, 49–63.

(104) Kumar, A.; Mishra, R.; Reinwald, Y.; Bhat, S. Cryogels: Freezing Unveiled by Thawing. *Mater. Today* **2010**, *13* (11), 42–44.

(105) Kim, T. K.; Yoon, J. J.; Lee, D. S.; Park, T. G. Gas Foamed Open Porous

Biodegradable Polymeric Microspheres. *file///Users/fei/Downloads/gas Form. open porous Biodegrad.* **2006**, *27* (2), 152–159.

(106) Chimene, D.; Lennox, K. K.; Kaunas, R. R.; Gaharwar, A. K. Advanced Bioinks for 3D Printing: A Materials Science Perspective. *Ann. Biomed. Eng.* **2016**, *44* (6), 2090–2102.

(107) Pataky, K.; Braschler, T.; Negro, A.; Renaud, P.; Lutolf, M. P.; Brugger, J. Microdrop Printing of Hydrogel Bioinks into 3D Tissue-Like Geometries. *Adv. Mater.* **2012**, *24* (3), 391–396.

(108) Hu, X.; Liu, S.; Zhou, G.; Huang, Y.; Xie, Z.; Jing, X. Electrospinning of Polymeric Nanofibers for Drug Delivery Applications. *J. Control. Release* **2014**, *185*, 12–21.

(109) Sill, T. J.; von Recum, H. A. Electrospinning: Applications in Drug Delivery and Tissue Engineering. *Biomaterials* **2008**, *29* (13), 1989–2006.

(110) Ji, Y.; Ghosh, K.; Li, B.; Sokolov, J. C.; Clark, R. A. F.; Rafailovich, M. H. Dual-Syringe Reactive Electrospinning of Cross-Linked Hyaluronic Acid Hydrogel Nanofibers for Tissue Engineering Applications. *Macromol. Biosci.* **2006**, *6* (10), 811–817.

(111) Huang, Z. M.; Zhang, Y. Z.; Kotaki, M.; Ramakrishna, S. A Review on Polymer Nanofibers by Electrospinning and Their Applications in Nanocomposites. *Compos. Sci. Technol.* **2003**, *63* (15), 2223–2253.

(112) Doshi, J.; Reneker, D. H. Electrospinning Process and Applications of Electrospun Fibers. *J. Electrostat.* **1995**, *35*, 151–160.

(113) Sill, T. J.; von Recum, H. A. Electrospinning: Applications in Drug Delivery and Tissue Engineering. *Biomaterials*. 2008, pp 1989–2006.

(114) Greiner, A.; Wendorff, J. H. Electrospinning: A Fascinating Method for the Preparation of Ultrathin Fibers. *Angew. Chemie - Int. Ed.* **2007**, *46* (30), 5670–5703.

(115) Beachley, V.; Wen, X. Effect of Electrospinning Parameters on the Nanofiber Diameter and Length. *Mater. Sci. Eng. C* **2009**, *29* (3), 663–668.

(116) Koski, A.; Yim, K.; Shivkumar, S. Effect of Molecular Weight on Fibrous PVA Produced by Electrospinning. *Mater. Lett.* **2004**, *58* (3–4), 493–497.

(117) Luo, C. J.; Nangrejo, M.; Edirisinghe, M. A Novel Method of Selecting Solvents for Polymer Electrospinning. *Polymer (Guildf).* **2010**, *51* (7), 1654–1662.

(118) Fong, H.; Fong, H.; Chun, I.; Chun, I.; Reneker, D.; Reneker, D. Beaded Nano Bers Formed during Electrospinning. *Polymer (Guildf).* **1999**, *40*, 4585–4592.

(119) Shenoy, S. L.; Bates, W. D.; Frisch, H. L.; Wnek, G. E. Role of Chain Entanglements on Fiber Formation during Electrospinning of Polymer Solutions: Good Solvent, Non-Specific Polymer-Polymer Interaction Limit. *Polymer (Guildf).*

2005, *46* (10), 3372–3384.

(120) Nie, H.; He, A.; Zheng, J.; Xu, S.; Li, J.; Han, C. C. Effects of Chain Conformation and Entanglement on the Electrospinning of Pure Alginate. *Biomacromolecules* **2008**, *9* (5), 1362–1365.

(121) Munir, M. M.; Suryamas, A. B.; Iskandar, F.; Okuyama, K. Scaling Law on Particle-to-Fiber Formation during Electrospinning. *Polymer (Guildf).* **2009**, *50* (20), 4935–4943.

(122) Yoshimoto, H.; Shin, Y. M.; Terai, H.; Vacanti, J. P. A Biodegradable Nanofiber Scaffold by Electrospinning and Its Potential for Bone Tissue Engineering. *Biomaterials* **2003**, *24* (12), 2077–2082.

(123) Ji, Y.; Ghosh, K.; Shu, X. Z.; Li, B.; Sokolov, J. C.; Prestwich, G. D.; Clark, R. A. F.; Rafailovich, M. H. Electrospun Three-Dimensional Hyaluronic Acid Nanofibrous Scaffolds. *Biomaterials* **2006**, *27* (20), 3782–3792.

(124) Elahi, M. F.; Lu, W. Core-Shell Fibers for Biomedical Applications-A Review. *J. Bioeng. Biomed. Sci.* **2013**, *03* (01), 1–14.

(125) Yu, D.-G.; Li, X.-Y.; Wang, X.; Yang, J.-H.; Bligh, S. W. A.; Williams, G. R. Nanofibers Fabricated Using Triaxial Electrospinning as Zero Order Drug Delivery Systems. *ACS Appl. Mater. Interfaces* **2015**, *7* (33), 18891–18897.

(126) Zhang, J.-F.; Yang, D.-Z.; Xu, F.; Zhang, Z.-P.; Yin, R.-X.; Nie, J. Electrospun Core−Shell Structure Nanofibers from Homogeneous Solution of Poly(Ethylene Oxide)/Chitosan. *Macromolecules* **2009**, *42* (14), 5278–5284.

(127) Li, D.; Xia, Y. Electrospinning of Nanofibers: Reinventing the Wheel? *Adv. Mater.* **2004**, *16* (14), 1151–1170.

(128) Jose, M. V; Thomas, V.; Johnson, K. T.; Dean, D. R.; Nyairo, E. Aligned PLGA/HA Nanofibrous Nanocomposite Scaffolds for Bone Tissue Engineering. *Acta Biomater.* **2009**, *5* (1), 305–315.

(129) Kishan, A. P.; Robbins, A. B.; Mohiuddin, S. F.; Jiang, M.; Moreno, M. R.; Cosgriff-Hernandez, E. M. Fabrication of Macromolecular Gradients in Aligned Fiber Scaffolds Using a Combination of In-Line Blending and Air-Gap Electrospinning. *Acta Biomater.* **2017**, *56*, 118–128.

(130) Baker, B. M.; Trappmann, B.; Wang, W. Y.; Sakar, M. S.; Kim, I. L.; Shenoy, V. B.; Burdick, J. a.; Chen, C. S. Cell-Mediated Fibre Recruitment Drives Extracellular Matrix Mechanosensing in Engineered Fibrillar Microenvironments. *Nat. Mater.* **2015**, *14* (12), 1262–1268.

Chapter 2

Structured Macroporous Hydrogels: Progress, Challenges, and Opportunities

Abstract

Structured macroporous hydrogels that have controllable porosities on both the nanoscale and the microscale offer both the swelling and interfacial properties of bulk hydrogels as well as the transport properties of "hard" macroporous materials. While a variety of techniques such as solvent casting, freeze drying, gas foaming, and phase separation have been developed to fabricate structured macroporous hydrogels, the typically weak mechanics and isotropic pore structures achieved as well as the required use of solvent/additives in the preparation process all limit the potential applications of these materials, particularly in biomedical contexts. This review highlights recent developments in the field of structured macroporous hydrogels aiming to increase network strength, create anisotropy and directionality within the networks, and utilize solvent-free or additive-free fabrication methods. Such functional materials are well-suited for not only biomedical applications like tissue engineering and drug delivery but also selective filtration, environmental sorption, and the physical templating of secondary networks.

2.1 Introduction

Hydrogels have attracted considerable research attention across a wide range of fields due to their versatility in composition, preparation, and resulting physical properties.[1] The soft mechanics, capacity for rapid internal diffusion of water-soluble components, tunable interfacial affinity for target molecules, and capacity for environmentally responsive physicochemical changes, all controllable based on the crosslink density and chemistry of

the hydrogel, make hydrogels highly relevant for biomedical,[1–3] bioseparations,[4–6] environmental,[7–9] and personal care applications,[10,11] among others. Biomedical applications including tissue engineering,[12] drug delivery,[13] and cell encapsulation[14] can particularly benefit from the properties of hydrogels, as hydrogels can effectively mimic the interfacial, chemical, mechanical, and biological functions of native extracellular matrix.[3]

The essential functionality of hydrogels in most applications is related to the pore size and pore distribution within the gel,[15] which directly regulates the transport properties of the gels. Porosity in conventional hydrogels is typically on the scale of a few to tens of nanometers, as defined by the average distance between crosslinks along the polymer chains comprising the hydrogel network.[16] Such porosity allows for facile internal diffusion of small molecules as well as some macromolecules, depending on their molecular weight relative to the size of the pores present. Larger porosity can in some cases be achieved via the phase separation of hydrogel components into domains, typically yielding larger pores between denser polymer clusters that can promote transport of larger molecules.[15] However, given the limitations in the molecular size of the constituent hydrogel precursor polymers as well as the magnitude of phase separation achievable within an elastic crosslinked network, swollen state porosity in conventional hydrogels is practically limited to <100 nm,[17,18] provided that one of the phases cannot be subsequently removed.[15] We would note that most papers claiming larger pore sizes in conventional hydrogels do so on the basis of scanning electron microscopy images, collected in the dry state typically following lyophilization of a frozen sample; as such, the porosities reported correspond not to the original porosity of the gel but rather the dimensions associated with ice crystal formation during the lyophilization process.[19,20] Although this dimension does have some correlation with hydrogel mechanics (i.e. stiffer materials restrict the growth of the ice crystals *in situ* inside the hydrogel), it is not an accurate representation of the actual swollen state morphology.

This practical limit on the achievable range of hydrogel porosity restricts the potential utility of hydrogels in applications such as bioadhesives and tissue engineering (in which the infiltration of cells of sizes on the order of tens of microns is desirable),[21–23] bioseparations (in which the pressure drop across the gel is extremely high due to the small pore size),[5,24] and sorbents (in which the desirable rapid influx of water is limited by the rate of water transport through the nanoporous network).[25–28] Even more interesting properties for some applications could be achieved if this introduction of larger micropores or macropores was combined with the effective alignment of those pores,[29] facilitating added benefits such as directional cell growth,[30] extremely low pressure drops,[4] and faster diffusion.[31] The shape and microarchitecture of the pores (i.e. whether they are cylindrical, lamellar, fibrous, etc.) can also be leveraged to influence phenomena such as oxygen and nutrient transport as well as cell migration and proliferation within the hydrogel,[21,22] with macroporous nanofibrous networks of particular interest for mimicking the fibrous nature of native extracellular matrix.[32]

Structured macroporous hydrogels are a class of hydrogels with porosities and/or feature sizes in the micron range that can effectively combine the desirable properties of conventional hydrogels with the transport properties of conventional porous media. The wide range of preparation techniques, highlighted below, allows for precise control over both pore size, pore orientation, and gel morphology, leading to highly functional materials for targeted applications including filtration, directing cell growth, and templating other materials.[23,26,33] In this review, we will discuss the current status of the preparation, characterization, and application of structured macroporous hydrogels as well as highlight ongoing challenges and opportunities associated with these materials to motivate future research activities in what is still a relatively new area of study.

2.2 Conventional Methods of Making Structured Hydrogels

Various methods have been developed to control structure/pore size and morphology in hydrogel scaffolds, summarized schematically in Figure 2.1.

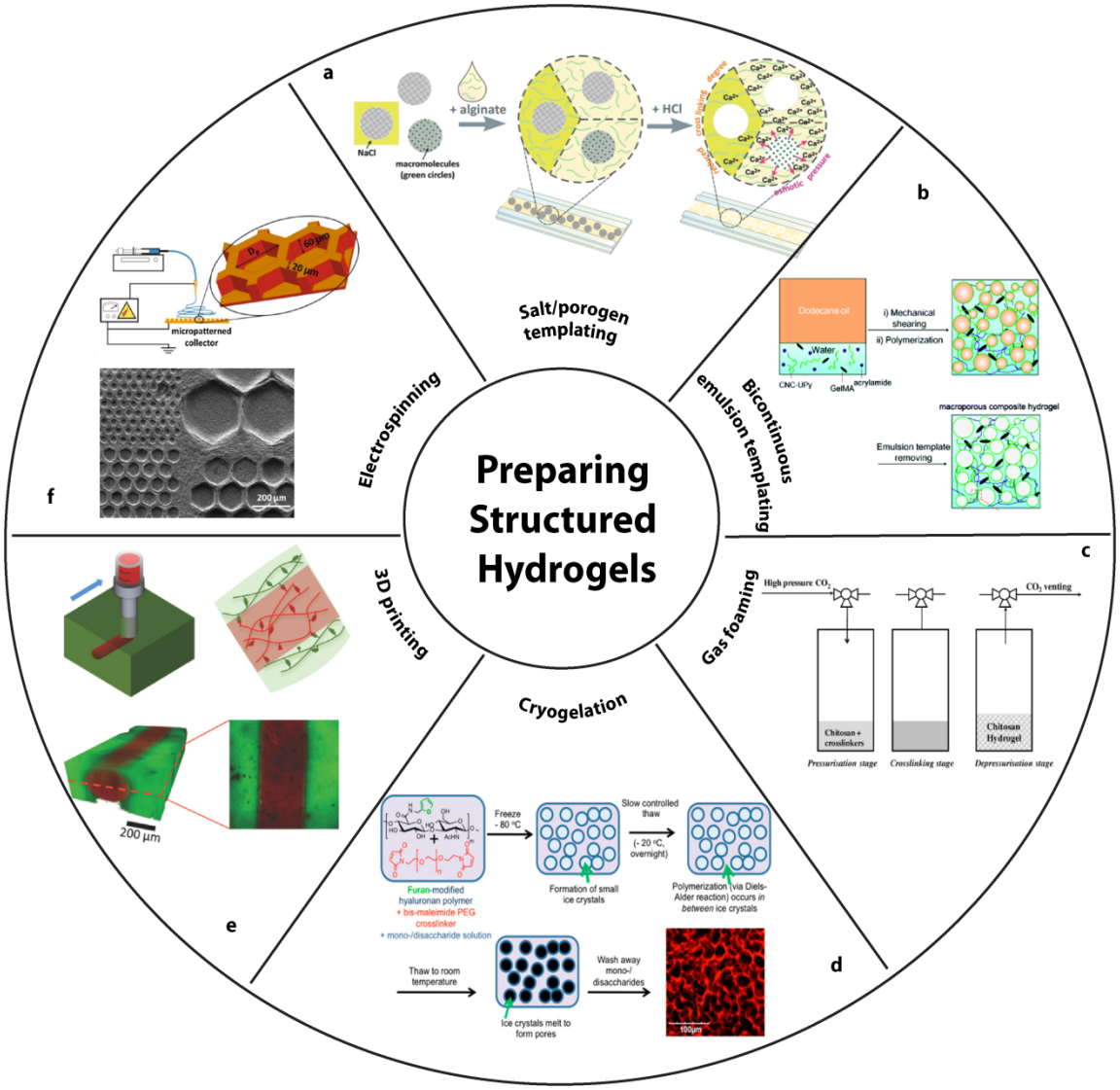

Figure 2.1 Conventional methods of preparing structured hydrogels: (a) salt/porogen templating, reproduced with permission from 34, copyright Wiley 2015; (b) bicontinuous emulsion templating, reproduced with permission from 35, copyright Royal Society of Chemistry 2017; (c) gas foaming, reproduced with permission from 36, copyright Elsevier 2011; (d) cryogelation, reproduced with permission from 37, copyright American Chemical Society 2016; (e) 3D printing, reproduced with permission from 38, copyright Wiley 2015; and (f) electrospinning, reproduced with permission from 39, copyright Elsevier 2015.

2.2.1 Salt/porogen templating

Salt templating is one of the most common methods to prepare porous hydrogel scaffolds due to its simplicity and low cost. In general, polymer precursors dissolved in aqueous media or (less commonly) an organic solvent are mixed with salt crystals and subsequently

polymerized and/or crosslinked to form monolithic scaffolds around the salt template. The salt is subsequently leached from the matrix (typically using water or weak bases), creating micro/macropores within the hydrogel matching the size of the salt crystal template. Sodium chloride salt crystals are most commonly used to prepare porous hydrogel scaffolds given their availability and bioinertness;[40,41] for example, porous photocrosslinked oligo (polyethylene glycol) fumarate (OPF) hydrogels have been fabricated with tunable pore sizes ranging from 100 to 500 μm using NaCl templates.[41] Other salts can also be applied, with $CaCO_3$ attracting particular interest given its low solubility at high/neutral pH values but significantly higher solubility in acidic conditions.[34] On this basis, hydrogels can be formed in aqueous conditions that can maintain the size/structure of the salt porogen without requiring the use of an organic solvent.

One notable limitation of salt templating is the high osmolarity induced by the high salt concentration required, and the potential for salt crystals to remain undissolved within the hydrogel scaffold (at least without highly exhaustive and slow dialysis processes). To solve this problem, degradable hydrogel microbeads have been explored for use as alternative porogens.[42,43] Relative to salt crystals, microbeads can be fabricated with more uniform sizes and consistent spherical geometries, increasing the regularity of the pore network formed while also undergoing programmed degradation to generate the macroporous structure. For example, Delaney et al. incorporated calcium alginate microspheres into bulk hydrogel networks, which could subsequently be solubilized and removed to form an open macroporous network [42],while Kim et al. reported a 3D porous poly(ε-caprolactone fumarate) (PCLF) scaffold containing different porogens including gelatin microparticles and poly(ethylene glycol) sebacic acid diacrylate (PEGSDA) microparticles.[43] Hwang et al. also used gelatin beads ranging from 150-300 μm as porogens to fabricate alginate hydrogels for cell encapsulation.[44] Importantly, unlike the salt templates that uniformly result in high osmolarity at minimum, these polymeric porogens are demonstrated to be non-toxic and cell compatible, opening possibilities to degrade the porogen (and thus create targeted macroporosities) over a defined time frame *in situ* during the use of the hydrogel

in a tissue engineering and/or drug delivery application.[45] For example, the Mikos group has described the controlled release of transforming growth factor-β1 (TGF-β1), from OPF hydrogels via the encapsulation of TGF-β1 within degradable microparticles throughout the gel, with the developing macroporosity (and thus ease of diffusion-based release) as the microparticles degrade helping to stabilize the drug release rate as a function of time.[46,47]

Porogen-based techniques, while widely used, do present significant limitations. Complete removal of the degraded polymer fractions from the gel network ultimately remains challenging even when using degradable polymer-based templates. Furthermore, regardless of the method of templating, porogens are inherently limited in applications in which a fully continuous pore structure is required for effective function (e.g. transport applications), as there will always be some statistically-significant fraction of pores that are not connected to others (at least at void fractions that would still enable the formation of a mechanically self-supporting network). The method is also relatively slow given the need for an extraction step, particularly if the application demands complete or almost complete removal of the template for effective function.

2.2.2 Gas foaming

Gas foaming works by either actively bubbling or (more commonly) *in situ*-generating gas bubbles within a polymer precursor solution as it gels/polymerizes, with the gas bubbles captured inside the matrix as the network forms to template pores. Sodium bicarbonate is the most widely used gas foaming agent given that it generates CO_2 in acidic conditions.[21] However, other carbonates (e.g. potassium carbonate, ammonium bicarbonate)[48,49] and nitrites (e.g. sodium nitrite)[50] have also been reported, with the ultimate choice of foaming agent decided based on cost and the safety of both the gas by-products produced as well as the residual products left behind within the formed gel; this latter considerations is particularly important to consider for biomedical applications.

As an alternative to the conventional solid foaming agents, which leave behind a residue following gas release, pressurized and/or supercritical CO_2 has more recently been

developed as a foaming agent that can dissolve within the forming gel network at high pressure and then rapidly evaporate to create pores upon release of the pressure, typically following at least partial crosslinking of the hydrogel.[36,51] The pressures used (corresponding to the total amount of CO_2 initially dissolved), the rate at which the pressures are changed, and the crosslink density of the gel at the time of depressurization can all be metered to gain some level of control over the porosity generated[52]. However, the low to moderate solubility of CO_2 in water is a drawback that limits the resulting porosity[53].

While gas foaming is relatively inexpensive in most cases, it suffers from the same key drawback of porogens: specifically, a lack of control over both the interconnectedness and directionality of the pore network formed. Note that the extraction of residues from solid gas foaming agents following gas formation is also a challenge in some applications, although gas foaming is significantly less problematic than porogens in this regard. In addition, unlike with porogens which can template a defined pore size and shape, gas foaming is a more random process that typically creates a highly heterogeneous pore size distribution within the network. Thus, compared to porogens, gas foaming typically trades an element of pore size control for increased speed and lower dependence on extraction prior to use of the scaffold.

2.2.3 Bicontinuous emulsion templating

Bicontinuous emulsions in which the pore-templating oil phase completely interpenetrates within an aqueous (and ultimately gelled) phase represent another popular and effective method of structuring hydrogels. Most commonly, high internal phase emulsions (polyHIPE) that by definition fill more >74% of the internal (dispersed) phase volume are used to create highly macroporous materials that avoid the formation of closed-cell porous structures common to porogen or gas foaming techniques.[54,55] Bicontinuous polyHIPEs are formed via polymerization of one of (or, in some examples, both of) the hydrophilic and hydrophobic phases, which can either be oil-in-water or water-in oil emulsions. For the

formation of polyHIPE-based structured hydrogels, the gel precursor monomers or polymer chains and crosslinker are typically dissolved in the aqueous phase, which is subsequently emulsified with an immiscible but relatively easy to extract organic solvent. For example, Ovadia et al. fabricated polyHIPE-based macroporous hydrogels of hydroxyethyl methacrylate (HEMA) and methacrylic acid (MAA) using cyclohexane as the organic phase to create hydrogels with higher water uptake due to the induced macroporosity,[56] while Zhou et al. reported an ion-responsive calcium-crosslinked alginate macroporous hydrogel using toluene as the organic phase which showed reversible swelling based on sodium citrate.[57] The polyHIPE method also makes the fabrication of pore-filled structured hydrogels easy by simply including water insoluble monomers in the organic phase and simultaneously (or sequentially if the mechanism is different) polymerizing both phases, with the collapse of one or the other phase resulting in templated macroporosity. As an example, Gitli described a hydrophilic-hydrophobic polymer system in which the hydrophobic phase was styrene or 2-ethylhexyl acrylate with divinylbenzene and the aqueous phase was acrylamide crosslinked with N,N-methylenebisacrylamide; upon swelling in water, the hydrophobic phase collapsed to create a macroporous and predominantly gel-like network.[58] Emulsion templating can also be combined with other pore-forming techniques (either porogen or, more commonly, gas foaming) to facilitate the generation of multi-scale porosities in gels,[59,60] although the partitioning of the porogen and/or gas foaming agent between the aqueous and organic phases must be well controlled to generate rational morphologies using such techniques.

The bicontinuous emulsion templating approach has advantages in terms of its relative simplicity and, most importantly relative to porogen templating, its generation of a hydrogel with a truly continuous macropore structure. The polyHIPE approach also can lead to the formation of networks with high overall porosities favorable in transport and cell scaffolding applications. However, the size and in particular the orientation of the pores produced using bicontinuous emulsification is difficult or impossible to control. While changing the emulsification shear rate can influence the average pore size, the pore structure generated is ultimately random in any published example (albeit interconnected).

In addition, the required use of an immiscible organic solvent can pose a challenge in terms of its efficient extraction as well as the incorporation of cells into the matrix if desired prior to those extraction steps.

2.2.4 Cryogelation

Cryogelation is a method that uses freeze/thaw cycles to generate ice crystals within aqueous pre-gel solutions that subsequently *in situ* template pores following polymerization/gelation, which is typically performed at sub-zero temperatures.[61,62] The formed ice crystals are subsequently removed by thawing or freeze drying to leave behind pores.[61,62] Due to the organized fractal nature of ice crystallization, cryogelation typically generates more interconnected pores than are achieved with conventional porogens. For example, Inci et al. prepared a gelatin cryogel crosslinked with oxidized dextran that displayed highly interconnected pores and a highly elastic nature,[63] while Thomas and Shea prepared poly ethylene glycol (PEG) hydrogels using cryotemplated photopolymerization that also demonstrated evidence of high pore interconnectivity.[64] In this way, cryogelation preserves the general advantages of porogen-based templating techniques while at least partially addressing the challenges of interconnectivity and template removal that limit the use of conventional porogens.

However, the sub-zero temperature processing limits the application of cryogelation in some applications, particularly in conjunction with potential cell loading for tissue engineering applications. That being said, the use of hydrogels as cryoprotectants for cells in conjunction with cryogelation processes has been demonstrated to successfully create cell-loaded macroporous gel scaffolds, albeit with some loss of cell activity following the freezing process.[65] Furthermore, although the rates of heating and cooling and the number of freeze/thaw cycles conducted can at least in part be used to rationally control the pore size and distribution generated,[66,67] the generated pores still typically have a broad pore size distribution and minimal if any directionality. Tam et al. have demonstrated the possible benefits of adding typical cryoprotectant carbohydrates such as D-galactose, D-glucose, D-trehalose or D-sucrose to the pre-gel solution, as all these sugars interact with water to alter

the nature of ice crystallization and thus create more transparent (in this case hyaluronan) hydrogels with improved pore size control.[37] However, further work is required to investigate what level of pore size/directionality control can be exerted using a cryogenic-based processing method.

2.2.5 Electrospinning

Electrospinning employs high voltages to overcome the surface tension of extruded polymer solutions to stretch them into nanofibers. It has attracted significant attention across a wide range of applications due to its simplicity and effectiveness of creating high surface area porous scaffolds, primarily using water insoluble polymers.[68–70] Both the parameters of the electrospinning process and the polymer solution can be adjusted to systematically alter the micro and nanostructure of the scaffolds.[71]

For nanofibers to be generated, high molecular weight polymers such as poly(ethylene oxide) (PEO) are typically required to facilitate sufficient polymer chain entanglement to favor nanofibers rather than electrosprayed droplet production.[68] Hydrogel fibers are typically produced by crosslinking gel precursor materials (monomers or prepolymers) either with or around high molecular weight electrospinning aids using an appropriate chemistry. The key to the successful hydrogel electrospinning is thus to identify a chemistry that can either rapidly gel the extruded nanofibers prior to deposition on the collector (preventing simple pooling of the solution on the collector) and/or post-gel dry fibers in a non-aqueous environment. Small molecule crosslinkers such as glutaraldehyde (GA) vapor can be used as a post-treatment or added to the polymer solution to crosslink the fibers *in situ*, provided the reaction time is balanced correctly with the processing time.[72,73]. Alternately, rapid photocrosslinking of the fibers during extrusion can capture the fibrous morphology prior to deposition, as demonstrated by Baker et al. for dextran methacrylate scaffolds[74] and Wade et al. for methacrylated hyaluronic acid (HA)-based nanofibers[75].

Electrospinning has significant benefits in terms of its potential for creating high surface area porous structures of various thicknesses (including very thin samples) that have inherently continuous pore structures due to the spaghetti-like nanofibrous product produced. The use of multiple spinnerets can accelerate the throughput of the process,[76,77] although care must be taken to avoid interfering electric fields and (even then) the production rate of porous materials is still slower than some other methods. Furthermore, micro-patterned collectors can be designed to obtain aligned porous scaffolds containing both micro/macropores and a nanofibrous structure without requiring additional control or post-processing steps[39,78]; gradients in both the radial direction and the longitudinal direction can also be directly incorporated into the macroporous hydrogel by designing appropriate mandrel-based collectors[79,80]. The main drawback of electrospinning is the stability of the resulting macroporous networks (particularly under pressure) given that there are typically no bonds between the fibers themselves, thus making them relatively easy to compress. In addition, while the nanofiber diameter can be precisely controlled, it is much more challenging to control the spacing between the fibers given the random whipping motion that occurs upon solvent evaporation. The relative kinetics of spinning and gelation must also be precisely optimized to maintain the templated feature sizes, often requiring substantial optimization of chemistry and/or processing. Finally, since an electrospinning aid such as high molecular weight PEO is typically required to induce fiber formation, this aid may have to be removed prior to use of the scaffold in the targeted application, adding time to the overall process.

2.2.6 3D printing

3D printing has recently gained increasing attention for the fabrication of hydrogel scaffolds with user-defined shapes as well as internal pore structures. In this technique, a 3D structure is rendered on a computer and printed layer-by-layer into the desired 3D structure. The mechanism by which the 3D structure is rendered depends on the nature of the gelation chemistry used for the hydrogel inks, which may be templated or free-form (Figure 2.2). In templated systems, the gel is deposited around a pre-printed sacrificial

template[81] or printed as a liquid that is subsequently polymerized *in situ*[82]; in either case, template removal results in the desired microporous structure. However, due to the requirement for templating, the same residual material and speed limitations associated with the use of porogens also apply to this technique, albeit without the likelihood of producing isolated pores (unless they are intentionally designed into the matrix). Two-photon techniques by which photopolymerization is localized in targeted 3D planes within a pre-gel solution offers a partial alternative to this issue with residual material[83] as well as exceptional resolution, achieving down to ~100 nm feature sizes. However, this technique still requires extraction of residual (unreacted) monomer following gelation and, as a raster-based technique, is extremely slow for making anything but very small scaffolds.

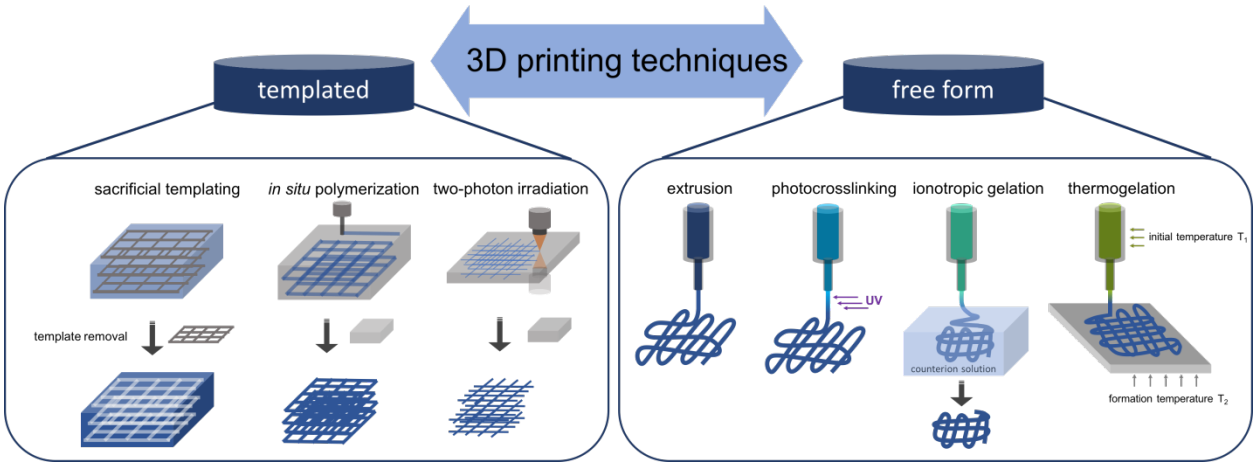

Figure 2.2 Common mechanisms for rendering structured hydrogels via 3D printing. Typically, scaffolds are either rendered via the use of a sacrificial template, or via direct writing, depending on the hydrogel gelation mechanism.

More promising is free-form printing techniques that can directly print a 3D gel structure in a single processing step using one of four approaches: (a) simple extrusion and deposition of pre-formed hydrogel tubes[84]; (b) printing and simultaneous rapid photocrosslinking of (meth)acrylated pre-polymer solutions to convert the liquid-like pre-polymer into a gel (also known as 3D printing stereolithography)[85]; (c) printing a polyelectrolyte into a counterion solution (e.g. sodium alginate into a calcium ion bath)[86] to facilitate near-instantaneous ionotropic gelation; or (d) extrusion of thermoresponsive

gelling pairs (e.g. sodium alginate/gelatin[87]) on a cooled or heated support that induces gelation on contact. Stereolithography has been particularly commonly exploited in this context given its capacity for processing different polymers. For example, Morris et al. fabricated ear-shaped scaffolds consisting of chitosan and polyethylene glycol diacrylate (PEGDA) that contained a macroporous interconnective pore structure,[88] Elomaa et al. created photocrosslinkable PEG-*co*-polydepsipeptide macromer to fabricate cell-laden hydrogels,[89] and Chan et al. used a commercial stereolithographic printer to prepare 3D structured PEG-based hydrogels.[90,91].

The clear advantage of 3D printing over all other described techniques is the precise detail on pore shape, alignment, size, and structure that can be designed into the product, as the resulting pore structure is neither the product of thermodynamics (emulsification), fluid mechanics (porogen distribution in the matrix), nor random events (nucleate evaporation in gas foaming, whipping in electrospinning). Such level of control may be particularly useful in tissue engineering applications to create well-defined geometric niches to direct cell behavior[83] in a way not possible with other techniques for fabricating structured macroporous hydrogels. However, current free-form printing strategies still suffer from two main drawbacks: (1) the resolution of the achievable feature sizes remains relatively low (at best ~10 μm aside from 2-photon techniques that are impractical for larger scaffolds), particularly problematic for extruded gels that are most common in current commercial printers and (2) for methods (c-d), a low diversity of chemistries can be used given that very rapid gelation is required to maintain the feature fidelity following printing[92,93] .

2.3 Challenges for Translational Structured Hydrogels

Although increased hydrogel porosity is extremely beneficial for rapid swelling and diffusion of solutes throughout the network, the preparation techniques described above all exhibit limitations. First, the typically desirable increased pore volume is directly

associated with a decrease in overall mechanical integrity of the network, as a fraction of the gel phase is replaced by water.[94] Given that hydrogels are already relatively weak materials, additional mechanical losses significantly limit the end use of many macroporous hydrogels, particularly in applications such as load-bearing tissues and/or pressure-driven separations where the mechanical stability of the structured hydrogel is essential to performance. Second, aside from 3D printing and to some extent electrospinning (both relatively slow processes), creating network anisotropy/directionality to better mimic native tissue striations or more efficiently direct solute diffusion remains difficult or infeasible. Third, most of the methods described (porogens, gas foaming, emulsification, and sometimes electrospinning and 3D printing) require the use of solvents/additives in the preparation process, increasing processing time/cost as well as introducing potential toxicity challenges associated with residual solvent/additive. In recognition of the importance of solving these three challenges, we will perform a more in-depth review of reported strategies to create structured macroporous hydrogels with high strength, anisotropic pore structures, and using solvent/additive-free processes.

2.3.1 High-Strength Hydrogels

Several techniques have been developed for improving the mechanical properties of bulk hydrogels,[95] with increasing the crosslink density[96] and/or the total solids content within the gel network[97] most typically used. However, these techniques have in general shown less success for structured hydrogels given that there is an inherent trade-off between mechanical performance and porosity; gels with higher mechanical strength typically have smaller or fewer pores. Significant effort has thus been invested in developing methods that can achieve sufficient mechanical strength but maximize the potential porosity of the structured macroporous hydrogel.

Controlling temperature during the gelation process has proven to be a relatively simple but effective method for mechanical enhancement. For example, both Plieva et al. and Rivero et al. have shown that performing the polymerization at sub-zero temperatures

(cryogelation/cryopolymerization) results in partitioning of acrylamide monomer toward the edges of the growing ice crystal, resulting in a macroporous structure with a dense (and strong) acrylamide phase comprising the walls.[98,99] Furthermore, by increasing the amount of initiator from 1.2 to 5%, Plieva et al. were able to enhance the compressive strength of these macroporous gels by nearly another order of magnitude.[98] Several groups have also explored freeze/thaw cycling – a process whereby hydrogel precursor materials are sequentially frozen – to induce strong physical crosslinking and enhance the mechanical properties of structured hydrogels.[100–102] When the number of freeze/thaw cycles is increased, the hydrogel components pack tighter to form a stronger, stiffer network. However, it must be noted that the porosity is also decreased upon increased cycling via the same mechanism,[100] limiting the practical utility of freeze/thaw processes for producing large pore volume materials.

Hydrogel nanocomposites have also attracted significant attention for mechanical enhancement. The incorporation of nanoparticles such as graphene oxide (GO),[103,104] silver nanoparticles,[105] , hydroxyapatite nanoparticles,[106] carbon nanotubes (CNT),[107] cellulose nanocrystals (CNCs),[35,108,109] and others have been used as reinforcing agents in macroporous hydrogels, with varying amounts of success. Notably, Huang et al. demonstrated that strong intermolecular interactions between GO and chitosan leads to the self-assembly of supramolecular macroporous composite hydrogels demonstrating enhanced mechanical performance versus chitosan-only gels.[103] Peng et al. showed similar mechanical enhancements by incorporating GO into directionally freeze-thawed polyvinyl alcohol (PVA) hydrogels, with 4 mg/mL GO leading to roughly 4-fold improvements in elastic modulus.[104] Our group has shown that the incorporation of rigid rod-like CNCs increased the compressive modulus of freeze-casted macroporous poly(oligoethylene glycol methacrylate) (POEGMA) hydrogels by nearly one order of magnitude as the CNC concentration was increased from 0.4 to 1.2 wt%.[108] Finally, the Khademhosseini group has shown that the incorporation of CNT into photo-crosslinkable gelatin methacrylate (GelMa) hydrogels led to a >3-fold increase in compressive modulus (Figure 2.3).[107] When

seeded with cardiomyocytes, these hydrogel scaffolds show promise as functional cardiac patches.

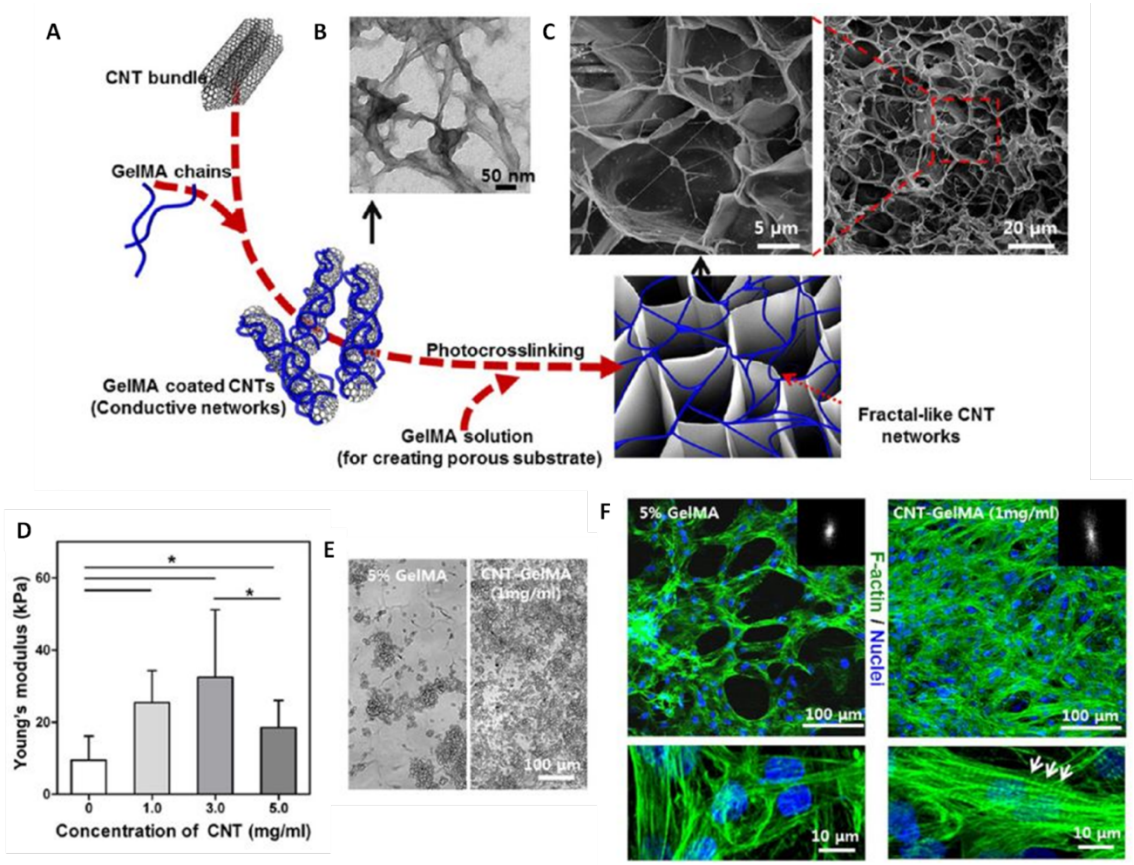

Figure 2.3 (A) Schematic representation of the preparation of CNT-GelMA macroporous hydrogel networks. (B) TEM and (C) SEM images of the nanocomposite networks. These networks show (D) enhanced Young's modulus, (E) more homogenous cardiac cell seeding, and (F) improved cell alignment versus pristine GelMA networks alone. Figure adapted with permission from reference [107], copyright 2013, American Chemical Society.

As an alternative to nanoparticle fillers, nanofibrous fillers have also been used, particularly in conjunction with 3D printing or other additive manufacturing gel fabrication approaches that can print gel in spatially controlled orientations around the reinforcing network. For example, Visser et al. utilized a 3D printing approach to reinforce soft hydrogels with highly organized polycaprolactone (PCL) microfiber networks (Figure 2.4). The stiffness of these gel/scaffold composites increases up to 54-fold versus pristine hydrogels and

approaches that of native articular cartilage, representing a feasible platform for producing functional tissue constructs.[110]

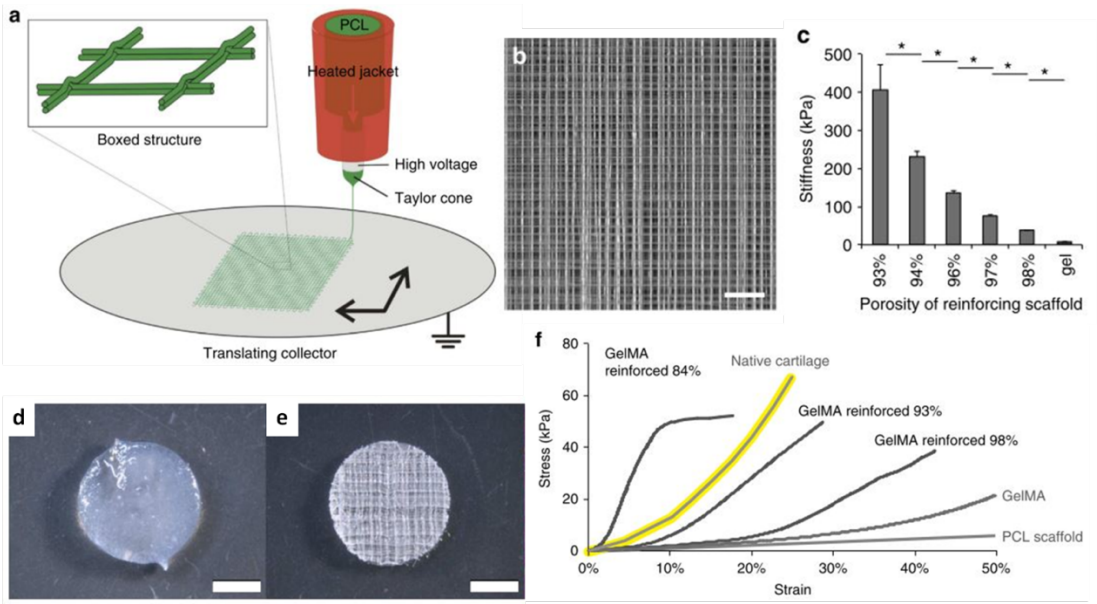

Figure 2.4 (a) Schematic representation of the fabrication of 3D printed PCL scaffolds for reinforcing soft hydrogels. (b) Stereomicroscopy image of the PCL grid network with spacing ranging from 0.2 mm (shown) to 1.0 mm (93% - 98% porosity, scale bar = 1 mm). (c, f) The lower the PCL network porosity, the greater the enhancement in the mechanical performance of GelMA composite networks. (d, e) Stereomicroscopy images of (d) pristine GelMa and (e) PCL reinforced networks (scale bars = 2 mm). Figure adapted with permission from reference **[110]**, copyright 2015, Nature Publishing Group.

One other common technique for enhancing the mechanical performance of structured hydrogels is through the creation of double (or interpenetrating) networks.[111,112] For example, Zhao et al. used a sequential cryopolymerization method whereby a polyacrylamide (PAM) network was prepared within a poly (N-isopropylacrylamide) (PNIPAM) network, [111] resulting in a greater than order of magnitude increase in Young's modulus versus either single network gel alone. Similarly, Zhang et al. demonstrated mechanical enhancements in PEG/gelatin interpenetrating networks via simple mixing, showing promise for cartilage regeneration applications.[112] Although not technically a double network gel, Li et al. also reported 2 – 20-fold enhancements in mechanical

performance when combining both cationic (poly(di- methyl diallyl ammonium chloride), PDMDAAC) and anionic (poly (acrylic acid), PAA) copolymers into a hybrid macroporous gel relative to an anionic network alone.[113]

2.3.2 Anisotropic Pore Structures

While a variety of anisotropic pore structures may be of interest, the generation of hydrogels with columnar or lamellar pore structures with well-defined directionality is of particularly attractive from an application perspective since such structures would allow for directional mass transfer/diffusion in filtration applications and more biomimetic scaffolds for the regeneration of biological tissues such as bone, muscle and tendon, all of which are composed of hierarchical structures. Typically, such materials are also inherently mechanically strong in at least one direction due to the aligned pore morphologies, addressing (at least in one dimension) the mechanical challenges previously described with most structured macroporous hydrogels.

Ice templating or directional freeze casting is an attractive option for creating uniaxial anisotropy in terms of both pore morphology and mechanical properties. In most cases, polymer precursor solutions are frozen and subsequently cryopolymerized through small molecule,[99,114–116] UV,[117–119] or radiation[105,113,120] initiated methods; however, physically crosslinked gels have also been reported,[121] including PVA-based anisotropic hydrogels prepared via directional freeze-thawing.[102,104] The direction of ice crystal growth determines the orientation of the pore while the rate of freezing predominantly influences the dimensionality is the aligned structures generated, with slower cooling rates resulting in slower ice crystal growth and ultimately the formation of larger ice platelets and thus larger pores following lyophilization.[118] Applications for such hydrogels have included 3D bacterial immobilization/culture for bioremediation and/or biocatalysis,[122] mammalian cell growth/guidance,[114] filtration,[123] and high surface area nanoparticle catalyst carriers.[105]

The use of “click-chemistry” in preparing freeze casted hydrogels has also been demonstrated,[108,124] which eliminates the need for additional crosslinking steps. Our group

has shown that varying the overall solids content and/or the weight ratio of aldehyde-functionalized CNCs to hydrazide-functionalized POEGMA can lead to structured macroporous hydrogels with tunable pore morphologies (e.g. fibrillar, columnar, or lamellar) via directional freeze casting (Figure 2.5).[108] The broad tunability of this system in terms of both the starting materials and the processing conditions (e.g. cooling rate, cooling temperature, cooling direction) allows for precise control over the anisotropic mechanical and swelling properties of the hydrogels produced. Furthermore, the aldehyde and hydrazide groups form reversible hydrazone cross-links under ambient conditions, stabilizing the structure of the hydrogels without requiring any form of post-polymerization or processing.[108]

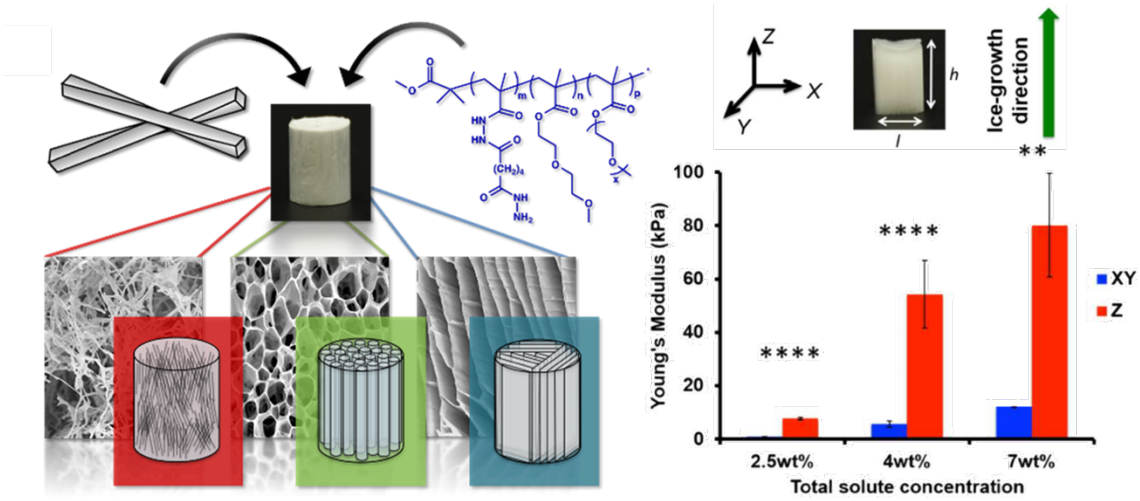

Figure 2.5 Schematic representation of the fabrication of macroporous anisotropic nanocomposite POEGMA-CNC hydrogels via freeze casting. By varying the total solute concentration and the ratio of CNC:POEGMA, the network morphology, swelling, and mechanical properties can be controlled in both directions perpendicular and parallel to ice crystal growth. Figure adapted with permission from reference [108], copyright 2016 American Chemical Society.

Alignment has also been explored in relation to modifications of other conventional techniques for macroporous hydrogel fabrication. In gas blowing, sodium bicarbonate is added to a pre-polymerization solution to create macroscopic ellipsoid-shaped pores in the direction of carbon dioxide gas escape (as directed via a vacuum).[125] However, intuitively,

the degree of anisotropy and the uniformity of the anisotropic structure achievable with a gas blowing technique are both significantly less than can be achieved in directional freezing. Porogens of various shapes can also be used to template anisotropic pores, particularly for the creation of ellipsoidal/channelled macropores within hydrogel networks. For example, Studenovska et al. polymerized HEMA in the presence of melt-spun aligned poly (L-lactide) fibers that were subsequently removed via either hydrolysis or aminolysis to create channelled hydrogels.[126] Spinning techniques can also readily be modified by using a rotating drum/disk or static parallel bar collector in order to generate aligned fibres.[127] Lee et al. used a wet spinning process with a rotating collector to directly fabricate aligned alginate microribbon hydrogels for cell encapsulation applications[128], while both Baek et al. and Yang et al. have fabricated aligned electrospun polylactic acid (PLA) fibers using rotating drum and static parallel bar collectors respectively.[129,130] These PLA fibres can then be used as templates for gel channels aiming to dictate the growth and orientation of cells within a collagen-based hydrogel.[129,130] Tonsomboon and Oyen demonstrated a comparable system using a rotating mandrel collector with electrospun gelatin fibers subsequently used to reinforce alginate hydrogels, showing control over hydrogel mechanical properties through fiber alignment.[131]

Directed phase separation has also been used to fabricate anisotropic macroporous hydrogels, although the consistency of the anisotropy resulting from such processes is typically lower than achieved using other approaches. For example, Renamayor et al. demonstrated that dimethylacrylamide hydrogels could form microheterogeneous structures varying from lamellar to cubic to hexagonal as the concentration of an anionic surfactant was increased and microphase separation was induced between the forming polymer/water phase and the surfactant phase.[132] These hydrogels do not however display macroscopic anisotropic properties. Alternately, Luo et al. demonstrated a method of creating hydrogels with well-defined gradient pore structures via hydrothermal synthesis, whereby NIPAM polymerization induces precipitation of polymer chains and therefore smaller (albeit isotropic) pores towards the bottom of the hydrogel,[31] resulting in controlled pore size along a directional gradient that leads to anisotropic swelling and potential

applications in programmable locomotion.[31] Similarly, Tripathi et al. prepared hybrid agarose-gelatin hydrogels through cryogelation that exhibited a gradient of pore sizes when prepared in water due to the viscosity differences between agarose and gelatin.[133]

Electrostatics can also be used to direct alignment. For example, hydrogels with two-dimensional interstitial voids/channels on the order of 10 μm have been created through the application of an external electric field to immobiline-functionalized polyacrylamide during polymerization.[134] These materials are useful as templates or microarrays, although the mechanical properties of the resulting scaffolds are not reported. Alternately, Yamamoto et al. demonstrated alginate gel scaffolds with honeycomb-like aligned pores prepared via ionotropic gelation, whereby adding a solution of calcium chloride on top of a solution of sodium alginate resulted in the formation of parallel channelled structures upon subsequent lyophilization.[135]

Another common method of creating anisotropic pore structures is through physical templating methods, whereby hydrogel precursor solutions are polymerized within either pre-defined or co-developed molds to form macroporous structures. Physical templating is performed primarily using lithographic techniques. For example, Bian et al. developed a soft lithography protocol to seed a mixture of muscle cells and fibrin gel within a PDMS mold, creating a muscle tissue sheet with elliptical pores that improved the directionality within the muscle fibres (Figure 2.6).[136] Similarly, Gauvin et al. used a 3D projection stereolithography technique to form a macroporous gelatin methacrylate hydrogel structures for cell growth and tissue engineering applications.[137] The Weidner group has also shown that templated microchanneled/capillary hydrogels fabricated through 3D projection stereolithography are effective as anisotropic scaffolds for promoting axonal regrowth.[138,139] Other materials can also be templated using lithographic techniques and then separately applied to direct hydrogel alignment. For example, Mao et al. used ice crystals formed within PDMS molds to structure silk fibroin-chitosan scaffolds that facilitated uniform cell seeding and nutrient delivery in 3D tissue engineering applications.[140]

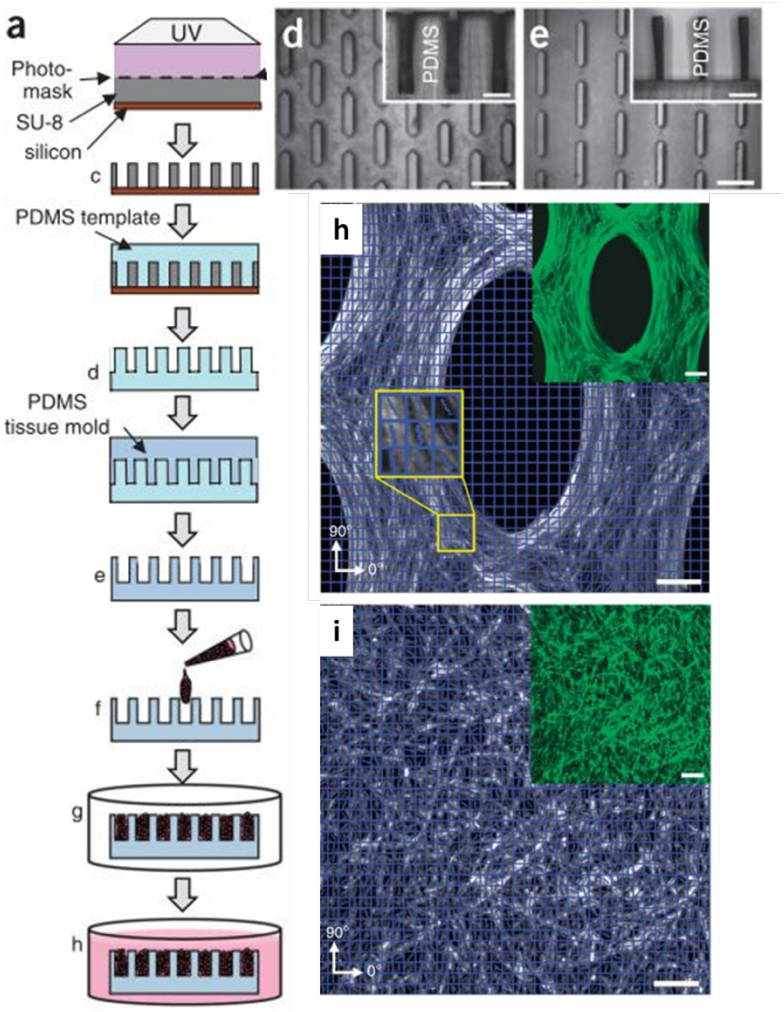

Figure 2.6 Fabrication process for creating bioartificial muscle tissue constructs. (a) A photomask is applied to SU-8 coated silicon wafers and exposed to UV light. (d) A PDMS negative replica and subsequently (e) a PDMS tissue mold are cast with elongated PDMS posts (scale bars = 1 mm, insets = 500 μm). (f) A cell-hydrogel solution is injected into the mold and incubated at 37°C to allow for gel polymerization and culture growth. (h) After 2 weeks of culture, muscle cell alignment is evidenced in the patterned hydrogel construct and is absent (i) in the unpatterned construct. Figure adapted with permission from reference [136], copyright 2009 Nature Publishing Group.

In situ-generated directional templates are typically based on directed crystallization protocols to create a structured template inside a pre-gel solution that is subsequently gelled around that template. For example, Zawko et al. developed such a "crystal templating"

technique whereby dendritic urea crystals were grown within methacrylated hyaluronic acid pre-gel solution that is subsequently photocrosslinked, followed by dissolution of the crystals to expose the pores.[141] Manipulating the density and placement of crystal seeds yields hydrogels with morphologies varying from radial to fibrillar, the latter of which is of potential interest for tissue engineering applications as templates for vascularization. Similarly, Mackova et al. used a freeze-casted sodium acetate salt crystal template to create pHEMA hydrogels with oriented pore structures.[142]

Finally, 3D printing techniques have a direct capacity to create highly aligned hydrogel structures with multiple dimensions and directionality, including the capacity to alter the directionality of the pores in the z-direction during the printing process if desired.[22,110,123,143] For example, Gou et al. utilized dynamic optical projection stereolithography (DOPsL) to 3D print a liver-mimetic device composed of a PEGDA matrix with incorporated nanoparticles for the neutralization of biological toxins.[123] This process uses a digital mirror array device to generate dynamic photomasks which can be translated into a 3D structure via layer by layer photopolymerization. Using a simpler 3D printing setup, Hong et al. developed a "stretching" method to condition 3D printed sodium alginate-PEG composite hydrogel meshes for cell encapsulation.[143] After 3D printing, these gels were photopolymerized in a separate UV chamber to crosslink, at which point they were seeded with cells, stretched, and fastened to a glass slide, leading to cellular elongation in the direction of stretching.

As 3D printing technology has improved so has the complexity of tissues produced, with biomimetic multilayer organs/organoids now having been generated containing different components and exhibiting different morphologies; although not strictly dedicated to macroporous hydrogels, reviews by Fedorovich et al. and Atala et al. summarize well such developments in 3D bioprinting of tissues and organs.[144,145] Notably, Kang et al. developed an integrated tissue-organ printer (ITOP) capable of producing human-scale tissue constructs with structural integrity.[146] This technique works by printing cell-laden hydrogels with sacrificial/biodegradable networks through the use of multiple cartridges

and clinical tissue imaging data to create integrated structures such as cartilage and skeletal muscle. Finally, it should be noted that while complex structures such as organs are achievable using 3D printing techniques, print resolution is ultimately governed by the diameter of the print nozzle used, practically limiting resolution to ~ 100 μm in most cases of cell-loaded structured macroporous hydrogels.

2.3.3 Solvent/Additive-Free Hydrogels

Avoiding both solvents and additives in the formation of structured macroporous hydrogels requires one of two approaches: (1) using water, ice, or biologically-acceptable gases (e.g. air, nitrogen, CO_2) as the pore-forming agent or (2) using chemistries that can facilitate *in situ*-gelation confined to fibers or other defined nanoscale features generated. Even in ice-templated materials, *in situ* gelation is often required to avoid the use of additives entirely; for example, both Kumar et al.[62] and Owen et al.[147,148] prepared oriented cryogels at sub-zero temperatures using ice crystals as the template but required small molecule crosslinkers or initiators to facilitate gelation around the template. As such, the development of *in situ*-gelling chemistries, particularly those that are cell-friendly in the context of potential tissue engineering applications and compatible with existing fabrication chemistries, is essential to remove the need for solvents or other additives. It should be emphasized that, while UV photopolymerization of (meth)acrylated polymer precursors in many ways does meet these criteria, such processes typically require the use of at least a small fraction of added photoinitiator and, depending on the required duration of UV exposure, may induce toxicity to cells included in the process either directly via DNA damage or indirectly by heating the scaffold[148,149]. Thus, while UV photopolymerization is certainly a viable option for avoiding solvent use is currently used as a water-based structuring chemistry with notable successes[89,150], its limitations should also be recognized.

A range of physical mechanisms including hydrophobic self-association[151], thermogelation[152,153], charge complexation[154,155], stereocomplexation[156], and host-guest

interactions[157] have been reported to enable *in situ* gelation in water. However, such interactions typically lead (at least alone) to weaker gels that are less predictably stable in a range of potential environments, particularly problematic in separations-based applications in which a range of different conditions may be used during a single separation process. Such instability can be mitigated by using the physical assembly process to enable the fast gelation kinetics required for many fabrication techniques and then a subsequent chemical crosslinking step to stabilize the structure. For example, Mironi-Harpaz et al. described 3D Pluronic-fibrinogen hydrogels fabricated using photolithography whereby the precursors were physically crosslinked at 37°C followed by UV irradiation using Irgacure 2959 as the photoinitiator to form stable covalent crosslinks and enhance the gel mechanics.[158] Covalent *in situ* gelation chemistries, meanwhile, offer the dual benefits of fast reactions as well as more predictable and tunable degradation kinetics (or, in some cases, non-degradability) have even broader potential utility. A variety of chemistries including amine-aldehyde (Schiff bases/imines)[159,160] , thiol-thiol (disulfide)[161], hydrazide-aldehyde (hydrazones)[162,163], hydroxylamine-aldehyde (oximes)[164], thiol-maleimide (thiosuccinimides)[165], (thiol or amine)-alkene (Michael adducts)[166], and alkyne-azide (triazoles)[167] has been reported that meets the criteria of fast reactions that occur spontaneously upon mixing in water, with the chemistries listed above in the approximate order of the stability of the resulting crosslink in water.

Combining various *in situ* gelling chemistries with electrospinning-based structured hydrogel fabrication techniques has met with the most success in terms of fabricating additive-free structured macroporous hydrogels, although most existing methods do have limitations. Wade et al. co-electrospun norbornene-functionalized HA with dithiothreitol (DTT) and subsequently UV irradiated sections of the scaffold (using a photomask) to locally crosslink the fibers and/or conjugate thiolated bioactive molecules to the scaffold via thiol-ene chemistry post-spinning[168]. While the spatial control gained via this post-modification approach was impressive, this method still required both a photoinitiator (Irgacure 2959) and a small molecule crosslinker (DTT) to work. Alternately, Ji et al. electrospun a matrix of thiolated 3,3'-dithiobis (propanoic dihydrazide)-modified

hyaluronic acid (HA-DTPH) that was subsequently mixed with PEGDA post-electrospinning and then dried, allowing Michael chemistry to induce gelation over a 24-hour period.[169,170] However, this approach is time-consuming and may not preserve in its entirety the initial electrospun structure based on the multiple post-treatment steps required.

Recently, we reported a fast reactive electrospinning technique that overcomes the challenges associated with these other approaches by co-delivering pairs of polymers that can undergo mixing-induced covalent *in situ* gelation using a double barrel syringe directly to an electrospinning needle. POEGMA oligomers were functionalized with hydrazide and aldehyde groups, allowing for rapid formation of hydrazone bonds upon mixing[163] that preserves the nanofiber structure on the collector (provided the residence time of the pre-gel solution between mixing and spinning is correctly optimized).[171] The resulting POEGMA electrospun scaffolds exhibit stable mechanical properties and nearly instantaneous swelling once exposed to water while retaining a nanofibrous morphology when wet. Moreover, the scaffolds can be degraded back into the oligomeric precursor polymers, slowly (over several months) at neutral pH and faster in acidic conditions (Figure 2.7). Using this method, *in situ* crosslinking to form stable gel nanofibers occurs at room temperature without any solvent, additives, crosslinker or post-treatment, making it significantly more cell-friendly than other strategies. It should however be noted that this method, as well as the two other approaches previously described in this section, use high molecular weight poly(ethylene oxide) (PEO) as an electrospinning aid, as the other polymers involved that ultimately make up the hydrogel nanofibers do not themselves exhibit sufficient chain entanglements for electrospinning. In each case, PEO is successfully extracted from the network following gelation via simple soaking; in addition, in the context of tissue engineering applications, a small amount of residual PEO is unlikely to have any adverse effects on cells given the known bioinert properties of PEO.[172]

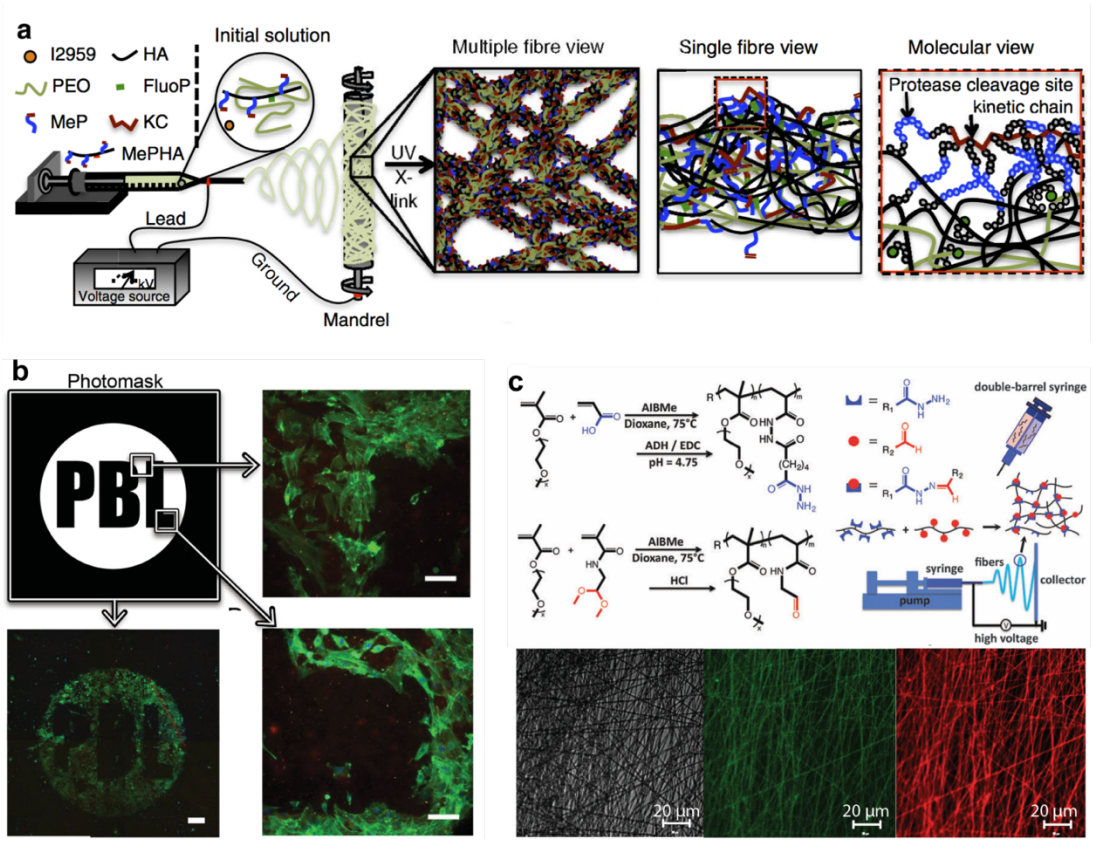

Figure 2.7 Solvent-free preparations for structured hydrogels: (a) Schematic of electrospun methacrylated peptide-functionalized HA (MePHA) degradable fibers with molecular composition; reproduced with permission from [75], copyright Nature Publishing Group, 2015. (b) Nanofibrous hydrogels with patterned biochemical ligands that affects adhesion of 3T3 fibroblasts; reproduced with permission from [168], copyright Wiley 2015. (c) POEGMA hydrogel nanofibers fabricated via reactive electrospinning; reproduced with permission from [171], copyright Royal Society of Chemistry, 2016.

The use of *in situ*-gelation chemistries in 3D printing is still in its infancy, aside from the ionotropic alginate-calcium gelation mechanism that forms the basis of most existing hydrogel 3D printers.[173–175] Thermogelation by printing on a heated platform (e.g. methacrylamide-PEG based triblock copolymer hydrogels[176]) or a cooled platform (e.g. sodium alginate/gelatin[87]) has also been demonstrated, although suffers from drawbacks associated with the stability of the resulting structures outside of the controlled temperature environment, the capacity to print thicker structures further away from the temperature-controlled base, and a lack of flexibility regarding the hydrogel components in order to

facilitate the required thermogelation. Combinations of physical gelation with UV photopolymerization have also been demonstrated. For example, Lewis's group has reported a bio-printed cell-laden gel with GelMA that forms a gelled network by cooling and can subsequently be photocrosslinked. The GelMA was used as bulk matrix to mimic native ECM and also as a cell carrier to encapsulate cells within the matrix (Figure 2.8).[177] Prestwich's group has reported the combination of thermogelation via gelatin (providing rapid physical gelation once cooled) with UV photopolymerization of pendant methacrylate groups (providing post-reaction stabilization and mechanical enhancement of the printed structure[178]), while Burdick's group has reported a combination of shear-disruptable host-guest physical interactions (providing rapid gelation once the nozzle shear is relieved) with UV photopolymerization as a 3D printable hydrogel ink capable of supporting cell growth.[179] However, to our knowledge, *in situ* covalent chemistry has not yet been reported in conjunction with 3D printing, likely attributable to the incompatibility of most current 3D printer designs for enabling the rapid mixing required for printing covalent *in situ* gelling polymers.

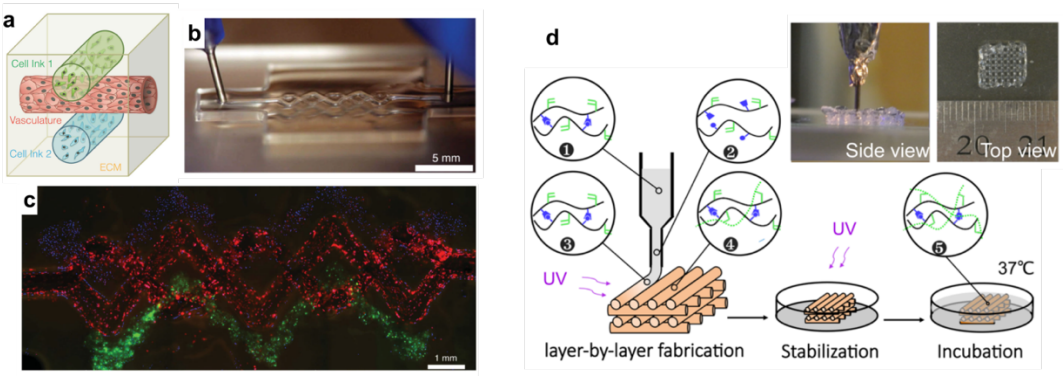

Figure 2.8 3D bio-printing of structured hydrogels: (a-c) co-printing of bioinks, GelMA, vasculature, and ECM to yield complex heterogeneous cell-laden hydrogel tissue constructs, reproduced with permission from ref [177], copyright Wiley 2014. (d) 3D printable supramolecular and UV curable multilayer HA hydrogel, reproduced with permission from ref [179], copyright American Chemical Society 2016.

2.4 Summary & Outlook

Although the field of structured hydrogels has made significant strides in recent years toward creating materials with high strength, controllable anisotropic pores, and using solvent/additive-free preparation techniques, there are several remaining challenges to address to fully realize the potential of structured gels in applications. First, the scale-up and reproducibility of various production methods poses a significant challenge to the commercialization of these materials. Although less of an issue for high value markets such as tissue engineering scaffolds, good manufacturing practices still need to be developed to consistently produce materials that can be approved by regulatory agencies even in cases in which cost is less problematic. Additive manufacturing techniques offer potential promise in this regard given the control that can be exerted in such processes over the product quality. Furthermore, *in vivo* screening in general and certainly clinical trials are lacking for most structured hydrogels developed to date, demanding studies of both the safety and efficacy of these materials in relevant and targeted biomedical applications. Alternately, outside the biomedical market, very little focus has been placed on developing these materials for other markets with far fewer barriers to entry; for example, anisotropic mechanical properties and diffusion gradients could be extremely beneficial in selective filtration/sorption applications. However, in this case, improving the scalability of the processing techniques is essential to make them economically viable for all but the highest value bioseparation applications (e.g. protein separation).

From a technical perspective, aside from challenges already described with increasing mechanical strength, introducing controlled anisotropy in the network, and minimizing or eliminating additives for structure generation or gelation already discussed, several outstanding issues still need to be addressed to improve the structural resolution and consistency of structured macroporous hydrogels for various applications. In particular, developing new 3D printing strategies that can efficiently print covalently *in situ* gelling hydrogels and/or significantly improve the resolution of printable feature sizes would greatly enhance the applicability of 3D printing in this context. Combining our knowledge

of how to control hydrogel swelling with some of the techniques already applied in soft lithography to create smaller features by e.g. swelling PDMS templates to narrow the spaces between the templated features may help to achieve this goal, although technical advances on the print heads and printing techniques used for 3D printing are ultimately likely required. Similarly, for electrospinning, developing new collectors that can take advantage of the electric fields present to better orient the fibers relative to each other (i.e. control not just alignment but also inter-fiber spacing) and further increase production rates while maintaining the quality of the nanofibers produced (i.e. avoiding undesirable overlaps between the electric fields associated with multiple spinnerets) would significantly broaden the applications of that technique.

Advances in even the more traditional techniques for macropore generation also have significant potential to address ongoing challenges. The use of aqueous two-phase systems that avoid organic solvents[180] or applying the lessons learned from surfactant or block copolymer-based templating of anisotropic nanoparticles to create more aligned or more regular pore sizes[33] would overcome many of the issues associated with bicontinuous emulsion techniques, which can already achieve the smaller resolution pores targeted by newer additive manufacturing approaches. New particulate templating techniques such as PRINT (Particle Replication in Non-wetting Templates)[181] may also be used to develop new shapes and sizes of easily dissolvable porogens that can create higher porosity networks with improved mechanics and better probabilities of pore interconnectivity relative to spheres; for example, porogens with sharper edges, controllable solubilization via blending, or smaller sizes may have higher probabilities of interlocking and thus creating a continuous pore structure while being easier to remove post-gelation. As such, while newer fabrication techniques are (perhaps deservedly) attracting more attention, using new knowledge gained from nanotechnology to refine older fabrication methods also holds promise for advancing the field.

Overall, we see particular potential for structured macroporous hydrogels with better control over pore size/shape/distribution/orientation, improved mechanics either

isotropically or anisotropically, and in particular co-fabricated with cells (facilitated by removing organic solvents or cytotoxic additives during processing) for addressing essential current challenges in the design of more biomimetic cell scaffolds for advanced tissue engineering applications. However, bioseparations and other filtration applications have been only peripherally explored thus far and represent substantial newer and beneficial uses for such hydrogels in easier-to-enter markets if suitable scalable production techniques are developed.

2.5 Acknowledgements

Funding from the Natural Sciences and Engineering Research Council of Canada (Discovery Grants RGPIN 356609 and 402329) as well as NSERC CREATE-IDEM (Integrated Design of Extracellular Matrices, Grant 398058) is gratefully acknowledged for the completion of our original work.

2.6 References

(1) Hoffman, A. S. Hydrogels for Biomedical Applications. *Adv. Drug Deliv. Rev.* **2002**, *54* (1), 3–12.

(2) Khademhosseini, A.; Langer, R. Microengineered Hydrogels for Tissue Engineering. *Biomaterials* **2007**, *28* (34), 5087–5092.

(3) Gaharwar, A. K.; Peppas, N. A.; Khademhosseini, A. Nanocomposite Hydrogels for Biomedical Applications. *Biotechnol. Bioeng.* **2014**, *111* (3), 441–453.

(4) Simhadri, J. J.; Stretz, H. A.; Oyanader, M.; Arce, P. E. Role of Nanocomposite Hydrogel Morphology in the Electrophoretic Separation of Biomolecules: A Review. *Ind. Eng. Chem. Res.* **2010**, *49* (23), 11866–11877.

(5) Tokarev, I.; Minko, S. Stimuli-Responsive Porous Hydrogels at Interfaces for Molecular Filtration, Separation, Controlled Release, and Gating in Capsules and Membranes. *Adv. Mater.* **2010**, *22* (31), 3446–3462.

(6) Kim, J. J.; Park, K. Smart Hydrogels for Bioseparation. *Bioseparation* **1999**, *7* (4–5), 177–184.

(7) Ma, J.; Li, X.; Bao, Y. Advances in Cellulose-Based Superabsorbent Hydrogels. *RSC Adv.* **2015**.

(8) Thakur, V. K.; Thakur, M. K. Recent Advances in Green Hydrogels from Lignin: A Review. *Int. J. Biol. Macromol.* **2015**, *72*, 834–847.

(9) Li, L.; Smitthipong, W.; Zeng, H. Mussel-Inspired Hydrogels for Biomedical and Environmental Applications. *Polym. Chem.* **2015**, *6*, 353–358.

(10) Zohuriaan-Mehr, M. J.; Omidian, H.; Doroudiani, S.; Kabiri, K. Advances in Non-Hygienic Applications of Superabsorbent Hydrogel Materials. *J. Mater. Sci.* **2010**, *45* (21), 5711–5735.

(11) Patravale, V. B.; Mandawgade, S. D. Novel Cosmetic Delivery Systems: An Application Update. *Int. J. Cosmet. Sci.* **2008**, *30* (1), 19–33.

(12) Billiet, T.; Vandenhaute, M.; Schelfhout, J.; Van Vlierberghe, S.; Dubruel, P. A Review of Trends and Limitations in Hydrogel-Rapid Prototyping for Tissue Engineering. *Biomaterials* **2012**, *33* (26), 6020–6041.

(13) Hoare, T. R.; Kohane, D. S. Hydrogels in Drug Delivery: Progress and Challenges. *Polymer (Guildf).* **2008**, *49* (8), 1993–2007.

(14) Brandl, F.; Sommer, F.; Goepferich, A. Rational Design of Hydrogels for Tissue Engineering: Impact of Physical Factors on Cell Behavior. *Biomaterials* **2007**, *28* (2), 134–146.

(15) Elbert, D. L. Liquid-Liquid Two-Phase Systems for the Production of Porous Hydrogels and Hydrogel Microspheres for Biomedical Applications: A Tutorial Review. *Acta Biomater.* **2011**, *7* (1), 31–56.

(16) Saul, J. M.; Williams, D. F. Hydrogels in Regenerative Medicine. *Princ. Regen. Med.* **2011**, 637–661.

(17) Anseth, K. S.; Bowman, C. N.; Brannon-Peppas, L. Mechanical Properties of Hydrogels and Their Experimental Determination. *Biomaterials* **1996**, *17* (17), 1647–1657.

(18) Ganji, F.; Vasheghani-Farahani, S.; Vasheghani-Farahani, E. Theoretical Description of Hydrogel Swelling: A Review. *Iran. Polym. J.* **2010**, *19* (5), 375–398.

(19) Apkarian, R. P.; Wright, E. R.; Seredyuk, V. a; Eustis, S.; Lyon, L. A.; Conticello, V. P.; Menger, F. M. In-Lens Cryo-High Resolution Scanning Electron Microscopy: Methodologies for Molecular Imaging of Self-Assembled Organic Hydrogels. *Microsc. Microanal.* **2003**, *9* (4), 286–295.

(20) Hermansson, A. M.; Buchheim, W. Characterization of Protein Gels by Scanning and Transmission Electron Microscopy. *J. Colloid Interface Sci.* **1981**, *81* (2), 519–530.

(21) Annabi, N.; Nichol, J. W.; Zhong, X.; Ji, C.; Koshy, S.; Khademhosseini, A.; Dehghani, F. Controlling the Porosity and Microarchitecture of Hydrogels for Tissue Engineering. *Tissue Eng. Part B. Rev.* **2010**, *16* (4), 371–383.

(22) Loh, Q. L.; Choong, C. Three-Dimensional Scaffolds for Tissue Engineering Applications: Role of Porosity and Pore Size. *Tissue Eng. Part B. Rev.* **2013**, *19* (6), 485–502.

(23) Staruch, R. M.; Glass, G. E.; Rickard, R.; Hettiaratchy, S. P.; Butler, P. Injectable Pore Forming Hydrogel Scaffolds for Complex Wound Tissue Engineering: Designing and Controlling Their Porosity and Mechanical Properties. *Tissue Eng. Part B Rev.* **2017**, *23* (2), 183–198.

(24) Yang, Q.; Adrus, N.; Tomicki, F.; Ulbricht, M. Composites of Functional Polymeric Hydrogels and Porous Membranes. *J. Mater. Chem.* **2011**, *21* (9), 2783–2811.

(25) Omidian, H.; Rocca, J. G.; Park, K. Advances in Superporous Hydrogels. *J. Control. Release* **2005**, *102* (1), 3–12.

(26) Mastropietro, D. J.; Omidian, H.; Park, K. Drug Delivery Applications for Superporous Hydrogels. *Expert Opin. Drug Deliv.* **2012**, *9* (1), 71–89.

(27) Kabiri, K.; Omidian, H.; Hashemi, S. A.; Zohuriaan-Mehr, M. J. Synthesis of Fast-Swelling Superabsorbent Hydrogels: Effect of Crosslinker Type and Concentration on Porosity and Absorption Rate. *Eur. Polym. J.* **2003**, *39* (7), 1341–1348.

(28) Kabiri, K.; Omidian, H.; Zohuriaan-Mehr, M. J. Novel Approach to Highly Porous Superabsorbent Hydrogels: Synergistic Effect of Porogens on Porosity and Swelling Rate. *Polym. Int.* **2003**, *52* (7), 1158–1164.

(29) Hollister, S. J. Porous Scaffold Design for Tissue Engineering. *Nat. Mater.* **2005**, *4* (July), 518–524.

(30) Li, Y.; Huang, G.; Zhang, X.; Wang, L.; Du, Y.; Lu, T. J.; Xu, F. Engineering Cell Alignment in Vitro. *Biotechnol. Adv.* **2014**, *32* (2), 347–365.

(31) Luo, R.; Wu, J.; Dinh, N. D.; Chen, C. H. Gradient Porous Elastic Hydrogels with Shape-Memory Property and Anisotropic Responses for Programmable Locomotion. *Adv. Funct. Mater.* **2015**, *25* (47), 7272–7279.

(32) Kumacheva, E. *Supramolecular Nanofibrillar Polymer Hydrogels*; 2015.

(33) Giese, M.; Blusch, L. K.; Khan, M. K.; MacLachlan, M. J. Functional Materials from Cellulose-Derived Liquid-Crystal Templates. *Angew. Chemie Int. Ed.* **2015**, *54* (10), 2888–2910.

(34) Sergeeva, A.; Feoktistova, N.; Prokopovic, V.; Gorin, D.; Volodkin, D. Design of Porous Alginate Hydrogels by Sacrificial CaCO3 Templates: Pore Formation Mechanism. *Adv. Mater. Interfaces* **2015**, *2* (18), 1–10.

(35) Liu, S.; Jin, M.; Chen, Y.; Gao, H.; Shi, X.; Cheng, W.; Ren, L.; Wang, Y. High Internal Phase Emulsions Stabilised by Supramolecular Cellulose Nanocrystals and Their Application as Cell-Adhesive Macroporous Hydrogel Monoliths. *J. Mater. Chem. B* **2017**, *5* (14), 2671–2678.

(36) Ji, C.; Annabi, N.; Khademhosseini, A.; Dehghani, F. Fabrication of Porous Chitosan Scaffolds for Soft Tissue Engineering Using Dense Gas CO2. *Acta Biomater.* **2011**, *7* (4), 1653–1664.

(37) Tam, R. Y.; Fisher, S. A.; Baker, A. E. G.; Shoichet, M. S. Transparent Porous Polysaccharide Cryogels Provide Biochemically Defined, Biomimetic Matrices for Tunable 3D Cell Culture. *Chem. Mater.* **2016**, *28* (11), 3762–3770.

(38) Highley, C. B.; Rodell, C. B.; Burdick, J. A. Direct 3D Printing of Shear-Thinning Hydrogels into Self-Healing Hydrogels. *Adv. Mater.* **2015**, *27* (34), 5075–5079.

(39) Nedjari, S.; Schlatter, G.; Hébraud, A. Thick Electrospun Honeycomb Scaffolds with Controlled Pore Size. *Mater. Lett.* **2015**, *142*, 180–183.

(40) Lee, S. B.; Kim, Y. H.; Chong, M. S.; Hong, S. H.; Lee, Y. M. Study of Gelatin-Containing Artificial Skin V: Fabrication of Gelatin Scaffolds Using a Salt-

Leaching Method. *Biomaterials* **2005**, *26* (14), 1961–1968.

(41) Dadsetan, M.; Hefferan, T. E.; Szatkowski, J. P.; Mishra, P. K.; Macura, S. I.; Lu, L.; Yaszemski, M. J. Effect of Hydrogel Porosity on Marrow Stromal Cell Phenotypic Expression. *Biomaterials* **2008**, *29* (14), 2193–2202.

(42) Delaney, J. T.; Liberski, A. R.; Perelaer, J.; Schubert, U. S. Reactive Inkjet Printing of Calcium Alginate Hydrogel Porogens—a New Strategy to Open-Pore Structured Matrices with Controlled Geometry. *Soft Matter* **2010**, *6* (5), 866.

(43) Kim, J.; Yaszemski, M. J.; Lu, L. Three-Dimensional Porous Biodegradable Polymeric Scaffolds Fabricated with Biodegradable Hydrogel Porogens. *Tissue Eng. Part C. Methods* **2009**, *15* (4), 583–594.

(44) Hwang, C. M.; Sant, S.; Masaeli, M.; Kachouie, N. N.; Zamanian, B.; Lee, S.-H.; Khademhosseini, A. Fabrication of Three-Dimensional Porous Cell-Laden Hydrogel for Tissue Engineering. *Biofabrication* **2010**, *2* (3), 035003.

(45) Shastri, V. P.; Hildgen, P.; Langer, R. In Situ Pore Formation in a Polymer Matrix by Differential Polymer Degradation. *Biomaterials* **2003**, *24* (18), 3133–3137.

(46) Holland, T. A.; Tessmar, J. K. V; Tabata, Y.; Mikos, A. G. Transforming Growth Factor-B1 Release from Oligo(Poly(Ethylene Glycol) Fumarate) Hydrogels in Conditions That Model the Cartilage Wound Healing Environment. *J. Control. Release* **2004**, *94* (1), 101–114.

(47) Park, H.; Temenoff, J. S.; Holland, T. A.; Tabata, Y.; Mikos, A. G. Delivery of TGF-B1 and Chondrocytes via Injectable, Biodegradable Hydrogels for Cartilage Tissue Engineering Applications. *Biomaterials* **2005**, *26* (34), 7095–7103.

(48) Kim, T. K.; Yoon, J. J.; Lee, D. S.; Park, T. G. Gas Foamed Open Porous Biodegradable Polymeric Microspheres. *file///Users/fei/Downloads/gas Form. open porous Biodegrad.* **2006**, *27* (2), 152–159.

(49) Kempen, D. H. R.; Lu, L.; Kim, C.; Zhu, X.; Dhert, W. J. A.; Currier, B. L.; Yaszemski, M. J. Controlled Drug Release from a Novel Injectable Biodegradable Microsphere/Scaffold Composite Based on Poly(Propylene Fumarate). *J. Biomed. Mater. Res. - Part A* **2006**, *77* (1), 103–111.

(50) Barbetta, A.; Gumiero, A.; Pecci, R.; Bedini, R.; Dentini, M. Gas-in-Liquid Foam

Templating as a Method for the Production of Highly Porous Scaffolds. *Biomacromolecules* **2009**, *10* (12), 3188–3192.

(51) Annabi, N.; Mithieux, S. M.; Weiss, A. S.; Dehghani, F. The Fabrication of Elastin-Based Hydrogels Using High Pressure CO2. *Biomaterials* **2009**, *30* (1), 1–7.

(52) Annabi, N.; Mithieux, S. M.; Weiss, A. S.; Dehghani, F. Cross-Linked Open-Pore Elastic Hydrogels Based on Tropoelastin, Elastin and High Pressure CO2. *Biomaterials* **2010**, *31* (7), 1655–1665.

(53) Barry, J. J. A.; Silva, M. M. C. G.; Popov, V. K.; Shakesheff, K. M.; Howdle, S. M. Supercritical Carbon Dioxide: Putting the Fizz into Biomaterials. *Philos. Trans. R. Soc. A Math. Phys. Eng. Sci.* **2006**, *364* (1838), 249 LP-261.

(54) Cameron, N. R.; Sherrington, D. C. High Internal Phase Emulsions (HIPEs) --- Structure, Properties and Use in Polymer Preparation. In *Biopolymers Liquid Crystalline Polymers Phase Emulsion*; Springer Berlin Heidelberg: Berlin, Heidelberg, 1996; pp 163–214.

(55) Zhang, H.; Cooper, A. I. Synthesis and Applications of Emulsion-Templated Porous Materials. *Soft Matter* **2005**, *1* (2), 107–113.

(56) Ovadia, M.; Silverstein, M. S. High Porosity, Responsive Hydrogel Copolymers from Emulsion Templating. *Polym. Int.* **2015**, No. August.

(57) Zhou, S.; Bismarck, A.; Steinke, J. H. G. Ion-Responsive Alginate Based Macroporous Injectable Hydrogel Scaffolds Prepared by Emulsion Templating. *J. Mater. Chem. B* **2013**, *1* (37), 4736–4745.

(58) Gitli, T.; Silverstein, M. S. Bicontinuous Hydrogel–Hydrophobic Polymer Systems through Emulsion Templated Simultaneous Polymerizations. *Soft Matter* **2008**, *4* (12), 2475.

(59) Partap, S.; Rehman, I.; Jones, J. R.; Darr, J. a. "Supercritical Carbon Dioxide in Water" Emulsion-Templated Synthesis of Porous Calcium Alginate Hydrogels. *Adv. Mater.* **2006**, *18* (4), 501–504.

(60) Lee, J.; Tan, B.; Cooper, A. I. CO 2 -in-Water Emulsion-Templated Poly (Vinyl Alcohol) Hydrogels Using Poly (Vinyl Acetate) -Based Surfactants. **2007**, 1955–

1961.

(61) Ricciardi, R.; Auriemma, F.; De Rosa, C. Structure and Properties of Poly(Vinyl Alcohol) Hydrogels Obtained by Freeze/Thaw Techniques. *Macromol. Symp.* **2005**, *222*, 49–63.

(62) Kumar, A.; Mishra, R.; Reinwald, Y.; Bhat, S. Cryogels: Freezing Unveiled by Thawing. *Mater. Today* **2010**, *13* (11), 42–44.

(63) Inci, I.; Kirsebom, H.; Galaev, I. Y.; Mattiasson, B.; Piskin, E. Gelatin Cryogels Crosslinked with Oxidized Dextran and Containing Freshly Formed Hydroxyapatite as Potential Bone Tissue-Engineering Scaffolds. *J. Tissue Eng. Regen. Med.* **2013**, *7* (7), 584–588.

(64) Thomas, A. M.; Shea, L. D. Cryotemplation for the Rapid Fabrication of Porous, Patternable Photopolymerized Hydrogels. *J. Mater. Chem. B* **2014**, *2* (28), 4521–4530.

(65) Vrana, N. E.; O'Grady, A.; Kay, E.; Cahill, P. A.; McGuinness, G. B. Cell Encapsulation within PVA-Based Hydrogels via Freeze-Thawing: A One-Step Scaffold Formation and Cell Storage Technique. *J. Tissue Eng. Regen. Med.* **2009**, *3* (6), 567–572.

(66) Hudson, S. D.; Hutter, J. L.; Nieh, M. P.; Pencer, J.; Millon, L. E.; Wan, W. Characterization of Anisotropic Poly(Vinyl Alcohol) Hydrogel by Small- and Ultra-Small-Angle Neutron Scattering. *J. Chem. Phys.* **2009**, *130*.

(67) Millon, L. E.; Nieh, M. P.; Hutter, J. L.; Wan, K. SANS Characterization of an Anisotropic Poly(Vinyl Alcohol) Hydrogel with Vascular Applications. *Macromolecules* **2007**, *40* (10), 3655–3662.

(68) Huang, Z. M.; Zhang, Y. Z.; Kotaki, M.; Ramakrishna, S. A Review on Polymer Nanofibers by Electrospinning and Their Applications in Nanocomposites. *Compos. Sci. Technol.* **2003**, *63* (15), 2223–2253.

(69) Li, D.; Xia, Y. Electrospinning of Nanofibers: Reinventing the Wheel? *Adv. Mater.* **2004**, *16* (14), 1151–1170.

(70) Doshi, J.; Reneker, D. H. Electrospinning Process and Applications of Electrospun Fibers. *J. Electrostat.* **1995**, *35*, 151–160.

(71) Greiner, A.; Wendorff, J. H. Electrospinning: A Fascinating Method for the Preparation of Ultrathin Fibers. *Angew. Chemie - Int. Ed.* **2007**, *46* (30), 5670–5703.

(72) Heydarkhan-Hagvall, S.; Schenke-Layland, K.; Dhanasopon, A. P.; Rofail, F.; Smith, H.; Wu, B. M.; Shemin, R.; Beygui, R. E.; MacLellan, W. R. Three-Dimensional Electrospun ECM-Based Hybrid Scaffolds for Cardiovascular Tissue Engineering. *Biomaterials* **2008**, *29* (19), 2907–2914.

(73) Schiffman, Jessica D. (Drexel University), Schauer, C. L. One-Step Electrospinning of Cross-Linked Chitosan Fibers. *Biomacromolecules* **2007**, *8*, 2665–2667.

(74) Baker, B. M.; Trappmann, B.; Wang, W. Y.; Sakar, M. S.; Kim, I. L.; Shenoy, V. B.; Burdick, J. a.; Chen, C. S. Cell-Mediated Fibre Recruitment Drives Extracellular Matrix Mechanosensing in Engineered Fibrillar Microenvironments. *Nat. Mater.* **2015**, *14* (12), 1262–1268.

(75) Wade, R. J.; Bassin, E. J.; Rodell, C. B.; Burdick, J. a. Protease-Degradable Electrospun Fibrous Hydrogels. *Nat. Commun.* **2015**, *6*, 6639.

(76) Varesano, A.; Carletto, R. A.; Mazzuchetti, G. Experimental Investigations on the Multi-Jet Electrospinning Process. *J. Mater. Process. Technol.* **2009**, *209* (11), 5178–5185.

(77) Persano, L.; Camposeo, A.; Tekmen, C.; Pisignano, D. Industrial Upscaling of Electrospinning and Applications of Polymer Nanofibers: A Review. *Macromol. Mater. Eng.* **2013**, *298* (5), 504–520.

(78) Nedjari, S.; Eap, S.; Hébraud, A.; Wittmer, C. R.; Benkirane-Jessel, N.; Schlatter, G. Electrospun Honeycomb as Nests for Controlled Osteoblast Spatial Organization. *Macromol. Biosci.* **2014**, *14* (11), 1580–1589.

(79) Kishan, A. P.; Robbins, A. B.; Mohiuddin, S. F.; Jiang, M.; Moreno, M. R.; Cosgriff-Hernandez, E. M. Fabrication of Macromolecular Gradients in Aligned Fiber Scaffolds Using a Combination of In-Line Blending and Air-Gap Electrospinning. *Acta Biomater.* **2017**, *56*, 118–128.

(80) Katta, P.; Alessandro, M.; Ramsier, R. D.; Chase, G. G. Continuous

Electrospinning of Aligned Polymer Nanofibers onto a Wire Drum Collector. *Nano Lett.* **2004**, *4* (11), 2215–2218.

(81) Lee, J. B.; Wang, X.; Faley, S.; Baer, B.; Balikov, D. A.; Sung, H.-J.; Bellan, L. M. Development of 3D Microvascular Networks Within Gelatin Hydrogels Using Thermoresponsive Sacrificial Microfibers. *Adv. Healthc. Mater.* **2016**, *5* (7), 781–785.

(82) Hinton, T. J.; Jallerat, Q.; Palchesko, R. N.; Park, J. H.; Grodzicki, M. S.; Shue, H.-J.; Ramadan, M. H.; Hudson, A. R.; Feinberg, A. W. Three-Dimensional Printing of Complex Biological Structures by Freeform Reversible Embedding of Suspended Hydrogels. *Sci. Adv.* **2015**, *1* (9).

(83) Xing, J.-F.; Zheng, M.-L.; Duan, X.-M. Two-Photon Polymerization Microfabrication of Hydrogels: An Advanced 3D Printing Technology for Tissue Engineering and Drug Delivery. *Chem. Soc. Rev.* **2015**, *44* (15), 5031–5039.

(84) Ozbolat, I. T.; Hospodiuk, M. Current Advances and Future Perspectives in Extrusion-Based Bioprinting. *Biomaterials* **2016**, *76*, 321–343.

(85) Hockaday, L. A.; Kang, K. H.; Colangelo, N. W.; Cheung, P. Y. C.; Duan, B.; Malone, E.; Wu, J.; Girardi, L. N.; Bonassar, L. J.; Lipson, H.; et al. Rapid 3D Printing of Anatomically Accurate and Mechanically Heterogeneous Aortic Valve Hydrogel Scaffolds. *Biofabrication* **2012**, *4* (3), 035005.

(86) Pataky, K.; Braschler, T.; Negro, A.; Renaud, P.; Lutolf, M. P.; Brugger, J. Microdrop Printing of Hydrogel Bioinks into 3D Tissue-like Geometries. *Adv. Mater.* **2012**, *24* (3), 391–396.

(87) He, Y.; Yang, F.; Zhao, H.; Gao, Q.; Xia, B.; Fu, J. Research on the Printability of Hydrogels in 3D Bioprinting. *Sci. Rep.* **2016**, *6*, 29977.

(88) Morris, V. B.; Nimbalkar, S.; Younesi, M.; McClellan, P.; Akkus, O. Mechanical Properties, Cytocompatibility and Manufacturability of Chitosan:PEGDA Hybrid-Gel Scaffolds by Stereolithography. *Ann. Biomed. Eng.* **2016**, *45* (1), 1–11.

(89) Elomaa, L.; Pan, C.-C.; Shanjani, Y.; Malkovskiy, A.; Seppälä, J. V.; Yang, Y. Three-Dimensional Fabrication of Cell-Laden Biodegradable Poly(Ethylene Glycol-Co-Depsipeptide) Hydrogels by Visible Light Stereolithography. *J. Mater.*

Chem. B **2015**, *3* (42), 8348–8358.

(90) Chan, V.; Zorlutuna, P.; Jeong, J. H.; Kong, H.; Bashir, R. Three-Dimensional Photopatterning of Hydrogels Using Stereolithography for Long-Term Cell Encapsulation. *Lab Chip* **2010**, *10* (16), 2062–2070.

(91) Chan, V.; Jeong, J. H.; Bajaj, P.; Collens, M.; Saif, T.; Kong, H.; Bashir, R. Multi-Material Bio-Fabrication of Hydrogel Cantilevers and Actuators with Stereolithography. *Lab Chip* **2012**, *12* (1), 88–98.

(92) Kumachev, A.; Greener, J.; Tumarkin, E.; Eiser, E.; Zandstra, P. W.; Kumacheva, E. High-Throughput Generation of Hydrogel Microbeads with Varying Elasticity for Cell Encapsulation. *Biomaterials* **2011**, *32* (6), 1477–1483.

(93) Lee, V. K.; Lanzi, A. M.; Ngo, H.; Yoo, S. S.; Vincent, P. A.; Dai, G. Generation of Multi-Scale Vascular Network System within 3D Hydrogel Using 3D Bio-Printing Technology. *Cell. Mol. Bioeng.* **2014**, *7* (3), 460–472.

(94) Stachowiak, A. N.; Bershteyn, A.; Tzatzalos, E.; Irvine, D. J. Bioactive Hydrogels with an Ordered Cellular Structure Combine Interconnected Macroporosity and Robust Mechanical Properties. *Adv. Mater.* **2005**, *17* (4), 399–403.

(95) Bin Imran, A.; Seki, T.; Takeoka, Y.; Imran, A. Bin. Recent Advances in Hydrogels in Terms of Fast Stimuli Responsiveness and Superior Mechanical Performance. *Polym. J.* **2010**, *42* (11), 839–851.

(96) Marklein, R. a.; Soranno, D. E.; Burdick, J. a. Magnitude and Presentation of Mechanical Signals Influence Adult Stem Cell Behavior in 3-Dimensional Macroporous Hydrogels. *Soft Matter* **2012**, *8* (31), 8113.

(97) Shi, X.; Hu, Y.; Tu, K.; Zhang, L.; Wang, H.; Xu, J.; Zhang, H.; Li, J.; Wang, X.; Xu, M. Electromechanical Polyaniline–Cellulose Hydrogels with High Compressive Strength. *Soft Matter* **2013**, *9* (42), 10129.

(98) Plieva, F.; Huiting, X.; Galaev, I. Y.; Bergenst?hl, B.; Mattiasson, B. Macroporous Elastic Polyacrylamide Gels Prepared at Subzero Temperatures: Control of Porous Structure. *J. Mater. Chem.* **2006**, *16* (41), 4065.

(99) Rivero, R. E.; Alustiza, F.; Rodríguez, N.; Bosch, P.; Miras, M. C.; Rivarola, C. R.; Barbero, C. A. Effect of Functional Groups on Physicochemical and Mechanical

Behavior of Biocompatible Macroporous Hydrogels. *React. Funct. Polym.* **2015**, *97*, 77–85.

(100) Guan, Y.; Bian, J.; Peng, F.; Zhang, X. M.; Sun, R. C. High Strength of Hemicelluloses Based Hydrogels by Freeze/Thaw Technique. *Carbohydr. Polym.* **2014**, *101* (1), 272–280.

(101) Chang, C.; Lue, A.; Zhang, L. Effects of Crosslinking Methods on Structure and Properties of Cellulose/PVA Hydrogels. *Macromol. Chem. Phys.* **2008**, *209* (12), 1266–1273.

(102) Zhang, L.; Zhao, J.; Zhu, J.; He, C.; Wang, H. Anisotropic Tough Poly(Vinyl Alcohol) Hydrogels. *Soft Matter* **2012**, *8*, 10439.

(103) Huang, Y.; Zeng, M.; Feng, Z.; Yin, D.; Xu, Q.; Fan, L. Graphene Oxide-Based Composite Hydrogels with Self-Assembled Macroporous Structures. *RSC Adv.* **2016**, *6* (5), 3561–3570.

(104) Peng, X.; He, C.; Liu, J.; Wang, H. Biomimetic Jellyfish-like PVA/Graphene Oxide Nanocomposite Hydrogels with Anisotropic and PH-Responsive Mechanical Properties. *J. Mater. Sci.* **2016**, *51* (12), 1–11.

(105) Mao, Q.; Shi, S.; Wang, H. Biomimetic Nanowire Structured Hydrogels as Highly Active and Recyclable Catalyst Carriers. *ACS Sustain. Chem. Eng.* **2015**, *3* (9), 1915–1924.

(106) Chang, C.; Peng, N.; He, M.; Teramoto, Y.; Nishio, Y.; Zhang, L. Fabrication and Properties of Chitin/Hydroxyapatite Hybrid Hydrogels as Scaffold Nano-Materials. *Carbohydr. Polym.* **2013**, *91* (1), 7–13.

(107) Shin, S. R.; Jung, S. M.; Zalabany, M.; Kim, K.; Zorlutuna, P.; Kim, S. B.; Nikkhah, M.; Khabiry, M.; Azize, M.; Kong, J.; et al. Carbon-Nanotube-Embedded Hydrogel Sheets for Engineering Cardiac Constructs and Bioactuators. *ACS Nano* **2013**, *7* (3), 2369–2380.

(108) Chau, M.; De France, K. J.; Kopera, B.; Machado, V. R.; Rosenfeldt, S.; Reyes, L.; Chan, K. J. W.; Förster, S.; Cranston, E. D.; Hoare, T.; et al. Composite Hydrogels with Tunable Anisotropic Morphologies and Mechanical Properties. *Chem. Mater.* **2016**, *28* (10), 3406–3415.

(109) De France, K. J.; Hoare, T.; Cranston, E. D. Review of Hydrogels and Aerogels Containing Nanocellulose. *Chem. Mater.* **2017**, acs.chemmater.7b00531.

(110) Visser, J.; Melchels, F. P. W.; Jeon, J. E.; van Bussel, E. M.; Kimpton, L. S.; Byrne, H. M.; Dhert, W. J. a; Dalton, P. D.; Hutmacher, D. W.; Malda, J. Reinforcement of Hydrogels Using Three-Dimensionally Printed Microfibres. *Nat. Commun.* **2015**, *6*, 6933.

(111) Zhao, Q.; Sun, J.; Wu, X.; Lin, Y. Macroporous Double-Network Cryogels: Formation Mechanism, Enhanced Mechanical Strength and Temperature/PH Dual Sensitivity. *Soft Matter* **2011**, *7* (9), 4284.

(112) Zhang, J.; Wang, J.; Zhang, H.; Lin, J.; Ge, Z.; Zou, X. Macroporous Interpenetrating Network of Polyethylene Glycol (PEG) and Gelatin for Cartilage Regeneration. *Biomed. Mater.* **2016**, *11* (3), 035014.

(113) Li, Y.; Peng, X.; Zhao, D.; Shi, S.; He, C.; Wang, H. Toughening Hydrogels by Immersing with Oppositely Charged Polymers. *J. Polym. Sci. Part B Polym. Phys.* **2016**, 1–10.

(114) Schulte, V. A.; Alves, D. F.; Dalton, P. P.; Moeller, M.; Lensen, M. C.; Mela, P. Microengineered PEG Hydrogels: 3D Scaffolds for Guided Cell Growth. *Macromol. Biosci.* **2013**, *13* (5), 562–572.

(115) Zhu, J.; Wang, J.; Liu, Q.; Liu, Y.; Wang, L.; He, C.; Wang, H. Anisotropic Tough Poly(2-Hydroxyethyl Methacrylate) Hydrogels Fabricated by Directional Freezing Redox Polymerization. *J. Mater. Chem. B* **2013**, *1* (7), 978–986.

(116) Yetiskin, B.; Okay, O. High-Strength Silk Fibroin Scaffolds with Anisotropic Mechanical Properties. *Polymer (Guildf).* **2017**, *112*, 61–70.

(117) Barrow, M.; Zhang, H. Aligned Porous Stimuli-Responsive Hydrogels via Directional Freezing and Frozen {UV} Initiated Polymerization. *Soft Matter* **2013**, *9* (9), 2723–2729.

(118) Bai, H.; Polini, A.; Delattre, B.; Tomsia, A. P. Thermoresponsive Composite Hydrogels with Aligned Macroporous Structure by Ice-Templated Assembly. *Chem. Mater.* **2013**, *25* (22), 4551–4556.

(119) Halake, K. S.; Lee, J. Superporous Thermo-Responsive Hydrogels by Combination

of Cellulose Fibers and Aligned Micropores. *Carbohydr. Polym.* **2014**, *105* (1), 184–192.

(120) Chen, M.; Zhu, J.; Qi, G.; He, C.; Wang, H. Anisotropic Hydrogels Fabricated with Directional Freezing and Radiation-Induced Polymerization and Crosslinking Method. *Mater. Lett.* **2012**, *89*, 8–11.

(121) Yokoyama, F.; Achife, E. C.; Momoda, J.; Shimamura, K.; Monobe, K. Morphology of Optically Anisotropic Agarose Hydrogel Prepared by Directional Freezing. *Colloid Polym. Sci.* **1990**, *268* (6), 552–558.

(122) Gutiérrez, M. C.; García-Carvajal, Z. Y.; Jobbágy, M.; Yuste, L.; Rojo, F.; Abrusci, C.; Catalina, F.; Del Monte, F.; Ferrer, M. L. Hydrogel Scaffolds with Immobilized Bacteria for 3D Cultures. *Chem. Mater.* **2007**, *19* (8), 1968–1973.

(123) Gou, M.; Qu, X.; Zhu, W.; Xiang, M.; Yang, J.; Zhang, K.; Wei, Y.; Chen, S. Bio-Inspired Detoxification Using 3D-Printed Hydrogel Nanocomposites. *Nat. Commun.* **2014**, *5* (May), 3774.

(124) Wu, J.; Zhao, Q.; Liang, C.; Xie, T. Enzymatically Degradable Oxidized Dextran–Chitosan Hydrogels with an Anisotropic Aligned Porous Structure. *Soft Matter* **2013**, *9* (46), 11136.

(125) Gemeinhart, R. A.; Park, H.; Park, K. Pore Structure of Superporous Hydrogels. *Polym. Adv. Technol.* **2000**, *11* (8–12), 617–625.

(126) Studenovská, H.; Šlouf, M.; Rypáček, F. Poly(HEMA) Hydrogels with Controlled Pore Architecture for Tissue Regeneration Applications. *J. Mater. Sci. Mater. Med.* **2008**, *19* (2), 615–621.

(127) Baji, A.; Mai, Y. W.; Wong, S. C.; Abtahi, M.; Chen, P. Electrospinning of Polymer Nanofibers: Effects on Oriented Morphology, Structures and Tensile Properties. *Compos. Sci. Technol.* **2010**, *70* (5), 703–718.

(128) Lee, S.; Tong, X.; Han, L.-H.; Behn, A.; Yang, F. Aligned Microribbon-like Hydrogels for Guiding Three-Dimensional Smooth Muscle Tissue Regeneration. *J. Biomed. Mater. Res. Part A* **2016**, *104* (5), 1064–1071.

(129) Baek, J.; Chen, X.; Sovani, S.; Jin, S.; Grogan, S. P.; D'Lima, D. D. Meniscus Tissue Engineering Using a Novel Combination of Electrospun Scaffolds and

Human Meniscus Cells Embedded within an Extracellular Matrix Hydrogel. *J. Orthop. Res.* **2015**, *33* (4), 572–583.

(130) Yang, Y.; Wimpenny, I.; Ahearne, M. Portable Nanofiber Meshes Dictate Cell Orientation throughout Three-Dimensional Hydrogels. *Nanomedicine Nanotechnology, Biol. Med.* **2011**, *7* (2), 131–136.

(131) Tonsomboon, K.; Oyen, M. L. Composite Electrospun Gelatin Fiber-Alginate Gel Scaffolds for Mechanically Robust Tissue Engineered Cornea. *J. Mech. Behav. Biomed. Mater.* **2013**, *21*, 185–194.

(132) Renamayor, C. S.; Pacios, I. E. Porous Structures Controlled by Segregation of Ordered Mesophases in Poly(N,N-Dimethylacrylamide) Hydrogels Polymerized from an Isotropic AOT/Water Medium. *Soft Matter* **2010**, *6* (9), 2013.

(133) Tripathi, A.; Kathuria, N.; Kumar, A. Elastic and Macroporous Agarose–Gelatin Cryogels with Isotropic and Anisotropic Porosity for Tissue Engineering. *J Biomed Mater Res* **2009**, *90* (October 2007), 680–694.

(134) Giunta, P. R.; Washington, R. P.; Campbell, T. D.; Steinbock, O.; Stiegman, A. E. Preparation of Mesoporous Silica Monoliths with Ordered Arrays of Macrochannels Templated from Electric-Field-Oriented Hydrogels. *Angew. Chemie Int. Ed.* **2004**, *43* (12), 1505–1507.

(135) Yamamoto, M.; James, D.; Li, H.; Butler, J.; Rafii, S.; Rabbany, S. Generation of Stable Co-Cultures of Vascular Cells in a Honeycomb Alginate Scaffold. *Tissue Eng. Part A* **2010**, *16* (1), 299–308.

(136) Bian, W.; Liau, B.; Badie, N.; Bursac, N. Mesoscopic Hydrogel Molding to Control the 3D Geometry of Bioartificial Muscle Tissues. *Nat. Protoc.* **2009**, *4* (10), 1522–1534.

(137) Gauvin, R.; Chen, Y. C.; Lee, J. W.; Soman, P.; Zorlutuna, P.; Nichol, J. W.; Bae, H.; Chen, S.; Khademhosseini, A. Microfabrication of Complex Porous Tissue Engineering Scaffolds Using 3D Projection Stereolithography. *Biomaterials* **2012**, *33* (15), 3824–3834.

(138) Prang, P.; Müller, R.; Eljaouhari, A.; Heckmann, K.; Kunz, W.; Weber, T.; Faber, C.; Vroemen, M.; Bogdahn, U.; Weidner, N. The Promotion of Oriented Axonal

Regrowth in the Injured Spinal Cord by Alginate-Based Anisotropic Capillary Hydrogels. *Biomaterials* **2006**, *27* (19), 3560–3569.

(139) Pawar, K.; Mueller, R.; Caioni, M.; Prang, P.; Bogdahn, U.; Kunz, W.; Weidner, N. Increasing Capillary Diameter and the Incorporation of Gelatin Enhance Axon Outgrowth in Alginate-Based Anisotropic Hydrogels. *Acta Biomater.* **2011**, *7* (7), 2826–2834.

(140) Mao, M.; He, J.; Liu, Y.; Li, X.; Li, D. Ice-Template-Induced Silk Fibroin–Chitosan Scaffolds with Predefined Microfluidic Channels and Fully Porous Structures. *Acta Biomater.* **2012**, *8* (6), 2175–2184.

(141) Zawko, S. A.; Schmidt, C. E. Crystal Templating Dendritic Pore Networks and Fibrillar Microstructure into Hydrogels. *Acta Biomater.* **2010**, *6* (7), 2415–2421.

(142) Mackova, H.; Plichta, Z.; Hlidkova, H.; Sedlacek, O.; Konefal, R.; Sadakbayeva, Z.; Duskova-Smrckova, M.; Horák, D.; Kubinova, S. Reductively Degradable Poly(2-Hydroxyethyl Methacrylate) Hydrogels with Oriented Porosity for Tissue Engineering Applications. *ACS Appl. Mater. Interfaces* **2017**, acsami.7b01513.

(143) Hong, S.; Sycks, D.; Chan, H. F. ai; Lin, S.; Lopez, G. P.; Guilak, F.; Leong, K. W.; Zhao, X. 3D Printing: 3D Printing of Highly Stretchable and Tough Hydrogels into Complex, Cellularized Structures. *Adv. Mater.* **2015**, *27* (27), 4034.

(144) Fedorovich, N. E.; Alblas, J.; de Wijn, J. R.; Hennink, W. E.; Verbout, A. J.; Dhert, W. J. a. Hydrogels as Extracellular Matrices for Skeletal Tissue Engineering: State-of-the-Art and Novel Application in Organ Printing. *Tissue Eng.* **2007**, *13* (8), 1905–1925.

(145) Atala, S. V. M. & A. 3D Bioprinting of Tissues and Organs. *Nat. Biotechnol.* **2014**, *32* (8), 773–785.

(146) Kang, H.-W.; Lee, S. J.; Ko, I. K.; Kengla, C.; Yoo, J. J.; Atala, A. A 3D Bioprinting System to Produce Human-Scale Tissue Constructs with Structural Integrity. *Nat. Biotechnol.* **2016**, *34* (3), 312–319.

(147) Owen, S. C.; Fisher, S. A.; Tam, R. Y.; Nimmo, C. M.; Shoichet, M. S. Hyaluronic Acid Click Hydrogels Emulate the Extracellular Matrix. *Langmuir* **2013**, *29* (24), 7393–7400.

(148) Liu, V. A.; Bhatia, S. N. Three-Dimensional Photopatterning of Hydrogels Containing Living Cells. *Biomed. Microdevices* **2002**, *4* (4), 257–266.

(149) Rouillard, A. D.; Berglund, C. M.; Lee, J. Y.; Polacheck, W. J.; Tsui, Y.; Bonassar, L. J.; Kirby, B. J. Methods for Photocrosslinking Alginate Hydrogel Scaffolds with High Cell Viability. *Tissue Eng. Part C. Methods* **2011**, *17* (2), 173–179.

(150) Ifkovits, J. L.; Burdick, J. a. Review: Photopolymerizable and Degradable Biomaterials for Tissue Engineering Applications. *Tissue Eng.* **2007**, *13* (10), 2369–2385.

(151) Adler-Abramovich, L.; Gazit, E. The Physical Properties of Supramolecular Peptide Assemblies: From Building Block Association to Technological Applications. *Chem. Soc. Rev.* **2014**, *43* (20), 6881–6893.

(152) Malmsten, M.; Lindman, B. Water Self-Diffusion in Aqueous Block Copolymer Solutions. *Macromolecules* **1992**, *25* (20), 5446–5450.

(153) Cho, I. S.; Cho, M. O.; Li, Z.; Nurunnabi, M.; Park, S. Y.; Kang, S.-W.; Huh, K. M. Synthesis and Characterization of a New Photo-Crosslinkable Glycol Chitosan Thermogel for Biomedical Applications. *Carbohydr. Polym.* **2016**, *144*, 59–67.

(154) Martinsen, A.; Skjåk-Bræk, G.; Smidsrød, O. Alginate as Immobilization Material: I. Correlation between Chemical and Physical Properties of Alginate Gel Beads. *Biotechnol. Bioeng.* **1989**, *33* (1), 79–89.

(155) Javvaji, V.; Baradwaj, A. G.; Payne, G. F.; Raghavan, S. R. Light-Activated Ionic Gelation of Common Biopolymers. *Langmuir* **2011**, *27* (20), 12591–12596.

(156) Hiemstra, C.; Zhou, W.; Zhong, Z.; Wouters, M.; Feijen, J. Rapidly in Situ Forming Biodegradable Robust Hydrogels by Combining Stereocomplexation and Photopolymerization. *J. Am. Chem. Soc.* **2007**, *129* (32), 9918–9926.

(157) Miyamae, K.; Nakahata, M.; Takashima, Y.; Harada, A. Self-Healing, Expansion–Contraction, and Shape-Memory Properties of a Preorganized Supramolecular Hydrogel through Host–Guest Interactions. *Angew. Chemie Int. Ed.* **2015**, *54* (31), 8984–8987.

(158) Mironi-Harpaz, I.; Hazanov, L.; Engel, G.; Yelin, D.; Seliktar, D. In-Situ Architectures Designed in 3D Cell-Laden Hydrogels Using Microscopic Laser

Photolithography. *Adv. Mater.* **2015**, *27* (11), 1933–1938.

(159) Li, L.; Wang, N.; Jin, X.; Deng, R.; Nie, S.; Sun, L.; Wu, Q.; Wei, Y.; Gong, C. Biodegradable and Injectable in Situ Cross-Linking Chitosan-Hyaluronic Acid Based Hydrogels for Postoperative Adhesion Prevention. *Biomaterials* **2014**, *35* (12), 3903–3917.

(160) Tan, H.; Chu, C. R.; Payne, K. A.; Marra, K. G. Injectable in Situ Forming Biodegradable Chitosan-Hyaluronic Acid Based Hydrogels for Cartilage Tissue Engineering. *Biomaterials* **2009**, *30* (13), 2499–2506.

(161) Ghosh, K.; Shu, X. Z.; Mou, R.; Lombardi, J.; Prestwich, G. D.; Rafailovich, M. H.; Clark, R. A. F. Rheological Characterization of in Situ Cross-Linkable Hyaluronan Hydrogels. *Biomacromolecules* **2005**, *6* (5), 2857–2865.

(162) Bulpitt, P.; Aeschlimann, D. New Strategy for Chemical Modification of Hyaluronic Acid: Preparation of Functionalized Derivatives and Their Use in the Formation of Novel Biocompatible Hydrogels. *J. Biomed. Mater. Res.* **1999**, *47* (2), 152–169.

(163) Smeets, N. M. B.; Bakaic, E.; Patenaude, M.; Hoare, T. Injectable and Tunable Poly(Ethylene Glycol) Analogue Hydrogels Based on Poly(Oligoethylene Glycol Methacrylate). *Chem. Commun.* **2014**, *50* (25), 3306–3309.

(164) Kalia, J.; Raines, R. T. Hydrolytic Stability of Hydrazones and Oximes. *Angew. Chemie* **2008**, *120* (39), 7633–7636.

(165) Phelps, E. A.; Enemchukwu, N. O.; Fiore, V. F.; Sy, J. C.; Murthy, N.; Sulchek, T. A.; Barker, T. H.; García, A. J. Maleimide Cross-Linked Bioactive PEG Hydrogel Exhibits Improved Reaction Kinetics and Cross-Linking for Cell Encapsulation and In Situ Delivery. *Adv. Mater.* **2012**, *24* (1), 64–70.

(166) Bencherif, S. A.; Siegwart, D. J.; Srinivasan, A.; Horkay, F.; Hollinger, J. O.; Washburn, N. R.; Matyjaszewski, K. Nanostructured Hybrid Hydrogels Prepared by a Combination of Atom Transfer Radical Polymerization and Free Radical Polymerization. *Biomaterials* **2009**, *30* (29), 5270–5278.

(167) Wang, Q.; Chan, T. R.; Hilgraf, R.; Fokin, V. V; Sharpless, K. B.; Finn, M. G. Bioconjugation by Copper(I)-Catalyzed Azide-Alkyne [3 + 2] Cycloaddition. *J.*

Am. Chem. Soc. **2003**, *125* (11), 3192–3193.

(168) Wade, R. J.; Bassin, E. J.; Gramlich, W. M.; Burdick, J. A. Nanofibrous Hydrogels with Spatially Patterned Biochemical Signals to Control Cell Behavior. *Adv. Mater.* **2015**, *27* (8), 1356–1362.

(169) Ji, Y.; Ghosh, K.; Li, B.; Sokolov, J. C.; Clark, R. A. F.; Rafailovich, M. H. Dual-Syringe Reactive Electrospinning of Cross-Linked Hyaluronic Acid Hydrogel Nanofibers for Tissue Engineering Applications. *Macromol. Biosci.* **2006**, *6* (10), 811–817.

(170) Ji, Y.; Ghosh, K.; Shu, X. Z.; Li, B.; Sokolov, J. C.; Prestwich, G. D.; Clark, R. A. F.; Rafailovich, M. H. Electrospun Three-Dimensional Hyaluronic Acid Nanofibrous Scaffolds. *Biomaterials* **2006**, *27* (20), 3782–3792.

(171) Xu, F.; Sheardown, H.; Hoare, T. Reactive Electrospinning of Degradable Poly(Oligoethylene Glycol Methacrylate)-Based Nanofibrous Hydrogel Networks. *Chem. Commun.* **2015**, *52*, 23–25.

(172) Gombotz, W. R.; Wang, G. H.; Horbett, T. A.; Hoffman, A. S. Protein Adsorption to Poly(Ethylene Oxide) Surfaces. *J. Biomed. Mater. Res.* **1991**, *25* (12), 1547–1562.

(173) Atala, S. V. M. & A. 3D Bioprinting of Tissues and Organs. *Nat. Biotechnol.* **2014**, *32* (8), 773–785.

(174) Wust, S.; Ralph, M.; Hofmann, S. 3D Bioprinting of Complex Channels — Effects of Material , Orientation , Geometry , and Cell Embedding. *J. Biomed. Res. part A* **2014**, 1–13.

(175) Müller, M.; Ozturk, E.; Arlov, O.; Gatenholm, P.; Zenobi-Wong, M. Alginate Sulfate-Nanocellulose Bioinks for Cartilage Bioprinting Applications. *Ann. Biomed. Eng.* **2017**, *45* (1), 210–223.

(176) Censi, R.; Schuurman, W.; Malda, J.; Di Dato, G.; Burgisser, P. E.; Dhert, W. J. A.; Van Nostrum, C. F.; Di Martino, P.; Vermonden, T.; Hennink, W. E. A Printable Photopolymerizable Thermosensitive p(HPMAm-Lactate)-PEG Hydrogel for Tissue Engineering. *Adv. Funct. Mater.* **2011**, *21* (10), 1833–1842.

(177) Kolesky, D. B.; Truby, R. L.; Gladman, A. S.; Busbee, T. A.; Homan, K. A.;

Lewis, J. A. 3D Bioprinting of Vascularized, Heterogeneous Cell-Laden Tissue Constructs. *Adv. Mater.* **2014**, *26* (19), 3124–3130.

(178) Skardal, A.; Zhang, J.; McCoard, L.; Xu, X.; Oottamasathien, S.; Prestwich, G. D. Photocrosslinkable Hyaluronan-Gelatin Hydrogels for Two-Step Bioprinting. *Tissue Eng. Part A* **2010**, *16* (8), 2675–2685.

(179) Ouyang, L.; Highley, C. B.; Rodell, C. B.; Sun, W.; Burdick, J. A. 3D Printing of Shear-Thinning Hyaluronic Acid Hydrogels with Secondary Cross-Linking. *ACS Biomater. Sci. Eng.* **2016**, *2* (10), 1743–1751.

(180) Lau, H. K.; Kiick, K. L. Opportunities for Multicomponent Hybrid Hydrogels in Biomedical Applications. *Biomacromolecules* **2015**, *16*, 28–42.

(181) Euliss, L. E.; DuPont, J. A.; Gratton, S.; DeSimone, J. Imparting Size, Shape, and Composition Control of Materials for Nanomedicine. *Chem. Soc. Rev.* **2006**, *35* (11), 1095–1104.

Chapter 3

High-throughput synthesis, analysis, and optimization of injectable hydrogels for protein delivery

Abstract

The development of *in situ*-gelling hydrogels that can enable prolonged protein release is of increasing importance due to the emerging area of protein-based therapeutics. Herein, we describe a high-throughput strategy to fabricate, characterize, and subsequently optimize hydrazone-gelling *in situ*-gelling hydrogels for protein delivery. Hydrogels are fabricated using an automated high-throughput robot to mix a variety of thermoresponsive, non-thermoresponsive, charged, neutral, naturally-sourced, and synthetic polymers functionalized with hydrazide and aldehyde groups, generating *in situ* gelling materials with well-defined compositions within a 96-well plate. High-throughput characterization strategies are subsequently developed to enable in-plate analysis of hydrogel swelling, mechanics, degradation, transparency, and ovalbumin release kinetics that yield results analogous to those collected using traditional bulk hydrogel analysis techniques. Given the rapid turnaround of the protocols developed (i.e. 126 hydrogels can be synthesized and screened in quadruplicate within hours), this approach offers particular promise for accelerating the identification of injectable hydrogel compositions relevant for both protein delivery as well as other biomedical applications for which clearly pre-defined materials properties are required.

Keywords: High throughput, hydrogel, protein release, characterization, thermoresponsive polymers, charged polymers

3.1 Introduction

Hydrogels have attracted significant attention in biomedical engineering based on their widespread applications in drug delivery[1–3], tissue engineering[4,5] wound dressings[6,7], diagnostics[8,9], anti-fouling coatings[10,11], and other applications. In particular, the high water content, controllable internal porosity, and easily tunable chemistry of hydrogels make hydrogels of particular relevance in controlled protein delivery applications[1,12–14] compared to alternative formulations such as polymeric micro/nanoparticles or lipid-based nanoparticles that require the use of organic solvents, high shear, and/or the creation of interfaces (all of which can induce protein denaturation). The high water content of hydrogels can promote the maintenance of the native conformation of the protein to prevent or minimize denaturation, essential to promote therapeutic efficacy while avoiding the potential immune responses associated with denatured proteins. The internal gel porosity, which is typically on the same few nm length scale of most proteins, can also be engineered by manipulating the crosslinker density[15] and/or the structure of the hydrogel building blocks[16,17] to control the diffusion of proteins through the hydrogel network. By engineering the pore size and pore size distribution of a hydrogel, proteins can either be irreversibly entrapped[18,19] or released at a rate proportional to the relative size of the protein and the pore network created.[20] Furthermore, by introducing affinity groups into the hydrogel that can interact with proteins (e.g. charged moieties or hydrophobic domains), the affinity of the protein for the gel phase can be engineered to further tune the release kinetics of the entrapped protein[21,22].

The emergence of *in situ* gelling hydrogels that can spontaneously gel in the body via physical[6,23,24] and/or chemical reactions[25,26] offers further advantages in the context of protein delivery by enabling the facile injection of low-viscosity precursor polymers at the desired site of delivery *in vivo*, avoiding the need for surgical intervention. If the *in situ* chemistry creates a degradable crosslink, further control over protein release kinetics can be achieved based on not only diffusion/affinity but also bulk matrix degradation, in both cases by engineering the gel composition and the crosslinker chemistry.[27–29] Collectively,

these properties have resulted in hydrogels providing demonstrated benefits for longer-term protein delivery *in vivo* for treating a range of diseases such as controlled release of vascular endothelium growth factor (VEGF) or bevacizumab for eye diseases[30,31], stimulus-responsive release of triamcinolone acetonide (TA) induced by an arthritis flare[32], or long-term release of anti-cancer drugs doxorubicin (DOX).[33,34]

In designing hydrogels for protein delivery applications, the choice of the constituent polymer is particularly critical. A range of both natural and synthetic polymers has been explored for this purpose.[28,35] The majority of effort has focused on one of two classes of polymers: (1) naturally-occurring polymers that can be degraded via various oxidative or enzymatic pathways *in vivo* and have an established track record of biocompatibility (e.g. alginate, chitosan, dextran, hyaluronic acid, and various soluble cellulose derivatives)[36,37] or (2) smart materials that can undergo physical changes in swelling upon exposure different environmental stimuli such as temperature, pH, or ionic strength.[38,39] Temperature-responsive smart materials such as poly(N-isopropylacrylamide) (PNIPAM)[40,41] or poly(ethylene oxide)/poly(propylene oxide) block copolymers (Pluronics[42]) have attracted particular interest given their potential to both facilitate *in situ* gelation upon heating from room temperature to physiological temperature as well as deswell in the body to entrap a protein cargo and thus prolong its release. Within this category, poly(oligo ethylene glycol methacrylate) (POEGMA) has more recently been explored as an alternative thermoresponsive polymer that exhibits similar properties to PNIPAM but avoids many of the regulatory issues that have limited the translation of PNIPAM-based materials to the clinic[22,25,43–45]. In addition, the lower critical solution temperature (LCST) of POEGMA-based polymers can easily be tuned from 22°C to >90 °C by changing the length of ethylene oxide (EO) side chain in the monomer.[44–46]

Both naturally-sourced and smart polymers have shown promising results in terms of facilitating prolonged protein release *in vivo*.[32,47,48] However, significant challenges are also inherent in optimizing both these classes of polymers for protein delivery. Naturally-

sourced polymers typically have defined degradation profiles that are hard to engineer and often offer limited potential for functionalization, in such cases restricting the range of gel mechanics and/or crosslinking chemistries accessible.[36] Alternately, smart polymers offer challenges around degradation[49,50] (since the conventional smart polymers are synthetic polymers based on carbon-carbon backbones) as well as avoiding convective burst release of the protein payload often observed as the gel deswells at physiological temperature[51,52], a process which (if it occurs) eliminates many of the benefits of smart hydrogels in the context of prolonging protein release.

Coupling these inherent limitations of conventional hydrogels for protein delivery with the multiple potential variables (e.g. hydrogel crosslink density, degradability, porosity, chemical affinity) that must be optimized for each specific protein to be delivered, the development of hydrogel-based protein delivery vehicles that can facilitate desirable release kinetics remains a challenging and largely trial-and-error process. Indeed, depending on the protein payload being delivered and the desired therapeutic timeline of the targeted therapy, different hydrogel compositions must be designed to suit each particular application. Given the sharply increasing number of protein-based therapeutics now transitioning into the clinic[53] (as enabled by advances in our capacity to engineer and manufacture customized proteins at large scales[54]), developing a rapid method to design a controlled delivery vehicle most suitable to deliver a given protein at the required dose over the required time is increasingly important.

In our previous work, we have extensively explored the use of hydrazide-aldehyde chemistry for creating functional *in situ*-gelling hydrogels based on PNIPAM[40], POEGMA[43], charged POEGMA derivatives[21,55], and natural polymers like carboxymethyl cellulose and dextran[56,57]. Hydrazone chemistry is attractive given its combination of rapid gelation (between seconds to minutes following mixing via co-extrusion through a double barrel syringe) and hydrolytic degradability (weeks to months at neutral pH).[21,43,51] In addition, by mixing different hydrazide and/or aldehyde precursor polymers with different properties (for example, natural degradable polymers and thermoresponsive polymers[50]

and/or thermoresponsive polymers with different phase transition temperatures[51]), we have demonstrated the potential to precisely tune hydrogel properties by simple additive mixing, including the potential to prolong the release of model proteins through the formation of phase-separated domains within hydrogels.[51] This mixing-based approach is attractive in that multiple hydrogels with significantly different properties can be fabricated by mixing a smaller set of precursor polymers in different ratios, reducing the required synthetic burden for hydrogel optimization. However, if a specific set of properties is desired, even this mixing approach becomes largely a trial-and-error process, particularly if the precursor polymers phase separate or interact in some way that makes the overall properties of the resulting hydrogel non-additive (and thus significantly less intuitive) based on the precursor polymer content.

Given the clear potential of precursor polymer mixing to generate hydrogels with targeted properties, applying high-throughput fabrication techniques to produce such hydrogels via automated mixing protocols offers a potential solution to this challenge. Although high-throughput screening techniques have been widely used in the field of drug/or cell-based assays[58,59], few reports have discussed the use of high-throughput robotics to fabricate and optimize hydrogels, likely due to the challenges inherent in characterizing the resulting hydrogel arrays generated. However, if these challenges can be overcome, the high amount of data that can be generated via high-throughput approaches is ideal for not only screening potential compositions directly but also for applying statistical optimization techniques that can fit multivariate mathematical models to the high-throughput experimental data and subsequently predict formulations that would offer better performance in terms of a specific set of property targets.

Herein, we report the development of high-throughput techniques to both fabricate and characterize hydrogel arrays based on the programmable mixing of 14 different polymer precursors (12 functionalized with hydrazide groups and 2 functionalized with aldehyde groups) and assess the potential of the fabricated hydrogels for protein delivery. In particular, precursor polymers with various charges (anionic, cationic, neutral),

degradabilities (i.e. naturally-sourced versus synthetic), and thermoresponsivities (using both PNIPAM and POEGMA with various LCST values) were used to fabricate 126 different hydrogels using a Tecan robot, with the precursor polymers specifically chosen to probe the effect of thermoresponsiveness, charge, and degradability on hydrogel physical and pharmacokinetic properties. We demonstrate the potential of this approach to more rapidly identify hydrogels with targeted properties, here aiming to achieve various combinations of high transparency, slow release kinetics, and high cumulative release percentages most relevant to ophthalmic drug delivery applications.

3.2 Experimental Section

3.2.1 Materials

Oligo (ethylene glycol) methyl ether methacrylate ($OEGMA_{475}$, M_n = 475 g/mol) and di(ethylene glycol) methyl ether methacrylate ($M(EO)_2MA$) were purchased from Sigma-Aldrich and were purified using an aluminum oxide (Sigma-Aldrich, type CG-20) column to remove the methyl ether hydroquinone (MEHQ) and butylated hydroxytoluene (BHT) inhibitors. *N*-(2,2-dimethoxyethyl) methacrylamide (DMEMAm) was synthesized following our previous protocol.[60] Dextran (M_w = 40,000 g/mol), chitosan (low molecular weight, CAS 9012-76-4), sodium carboxymethyl cellulose (CMC, M_w = 90,000 g/mol, DS = 0.9), N,N-dimethylaminoethyl methacrylate (DMAEMA), *N*-isopropylacrylamide (NIPAM, 99%), acrylic acid (AA, 99%), thioglycolic acid (TGA, 98%), N-hydroxysuccinimide (NHS, 97%), and monochloroacetic acid (MACC) were purchased from Sigma-Aldrich and used as received. Adipic acid dihydrazide (ADH, Alfa Aesar, 98%), *N'*-ethyl-*N*-(3-dimethylaminopropyl)-carbodiimide (EDC, Carbosynth, Compton CA, commercial grade), 2,2-azobisisobutryic acid dimethyl ester (AIBMe, Wako Chemicals, 98.5%) and dioxane (Caledon Labs, 99%) were used as received. Sodium hydroxide (NaOH) and hydrogen chloride (HCl) was purchased from LabChem Inc. and used as received. NIH 3T3 mouse fibroblast cells were purchased from ATCC (Cedarlane Laboratories, Burlington, ON, Canada). Dulbecco's Modified Eagle's Medium (DMEM,

Life Technologies), fetal bovine serum (FBS, ThermoFisher), penicillin-streptomycin (PS, ThermoFisher), PrestoBlue cell viability reagent (ThermoFisher), a Bradford reagent kit (Sigma-Aldrich) and albumin from chicken egg white (ovalbumin, Sigma Aldrich) were used as received. 10 mM PBS (pH 7.4) prepared with Milli-Q grade distilled deionized water (DIW) was used for all experiments.

3.2.2 Synthesis and characterization of polymer precursors

Chemical characterization. ^{1}H-NMR was performed using a Bruker 600 MHz spectrometer using deuterated chloroform as the solvent. The carboxylic acid content of relevant polymer precursors was determined by base-into-acid titration (ManTech Associates) using 100 mM NaOH as the base. The lower critical solution temperatures (LCST) of the polymer precursors were determined in a 10 mg/mL solution of polymer in 10 mM PBS using a Variant Cary Bio 100 UV-vis spectrophotometer ramped over a temperature range of 20-80 °C at a rate of 0.5 °C/min.

Hydrazide-functionalized POEGMA. The synthetic recipes and resulting chemical properties of POEGMA hydrazide precursor polymers produced are shown in Table 3.1. All hydrazide functionalized POEGMA polymers were synthesized following recipes previously reported.[61] In brief, diethylene glycol methacrylate ($M(EO)_2MA$, n=2), oligo ethylene glycol methacrylate ($OEGMA_{475}$, n=8,9), acrylic acid (AA), 2,2-azobisisobutryic acid dimethyl ester (AIBMe), thioglycolic acid (TGA) and 20 mL dioxane were added to a 50 mL Schlenk three-neck flask and were purged with nitrogen for 30 minutes before placed into a 75 °C oil bath. The polymerization was completed in 4 hours under magnetic stirring to obtain poly(OEGMA-co-AA) copolymer following by rotary evaporation to remove dioxane. Subsequently, poly(OEGMA-co-AA) was re-dissolved in 100 mL DIW and the acrylic acid residues were functionalized with hydrazide groups by grafting a 5-fold excess of adipic acid dihydrazide using a 2.5-fold molar excess of EDC at pH =4.75. The resulting POEGMA precursor polymers are coded as PO_xH_y, where x represents the mole percentage of $OEGMA_{475}$ relative to the sum of the $OEGMA_{475}$ (long chain, high

transition temperature) and $M(EO)_2MA$ (short chain, low transition temperature) OEGMA monomers and y is overall mol% of monomer residues bearing hydrazide groups. By changing the ratio of $OEGMA_{475}$: $M(EO)_2MA$, the LCST of POEGMA precursors was adjusted from low (PO_0H_{30} and $PO_{10}H_{30}$) to medium ($PO_{50}H_{30}$) to high ($PO_{100}H_{30}$).[46,51] The hydrazide content was determined by the difference in the titrated -COOH content of the polymers before and after ADH functionalization. The charged POEGMA precursors $PO_{100}H_{30}$-cationic and $PO_{100}H_{30}$-anionic were synthesized using the same protocols but adding 20 mol% of N,N-dimethylaminoethyl methacrylate (cationic) and acrylic acid (anionic) (Table 3.1), respectively. [21,55] All precursors were dialyzed for purification (6+ hours for 6 cycles, using dialysis tubing with molecular weight cut-off of 3.5 kDa), lyophilized, and stored in a 15 wt% solution of 10 mM PBS at 4 °C.

Hydrazide-functionalized PNIPAM (PNIPAM-Hzd). PNIPAM-Hzd precursor was synthesized following previous work.[40,62] In brief, 4.00 g of NIPAM, 1.00 g of acrylic acid, 87 μL of TGA (chain transfer agent) and 55.5 mg of AIBMe (initiator) were dissolved in 20 mL of ethanol and polymerized overnight at 56 °C under nitrogen. The solution was then lyophilized, re-dissolved in DIW, and functionalized with hydrazide groups using ADH/EDC chemistry as described for the POEGMA precursors. The resulting PNIPAM-Hzd polymer was then dialyzed (6+ hours for 6 cycles, using dialysis tubing with molecular weight cut-off (MWCO) of 3.5 kDa) and lyophilized for storage. The hydrazide content was determined by the difference in the titrated -COOH content of the polymers before and after ADH functionalization.

Hydrazide-functionalized dextran (Dextran-Hzd). Hydrazide-functionalized dextran was prepared following previous work.[14,63,64] 5 g of dextran from Leuconstroc spp (Sigma-Aldrich, M_r = 500 000) was dissolved in 42 mL of a 3 M solution of NaOH, after which 7.29 g of chloroacetic acid was added and stirred at room temperature until dissolution. Subsequently, the solution was heated to 70 °C for 90 minutes, cooled back to room temperature, and neutralized to pH 7.0 by adding glacial acetic acid. The product was

precipitated with methanol and collected through vacuum filtration to acquire a crude product that was subsequently stirred in acetone overnight to fully precipitate. Subsequently, the resulting product was washed with acetone and dried in an oven at 60 °C to obtain a white carboxymethylated dextran product. This product was then functionalized with hydrazide groups by adding a 2.5-fold molar excess of EDC and 5-fold molar excess of ADH to an aqueous solution of carboxymethylated dextran and maintaining the pH at 4.75 for at least four hours or until no further pH change is observed. The final product was obtained by dialysis (6+ hours for 6 cycles, MWCO of 12 kDa) and lyophilized for storage. The hydrazide content was determined by the difference in the titrated -COOH content between the carboxymethylated dextrans before and after ADH functionalization.

Hydrazide-functionalized chitosan (Chitosan-Hzd). Chitosan-Hzd was prepared following previously reported protocols.[65,66] 1 g of chitosan was gradually added to a solution of sodium 1 M NaOH in 2 mL of DIW under magnetic stirring, allowing the chitosan granules to swell. 8 mL of 2-propanol was then added, and the mixture was kept stirring for one hour. Subsequently, 1.75 g of monochloroacetic acid pre-dissolved in 2 mL of isopropanol was added and reacted for 4 hours, after which the reaction was stopped by adding 50 mL of 70% ethanol. The resulting carboxymethylated chitosan was then purified by dialysis (6+ hours for 6 cycles, MWCO = 12 kDa) and functionalized with hydrazide groups using the same EDC/ADH chemistry outlined for dextran. The final product was dialyzed and lyophilized for storage. The hydrazide content was determined by the difference in the titrated -COOH content between the carboxymethylated chitosan before and after ADH functionalization.

Hydrazide-functionalized sodium carboxymethyl cellulose (CMC-Hzd). Synthesis of CMC-Hzd followed protocols reported in previous work.[64] 1.0 g CMC and 3 g ADH were dissolved in 200 mL DIW. Following, pre-made solutions of 0.07 g NHS (suspended in 4 mL of a 1:1 DMSO/H_2O solution) and 0.3 g EDC (dissolved in 1 mL of a 1:1 DMSO/H_2O solution) were added to the flask sequentially. The pH of CMC solution was adjusted to pH 6.8 using 0.1 M NaOH or HCl until it no longer changed (~4 hours). The resulting

hydrazide-functionalized polymer was dialyzed dialysis (6+ hours for 6 cycles, MWCO = 12 kDa) and lyophilized for storage. The hydrazide content was determined by the difference in the titrated -COOH content before and after ADH functionalization.

Aldehyde-functionalized POEGMA polymer precursors. Aldehyde-functionalized POEGMA precursors were synthesized as previously described.[25,60] Briefly, diethylene glycol methacrylate ($M(EO)_2MA$, n=2), oligo ethylene glycol methacrylate ($OEGMA_{475}$, n=8,9), *N*-(2,2-dimethoxyethyl) methacrylamide (DMEMAm), AIBMe initiator, and TGA chain transfer agent were dissolved in 20 mL dioxane and reacted for 4 hours at 75 °C under nitrogen. The resulting poly(OEGMA-co-DMEMAm) polymer precursors were subsequently dissolved in 75 mL DIW, to which 25 mL of 1.0 M HCl was added and allowed to reacted at room temperature for 24 hours to convert the acetal groups in the DMEMAm residues to aldehyde groups. The aldehyde polymers are coded as PO_xA_y, where x represents the $OEGMA_{475}/M(EO)_2MA$ ratio (as with the hydrazide polymers) and y represents the overall mole fraction of monomers bearing an aldehyde group (Table 1). The resulting precursors were dialyzed (6+ hours for 6 cycles, MWCO = 3.5 kDa) , lyophilized, and stored in 15 wt% solutions in 10 mM PBS at 4 °C. The aldehyde content of the polymers was determined by ^1H NMR in deuterated DMSO by comparing the integration of the aldehyde proton (ppm ~ 9) with that of the methoxy proton (ppm ~ 3.5).

Table 3.1 Synthetic recipes for POEGMA polymer precursors

	$OEGMA_{475}$ [g]	$M(EO)_2MA$ [g]	AA [g]	DMEMAm [g]	TGA [μL]	AIBMe [mg]	DMAEMA [g]
PO_0H_{30}	0.0	4.0	0.65	-	7.5	37	-
$PO_{10}H_{30}$	0.9	3.1	0.55	-	7.5	37	-
$PO_{50}H_{30}$	2.9	1.1	0.35	-	7.5	37	-
$PO_{100}H_{30}$	4.0	0.0	0.25	-	1.0	37	-
$PO_{100}H_{30}C_{20}$	4.0	0.0	0.35	-	1.0	37	0.55
$PO_{100}H_{30}A_{20}$	4.0	0.0	0.65	-	1.0	37	-
$PO_{10}A_{30}$	0.9	3.1	-	1.3	7.5	50	-
$PO_{100}A_{30}$	4.0	0.0	-	0.6	1.0	50	-

Table 3.2 Chemical characterization of polymer precursors

Category	Polymers	Functional group	Charge	LCST °C	Concentration mg/ml
Thermoresponsive vs. non-thermoresponsive precursors	PO_0H_{30}	$NHNH_2$	neutral	36.6	150
	$PO_{10}H_{30}$	$NHNH_2$	neutral	52.6	150
	$PO_{50}H_{30}$	$NHNH_2$	neutral	>80	150
	$PO_{100}H_{30}$	$NHNH_2$	neutral	>80	150
	PNIPAM-Hzd	$NHNH_2$	neutral	32.0	60
	CMC_{40}-Hzd	$NHNH_2$	neutral	>80	40
	$PO_{10}A_{30}$	CHO	neutral	44.5	150
Charged vs. neutral precursors	$PO_{100}H_{30}$	$NHNH_2$	neutral	>80	150
	$PO_{100}H_{30}C_{20}$	$NHNH_2$	cationic	>80	150
	$PO_{100}H_{30}A_{20}$	$NHNH_2$	anionic	>80	150
	CMC_{20}-Hzd	$NHNH_2$	neutral	>80	20
	Dextran-Hzd	$NHNH_2$	anionic	>80	15
	Chitosan-Hzd	$NHNH_2$	cationic	>80	20
	$PO_{100}A_{30}$	CHO	neutral	>80	150

3.2.3 Hydrogel preparations

Hydrogels were prepared using an automated materials screening high-throughput robotics system (Tecan Evo 200). Eight available robotic arms were used to aspirate pre-programmed volumes of each hydrazide precursor polymer (initially loaded into different columns of a 24-well plate) into different wells of a 96 well-plate (Greiner, VWR) using a factorial design strategy, in which each possible equal volume combination of the six hydrazide precursor polymers within each polymer series (Table 3.2) was pipetted sequentially into each well (Figure 3.1; see Tables S3.1 and S3.2 for detailed recipes of which polymers were dispensed into each well). The pipetting parameters must be optimized for different range of liquid types. After dispensing all the hydrazide precursor polymers, the plate was automatically moved to a vibrating shaker operating at 500 rpm for 5 minutes to ensure uniform mixing of all added hydrazide components. The plate was then moved back to the pipetting platform and the relevant aldehyde precursor polymer was added column by column to the plate, with the plate moved to the same vibrating shaker immediately after each column of aldehyde polymer was added to ensure complete mixing of the added aldehyde and all the component hydrazide polymers prior to gelation. To avoid bubbles when adding aldehyde polymer precursors, 65 μL of POA was aspirated but only 60 μL was dispensed into each well and the pipette tips were immersed directly in the hydrazide precursor solutions during dispensing, the latter of which also promotes efficient mixing of the reactive precursor polymers.

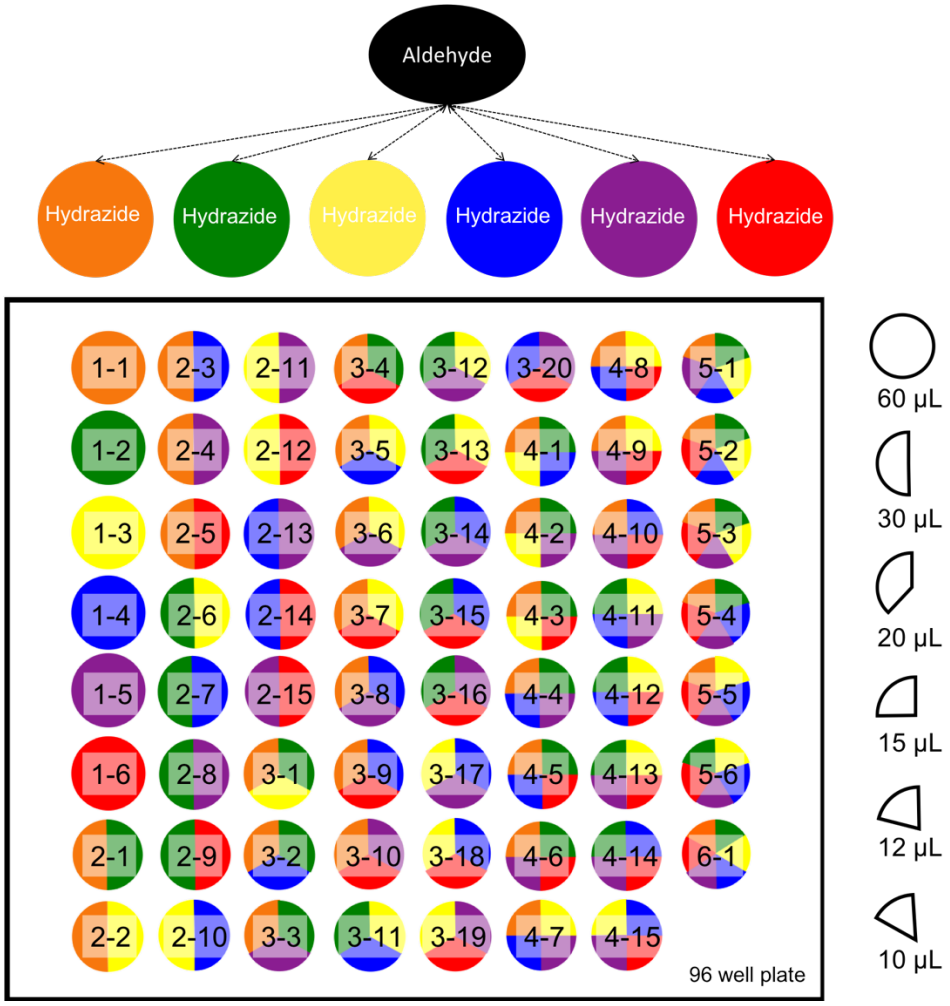

Figure 3.1 Schematic of compositions of hydrazide polymer precursors in 96-well plate. The number codes in each well correspond to the m-n sample names assigned throughout the paper, where m is the number of different hydrazide components mixed together and n is the number corresponding to each mixture type.

3.2.4 High-throughput hydrogel characterization

Hydrogel swelling. 120 µL of 10 mM PBS was added to each well containing hydrogel and incubated for 48 h at 22 °C, a time confirmed to achieve equilibrium swelling in previous experiments[21,43] and a temperature below the LCST values of each precursor polymer used. The "find contact" function of a Mach-1 micromechanical tester fitted with a 1 mm diameter rounded tip indenter and a multiwell plate attachment (Biomomentum, Laval, Canada) was used to track the change in the height of hydrogel in each well before

and after swelling, with the swelling ratio of the hydrogel subsequently calculated based on the measured height change as per Equation (1), normalizing the measured height at gel contact following swelling to the pre-measured height at gel contact prior to the swelling measurement.

$$\text{Normalized volume} = \frac{V_{final}}{V_{initial}} = \frac{A \times H_{gel}}{120\mu L} \qquad (1)$$

V_{final} and $V_{initial}$ are the volumes of gel before and after swelling respectively, A is the cross-sectional area of each well in 96 well-plate (0.34 cm^2), and H_{gel} is the height of gel (relative to the height of the same gel prior to swelling as the z=0 point) as measured by the Mach-1 tester. Error bars represent the standard deviation of four independent measurements (n=4).

Hydrogel mechanics. The compressive modulus of the hydrogels was measured inside the 96-well plates using a 1 mm diameter rounded tip indenter and the Mach-1 micromechanical tester with a multiwell plate attachment. The modulus was measured by first finding the contact in each well and subsequently performing a 10% compression relative to the pre-measured height of an empty well, with the modulus corresponding to the slope of the resulting stress versus strain curve. Error bars represent the standard deviation of four independent measurements (n=4).

Hydrogel degradation. Hydrogel degradation was determined by tracking the change in the compressive modulus of the hydrogels in acid-accelerated conditions that allow for comparisons to be made between the degradation rates of different hydrogels under practical-to-measure timeframes. Following an equilibrium swelling step (120 µL PBS/well, 22 °C, 72 h), the PBS was removed, and a compressive modulus measurement was done in each well using the Mach-1 micromechanical tester as described above. Subsequently, 100 mM HCl was added to each well and the compressive modulus measurement was repeated at predetermined time intervals until complete gel degradation

was visually observed or until the modulus of the residual hydrogel was below the detection threshold of the find contact measurement (normal force normal force <0.005 N). Error bars represent the standard deviation of four independent measurements (n=4).

Transparency. The transmittance of each hydrogel was determined using a VICTOR 3 multilabel microplate reader operating at a wavelength of 595 nm. The transmittance was scanned over a temperature range of 25°C to 40 °C. Error bars represent the standard deviation of four independent measurements (n=4).

Drug release kinetics. Hydrogels were prepared as described above using the high-throughput robotics system but dissolving 5 mg/mL ovalbumin in each POA precursor polymer, ensuring that the same concentration of ovalbumin was added to each well without requiring an additional pipetting step. For drug release experiment, hydrogels were first fabricated inside a 96-well MultiScreen-Mesh filter plate instead of the conventional hard-bottom 96 well plate used for the other assays. The hydrogel-filled filter plates were then submerged into a 96-well receiver (see Supporting Information Figure S3.1). 100 μL PBS was added on the top of each hydrogel as well as in the corresponding receiving well, allowing for full wetting of the hydrogel sample above and below the gel samples. The samples were incubated at 37 °C for pre-determined time intervals. At each sampling time over the one month experimental period, 20 μL of medium was removed from the receiving chamber and assayed for protein concentration using a Bradford assay, with the concentration calculated based on a calibration of standard ovalbumin concentrations (R^2 =0.99). The removed volume was replaced with fresh PBS and the plate was returned to the incubator until the next sampling point. Error bars represent the standard deviation of four independent measurements (n=4).

3. 3 Results and Discussion

3.3.1 Synthesis of hydrogel precursors

Six hydrazide-functionalized hydrogel precursor polymers were synthesized for each series of materials studied (i.e. thermoresponsive vs. non-thermoresponsive and charged vs. neutral). This number was chosen given that all possible combinations of each of the six precursor polymers in each series could be prepared in a single 96-well plate (63 total hydrogels/series), facilitating high-throughput characterization of hydrogel swelling, degradation, transparency, and drug release kinetics for each hydrogel series. The two series of polymers were selected based on the integral roles of both hydrogel porosity (regulated by the water affinity and, by extension, thermoresponsiveness) and protein-hydrogel interactions (regulated by both the hydrophobicity of the phase transition and charge) on controlling protein release kinetics from hydrogels.

All synthetic polymers (POEGMA, PNIPAM) were synthesized via free radical copolymerization using a chain transfer agent to limit the molecular weight of polymers. The measured number average molecular weight (M_n) of both hydrazide and aldehyde-functionalized POEGMA or PNIPAM polymers was measured to lie between 16-22 $\times 10^3$ g/mol, below the M_n ~40×10^3 g/mol associated with *in vivo* renal clearance (Table 3.2).[50,67] Similarly, the degree of hydrazide or aldehyde functionalization between the different POEGMA precursor polymers is similar, such that the degree of crosslinking is likely to be similar between different mixed combinations. However, it must be emphasized that such functional equivalence is not required for the high throughput assay to meet our aims of optimizing hydrogel properties based on a given set of starting materials. The lower critical solution temperatures of the PO_x POEGMA-based hydrazide-functionalized precursor polymers varied between ~37 °C for PO_0H_{30} to >80°C for $PO_{50}H_{30}$ and $PO_{100}H_{30,}$ consistent with our previous reports.[51,67] Note that the resulting VPTT of the single-component hydrogels was significantly lower than the precursor LCST due to the consumption of the more polar hydrazide and aldehyde groups upon hydrazone bond formation, resulting in hydrogel VPTT values ranging from ~26 °C for PO_0 (collapsed at 37 °C), ~32-33 °C for

PO_{10} (partially collapsed at 37 °C), >80 °C for PO_{50} (swollen at 37 °C) and >80 °C for PO_{100} (swollen at 37 °C)[51,67]; this range allows us to explore the full effect of the phase transition temperature on drug release kinetics under physiological conditions. CMC-Hzd was included in the thermoresponsive series as a non-thermoresponsive carbohydrate component for comparison with the high transition temperature PO_{50} and PO_{100} components to assess how using a temperature-independent but more highly viscous precursor component would affect the protein release properties.

Charge was introduced into the precursor polymers by (1) copolymerizing the cationic comonomer DMAEMA (cationic, $PO_{100}H_{30}C_{20}$) or the anionic comonomer AA (anionic, $PO_{100}H_{30}A_{20}$) to form 20 mol% charged comonomer POEGMA-based synthetic copolymers or (2) selecting natively cationic (chitosan) or anionic (carboxymethyl cellulose) naturally-sourced polymers. In this manner, different cationic, anionic and amphoteric hydrogels with different charge contents can be prepared by mixing different combinations of cationic, anionic, and neutral PO_{100}-based hydrazide precursors together with the non-thermoresponsive neutral aldehyde polymer $PO_{100}A_{30}$.

The concentrations of each polymer used were selected based on (1) the viscosity of the precursor polymers (ensuring that robotic pipetting is feasible), (2) the concentration at which the single component hydrazide and aldehyde gelling pair gels within < 5 minutes for thermoresponsive series and ~ 30-40 minutes for charge series (ensuring that mixing is possible prior to gelation), and (3) published recipes of single component hydrazide and aldehyde gelling pairs that have been demonstrated to yield mechanically robust hydrogels with relevant biomedical properties.[14,40,55,57,61,64,67] As such, while the mass concentration and/or functional group density of polymer in each combination gel does not necessarily match, the resulting hydrogels all have similar gelation times and compressive moduli on the same order of magnitude (tens of kPa, Supporting Figure S3.2)

Cytotoxicity measurements using the Presto Blue assay in conjunction with NIH 3T3 mouse fibroblast cells indicated that high cell viability was maintained after 24 hours of incubation with each hydrogel precursor at concentrations of at least 2 mg/mL, a relatively high concentration for *in vitro* cytotoxicity screening (Supporting Information, Figure S3.3). As such, coupled with the degradability of the hydrogel networks (enabled by the presence of the naturally-sourced polymers and/or the hydrolytically labile hydrazone crosslinks), both sets of combinatorial hydrogels tested have potential for *in vivo* use.

3.3.2 Preparation of multi-component hydrogels using high throughput robotics

Multi-component hydrogels were prepared using a Tecan Evo 200 robot to mix pre-formed solutions of hydrogel precursor solutions in 10 mM PBS at pre-programmed ratios, as shown visually in Figure 3.1. Two categories of materials were separately assayed: thermoresponsive vs. non-thermoresponsive hydrogels (T) and charged vs. neutral hydrogels (C). Each possible combination of the six hydrazide precursor polymers in each set was pipetted by the robot into separate wells of a 96-well plate according to combinatorial theory (Equation 2).

$$C_6^1 + C_6^2 + C_6^3 + C_6^4 + C_6^5 + C_6^6 = 63. \qquad (2)$$

For example, C_6^2 refers to gels formed from each possible combination of two premixed hydrazide polymers crosslinked with one aldehyde polymer (15 combinations total). A total of 60 μL of hydrazide precursor polymer is dispensed into each well for each combination tested, resulting in 30 μL of each precursor polymer if two precursor polymers were dispensed, 20 μL of each precursor polymer if three precursor polymers were dispensed, etc.; this facilitates the preparation of the precursor polymer combinations listed above without changing the total gel volume. The result of this protocol was that 126 different hydrogels could be fabricated in just ~25 minutes, enabling the rapid preparation of multiple types of *in situ*-gelling hydrogels through a fully automated method. Note that all tested compositions gelled within 5-20 minutes following addition of the aldehyde

polymer, enabling mixing of all added components prior to gelation and consistent with bulk hydrogel data associated with each polymer precursor and precursor solution concentration chosen for the screen.

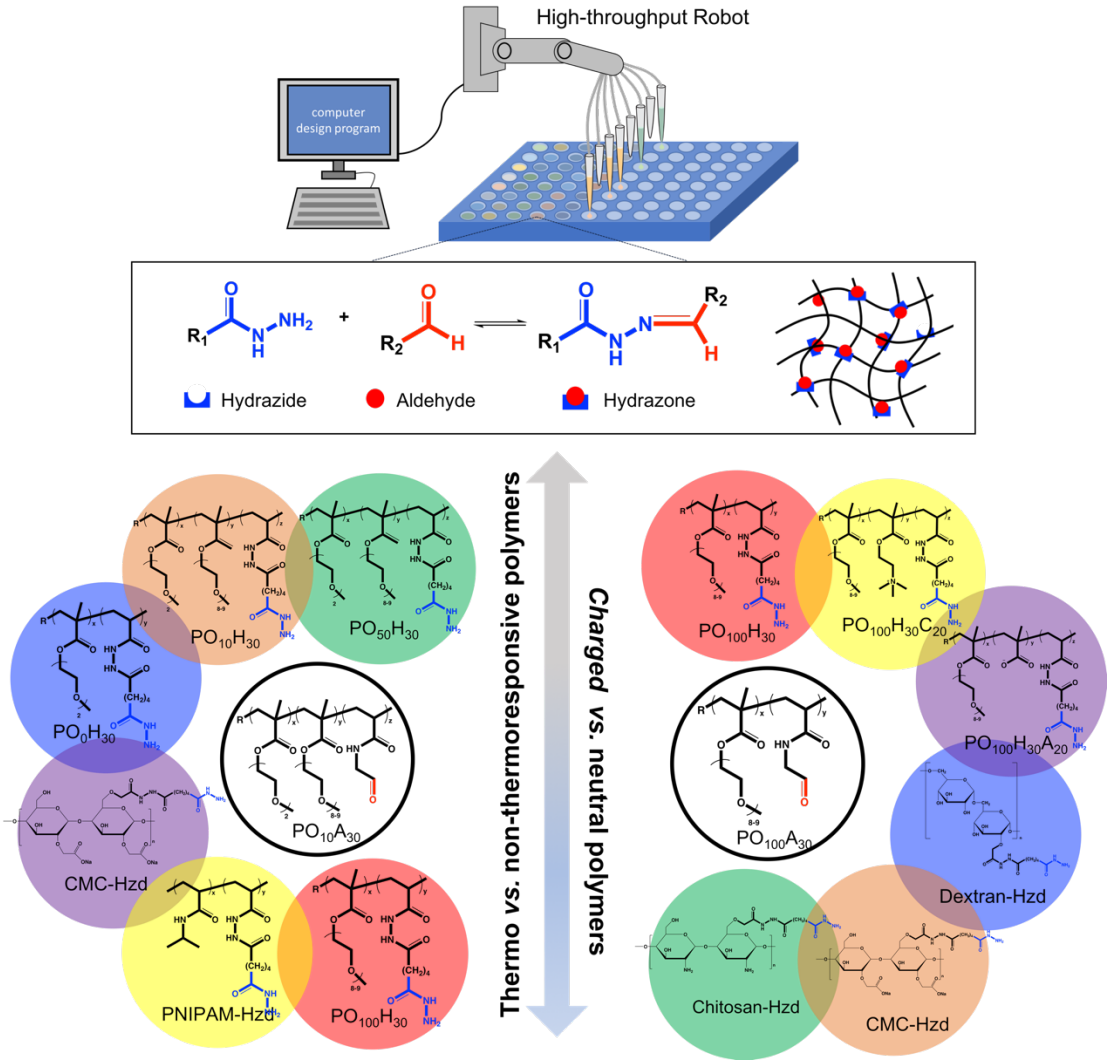

Figure 3.2 Schematic of the high-throughput robotics-based fabrication approach for preparing mixing-induced *in situ*-gelling hydrogels and the structures of the hydrazide and aldehyde-functionalized polymer precursors used for the preparation of each hydrogel series

3.3.3 Physiochemical properties of combinatorial hydrogels

To address the key challenge of high-throughput materials screening (i.e. the characterization of the properties of the fabricated materials), we developed a series of analytical techniques for assessing the properties of hydrogels particularly relevant for biomedical applications (mechanics, swelling, degradation, and transparency) that could be performed reliably at reasonably high speeds (<2 hour per plate of 63 hydrogels) in an automated fashion without requiring removal of the hydrogels from the wells. Mechanics, swelling, and degradation measurements were all performed using a Mach-1 micromechanical tester fitted with a multiwell plate adapter that allows the instrument to individually address each well of a 96-well plate.

Swelling. Hydrogel swelling was measured by comparing the point at which the microindenter contacted the hydrogel interface (i.e. normal force >0.0051 N) before and after equilibrium swelling over 48 hours in 10 mM PBS at 22 °C, with the temperature chosen to minimize the effect of the phase transition of thermoresponsive hydrogels on the measured swelling results. Note that the normal force threshold allows the indenter to freely penetrate through PBS without detecting an interface, enabling swelling measurements *in situ* without the removal of the PBS swelling solvent. Figure 3 shows the swelling responses of single-component hydrogels in each series, while Supporting Information Fig. S3.4 (thermoresponsive series) and Fig. S3.5 (charged series) show the results for each combinatorial hydrogel fabricated. As anticipated, both PO_0H and PNIPAM-Hzd single component hydrogels de-swelled over the test period, yielding equilibrium swelling ratios of 0.91 ± 0.09 (PO_0H) and 0.82 ± 0.11 (PNIPAM) respectively relative to their initial volume. This result is consistent with previous results on bulk hydrogels tested using conventional swelling protocols[67], confirming the efficacy of the high-throughput swelling measurement protocol. Similarly, mixing PO_0H or PNIPAM-Hzd with any of $PO_{10}H$, $PO_{50}H$, $PO_{100}H$ or CMC-Hzd resulted in hydrogels with significantly suppressed swelling over the 48 hour incubation period for any binary or ternary combination tested (Supporting Information Fig. S3.4 A, B). Of particular note,

the binary combination of PO_0H + CMC-Hzd (T2-12) deswelled more than PO_0H single component gel (deswelling ratio = 0.70 ± 0.06) despite the fact that CMC-Hzd single component gels swell over the same time period (Fig. 3.3A); furthermore, the ternary combination of $PO_{10}H_{30}$ + $PO_{100}H_{30}$ + PNIPAM-Hzd (T3-3) exhibited a similarly significant deswelling ratio (0.70 ± 0.07) despite the presence of just one precursor polymer (PNIPAM-Hzd) that deswelled in its single component gel (Fig. 3.3A). In contrast, each five-component hydrogel in which PO_0H and PNIPAM-Hzd represent two of the five components (i.e. comprise 40% of the total volume and >50% of the total polymer mass, Supporting Information Fig. S3.4D) exhibited substantial swelling upon incubation in PBS. We attribute these anomalous swelling responses to probable phase separation between the different precursor polymers upon mixing, leading to potential non-linear responses in hydrogel swelling upon gelation.

Swelling ratios for the charged hydrogel series also showed non-linear effects, although the general trends were more consistent with predictions from single component gels. Comparing Figs. 3.3A and 3.3B, the swelling ratios in Fig. 3.3B were typically higher, consistent with the higher hydrophilicity of the crosslinking polymer ($PO_{100}A$ compared to $PO_{10}A$) as well as the charged nature of many of the hydrazide precursor polymers; indeed, all gels tested swelled within the 48 h test period due to the lack of a thermoresponsive component in these hydrogels. Combinations of two, five, or six precursor polymers (Supporting Information Fig. S3.5A, D) all resulted in hydrogels with generally similar swelling ratios to the single component hydrogels; in contrast, multiple combinations of three or four precursor polymers (Supporting Information Fig. S3.5B, C) resulted in hydrogels with significantly higher swelling ratios. Of particular note, the amphoteric hydrogel combinations of $PO_{100}H_{30}A_{20}$ + Dextran-Hzd + Chitosan-Hzd (C3-19) and $PO_{100}H_{30}A_{20}$ + CMC-Hzd + Dextran-Hzd + Chitosan-Hzd (C4-15) showed swelling ratios particularly higher than those achieved with the single component hydrogels alone (1.9 ± 0.4 and 2.2 ± 0.1 respectively). As such, combinatorial mixing can access a broader potential range of hydrogel swelling responses than possible with the single-component

hydrogels, suggesting the potential utility of this mixing approach to generate new and/or optimized protein release kinetics.

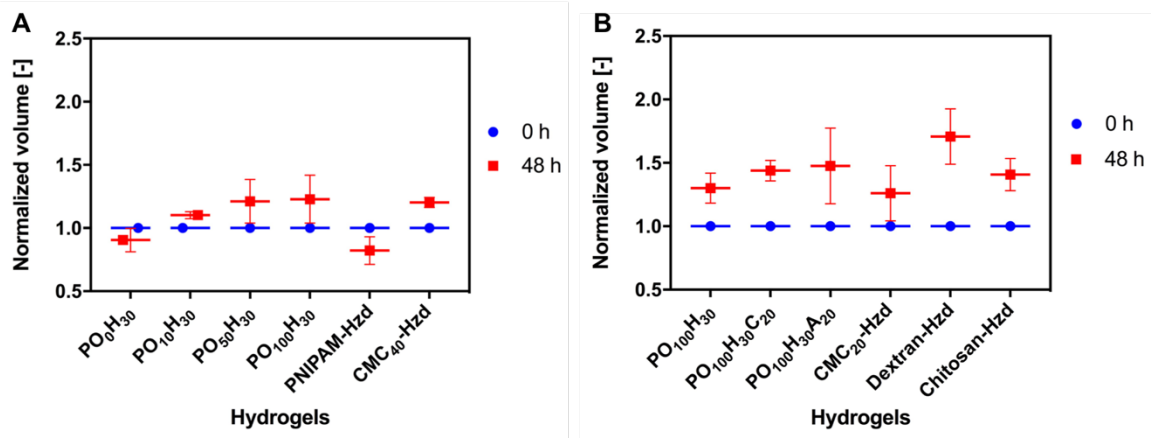

Figure 3.3 Volume-based swelling ratios of (A) thermoresponsive vs. non-thermoresponsive (T series) single-component hydrogels and (B) charged vs. neutral (C series) single-component hydrogels before and after swelling for 48 hours in 10 mM PBS at room temperature (22 °C) (n=4). See Supporting Figures S1-S2 for the corresponding results for the combinatorial hydrogels.

Mechanics. A simple 10% compression protocol from the point of contact was used in combination with the high throughput testing accessory of the Mach-1 micromechanical tester to measure the compressive modulus following the incubation of the hydrogels in 10 mM PBS at room temperature (22 °C) for 72 h, with the pre-swelling step performed to ensure all gels reach equilibrium swelling prior to measurement. The compressive modulus of POEGMA hydrogels decreased from PO_0 (59 ± 34 kPa) to PO_{100} (33 ± 5 kPa) (Figure 3.4A, time t = 0 h) , consistent with previous observations on bulk gels as the proportion of the long-chain $OEGMA_{475}$ monomer is reduced[67]. Furthermore, charged hydrogels prepared with POEGMA-based precursor polymers exhibited substantially higher moduli than those prepared based on naturally-sourced precursors (Figure 3.4B, time t = 0 h), again consistent with our previous reports.[50]

Mixing different precursor polymers again demonstrates non-linear effects (Supporting Information, Figures S3.6 and S3.7). For example, among the binary thermoresponsive

combinations (Fig. S3.6A), the combination of PO_0H_{30} + $PO_{50}H_{30}$ (T2-10, in which one component is thermoresponsive and the other is not at physiological temperature) exhibited a compressive modulus of 89 ± 21 kPa, equivalent to a PO_0H_{30} single-component gel and substantially higher than a $PO_{50}H_{30}$ single-component gel; in contrast, the combination of PO_0H_{30} + $PO_{10}H_{30}$ (T2-2, in which both components are thermoresponsive but to different degrees at physiological temperature) resulted in a hydrogel with a compressive modulus of 15 ± 7 kPa, substantially weaker than either single-component gel. We hypothesize this difference is again related to differences in phase separation, with the double thermoresponsive binary gel (T2-2) more likely to generate bulk phase-segregated domains with potentially weaker crosslinking between the phases while the single thermoresponsive component binary gel (T2-10) is more likely to form a continuous non-responsive phase with collapsed thermoresponsive domains that may serve to mechanically reinforce the bulk hydrogel. Such differences are suppressed as more components are added to the gels and the probability of some form of macroscopic phase separation is increased, with all of the five and six-component hydrogels exhibiting similar moduli within experimental error. Similar general trends are observed with the charged precursor data (Fig. S3.7); binary and ternary combinations (Figs. S3.7A and S3.7B) exhibit substantially higher variability in modulus values than the five and six-component mixtures (Fig. S3.7D). Amphoteric hydrogels such as $PO_{100}H_{30}$ + $PO_{100}H_{30}C_{20}$ + $PO_{100}H_{30}A_{20}$ (C3-1) exhibited particularly high moduli consistent with the demonstrated high capacity of amphoteric hydrogels for retaining water in the presence of salt (i.e. PBS) and/or facilitating dual ionic/covalent crosslinking at physiological pH[55].

Degradation. Degradation kinetics were assessed by tracking the decrease in the compressive modulus of the hydrogels over time upon exposure to acidic degradation conditions (0.1 M HCl, 22 °C). Note that these conditions were chosen to accelerate the degradation of the hydrazone bond to enable comparisons between the degradation potential of various hydrogel compositions on a shorter time scale. Upon exposure to 0.1 M HCl, the compressive modulus of most hydrogels decreased to ~ 50 % or less of their initial modulus within two hours (comparing t = 0 h and 2 h in Figs. 3.5A and 3.6B), with

the modulus of most of the single-component charged series hydrogels (C series) decreasing to nearly zero by 24 h indicative of complete gel degradation. In contrast, thermoresponsive hydrogels based on POEGMA or, in particular, PNIPAM (which deswells the most relative to its preparation state at room temperature, Fig. 3.3A) retained at least ~20-50 % of their initial modulus after 24 hours and persisted for at least 72 hours in the presence of 0.1 M HCl. This notably slow degradation of the PNIPAM-Hzd-based hydrogel is consistent with previous observations[40,50]. The general trends in degradation times also conform to theory in that reducing the water content of the hydrogel increases the resistance of the hydrogel to hydrolytic degradation; introducing charge promotes swelling (and thus faster degradation, Fig. 3.4B) while introducing thermoresponsive components suppresses swelling (Fig. 3.3A) and thus also degradation. As such, the accuracy of the high-throughput measurement protocol used for probing degradation rates is supported by fundamental expectations.

Synergistic effects are again observed in the combinatorial hydrogels, particularly in the thermoresponsive binary and ternary mixture hydrogels (Figs. S3.6A and S3.6B). Of particular note, PO_0H_{30} + PNIPAM-Hzd (T2-11) and $PO_{10}H_{30}$ + PO_0H_{30} + PNIPAM-Hzd (T3-6), both of which contain mixtures of only thermoresponsive polymers, exhibit notably higher retained moduli after 72 hours of acid exposure compared to either single component hydrogel, with no significant change observed in the compressive modulus of both hydrogels over this time period. Combining the naturally-sourced non-thermoresponsive (but more viscous) CMC component with the PO_0H_{30}/NIPAM-Hzd combination (T3-19) similarly suppresses degradation over the 72 hour test period. While the results are less dramatic with the charged series, more neutral binary and ternary combinations such as $PO_{100}H_{30}$ + Dextran-Hzd (C2-4) or $PO_{100}H_{30}$ + $PO_{100}H_{30}$-cat + Dextran-Hzd (C3-3) also show somewhat reduced degradation rates.

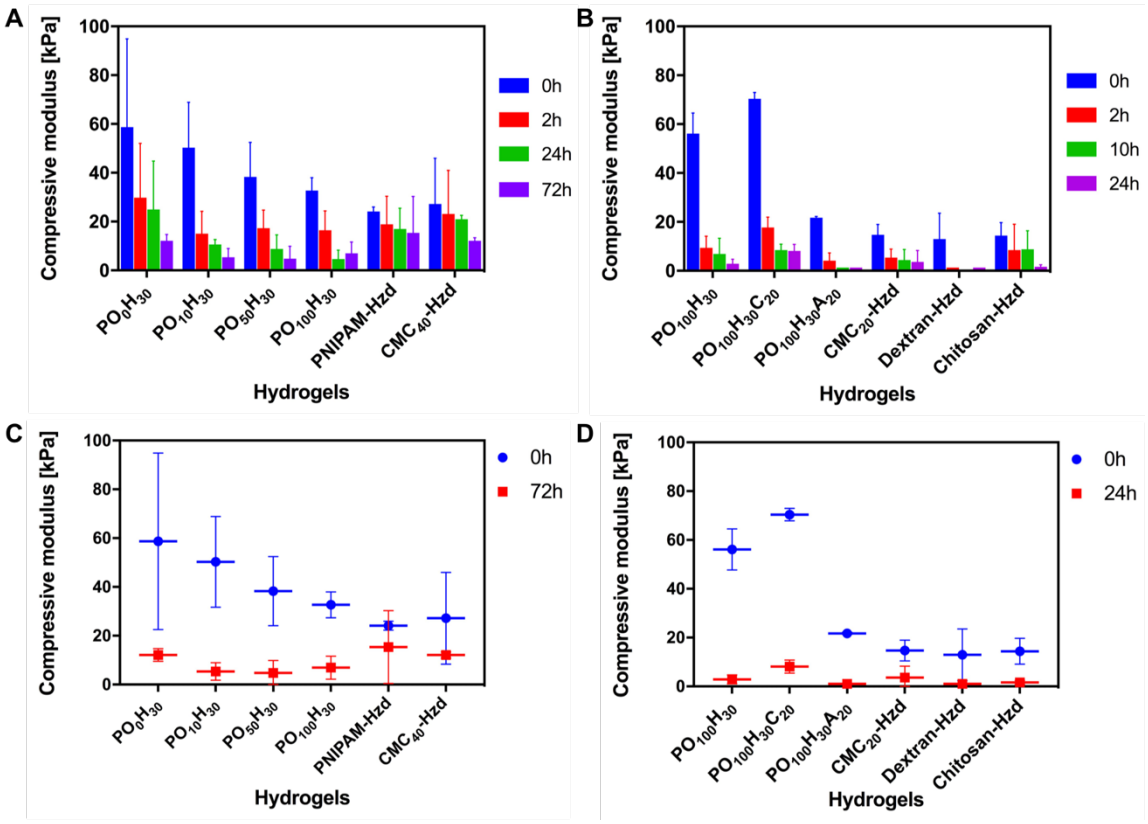

Figure 3.4. Compressive modulus (t = 0 h data points) and degradation kinetics (tracked by changes in the measured compressive modulus over time of exposure to 0.1 M HCl at 22 °C) for (A) thermoresponsive vs. non-thermoresponsive (T series) single-component hydrogels and (B) charged vs. neutral (C series) single-component hydrogels (n=4); (C) Comparison of the compressive modulus of T series hydrogels before and after degradation over 72 hours; (D) Comparison of the compressive modulus of C series hydrogels before and after degradation over 24 hours. See Supporting Figures S3-S4 for the corresponding results for the combinatorial hydrogels.

Transparency. Optical transparency is an important parameter in some applications of injectable hydrogels (e.g. ophthalmic delivery) relevant to protein-based therapies[68]. Transmittance as a function of temperature was measured by ramping a microplate reader from 25 °C to 40 °C and tracking the resulting transmittance at 595 nm. Since this wavelength is far outside the window in which any of the precursor polymers would absorb, the transmittance measurement corresponds primarily to the degree of phase separation in each hydrogel. As expected, low VPTT hydrogels such as PO_0H_{30} and PNIPAM-Hzd showed lower transmittance at 25 °C (48% for PO_0H_{30} and 45% for PNIPAM-Hzd,

consistent with the deswelling response observed for both these hydrogels at room temperature in Fig. 3.3A) and further decreased transmittance as the temperature was increased to 40 °C (29% for PO_0H_{30}, 30% for PNIPAM-Hzd). In contrast, only a slight reduction in transmittance was observed for the $PO_{10}H_{30}$ single-component hydrogel (consistent with its ~33 °C onset transition temperature) and no change in transparency was observed for higher transition temperature or non-thermoresponsive single-component gels over the same temperature range. As expected, none of the charged gels exhibited a thermal phase transition (Fig. 3.4B), with all gels showing transmittance values of >95%.

Combinatorial mixing results in a substantially higher range of transmittances between the hydrogels. The thermoresponsive hydrogels (T series) showed transmittances ranging from ~20% to >95% (Figure S3.5), while the charged hydrogels (C series) yield transmittances as low as ~60% (Figure S3.6) despite all single-component charged gels being highly transparent. For example, the $PO_{10}H_{30}$ + $PO_{100}H_{30}$ + PNIPAM-Hzd hydrogel (T3-3) noted to have a particularly large deswelling response (Fig. 3.2A) also exhibited a particularly low transparency (<20% over the full temperature range). This result is consistent with phase separation among the different transition temperature thermoresponsive components of this hydrogel. In comparison, the PO_0H_{30} + CMC-Hzd hydrogel (T2-12) that exhibited similarly high deswelling maintained a transparency of ~50% at 25 °C, albeit decreasing to ~20% transparency by 40 °C consistent with thermal response). The PNIPAM-Hzd component particularly appears to drive lower transparencies among the mixed hydrogels. For example, in the five-component thermoresponsive combinatorial gels demonstrated to suppress bulk deswelling (Fig. S3.1D), the one hydrogel prepared without the PNIPAM-Hzd component (T5-2) still maintained >60% transmittance while all formulations containing PNIPAM-Hzd had transmittances <40%.

For the charged series, binary mixtures of different carbohydrates such as CMC-Hzd + Chitosan-Hzd (C2-14) or CMC-Hzd + Dextran-Hzd (C2-15) appear to result in significantly lower transparency than mixing different POEGMA precursor polymers. This

result is consistent with the more different base chemistries of the carbohydrates (making phase separation more likely) as well as the higher viscosities of the carbohydrate starting materials that makes intimate mixing during high-throughput synthesis more challenging. Of particular note, multi-component mixtures including Chitosan-Hzd (e.g. C4-10, C4-12, C4-15, or any of the five-component gels aside from C5-1) all exhibit lower transmittances than corresponding combinations excluding Chitosan-Hzd. We attribute this result to the reduced solubility of the carboxymethylated chitosan at physiological pH following the consumption of a portion of those carboxyl groups during the hydrazide functionalization process, presenting a higher driving force for phase separation in such mixtures as the polar hydrazide groups are reacted to form hydrazone crosslinks. As such, the data suggests minimizing the use of PNIPAM-Hzd and Chitosan-Hzd improves transparency without necessarily changing the observed swelling responses.

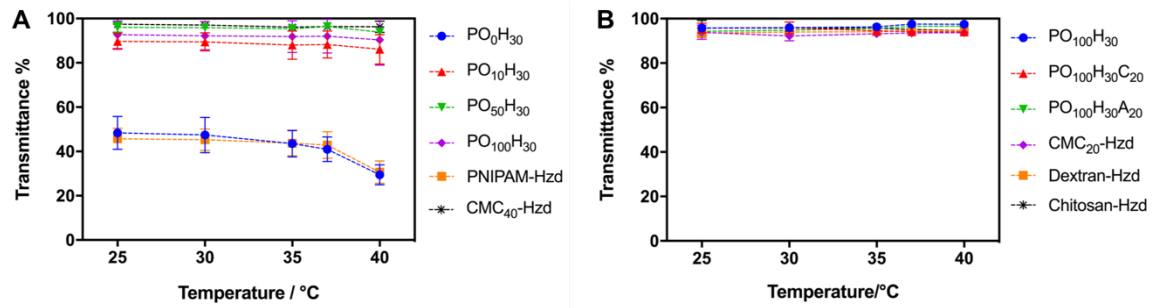

Figure 3.5 Transmittance of (A) thermoresponsive vs. non-thermoresponsive (T series) single-component hydrogels and (B) charged vs. neutral (C series) single-component hydrogels as a function of temperature (n=4). See Supporting Figures S5-S6 for the corresponding results for the combinatorial hydrogels.

3.3.4 Drug release kinetics

To assess the kinetics of protein release from the combinatorial hydrogels, ovalbumin was dissolved in the aldehyde precursor solution used to prepare gels in each set ($PO_{10}A_{30}$ in the T series and $PO_{100}A_{30}$ in the C series), resulting in a uniform overall loading of 2.5 mg/mL ovalbumin in each hydrogel. By using a multiwell filter plate with individual well collectors, the cumulative protein release from each sample can be individually tracked over a one month release period in high throughput. Figure 6 shows the cumulative

ovalbumin release profiles for each single-component gel. Thermoresponsive hydrogels showed higher % drug release than non-thermoresponsive hydrogels over the test period (Fig. 3.6A) depending on the degree of deswelling observed in each gel. PNIPAM-Hzd gels, which deswell the most relative to the fabricated volume of any single-component gel (Fig. 3.3A), show the highest total drug release (89.2 %) and day one burst release (69.5 %) of all hydrogels tested, consistent with convective transport of the protein out of the gel as the thermal collapse occurs. In contrast, non-thermoresponsive gels such as CMC-Hzd and $PO_{100}H_{30}$ exhibited substantially lower burst releases (~32% day one release for both) but also significant retention of protein, with <45 % of the loaded protein released after one month. In comparison, the intermediate transition temperature $PO_{50}H_{30}$ single component hydrogel exhibited comparable lower burst release to the non-thermoresponsive gels (~40 % day one release) but also significantly higher total release over the test period (~60%), suggesting that moderate thermoresponsiveness may be beneficial for prolonged protein release.

The charged single component hydrogels (Fig. 3.6B) showed significantly less burst release (~10 % to 28 % after 1 day compared to ~42% for the neutral $PO_{100}H_{30}$ control) but also significantly higher protein retention. Ovalbumin retention is particularly high for the carbohydrate-based hydrogels, which retained between 58-68% of their cargo even after one month. However, it must be noted that the oxidative degradation mechanism of carbohydrate-based hydrogels *in vivo* is not well modeled in this *in vitro* test. Regardless, this general result is consistent with the increased affinity of the charged gels for proteins, a result further demonstrated by the longer time frame of controlled release observed in the charged gels (up to 10 days) relative to the thermoresponsive gels (up to 5 days) despite the significantly higher water contents and thus lower diffusion resistances with the charged hydrogel series (Fig. 3.2B).

The combinatorial hydrogels again show interesting results in terms of manipulating the burst release, total duration of significant protein release, and the entrapped protein fraction of *in situ*-gelling hydrogels (Supporting Information Figures S3.8 - S3.14). While the

charged combinations all trended similarly (i.e. samples with less burst release also released less total protein, Fig. S3.10), the thermoresponsive hydrogels showed some independence among these variables. For example, the $PO_{10}H_{30}$ + $PO_{100}H_{30}$ + PO_0H_{30} hydrogel containing a mixture of POEGMA-based polymers with different phase transition temperatures (T3-1) exhibited a high burst release of ~60% and a high cumulative release of >90% but effectively sustained ovalbumin release effectively over ~10 days; in contrast, the T3-3 gel in which the PO_0H_{30} component is replaced with PNIPAM-Hzd exhibited similar burst and total ovalbumin release but a substantially shorter release time of ~3 days. The binary combinations exhibiting the highest degree of deswelling (T2-2 and T2-10, Fig. S3.1A) also exhibited the fastest and highest total convective ovalbumin release, while binary hydrogels formed by combining CMC-Hzd with an intermediate transition temperature POEGMA precursor such as $PO_{10}H_{30}$ + CMC-Hzd (T2-5) or $PO_{50}H_{30}$ + CMC-Hzd (T2-14) exhibited the lowest total release over much more extended periods. These results demonstrate that mixing different precursor polymers can effectively manipulate protein release from hydrogels in non-additive ways.

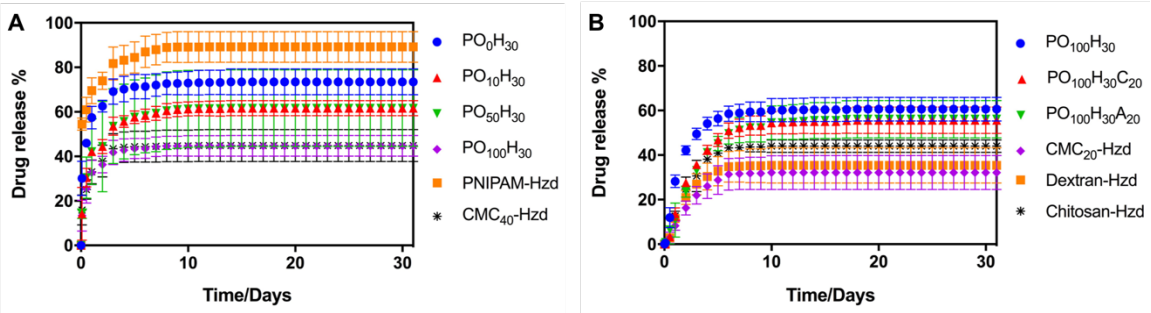

Figure 3.6 Cumulative ovalbumin release kinetics from (A) thermoresponsive vs. non-thermoresponsive (T series) single component hydrogels and (B) charged vs. neutral (C series) single component hydrogels in 10 mM PBS at 37 °C (n=4). See Supporting Figures S7-S8 for the corresponding results for the combinatorial hydrogels.

3.4 Conclusions

We demonstrate the potential of automated high-throughput synthesis and characterization strategies to prepare and screen *in situ*-gelling hydrogel compositions for targeted applications. In particular, we show how mixtures of charged and thermoresponsive

precursor polymers can reduce burst release, maximize total release, and slow the overall kinetics of release of a model protein (here, ovalbumin), with all beneficial properties toward achieving long-term protein delivery. The use of a high-throughput strategy to rapidly collect large amounts of data, as enabled by the development of the suite of high-throughput hydrogel characterization protocols developed and optimized in this paper, facilitates fast screening of potential hydrogel delivery vehicle compositions in a manner similar to current approaches to screen drugs or cell interactions, offering potential to substantially accelerate the discovery of biomedical hydrogels with targeted sets of properties. It could also be applied as a trial-and-error high content screening technique to quickly identify promising formulations for follow-up study.

3.5 Acknowledgements

Funding from the Natural Sciences and Engineering Research Council of Canada (Strategic Project Grant # STPGP447372-13) is gratefully acknowledged. ProMV software for performing the latent variable analysis was provided free of charge by ProSensus Inc.

3.6 References

(1) Hoare, T. R.; Kohane, D. S. Hydrogels in Drug Delivery: Progress and Challenges. *Polymer (Guildf).* **2008**, *49* (8), 1993–2007.

(2) S., F. O.; N., O. K.; S., P. P.; J., M. M.; Robert, L. Advances in Biomaterials for Drug Delivery. *Adv. Mater.* **2018**, *0* (0), 1705328.

(3) Jiang, Y.; Chen, J.; Deng, C.; Suuronen, E. J.; Zhong, Z. Click Hydrogels, Microgels and Nanogels: Emerging Platforms for Drug Delivery and Tissue Engineering. *Biomaterials* **2014**, *35* (18), 4969–4985.

(4) Drury, J. L.; Mooney, D. J. Hydrogels for Tissue Engineering: Scaffold Design Variables and Applications. *Biomaterials* **2003**, *24* (24), 4337–4351.

(5) Vlierberghe, S. Van; Dubruel, P.; Schacht, E. Biopolymer-Based Hydrogels As Scaffolds for Tissue Engineering Applications : A Review. **2011**, 1387–1408.

(6) Hoffman, A. S. Hydrogels for Biomedical Applications. *Adv. Drug Deliv. Rev.*

2002, *54* (1), 3–12.

(7) Boateng, J. S.; Matthews, K. H.; Stevens, H. N. E.; Eccleston, G. M. Wound Healing Dressings and Drug Delivery Systems: A Review. *J. Pharm. Sci.* **2008**, *97* (8), 2892–2923.

(8) Jung, I. Y.; Kim, J. S.; Choi, B. R.; Lee, K.; Lee, H. Hydrogel Based Biosensors for In Vitro Diagnostics of Biochemicals, Proteins, and Genes. *Adv. Healthc. Mater.* **2017**, *6* (12), 1601475.

(9) Puchberger-Enengl, D.; Krutzler, C.; Keplinger, F.; Vellekoop, M. J. Single-Step Design of Hydrogel-Based Microfluidic Assays for Rapid Diagnostics. *Lab Chip* **2014**, *14* (2), 378–383.

(10) Xie, L.; Hong, F.; He, C.; Ma, C.; Liu, J.; Zhang, G.; Wu, C. Coatings with a Self-Generating Hydrogel Surface for Antifouling. *Polymer (Guildf).* **2011**, *52* (17), 3738–3744.

(11) Liu, S. Q.; Yang, C.; Huang, Y.; Ding, X.; Li, Y.; Fan, W. M.; Hedrick, J. L.; Yang, Y.-Y. Antimicrobial and Antifouling Hydrogels Formed In Situ from Polycarbonate and Poly(Ethylene Glycol) via Michael Addition. *Adv. Mater.* **2012**, *24* (48), 6484–6489.

(12) Veronese, F. M.; Pasut, G. PEGylation, Successful Approach to Drug Delivery. *Drug Discov. Today* **2005**, *10* (21), 1451–1458.

(13) Ishii, S.; Kaneko, J.; Nagasaki, Y. Development of a Long-Acting, Protein-Loaded, Redox-Active, Injectable Gel Formed by a Polyion Complex for Local Protein Therapeutics. *Biomaterials* **2016**, *84*, 210–218.

(14) Mateen, R.; Hoare, T. Injectable, in Situ Gelling, Cyclodextrin-Dextran Hydrogels for the Partitioning-Driven Release of Hydrophobic Drugs. *J. Mater. Chem. B* **2014**, *2* (32), 5157–5167.

(15) Takeoka, Y.; Watanabe, M. Tuning Structural Color Changes of Porous Thermosensitive Gels through Quantitative Adjustment of the Cross-Linker in Pre-Gel Solutions. *Langmuir* **2003**, *19* (22), 9104–9106.

(16) Breulmann, M.; Davis, S. A.; Mann, S.; Hentze, H.-P.; Antonietti, M. Polymer–Gel Templating of Porous Inorganic Macro-Structures Using Nanoparticle Building

Blocks. *Adv. Mater.* **2000**, *12* (7), 502–507.

(17) Griffin, D. R.; Weaver, W. M.; Scumpia, P. O.; Di Carlo, D.; Segura, T. Accelerated Wound Healing by Injectable Microporous Gel Scaffolds Assembled from Annealed Building Blocks. *Nat Mater* **2015**, *14* (7), 737–744.

(18) Mateen, R.; Ali, M. M.; Hoare, T. A Printable Hydrogel Microarray for Drug Screening Avoids False Positives Associated with Promiscuous Aggregating Inhibitors. *Nat. Commun.* **2018**, *9* (1), 602.

(19) Lin, C.-C.; Anseth, K. S. PEG Hydrogels for the Controlled Release of Biomolecules in Regenerative Medicine. *Pharm. Res.* **2009**, *26* (3), 631–643.

(20) Yu, Y.; Chau, Y. Formulation of In Situ Chemically Cross-Linked Hydrogel Depots for Protein Release: From the Blob Model Perspective. *Biomacromolecules* **2015**, *16* (1), 56–65.

(21) Bakaic, E.; Smeets, N. M. B.; Badv, M.; Dodd, M.; Barrigar, O.; Siebers, E.; Lawlor, M.; Sheardown, H.; Hoare, T. Injectable and Degradable Poly(Oligoethylene Glycol Methacrylate) Hydrogels with Tunable Charge Densities as Adhesive Peptide-Free Cell Scaffolds. *ACS Biomater. Sci. Eng.* **2017**.

(22) Smeets, N. M. B.; Patenaude, M.; Kinio, D.; Yavitt, F. M.; Bakaic, E.; Yang, F.-C.; Rheinstadter, M.; Hoare, T. Injectable Hydrogels with in Situ-Forming Hydrophobic Domains: Oligo(D{,}l-Lactide) Modified Poly(Oligoethylene Glycol Methacrylate) Hydrogels. *Polym. Chem.* **2014**, *5* (23), 6811–6823.

(23) Loh, X. J.; Peh, P.; Liao, S.; Sng, C.; Li, J. Controlled Drug Release from Biodegradable Thermoresponsive Physical Hydrogel Nanofibers. *J. Control. Release* **2010**, *143* (2), 175–182.

(24) Zhang, J.; Muirhead, B.; Dodd, M.; Liu, L.; Xu, F.; Mangiacotte, N.; Hoare, T.; Sheardown, H. An Injectable Hydrogel Prepared Using a PEG/Vitamin E Copolymer Facilitating Aqueous-Driven Gelation. *Biomacromolecules* **2016**, *17* (11), 3648–3658.

(25) Bakaic, E.; Smeets, N. M. B.; Hoare, T. Injectable Hydrogels Based on Poly(Ethylene Glycol) and Derivatives as Functional Biomaterials. *RSC Adv.* **2015**, *5* (45), 35469–35486.

(26) Fenoli, C. R.; Bowman, C. N. The Thiol-Michael Addition Click Reaction: A Powerful and Widely Used Tool in Materials Chemistry. **2013**.

(27) Koehler, K. C.; Anseth, K. S.; Bowman, C. N. Diels–Alder Mediated Controlled Release from a Poly(Ethylene Glycol) Based Hydrogel. *Biomacromolecules* **2013**, *14* (2), 538–547.

(28) Buwalda, S. J.; Boere, K. W. M.; Dijkstra, P. J.; Feijen, J.; Vermonden, T.; Hennink, W. E. Hydrogels in a Historical Perspective: From Simple Networks to Smart Materials. *J. Control. Release* **2014**, *190*, 254–273.

(29) Hennink, W. E.; van Nostrum, C. F. Novel Crosslinking Methods to Design Hydrogels. *Adv. Drug Deliv. Rev.* **2012**, *64*, 223–236.

(30) Yu, Y.; Lau, L. C. M.; Lo, A. C.; Chau, Y. Injectable Chemically Crosslinked Hydrogel for the Controlled Release of Bevacizumab in Vitreous: A 6-Month In Vivo Study. *Transl. Vis. Sci. Technol.* **2015**, *4* (2), 5.

(31) Lau, C. M. L.; Yu, Y.; Jahanmir, G.; Chau, Y. Controlled Release Technology for Anti-Angiogenesis Treatment of Posterior Eye Diseases: Current Status and Challenges. *Adv. Drug Deliv. Rev.* **2018**, *126*, 145–161.

(32) Joshi, N.; Yan, J.; Levy, S.; Bhagchandani, S.; Slaughter, K. V; Sherman, N. E.; Amirault, J.; Wang, Y.; Riegel, L.; He, X.; et al. Towards an Arthritis Flare-Responsive Drug Delivery System. *Nat. Commun.* **2018**, *9* (1), 1275.

(33) Basu, K.; Baral, A.; Basak, S.; Dehsorkhi, A.; Nanda, J.; Bhunia, D.; Ghosh, S.; Castelletto, V.; Hamley, I. W.; Banerjee, A. Peptide Based Hydrogels for Cancer Drug Release: Modulation of Stiffness, Drug Release and Proteolytic Stability of Hydrogels by Incorporating d-Amino Acid Residue(S). *Chem. Commun.* **2016**, *52* (28), 5045–5048.

(34) Qiu, M.; Wang, D.; Liang, W.; Liu, L.; Zhang, Y.; Chen, X.; Sang, D. K.; Xing, C.; Li, Z.; Dong, B.; et al. Novel Concept of the Smart NIR-Light–Controlled Drug Release of Black Phosphorus Nanostructure for Cancer Therapy. *Proc. Natl. Acad. Sci.* **2018**, *115* (3), 501 LP-506.

(35) Lutolf, M. P.; Hubbell, J. a. Synthetic Biomaterials as Instructive Extracellular Microenvironments for Morphogenesis in Tissue Engineering. *Nat. Biotechnol.*

2005, *23* (1), 47–55.

(36) Dang, J. M.; Leong, K. W. Natural Polymers for Gene Delivery and Tissue Engineering. *Adv. Drug Deliv. Rev.* **2006**, *58* (4), 487–499.

(37) B., S. N.; Roshan, J.; T., L. C.; G., K. S. Polysaccharide Biomaterials for Drug Delivery and Regenerative Engineering. *Polym. Adv. Technol.* **2014**, *25* (5), 448–460.

(38) Li, L.; Smitthipong, W.; Zeng, H. Mussel-Inspired Hydrogels for Biomedical and Environmental Applications. *Polym. Chem.* **2015**, *6*, 353–358.

(39) Qiu, Y.; Park, K. Environment-Sensitive Hydrogels for Drug Delivery. *Adv. Drug Deliv. Rev.* **2001**, *53* (3), 321–339.

(40) Patenaude, M.; Hoare, T. Injectable, Degradable Thermoresponsive Poly(N-Isopropylacrylamide) Hydrogels. *ACS Macro Lett.* **2012**, *1* (3), 409–413.

(41) Sivakumaran, D.; Bakaic, E.; Campbell, S. B.; Xu, F.; Mueller, E.; Hoare, T. Fabricating Degradable Thermoresponsive Hydrogels on Multiple Length Scales via Reactive Extrusion, Microfluidics, Self-Assembly, and Electrospinning. *J. Vis. Exp.* **2018**, *2018* (134), 1–12.

(42) Jin, Y. J.; Jung, C. H.; Gwan, P. T. Photo-Crosslinkable and Biodegradable Pluronic/Heparin Hydrogels for Local and Sustained Delivery of Angiogenic Growth Factor. *J. Biomed. Mater. Res. Part A* **2007**, *83A* (3), 597–605.

(43) Smeets, N. M. B.; Bakaic, E.; Patenaude, M.; Hoare, T. Injectable and Tunable Poly(Ethylene Glycol) Analogue Hydrogels Based on Poly(Oligoethylene Glycol Methacrylate). *Chem. Commun.* **2014**, *50* (25), 3306–3309.

(44) Lutz, J.-F.; Akdemir, Ö.; Hoth, A. Point by Point Comparison of Two Thermosensitive Polymers Exhibiting a Similar LCST: Is the Age of Poly(NIPAM) Over? *J. Am. Chem. Soc.* **2006**, *128* (40), 13046–13047.

(45) Jean-François, L. Thermo-Switchable Materials Prepared Using the OEGMA-Platform. *Adv. Mater.* **2011**, *23* (19), 2237–2243.

(46) Lutz, J.-F.; Hoth, A. Preparation of Ideal PEG Analogues with a Tunable Thermosensitivity by Controlled Radical Copolymerization of 2-(2-Methoxyethoxy)Ethyl Methacrylate and Oligo(Ethylene Glycol) Methacrylate.

Macromolecules **2006**, *39* (2), 893–896.

(47) Dhar, S.; Kolishetti, N.; Lippard, S. J.; Farokhzad, O. C. Targeted Delivery of a Cisplatin Prodrug for Safer and More Effective Prostate Cancer Therapy in Vivo. *Proc. Natl. Acad. Sci.* **2011**, *108* (5), 1850 LP-1855.

(48) Yu, Y.; Chow, D.; Back, W.; Xu, J.; Chau, Y. Effects of Twice per Day KN-A01, a Modified Hyaluronic Acid Based Hydrogel, for the Treatment of Dry Eye Syndrome in Dog Patients. *Invest. Ophthalmol. Vis. Sci.* **2018**, *59* (9), 3824.

(49) Zhang, Y. S.; Khademhosseini, A. Advances in Engineering Hydrogels. *Science (80-.).* **2017**, *356* (6337).

(50) Patenaude, M.; Hoare, T. Injectable, Mixed Natural-Synthetic Polymer Hydrogels with Modular Properties. *Biomacromolecules* **2012**, *13* (2), 369–378.

(51) Ward, M. A.; Georgiou, T. K. Thermoresponsive Polymers for Biomedical Applications. *Polymers* . 2011.

(52) Bakaic, E.; Smeets, N. M. B.; Dorrington, H.; Hoare, T. "Off-the-Shelf" Thermoresponsive Hydrogel Design: Tuning Hydrogel Properties by Mixing Precursor Polymers with Different Lower-Critical Solution Temperatures. *RSC Adv.* **2015**, *5* (42), 33364–33376.

(53) Caló, E.; Khutoryanskiy, V. V. Biomedical Applications of Hydrogels: A Review of Patents and Commercial Products. *Eur. Polym. J.* **2015**, *65*, 252–267.

(54) Vermonden, T.; Censi, R.; Hennink, W. E. Hydrogels for Protein Delivery. *Chem. Rev.* **2012**, *112* (5), 2853–2888.

(55) Bakaic, E.; Smeets, N. M. B.; Barrigar, O.; Alsop, R.; Rheinstädter, M. C.; Hoare, T. PH-Ionizable in Situ Gelling Poly(Oligo Ethylene Glycol Methacrylate)-Based Hydrogels: The Role of Internal Network Structures in Controlling Macroscopic Properties. *Macromolecules* **2017**, *50* (19), 7687–7698.

(56) Sivakumaran, D.; Maitland, D.; Hoare, T. Injectable Microgel-Hydrogel Composites for Prolonged Small-Molecule Drug Delivery. *Biomacromolecules* **2011**, *12* (11), 4112–4120.

(57) Campbell, S. B.; Patenaude, M.; Hoare, T. Injectable Superparamagnets: Highly Elastic and Degradable Poly(N-Isopropylacrylamide)–Superparamagnetic Iron

Oxide Nanoparticle (SPION) Composite Hydrogels. *Biomacromolecules* **2013**, *14* (3), 644–653.

(58) Demirci, F. X. and J. W. and S. W. and N. G. D. and U. A. G. and U. Microengineering Methods for Cell-Based Microarrays and High-Throughput Drug-Screening Applications. *Biofabrication* **2011**, *3* (3), 34101.

(59) Fernandes, T. G.; Diogo, M. M.; Clark, D. S.; Dordick, J. S.; Cabral, J. M. S. High-Throughput Cellular Microarray Platforms: Applications in Drug Discovery, Toxicology and Stem Cell Research. *Trends Biotechnol.* **2009**, *27* (6), 342–349.

(60) Smeets, N. M. B.; Bakaic, E.; Patenaude, M.; Hoare, T. Injectable and Tunable Poly(Ethylene Glycol) Analogue Hydrogels Based on Poly(Oligoethylene Glycol Methacrylate). *Chem. Commun.* **2014**, *50* (25), 3306–3309.

(61) Bakaic, E.; Smeets, N. M. B.; Dorrington, H.; Hoare, T. "Off-the-Shelf" Thermoresponsive Hydrogel Design: Tuning Hydrogel Properties by Mixing Precursor Polymers with Different Lower-Critical Solution Temperatures. *RSC Adv.* **2015**, *5* (42), 33364–33376.

(62) Campbell, S.; Maitland, D.; Hoare, T. Enhanced Pulsatile Drug Release from Injectable Magnetic Hydrogels with Embedded Thermosensitive Microgels. *ACS Macro Lett.* **2015**, *4* (3), 312–316.

(63) Mateen, R.; Hoare, T. Carboxymethyl and Hydrazide Functionalized β-Cyclodextrin Derivatives: A Systematic Investigation of Complexation Behaviours with the Model Hydrophobic Drug Dexamethasone. *Int. J. Pharm.* **2014**, *472* (1), 315–326.

(64) Yang, X.; Bakaic, E.; Hoare, T.; Cranston, E. D. Injectable Polysaccharide Hydrogels Reinforced with Cellulose Nanocrystals: Morphology, Rheology, Degradation, and Cytotoxicity. *Biomacromolecules* **2013**, *14* (12), 4447–4455.

(65) Anitha, A.; Maya, S.; Deepa, N.; Chennazhi, K. P.; Nair, S. V; Tamura, H.; Jayakumar, R. Efficient Water Soluble O-Carboxymethyl Chitosan Nanocarrier for the Delivery of Curcumin to Cancer Cells. *Carbohydr. Polym.* **2011**, *83* (2), 452–461.

(66) Xiao, F. L.; Yun, L. G.; Dong, Z. Y.; Zhi, L.; Kang, D. Y. Antibacterial Action of

Chitosan and Carboxymethylated Chitosan. *J. Appl. Polym. Sci.* **2000**, *79* (7), 1324–1335.

(67) Smeets, N. M. B.; Bakaic, E.; Patenaude, M.; Hoare, T. Injectable Poly(Oligoethylene Glycol Methacrylate)-Based Hydrogels with Tunable Phase Transition Behaviours: Physicochemical and Biological Responses. *Acta Biomater.* **2014**, *10* (10), 4143–4155.

(68) Ng, E. W. M.; Shima, D. T.; Calias, P.; Cunningham Jr., E. T.; Guyer, D. R.; Adamis, A. P. Pegaptanib, a Targeted Anti-VEGF Aptamer for Ocular Vascular Disease. *Nat. Rev. Drug Discov.* **2006**, *5*, 123.

3.7 Support Information

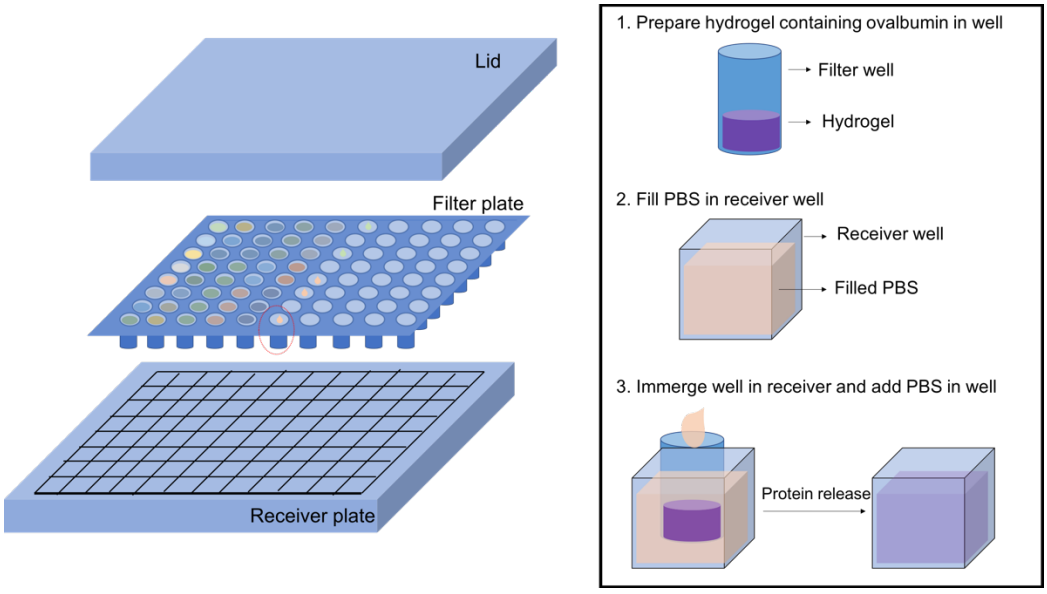

Figure S3.1 Schematic of drug release set-up in 96 well-plate using high-throughput measurement.

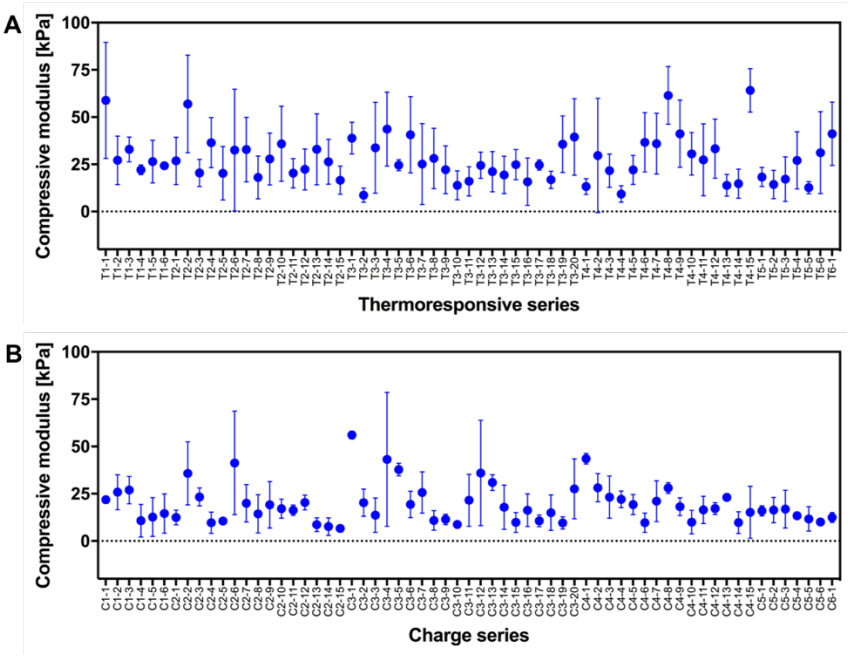

Figure S3.2 Compression modulus of each hydrogel before swelling.

Cytocompatibility testing. The *in vitro* cytocompatibility of all the polymer precursors was assessed using NIH 3T3 mouse fibroblasts. Cells were cultured in DMEM containing 10% FBS and 1% PS at 37 °C with 5 % CO_2 to ~80% confluence before use. 10,000 cells were plated in each well of 96 well-plate and incubated overnight in 100 μL DMEM medium. Following, the DMEM was aspirated and replaced with polymer precursor solutions at concentrations of 1 mg/mL and 2 mg/mL in the same DMEM media and incubated for an additional 24 h. Following, cell viability was assessed using the PrestoBlue assay following the standard protocol, with absorbances measured using a microplate reader (Infinite M200 Pro) at wavelength of 570 nm. Cell viabilities were calculated by comparing the measured PrestoBlue signal in the presence of the polymers to cell-only and media-only controls. Error bars represent the standard deviation of four independent measurements (n=4).

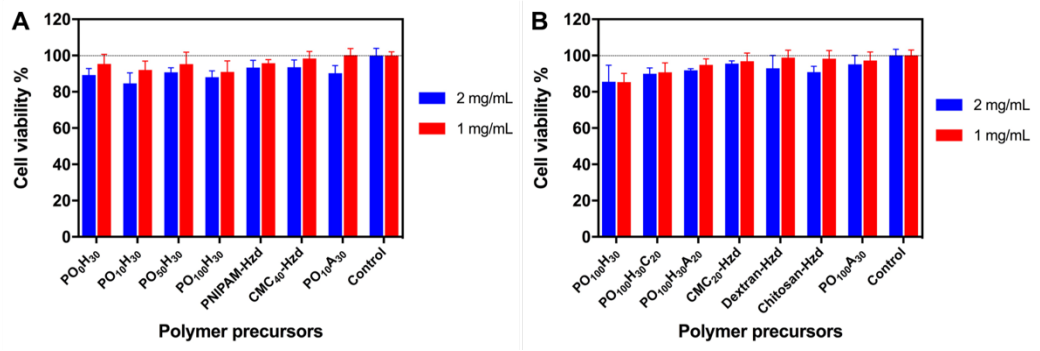

Figure S3.3 3T3 mouse fibroblast cell viability (relative to cell-only control) of polymer precursors used to produce (A) thermoresponsive vs. non-thermoresponsive combinatorial hydrogels (T series) and (B) charged vs. neutral (C series) combinatorial hydrogels (n=4).

Table S3.1. Compositions of thermoresponsive vs. non-thermoresponsive combinatorial hydrogels

Number	Group	Label	Components of hydrazide polymer precursors	Volume of each component
1		T1-1	PO_0H_{30}	
2		T1-2	$PO_{10}H_{30}$	
3	C_6^1	T1-3	$PO_{50}H_{30}$	60 µL
4		T1-4	$PO_{100}H_{30}$	
5		T1-5	PNIPAM-Hzd	
6		T1-6	CMC_{40}-Hzd	
7		T2-1	$PO_{10}H_{30}$ + $PO_{100}H_{30}$	
8		T2-2	$PO_{10}H_{30}$ + PO_0H_{30}	
9		T2-3	$PO_{10}H_{30}$ + $PO_{50}H_{30}$	
10		T2-4	$PO_{10}H_{30}$ + PNIPAM-Hzd	
11		T2-5	$PO_{10}H_{30}$ + CMC_{40}-Hzd	
12		T2-6	$PO_{100}H_{30}$ + PO_0H_{30}	
13		T2-7	$PO_{100}H_{30}$ + $PO_{50}H_{30}$	
14	C_6^2	T2-8	$PO_{100}H_{30}$ + PNIPAM-Hzd	30 µL
15		T2-9	$PO_{100}H_{30}$ + CMC_{40}-Hzd	
16		T2-10	PO_0H_{30} + $PO_{50}H_{30}$	
17		T2-11	PO_0H_{30} + PNIPAM-Hzd	
18		T2-12	PO_0H_{30} + CMC_{40}-Hzd	
19		T2-13	$PO_{50}H_{30}$ + PNIPAM-Hzd	

20		T2-14	$PO_{50}H_{30}$ + CMC_{40}-Hzd	
21		T2-15	PNIPAM-Hzd + CMC_{40}-Hzd	
22		T3-1	$PO_{10}H_{30}$ + $PO_{100}H_{30}$ + PO_0H_{30}	
23		T3-2	$PO_{10}H_{30}$ + $PO_{100}H_{30}$ + $PO_{50}H_{30}$	
24		T3-3	$PO_{10}H_{30}$ + $PO_{100}H_{30}$ + PNIPAM-Hzd	
25		T3-4	$PO_{10}H_{30}$ + $PO_{100}H_{30}$ + CMC_{40}-Hzd	
26		T3-5	$PO_{10}H_{30}$ + PO_0H_{30} + $PO_{50}H_{30}$	
27		T3-6	$PO_{10}H_{30}$ + PO_0H_{30} + PNIPAM-Hzd	
28		T3-7	$PO_{10}H_{30}$ + PO_0H_{30} + CMC_{40}-Hzd	
29		T3-8	$PO_{10}H_{30}$ + $PO_{50}H_{30}$ + PNIPAM-Hzd	20 μL
30		T3-9	$PO_{10}H_{30}$ + $PO_{50}H_{30}$+ CMC_{40}-Hzd	
31	C_6^3	T3-10	$PO_{10}H_{30}$ + PNIPAM-Hzd + CMC_{40}-Hzd	
32		T3-11	$PO_{100}H_{30}$ + PO_0H_{30} + $PO_{50}H_{30}$	
33		T3-12	$PO_{100}H_{30}$ + PO_0H_{30} + PNIPAM-Hzd	
34		T3-13	$PO_{100}H_{30}$ + PO_0H_{30} + CMC_{40}-Hzd	
35		T3-14	$PO_{100}H_{30}$ + $PO_{50}H_{30}$ + PNIPAM-Hzd	
36		T3-15	$PO_{100}H_{30}$ + $PO_{50}H_{30}$ + CMC_{40}-Hzd	
37		T3-16	$PO_{100}H_{30}$ + PNIPAM-Hzd + CMC_{40}-Hzd	
38		T3-17	PO_0H_{30} + $PO_{50}H_{30}$ + PNIPAM-Hzd	
39		T3-18	PO_0H_{30} + $PO_{50}H_{30}$ + CMC_{40}-Hzd	
40		T3-19	PO_0H_{30} + PNIPAM-Hzd + CMC_{40}-Hzd	
41		T3-20	$PO_{50}H_{30}$ + PNIPAM-Hzd + CMC_{40}-Hzd	
42		T4-1	$PO_{10}H_{30}$ + $PO_{100}H_{30}$ + PO_0H_{30} + $PO_{50}H_{30}$	
43		T4-2	$PO_{10}H_{30}$ + $PO_{100}H_{30}$ + PO_0H_{30} + PNIPAM-Hzd	
44		T4-3	$PO_{10}H_{30}$ + $PO_{100}H_{30}$ + PO_0H_{30} + CMC_{40}-Hzd	
45		T4-4	$PO_{10}H_{30}$ + $PO_{100}H_{30}$ + $PO_{50}H_{30}$ + PNIPAM-Hzd	
46		T4-5	$PO_{10}H_{30}$ + $PO_{100}H_{30}$ + $PO_{50}H_{30}$ + CMC_{40}-Hzd	
47		T4-6	$PO_{10}H_{30}$ + $PO_{100}H_{30}$ + PNIPAM-Hzd + CMC_{40}-Hzd	
48		T4-7	$PO_{10}H_{30}$ + PO_0H_{30} + $PO_{50}H_{30}$ + PNIPAM-Hzd	15 μL
49	C_6^4	T4-8	$PO_{10}H_{30}$ + PO_0H_{30} + $PO_{50}H_{30}$ +CMC_{40}-Hzd	
50		T4-9	$PO_{10}H_{30}$ + PO_0H_{30} + PNIPAM-Hzd + CMC_{40}-Hzd	
51		T4-10	$PO_{10}H_{30}$ + $PO_{50}H_{30}$ + PNIPAM-Hzd + CMC_{40}-Hzd	
52		T4-11	$PO_{100}H_{30}$ + PO_0H_{30} + $PO_{50}H_{30}$ + PNIPAM-Hzd	
53		T4-12	$PO_{100}H_{30}$ + PO_0H_{30} + $PO_{50}H_{30}$ + CMC_{40}-Hzd	
54		T4-13	$PO_{100}H_{30}$ + PO_0H_{30} + PNIPAM-Hzd + CMC_{40}-Hzd	

55		T4-14	$PO_{100}H_{30}$ + $PO_{50}H_{30}$ + PNIPAM-Hzd + CMC_{40}-Hzd	
56		T4-15	$PO_{0}H_{30}$ + $PO_{50}H_{30}$ + PNIPAM-Hzd + CMC_{40}-Hzd	
57		T5-1	$PO_{10}H_{30}$ + $PO_{100}H_{30}$ + $PO_{0}H_{30}$ + $PO_{50}H_{30}$ + PNIPAM-Hzd	
58		T5-2	$PO_{10}H_{30}$ + $PO_{100}H_{30}$ + $PO_{0}H_{30}$ + $PO_{50}H_{30}$ + CMC_{40}-Hzd	
59		T5-3	$PO_{10}H_{30}$ + $PO_{100}H_{30}$ + $PO_{0}H_{30}$ + PNIPAM-Hzd + CMC_{40}-Hzd	
60	C_6^5	T5-4	$PO_{10}H_{30}$ + $PO_{100}H_{30}$ + $PO_{50}H_{30}$ + PNIPAM-Hzd + CMC_{40}-Hzd	12 μL
61		T5-5	$PO_{10}H_{30}$ + $PO_{0}H_{30}$ + $PO_{50}H_{30}$ + PNIPAM-Hzd + CMC_{40}-Hzd	
62		T5-6	$PO_{100}H_{30}$ + $PO_{0}H_{30}$ + $PO_{50}H_{30}$ + PNIPAM-Hzd + CMC_{40}-Hzd	
63	C_6^6	T6-1	$PO_{10}H_{30}$ + $PO_{100}H_{30}$ + $PO_{0}H_{30}$ + $PO_{50}H_{30}$ + PNIPAM-Hzd + CMC_{40}-Hzd	10 μL

∗ The combinations of hydrazide polymers listed above were each mixed with a single aldehyde precursor polymer ($PO_{10}A_{30}$, 60 μL) to facilitate gelation. The total volume of each gel was 120 μL.

Table S3.2. Compositions of charged vs. neutral combinatorial hydrogels

Number	Group	Label	Components of hydrazide polymer precursors	Volume of each component
1		C1-1	$PO_{100}H_{30}$	
2		C1-2	$PO_{100}H_{30}C_{20}$	
3	C_6^1	C1-3	$PO_{100}H_{30}A_{20}$	60 μL
4		C1-4	CMC_{20}-Hzd	
5		C1-5	Dextran-Hzd	
6		C1-6	Chitosan-Hzd	
7		C2-1	$PO_{100}H_{30}$ + $PO_{100}H_{30}C_{20}$	
8		C2-2	$PO_{100}H_{30}$ + $PO_{100}H_{30}A_{20}$	
9		C2-3	$PO_{100}H_{30}$ + CMC_{20}-Hzd	
10		C2-4	$PO_{100}H_{30}$ + Dextran-Hzd	
11		C2-5	$PO_{100}H_{30}$ + Chitosan-Hzd	

12		C2-6	$PO_{100}H_{30}C_{20}$ + $PO_{100}H_{30}A_{20}$	
13		C2-7	$PO_{100}H_{30}C_{20}$ + CMC_{20}-Hzd	
14	C_6^2	C2-8	$PO_{100}H_{30}C_{20}$ + Dextran-Hzd	30 μL
15		C2-9	$PO_{100}H_{30}C_{20}$ + Chitosan-Hzd	
16		C2-10	$PO_{100}H_{30}A_{20}$ + CMC_{20}-Hzd	
17		C2-11	$PO_{100}H_{30}A_{20}$ + Dextran-Hzd	
18		C2-12	$PO_{100}H_{30}A_{20}$ + Chitosan-Hzd	
19		C2-13	CMC_{20}-Hzd + Dextran-Hzd	
20		C2-14	CMC_{20}-Hzd + Chitosan-Hzd	
21		C2-15	Dextran-Hzd + Chitosan-Hzd	
22		C3-1	$PO_{100}H_{30}$ + $PO_{100}H_{30}C_{20}$ + $PO_{100}H_{30}A_{20}$	
23		C3-2	$PO_{100}H_{30}$ + $PO_{100}H_{30}C_{20}$ + CMC_{20}-Hzd	
24		C3-3	$PO_{100}H_{30}$ + $PO_{100}H_{30}C_{20}$ + Dextran-Hzd	
25		C3-4	$PO_{100}H_{30}$ + $PO_{100}H_{30}C_{20}$ + Chitosan-Hzd	
26		C3-5	$PO_{100}H_{30}$ + $PO_{100}H_{30}A_{20}$ + CMC_{20}-Hzd	
27		C3-6	$PO_{100}H_{30}$ + $PO_{100}H_{30}A_{20}$ + Dextran-Hzd	
28		C3-7	$PO_{100}H_{30}$ + $PO_{100}H_{30}$ A_{20} + Chitosan-Hzd	
29		C3-8	$PO_{100}H_{30}$ + CMC_{20}-Hzd + Dextran-Hzd	20 μL
30		C3-9	$PO_{100}H_{30}$ + CMC_{20}-Hzd + Chitosan-Hzd	
31	C_6^3	C3-10	$PO_{100}H_{30}$ + Dextran-Hzd + Chitosan-Hzd	
32		C3-11	$PO_{100}H_{30}C_{20}$ + $PO_{100}H_{30}A_{20}$ + CMC_{20}-Hzd	
33		C3-12	$PO_{100}H_{30}C_{20}$ + $PO_{100}H_{30}A_{20}$ + Dextran-Hzd	
34		C3-13	$PO_{100}H_{30}C_{20}$+ $PO_{100}H_{30}A_{20}$ + Chitosan-Hzd	
35		C3-14	$PO_{100}H_{30}C_{20}$ + CMC_{20}-Hzd + Dextran-Hzd	
36		C3-15	$PO_{100}H_{30}C_{20}$ + CMC_{20}-Hzd + Chitosan-Hzd	
37		C3-16	$PO_{100}H_{30}C_{20}$ + Dextran-Hzd + Chitosan-Hzd	
38		C3-17	$PO_{100}H_{30}A_{20}$ + CMC_{20}-Hzd + Dextran-Hzd	
39		C3-18	$PO_{100}H_{30}A_{20}$ + CMC_{20}-Hzd + Chitosan-Hzd	
40		C3-19	$PO_{100}H_{30}A_{20}$ + Dextran-Hzd + Chitosan-Hzd	
41		C3-20	CMC_{20}-Hzd + Dextran-Hzd + Chitosan-Hzd	
42		C4-1	$PO_{100}H_{30}$ + $PO_{100}H_{30}C_{20}$ + $PO_{100}H_{30}A_{20}$ + CMC_{20}-Hzd	
43		C4-2	$PO_{100}H_{30}$ + $PO_{100}H_{30}C_{20}$ + $PO_{100}H_{30}A_{20}$ + Dextran-Hzd	
44		C4-3	$PO_{100}H_{30}$ + $PO_{100}H_{30}C_{20}$ + $PO_{100}H_{30}A_{20}$ + Chitosan-Hzd	
45		C4-4	$PO_{100}H_{30}$ + $PO_{100}H_{30}C_{20}$ + CMC_{20}-Hzd + Dextran-Hzd	
46		C4-5	$PO_{100}H_{30}$ + $PO_{100}H_{30}C_{20}$+ CMC_{20}-Hzd + Chitosan-Hzd	

47		C4-6	$PO_{100}H_{30}$ + $PO_{100}H_{30}C_{20}$+ Dextran-Hzd + Chitosan-Hzd	15 μL
48	C_6^4	C4-7	$PO_{100}H_{30}$ + $PO_{100}H_{30}A_{20}$+ CMC_{20}-Hzd + Dextran-Hzd	
49		C4-8	$PO_{100}H_{30}$ + $PO_{100}H_{30}A_{20}$+ CMC_{20}-Hzd + Chitosan-Hzd	
50		C4-9	$PO_{100}H_{30}$ + $PO_{100}H_{30}A_{20}$+ Dextran-Hzd + Chitosan-Hzd	
51		C4-10	$PO_{100}H_{30}$ + CMC_{20}-Hzd + Dextran + Chitosan	
52		C4-11	$PO_{100}H_{30}C_{20}$ + $PO_{100}H_{30}A_{20}$ + CMC_{20}-Hzd + Dextran-Hzd	
53		C4-12	$PO_{100}H_{30}C_{20}$ + $PO_{100}H_{30}A_{20}$ + CMC_{20}-Hzd + Chitosan-Hzd	
54		C4-13	$PO_{100}H_{30}C_{20}$ + $PO_{100}H_{30}A_{20}$ + Dextran-Hzd + Chitosan-Hzd	
55		C4-14	$PO_{100}H_{30}C_{20}$ + CMC_{20}-Hzd + Dextran-Hzd + Chitosan-Hzd	
56		C4-15	$PO_{100}H_{30}A_{20}$ + CMC_{20}-Hzd + Dextran-Hzd + Chitosan-Hzd	
57		C5-1	$PO_{100}H_{30}$ + $PO_{100}H_{30}C_{20}$ + CMC_{20}-Hzd + CMC_{20}-Hzd + Dextran-Hzd	
58	C_6^5	C5-2	$PO_{100}H_{30}$ + $PO_{100}H_{30}C_{20}$ + CMC_{20}-Hzd + CMC_{20}-Hzd + Chitosan-Hzd	12 μL
59		C5-3	$PO_{100}H_{30}$ + $PO_{100}H_{30}C_{20}$ + CMC_{20}-Hzd + Dextran-Hzd + Chitosan-Hzd	
60		C5-4	$PO_{100}H_{30}$ + $PO_{100}H_{30}C_{20}$ + CMC_{20}-Hzd + Dextran-Hzd + Chitosan-Hzd	
61		C5-5	$PO_{100}H_{30}$ + $PO_{100}H_{30}A_{20}$+ CMC_{20}-Hzd + Dextran-Hzd + Chitosan-Hzd	
62		C5-6	$PO_{100}H_{30}C_{20}$ + $PO_{100}H_{30}A_{20}$+ CMC_{20}-Hzd + Dextran-Hzd + Chitosan-Hzd	
63	C_6^6	C6-1	$PO_{100}H_{30}$ + $PO_{100}H_{30}C_{20}$ + $PO_{100}H_{30}A_{20}$ + CMC_{20}-Hzd + Dextran-Hzd + Chitosan-Hzd	10 μL

∗ The combinations of hydrazide polymers listed above were each mixed with a single aldehyde precursor polymer ($PO_{100}A_{30}$, 60 μL) to facilitate gelation. The total volume of each gel was 120 μL.

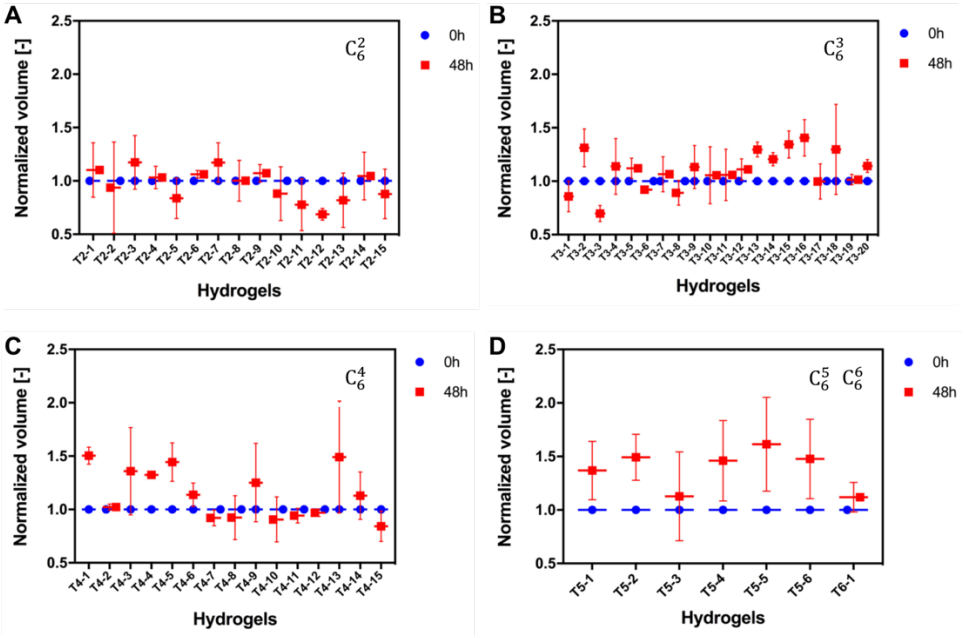

Figure S3.4 Volume-based swelling ratios of combinatorial thermoresponsive vs. non-thermoresponsive hydrogels (T series) before and after swelling for 48 hours in 10 mM PBS at room temperature (22 °C) (n=4). The gel composition corresponding to each label along the x-axis can be referenced in Table S1.

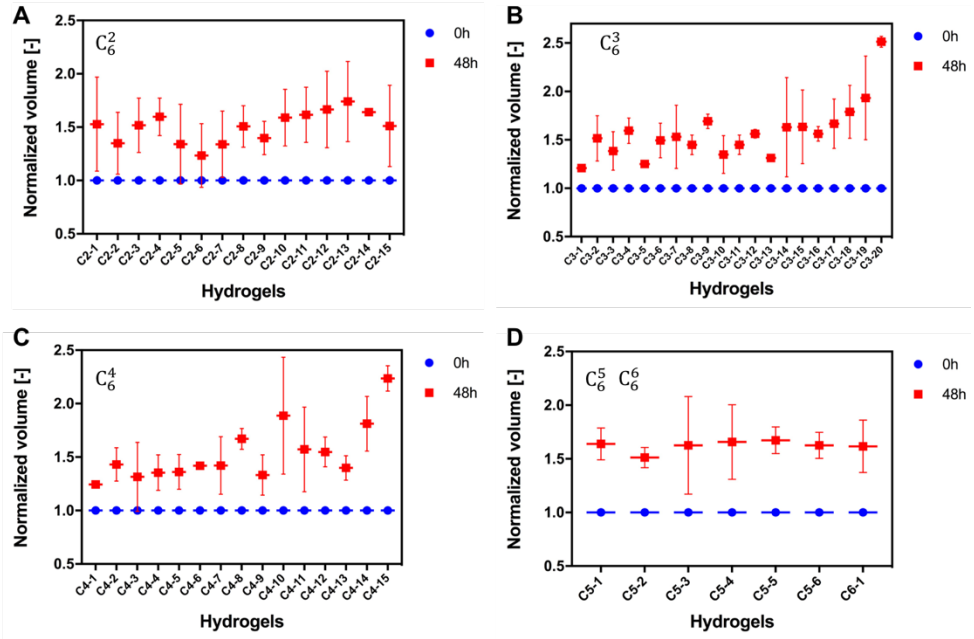

Figure S3.5 Volume-based swelling ratios of combinatorial charged vs. neutral hydrogels (C series) before and after swelling for 48 hours in 10 mM PBS at room temperature (22 °C) (n=4). The gel composition corresponding to each label along the x-axis can be referenced in Table S2.

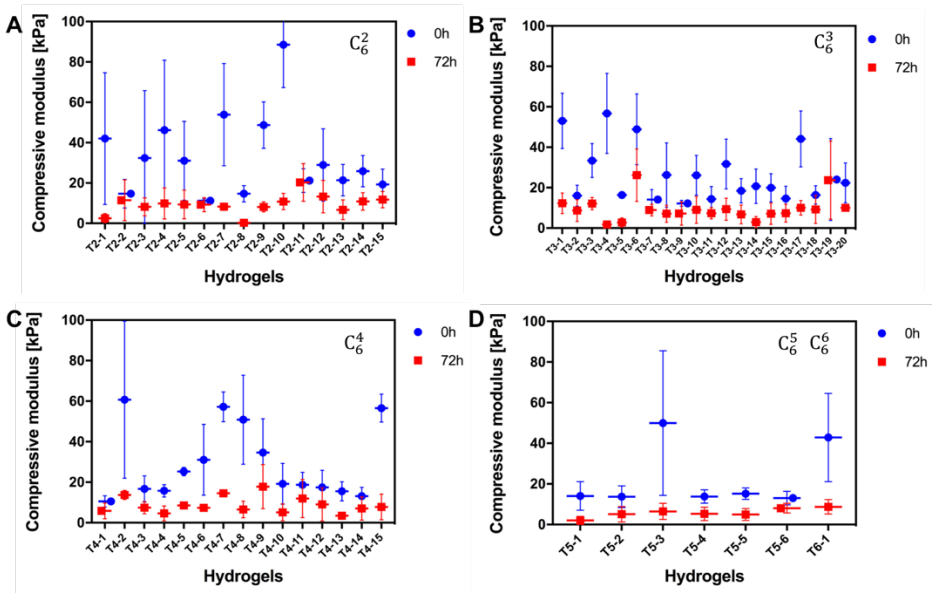

Figure S3.6 Compressive moduli of combinatorial thermoresponsive vs. non-thermoresponsive hydrogels (T series) immediately after fabrication (blue, corresponding to the reported compressive modulus results in Fig. S1) and after 72 hours immersed in 100 mM HCl (red, corresponding to the reported degradation results) at room temperature (22 °C) (n=4). The gel composition corresponding to each label along the x-axis can be referenced in Table S1.

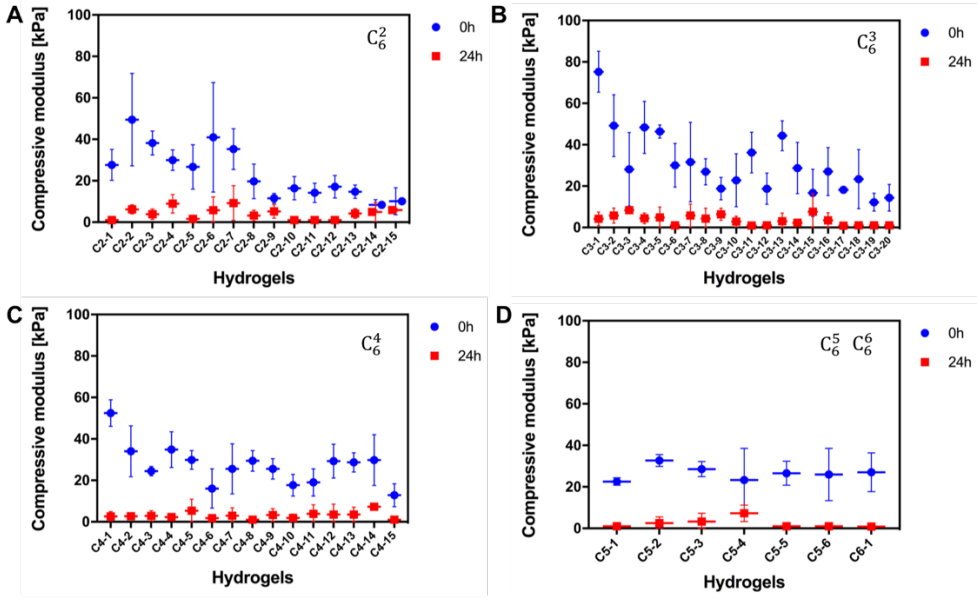

Figure S3.7 Compressive moduli of combinatorial charged vs. neutral hydrogels (C-series) immediately after fabrication (blue, corresponding to the reported compressive modulus results) and after 72 hours immersed in 100 mM HCl (red, corresponding to the reported degradation results) at room temperature (22 °C) (n=4). The gel composition corresponding to each label along the x-axis can be referenced in Table S2

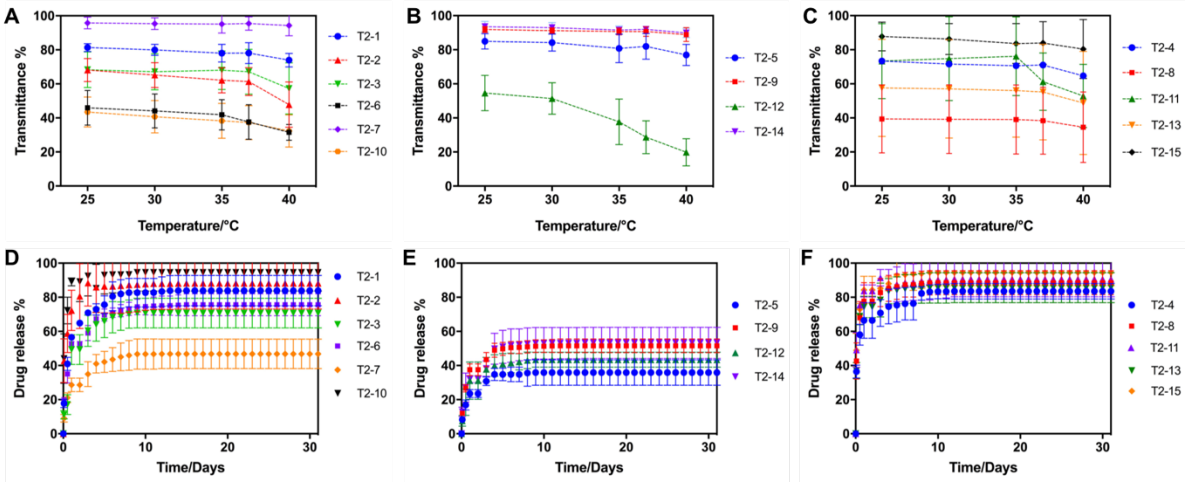

Figure S3.8 Transmittance (A-C) and ovalbumin release kinetics (D-F) of two-component thermoresponsive vs. non-thermoresponsive (T series) combinatorial hydrogels containing (A,D) various combinations of only POEGMA-Hzd precursor polymers with different phase transition temperatures; (B,E) CMC-Hzd as one of the precursor polymers; and (C-F) PNIPAM-Hzd as one of the precursor polymers. The full gel composition corresponding to each label in the legend can be referenced in Table S1. Protein release was measured in 10 mM PBS at 37 °C (n=4).

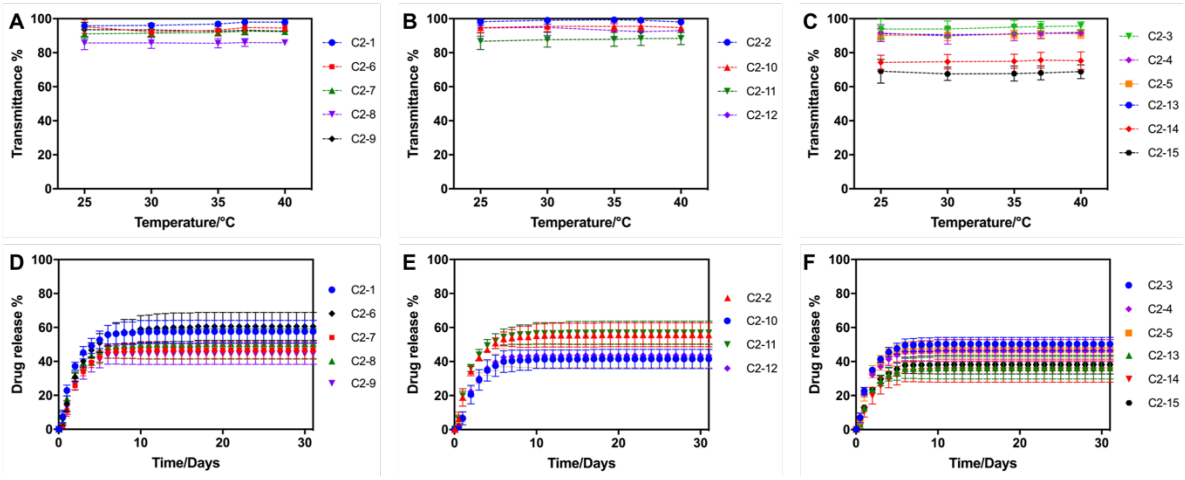

Figure S3.9 Transmittance (A-C) and ovalbumin release kinetics (D-F) of two-component charged vs. neutral (C-series) combinatorial hydrogels containing (A,D) $PO_{100}H_{30}C_{20}$ (cationic) as one of the precursor polymers; (B,E) $PO_{100}H_{30}A_{20}$ (anionic) as one of the precursor polymers; and (C,F) neither $PO_{100}H_{30}C_{20}$ nor $PO_{100}H_{30}A_{20}$ as one of the precursor polymers. The full gel composition corresponding to each label in the legend can be referenced in Table S2. Protein release was measured in 10 mM PBS at 37 °C (n=4).

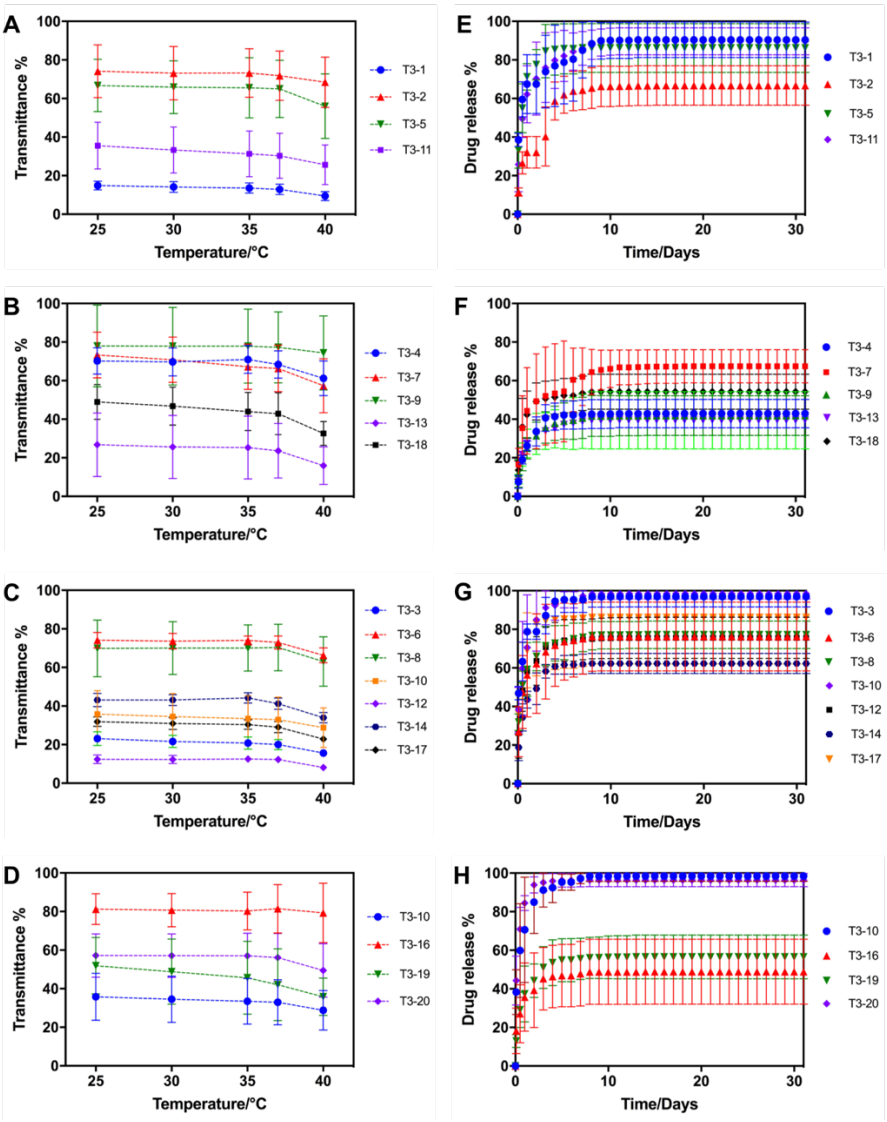

Figure S3.10 Transmittance (A-D) and ovalbumin release kinetics (E-H) of three-component thermoresponsive vs. non-thermoresponsive (T series) combinatorial hydrogels containing (A,E) various combinations of only POEGMA-Hzd precursor polymers with different phase transition temperatures; (B,F) POEGMA-Hzd and CMC-Hzd as two of the precursor polymers; (C,G) POEGMA-Hzd and PNIPAM-Hzd as two of the precursor polymers; and (D,H) CMC-Hzd and PNIPAM-Hzd as two of the precursor polymers. The full gel composition corresponding to each label in the legend can be referenced in Table S1. Protein release was measured in 10 mM PBS at 37 °C (n=4).

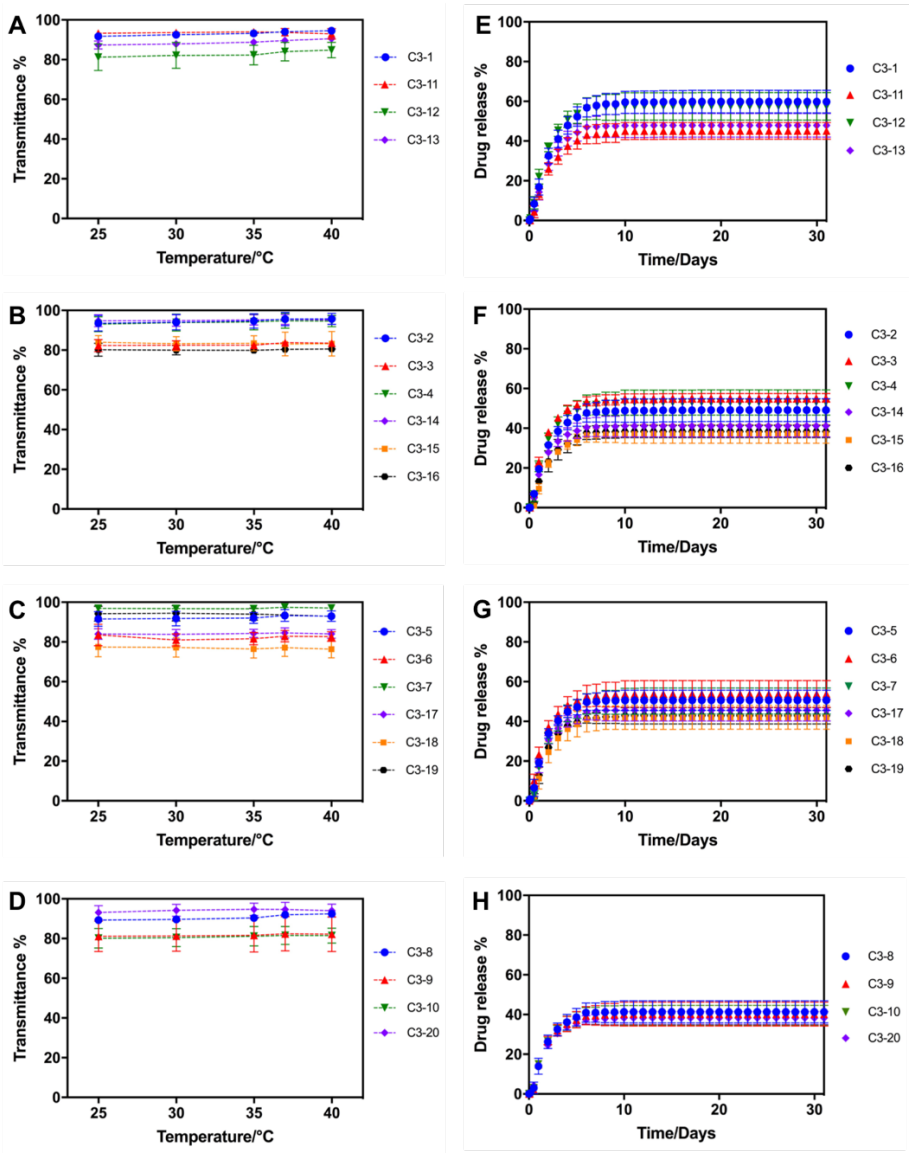

Figure S3.11 Transmittance (A-D) and ovalbumin release kinetics (E-H) of three-component charged vs. neutral (C series) combinatorial hydrogels containing (A,E) both synthetic charged polymers $PO_{100}H_{30}C_{20}$ and $PO_{100}H_{30}A_{20}$; (B,F) $PO_{100}H_{30}C_{20}$ but not $PO_{100}H_{30}A_{20}$ included; (C,G) $PO_{100}H_{30}A_{20}$ but not $PO_{100}H_{30}C_{20}$ included; and (D,H) neither $PO_{100}H_{30}C_{20}$ or $PO_{100}H_{30}A_{20}$ included. The full gel composition corresponding to each label in the legend can be referenced in Table S2. Protein release was measured in 10 mM PBS at 37 °C (n=4).

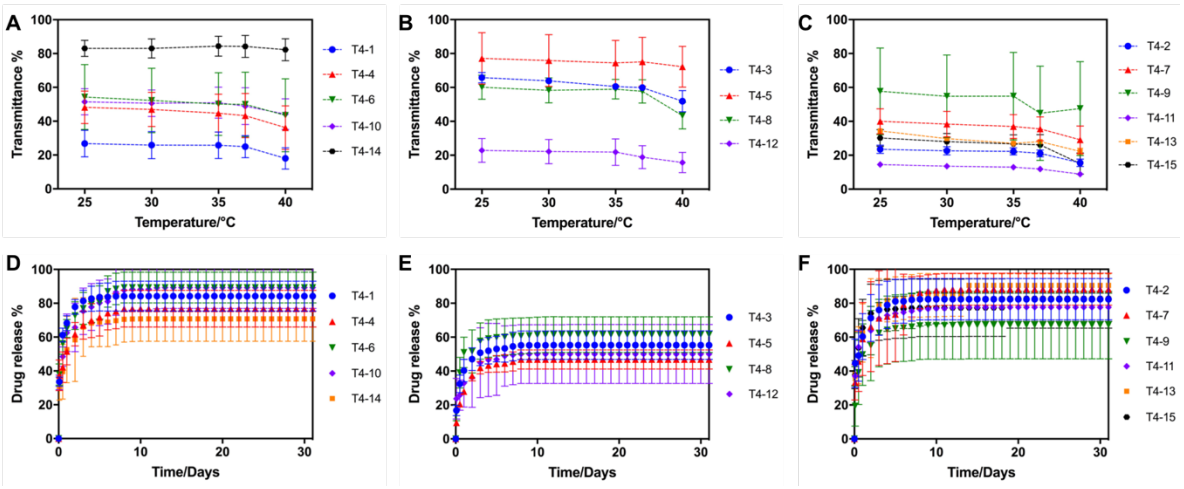

Figure S3.12 Transmittance (A-C) and ovalbumin release kinetics (D-F) of four-component thermoresponsive vs. non-thermoresponsive (T series) combinatorial hydrogels containing (A,D) various combinations of only POEGMA-Hzd precursor polymers with different phase transition temperatures; (B,E) CMC-Hzd but no PNIPAM-Hzd; and (C,F) both PO_0H_{30} and PNIPAM-Hzd. The full gel composition corresponding to each label in the legend can be referenced in Table S1. Protein release was measured in 10 mM PBS at 37 °C (n=4).

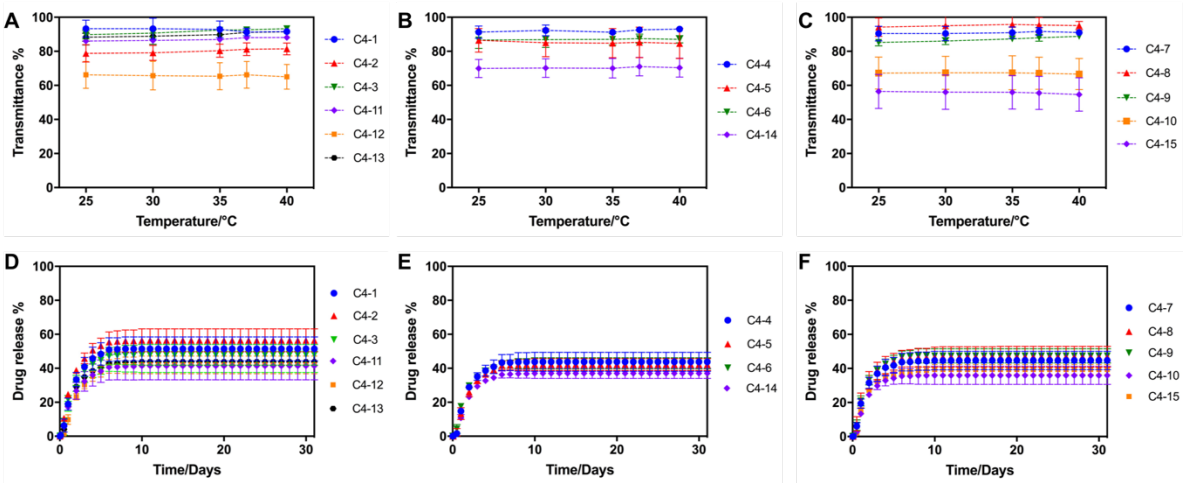

Figure S3.13 Transmittance (A-C) and ovalbumin release kinetics (D-F) of four-component charged vs. neutral (C series) combinatorial hydrogels including (A,D) both synthetic charged polymers $PO_{100}H_{30}C_{20}$ and $PO_{100}H_{30}A_{20}$; (B,E) $PO_{100}H_{30}C_{20}$ but no $PO_{100}H_{30}A_{20}$; (C,F) $PO_{100}H_{30}A_{20}$ but no $PO_{100}H_{30}C_{20}$. The full gel composition corresponding to each label in the legend can be referenced in Table S2. Protein release was measured in 10 mM PBS at 37 °C (n=4).

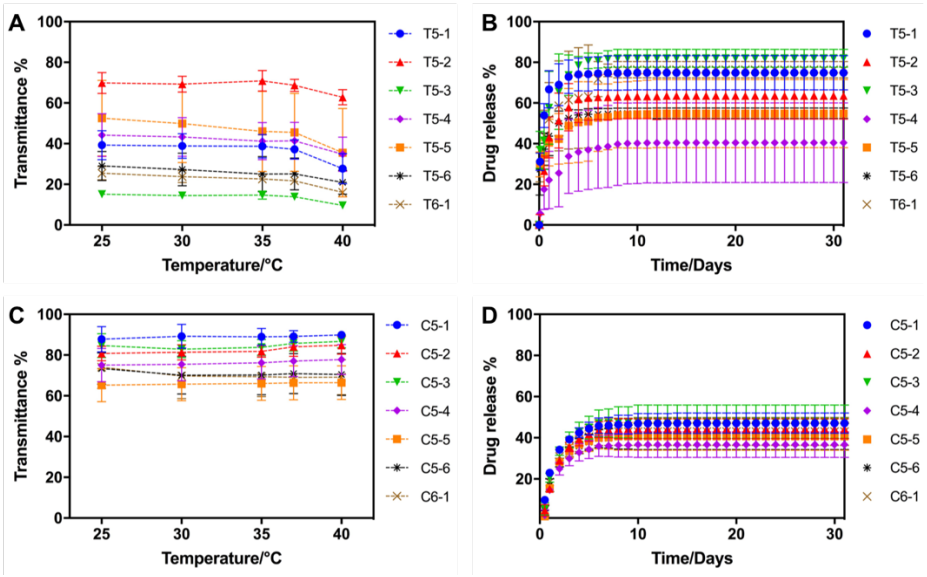

Figure S3.14. Transmittance (A, C) and ovalbumin release kinetics (B, D) of five-component and six-component thermoresponsive vs. non-thermoresponsive (T series, A-B) and charged vs. neutral (C series, C-D) combinatorial hydrogels. The full gel composition corresponding to each label in the legend can be referenced in Tables S1 (A,B) and S2 (C,D). Protein release was measured in 10 mM PBS at 37 °C (n=4).

Chapter 4

Reactive Electrospinning of Degradable Poly(oligoethylene glycol methacrylate)-Based Nanofibrous Hydrogel Networks

Abstract

A direct, all-aqueous electrospinning method for fabricating degradable nanofibrous hydrogel networks is reported in which hydrazide and aldehyde-functionalized poly(oligoethylene glycol methacrylate) (POEGMA) polymers are simultaneously electrospun and cross-linked. The resulting networks are spatially well-defined, mechanically stable (both dry and wet), and offer extremely fast swelling responses, suggesting potential utility as smart hydrogels and tunable tissue engineering matrices.

Keywords: Reactive electrospinning; Hydrogel; Nanofiber; POEGMA

4.1 Introduction

Hydrogels have attracted significant attention in biomedical applications due to their physicochemical and mechanical similarities to native extracellular matrix (ECM). While most hydrogels studied in this context have relatively homogeneous networks with pore sizes on the tens of nanometre scale, native ECM typically consists of gels constructed from a matrix of protein nanofibrils (primarily based on collagen and elastin). This fibrous structure has been demonstrated to play a key role in regulating how cells interact with the native ECM, influencing cell adhesion, spreading, and propagation.[1] However, replicating this nanofibrous hydrogel structure *in vitro,* particularly with synthetic polymers that offer the advantages of potentially reduced

immunogenicity and increased tunability compared to natural polymers, has generally been challenging. Several examples of peptide-based nanofibrous hydrogels have been reported that exploit either the innate self-assembly of peptides or the directed self-assembly of typically hydrophobically modified peptides.[2–4] Research has also been done using synthetic small molecule amphiphiles[5,6] and synthetic block copolymers[7] as gelators to form nanofibrous hydrogels, although the physical nature of such self-assembly offers challenges for tuning hydrogel mechanics and stability to match specific application needs.

As an alternative to these physical self-assembly mechanisms for nanofiber formation, electrospinning represents a versatile technique for nanofiber preparation due to its low cost, high-throughput, and ready tunability based on changing process conditions (e.g. flow rates, voltages, collector distances)[8] While conventional electrospinning approaches generate solid nanofibers based on the rapid evaporation of volatile organic solvents between the spinner nozzle and the collector, organic solvent use limits the direct applicability of such methods in cell applications. Aqueous electrospinning of water-soluble polymers to form nanofibrous hydrogels is possible[9,10] but requires a method to stabilize the nanofibers (applied either during or after the spinning process) to form a hydrogel and prevent rapid dissolution upon re-exposure to water[11]. A variety of crosslinking methods have been reported, including chemical post-crosslinking by glutaraldehyde vapour[12,13] or by genipin[14] following nanofiber spinning, *in situ* crosslinking by glutaraldehyde using HCl as a catalyst[15] or maleic acid using vitriolic acid as catalyst[16], photocrosslinking by UV light during electrospinning[17–19] or physical crosslinking by heat treatment following electrospinning[20]. However, these methods may induce cytotoxicity, limiting their biomedical use. In addition, any post-treatment method mandates an additional processing step, and the resulting crosslink is either non-degradable (glutaraldehyde, photocrosslinking) or non-covalent. In this context, a single-step aqueous electrospinning method enabling production of a degradable, covalently crosslinked nanofibrous scaffold would be beneficial. The only such example is the work of Ji

et al., who used Michael chemistry between thiolated hyaluronic acid and polyethylene glycol diacrylate to produce a nanofibrous hydrogel with promising cell migration and adhesion properties.[21,22] However, translation of this approach to synthetic polymers with non-degradable backbones would result in a non-degradable scaffold, again limiting biomedical applications.

Recently, we have reported injectable, covalently cross-linked poly(ethylene glycol) (PEG)-analogue hydrogels based on poly(oligoethylene glycol methacrylate) (POEGMA) formed via *in situ* gelation of low molecular weight precursor polymers functionalized with hydrazide and aldehyde functional groups. Poly (ethylene glycol) (PEG) is a hydrophilic, non-immunogenic, non-cytotoxic, and highly protein-repellent polymer[23–25], and PEG-based hydrogels are thus among the most widely used synthetic biomaterials for tissue engineering.[26,27] POEGMA offers many of the same properties as PEG (i.e. hydrophilicity, non-cytotoxicity, low protein adsorption)[28,29] but can be polymerized using standard free radical chemistries, enabling facile functionalization of POEGMA-based networks to tune the mechanical and biological properties as desired. With our particular approach, covalent crosslinking of hydrazide and aldehyde-functionalized precursor polymers via the formation of hydrolytically and enzymatically-degradable hydrazone bonds offers additional advantages. Hydrazone bond formation facilitates rapid gelation and tunable degradation according to the structure and reactive functional group density of the POEGMA precursor polymer. The absence of any small molecule crosslinkers or need for heat/UV light to facilitate gelation promotes higher cytocompatibility relative to other possible strategies, with cell viability demonstrated in both 2D and 3D culture.[30] The ease of functionalizing POEGMA backbones by copolymerization enables conjugation of controlled densities of cell adhesion-modifying peptides or other ligands to engineer the cell-hydrogel interface.[30] Furthermore, depending on the length of the oligo(ethylene glycol) side chain in the OEGMA monomer used, the hydrogel can be engineered to exhibit "smart" thermoresponsive properties that can further be applied to (for example)

dynamically tune cell-gel interactions[31] or facilitate environmentally-responsive drug delivery.[32] Of note, given the typically sluggish swelling kinetics of thermoresponsive bulk hydrogels, the formation of nanofibrous (macroporous) hydrogels based on POEGMA in a single step without requiring any pore-forming additives offers potential to enhance the rate and reversibility of thermal swelling/deswelling transitions[33] while maximizing the network cytocompatibility.

4.2 Materials and Methods

4.2.1 Materials

Poly (ethylene oxide) (PEO, M_w = 600,000 g/mol) was purchased from Sigma-Aldrich. Oligo(ethylene glycol) methyl ether methacrylate (OEGMA, M_n = 475 g/mol, Sigma Aldrich, 95%) was purified by passing through a column of basic aluminum oxide (Sigma Aldrich, type CG-20) to remove the methyl ether hydroquinone (MEHQ) and butylated hydroxytoluene (BHT) inhibitors. Acrylic acid (AA, Sigma Aldrich, 99%), 2,2-azobisisobutryic acid dimethyl ester (AIBMe, Wako Chemicals, 98.5%), dioxane (Caledon Labs, 99%), adipic acid dihydrazyde (ADH, Alfa Aesar, 98%), N'-ethyl-N-(3-dimethylaminopropyl)-carbodiimide (EDC, Carbosynth, Compton CA, commercial grade), aminoacetaldehyde dimethyl acetal (Sigma Aldrich, 99%), methacryloyl chloride (Sigma Aldrich, purum), rhodamine 123 (Sigma Aldrich, 85%), and fluorescein isothiocyanate (FITC, Sigma Aldrich, 90%) were all used as received. For all experiments, Milli-Q grade distilled deionized water (DIW) was used. N-(2,2-dimethoxyethyl)methacrylamide (DMEMAm) was synthesized as previously reported (see N. M. B. Smeets, E. Bakaic, M. Patenaude and T. Hoare, Chem. Commun., 2014, 50, 3306–3309).

4.2.2 Synthesis of POEGMA precursors

Synthesis of hydrazide-functionalized POEGMA (POH): AIBMe (37 mg, 0.16 mmol), OEGMA (4.0 g, 8.4 mmol), AA (0.25 g, 3.5 mmol) and dioxane (20 mL) were added to a 50 mL Schlenk three-neck flask and were purged with nitrogen for 30 minutes. Subsequently the solution was placed in an oil bath at 75 °C for 4 hours under magnetic

stirring. After removing the solvent, poly(OEGMA-*co*-AA) polymer was purified by dialysis (6+ hours for 6 cycles) and lyophilized. The purified copolymer was dissolved in 100 mL DIW, after which ADH (2.65 g, 15.2 mmol) and EDC (1.18 g, 7.6 mmol) were added to the polymer solution. The pH of the solution was adjusted to pH = 4.75 using 0.1 M HCl continually over the reaction until the pH stabilized (~ 4 hours). The solution was stirred overnight and then purified by dialysis (6+ hours for 6 cycles). The final polymer was obtained by lyophilization and was stored as a 15 w/w% solution in DIW at 4 °C.

Synthesis of aldehyde-functionalized POEGMA (POA): AIBMe (50 mg, 0.22 mmol), OEGMA (4.0 g, 8.4 mmol), DMEMAm (0.60 g, 3.5 mmol) and dioxane (20 mL) were added to a 50 mL Schlenk three-neck flask and purged with nitrogen for 30 minutes. Subsequently the solution was placed in an oil bath at 75 °C for 4 hours under magnetic stirring. After removing the solvent, poly(OEGMA-*co*-DMEMAm) was dissolved in 100 mL of 0.25 M HCl. The solution was stirred for 24 hours and then purified by dialysis (6+ hours for 6 cycles). The final product was obtained by lyophilization and was stored as a 15 w/w% solution in DIW at 4 °C.

4.2.3 Characterization of reactive precursor polymers

The molecular weight of the precursor polymers was analyzed using gel permeation chromatography (GPC) (Waters, Mississauga, ON). Aqueous GPC was performed with a system consisting of a Waters 515 HPLC pump, Waters 717 plus Autosampler and three columns (Waters Ultrahydrogel-120, -250, -500; 7.8 × 300 mm; 6 μm particles). Samples run in an aqueous buffer consisting of 0.5 M sodium nitrate and 25 mM 2-(cyclohexylamino) ethanesulfonic acid maintained at pH 10.0 at 30 °C. The degree of hydrazide functionalization in POH was determined by conductometric base-into-acid titration (Mantech), comparing the number of –COOH groups in the polymer before and after functionalization. The degree of aldehyde functionalization in POA was determined by ^{1}H-NMR (600 MHz, Bruker), taking the ratio of the aldehyde proton signal at 9.52 ppm to the

methyl proton signal at 0.81 ppm. The resulting properties of the POH and POA pre-polymers are summarized in Table S4.1.

4.2.4 Synthesis of fluorescein isothiocyanate (FITC)-labeled POH

FITC-labeled POH was prepared by reacting FITC (5 mg) with POH solution (1 g, 15 w/w% in DIW) under magnetic stirring for 12 hours at room temperature. A total of 2 mol% of the available hydrazide groups were targeted for labelling with FITC. The solution was dialyzed (6+ hours for 6 cycles) and lyophilized. FITC-labeled POH was stored at 15 w/w% in DIW at 4°C. All reaction vessels and storage containers were covered by aluminum foil to prevent photobleaching.

4.2.5 Synthesis of rhodamine 123-labeled POA

Rhodamine 123-labeled POA was prepared by reacting rhodamine 123 (5 mg) with POA solution (1g, 15 w/w% in DIW) under magnetic stirring for 24 hours. Sodium cyanoborohydride (8.25 mg, 10 mol eq. to rhodamine 123) was then added to the solution to generate a stable conjugate via reductive amination, after which the solution was stirred for another 48 hours. The resulting polymer solution was dialyzed (6+ hours for 6 cycles) and lyophilized to dryness. The rhodamine 123-labeled POA was stored at 15w/w% in in DIW at 4 °C. All reaction vessels and storage containers were covered by aluminum foil to prevent photobleaching.

4.2.6 Preparation of electrospun nanofibrous hydrogel

PEO (2.5 w/w%) and either POH or POA (7.5 w/w%) were co-dissolved in DIW, with the resulting PEO/POH and PEO/POA solutions subsequently loaded into separate barrels of a double barrel syringe equipped with a static mixer followed by a blunt-tip 18 G needle. A voltage of 8.5 kV was applied to the tip of the blunt needle. Aluminum foil and aluminum disk were used as collectors for electrospinning, the former for collecting films and the latter for collecting thicker scaffolds. The distance between the needle and the collector was maintained at 10 cm. All electrospun scaffolds were prepared at room temperature.

4.2.7 Differential scanning calorimetry (DSC) analysis

DSC experiments were conducted using Auto Q20 (TA Instruments) to assess the efficacy of the swelling step for removing the PEO electrospinning aid. First, all samples were heated to 150 °C at a rate of 10 °C/min to eliminate any thermal history. Second, all samples were cooled down to 20 °C at a rate of 5 °C/min and subsequently heated back to 150 °C at a rate of 2 °C/min. Figure S4.2 shows that melting point endotherms were observed with maximum absolute values of 66 °C and 63 °C for PEO and POH/POA+PEO electrospun nanofiber thermograms respectively due to the crystallization of the high molecular weight PEO; in contrast, a POH/POA bulk hydrogel (prepared without PEO and lyophilized to dryness to match the dry state of the nanofibers) exhibits no transition whatsoever. After the POH/POA+PEO electrospun scaffold was immersed in DIW overnight and then lyophilized, the endotherm disappeared, suggesting that the PEO electrospinning aid could effectively be removed by swelling the scaffold. Note that the degradation results as well as SEM imaging of the scaffolds following the 24 hour time over which DSC indicated complete removal of the PEO fraction (Figure S4.3) confirm the scaffold remained intact during this time, again confirming that POH/POA gelation is occurring in this electrospun system.

4.2.8 Microscopy

Optical microscopy of the nanofibrous hydrogels was conducted using a Nikon Eclipse LV100N POL epifluorescence microscope (Nikon Instruments, Mississauga, Ontario, 10× objective lens) that enables direct imaging of the hydrogel when swollen in 10 mM phosphate buffered saline. Nanostructural analysis of the nanofibrous hydrogels in the dry state was conducted using scanning electron microscopy (SEM, Tecan Vega II LSU instrument) using an operating voltage of 10 kV. Samples were imaged directly following electrospinning or lyophilized immediately after swelling in water and sputter-coated with a ~30 nm gold layer prior to imaging to prevent charging. Co-localization of hydrazide and aldehyde-functionalized POEGMA within the hydrogel fibers was confirmed by preparing scaffolds using POH-fluorescein and POH-rhodamine (at the same concentrations outlined

above) and observing the resulting scaffolds using confocal laser scanning microscopy (Zeiss LSM 510). Excitation wavelengths of 488 nm (fluorescein) and 543 nm (rhodamine) were used for imaging.

4.2.9 Swelling kinetics

Swelling kinetics were measured at 37 °C in 10 mM PBS at pH 7.4. Electrospun scaffolds were placed into cell culture inserts that were subsequently placed inside a 24-well plate and submerged with 4 mL PBS. At predetermined time intervals, the inserts were removed, excess PBS was wicked off the surface of the hydrogels using a Kimwipe, and the inserts were weighed. The water content was calculated based on this gravimetric data using the equation

$$Swelling\ ratio\ \% = \frac{W_{swollen} - W_{initial}}{W_{initial}} \times 100\%$$

$$Water\ content\ \% = \frac{W_{swollen} - W_{dry}}{W_{swollen}} \times 100\%$$

Error bars represent the standard deviation of the replicate measurements (n=4). Videos of the short-term swelling of PEO-only scaffolds as well as POH/POA+PEO scaffolds are also available as supplementary information for viewing. As a control, a bulk hydrogel prepared with the same overall composition (2.5 wt% PEO, 7.5 wt% of each POEGMA precursor polymer) was prepared via simple injection of the precursors into a silicone mold with comparable thickness to the electrospun sample tested (1.7 ± 0.2 mm height for the bulk gels compared to 0.4 ± 0.1 mm height for the electrospun samples). Note that precisely matching these dimensions is technically difficult using the molding process; however, all samples were kept thin such that the small differences in height would have minimal impact on changing any swelling kinetics measured (at least in comparison to the differences in swelling kinetics measured). The bulk hydrogel sample was dried overnight at room temperature (to match the electrospinning sample treatment), after which its swelling was tested using the same gravimetric method outlined above for the nanofibrous hydrogels.

4.2.10 Degradation kinetics

Degradation kinetics were determined using the same gravimetric method described above for the swelling kinetics measurements but substituting the PBS for 1 M HCl at 37 °C; the acid-catalyzed conditions were selected to provide an effective and rapid assay to compare the degradation of the nanofibrous scaffolds with a corresponding bulk hydrogel prepared as described above for the swelling measurements. Degradation was also tracked in 10 mM PBS as the buffer by continuing to observe the swelling kinetics samples until no residual gel was present in the cell culture insert. In a parallel experiment, samples were collected at different times, immediately lyophilized, and imaged using SEM as per the previously described protocol to track the morphology of the nanofibrous network during degradation. Error bars represent the standard deviation of the replicate measurements (n=4).

4.2.11 Mechanical properties

The tensile properties of dry electrospun scaffolds were tested using a MicroSquisher (CellScale Biomaterials Testing, Waterloo Canada). Samples were mounted via puncture with five pins spaced 0.7 cm apart, then pulled to 10% (swollen samples) or 20% (dry samples) elongation and subsequently allowed to relax. At least 80 cycles were tested, with loading and recovery durations of 20 seconds used for each cycle. Compressive mechanical properties of the swollen nanofibrous hydrogels were subsequently measured directly in 10 mM PBS buffer at room temperature, also using a MicroSquisher. Cantilevers were fabricated using a 559 μm gauge cantilever and a square, 3 mm stainless steel plate. A displacement of 50% compression was used per cycle, with 40 cycles tested and loading and recovery durations of 20 seconds per cycle applied. Videos showing each micromechanical test performed are uploaded for viewing as supplementary information.

4.2.12 Enzyme Activity

β-galactosidase (β-gal, Grade VI, M_w = 464 kDa, Sigma Aldrich) and alkaline phosphatase (AP, from calf intestine, Roche) was encapsulated in POH/POA+PEO nanofibers directly

during the electrospinning process by dissolving the enzyme in the POH precursor solution at concentrations of 2.65U/mL and 2.5U/mL respectively. The resulting POH/POA+PEO scaffolds were then swollen in 10 mM PBS buffer (pH=7.4) at 37 °C. The released protein concentration was measured using a Bradford protein assay (595 nm, Tecan M 1000 plate reader), while the relative enzyme activity was then assessed by adding the chlorophenol red β-galactopyranoside (CPRG) substrate for β-gal and the 3,3',5,5'-tetramethylbenzidine substrate for AP (without removing the scaffolds) and tracking their conversions at 550 nm and 405 nm, respectively, 30 minutes (β-gal) and 5 minutes (AP) after substrate addition (Tecan M 1000 plate reader). The relative (%) enzyme activity was calculated based on a calibration curve constructed from a fresh solution of the enzyme prepared at the same overall concentration in the same PBS buffer.

4.3 Results and discussion

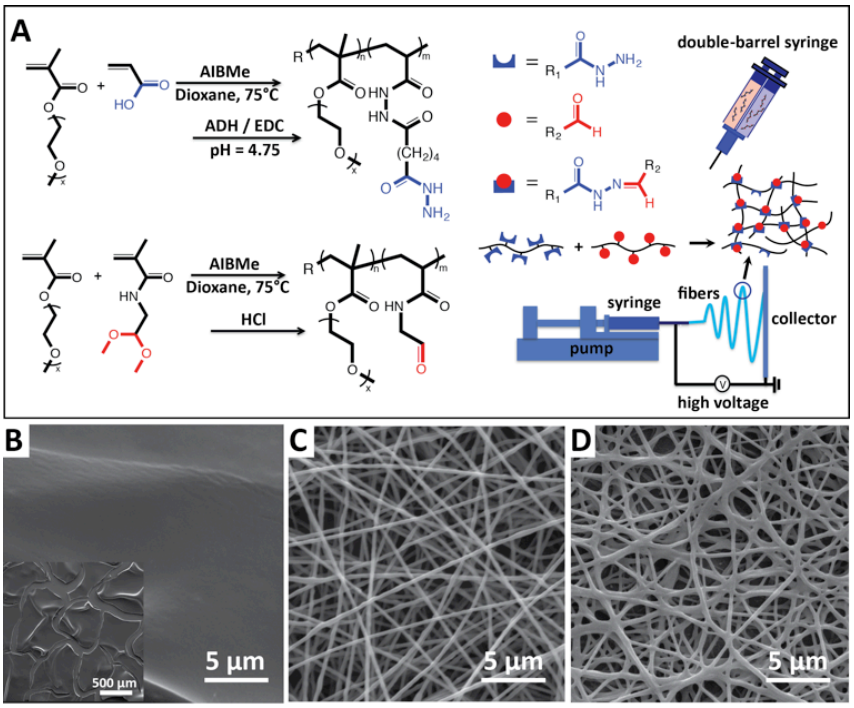

Figure 4.1 Reactive electrospinning of degradable POEGMA hydrogel nanofibers: (A) scheme showing polymer precursor chemistry and electrospinning strategy; (B-D) electrospun POH/POA only (B), PEO only (C), and POH/POA+PEO (D).

To leverage these favorable properties of POEGMA and nanofibrous hydrogels, we have developed a reactive electrospinning process to directly fabricate degradable nanofibrous POEGMA hydrogels in a single step (Figure 4.1A). POEGMA precursor polymers with molecular weights on the order ~30 kDa (to facilitate kidney clearance following gel degradation via hydrolysis, Table S4.1) were functionalized with 30 mol% hydrazide groups (POH, via carbodiimide-mediated adipic acid dihydrazide conjugation to an acrylic acid-functionalized POEGMA polymer) and aldehyde groups (POA, via copolymerization of OEGMA with a diacetal-containing monomer followed by acid-catalyzed cleavage of the diacetal to an aldehyde) following reported protocols.[30] Each polymer was then dissolved at 15% w/v in deionized water and loaded into separate barrels of a double barrel syringe attached to a static mixer with a blunt 18G needle at its outlet. This syringe was mounted on a syringe pump and connected to an electrospinning platform. The bulk gelation time of the POEGMA prepolymers used was ~45 minutes; a flow rate of 8 μL/min was subsequently selected to match the residence time of the polymer in the mixing channel to the gelation rate and thus ensure both spinnability (i.e. minimal increases in viscosity prior to jetting) and stable nanofiber formation on the collector. The increase in polymer concentration during the spinning step assists with enabling both these competing requirements, as a solution just below its gel point can be ejected but then rapidly stabilized via covalent network formation as it is concentrated upon water evaporation. A voltage of 8.5 kV was applied to the conductive needle, with either aluminium foil (for films) or an aluminium disk (for bulk scaffolds) used as a collector (Figure S4.1). Using POEGMA alone (POA/POH, Figure 4.1B) resulted in electrospray at all process conditions tested; we anticipate this observation is a result of both the high hygroscopicity and low entanglement potential of the low molecular weight and highly side chain-branched POEGMA polymer, properties previously shown to inhibit polymer spinnability[34–36]. In response, a small concentration of high molecular weight poly(ethylene oxide) (PEO, M_v = 600×10^3 g/mol, 5% w/v dissolved in deionized water, 1:3 weight ratio PEO:POEGMA) was introduced as an electrospinning aid. The high molecular

weight and chain flexibility of PEO enables its electrospinning from aqueous solutions to form well-defined nanofibers[9,37,38] (Figure 4.1C); furthermore, its chemical similarity to POEGMA facilitates mixing without phase separation during electrospinning or drying. PEO nanofibers alone exhibited a diameter of 287 ± 80 nm (Fig. 4.1C); when PEO was mixed with hydrazide and aldehyde POEGMA precursors (POH/POA+PEO, Figure 4. 1D), a single nanofibrous network with an average fiber diameter of 341 ± 82 nm was achieved, with no evidence of electrosprayed nanoparticle generation visually or microscopically (Figure 4. 1D).

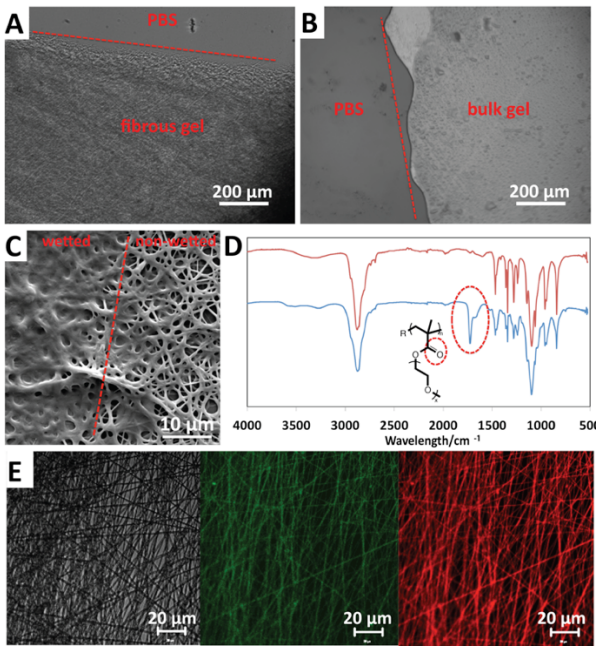

Figure 4.2. Confirmation of hydrogel structure of POH/POA+PEO nanofibers: (A, B) light microscopy images of electrospun nanofibers (A) relative to a bulk hydrogel of the same chemical composition (B) in 10 mM PBS; (C) scanning electron microscopy image of nanofibers dipped halfway in water; (D) ATR-FTIR analysis of PEO-only (red) and POH/POA+PEO (blue) nanofibers; (E) co-localization of POH-fluorescein (488 nm excitation, green) and POA-rhodamine (543 nm excitation, red) throughout nanofiber structure (visible light, grey).

Upon exposure to phosphate buffered saline (PBS), PEO-only nanofibers dissolved fully within one minute; in contrast, the POH/POA+PEO electrospun matrix quickly hydrated and swelled but remained present as a gel matrix (see video in Supplementary

Information). The disappearance of the characteristic PEO phase transition peak at ~65-70°C via differential scanning calorimetry following soaking of the gel in deionized water overnight indicates that PEO electrospinning aid can be effectively removed from the matrix while maintaining the nanofibrous structure (Figs. S4.2 and S4.3). Light microscopy analysis of the swollen fiber mat confirmed the presence of a fibrous structure (Fig. 4.2A) relative to the bulk hydrogel prepared from the same starting components (Fig. 4.2B); furthermore, when half the POA/POH+PEO scaffold was dipped in water, scanning electron microscopy imaging of the subsequently lyophilized sample indicated a clear increase in nanofiber diameter between the swollen (wetted) matrix (1.33 ± 0.20 μm) and the still-dry nanofibers not exposed to water (0.34 ± 0.08 μm), although a textured nanofibrous structure was maintained in the swollen state (Fig. 4.2C). Confocal microscopy of electrospun POH/POA+PEO nanofibers using POH labelled with fluorescein isothiocyanate (green, 488 nm) and POA labelled with rhodamine (red, 543 nm) demonstrated that both fluorescent signals were uniformly present throughout the nanofiber mat (Fig. 4.2E), confirming the co-localization of reactive precursor polymers as required for gelation. The presence of POEGMA in the nanofibers following soaking was also confirmed by ATR-FTIR via the presence of a C=O ester stretch at ~1700 cm-1 corresponding to the attachment point between the methacrylate backbone and the oligo(ethylene glycol) side chains (Fig. 4.2D). Thus, the nanofibers following soaking appear to consist primarily of cross-linked POEGMA and behave as a hydrogel matrix.

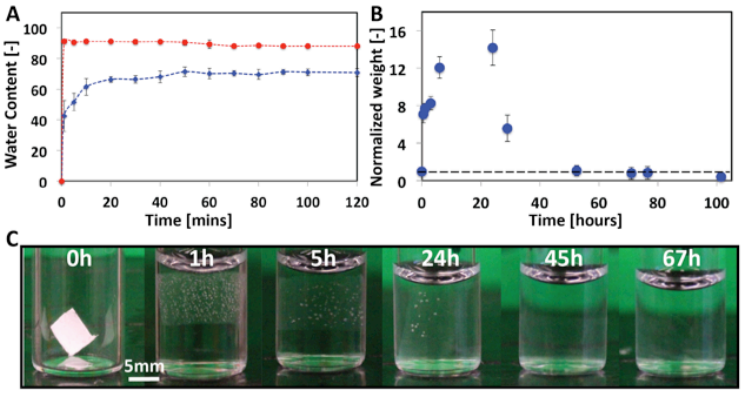

Figure 4.3. Swelling and degradation of POH/POA+PEO nanofibers: (A) swelling of nanofiber mat (red) relative to a bulk hydrogel (blue) of the same composition (PBS, 37°C); (B, C) gravimetric (B) and visual (C) degradation (normalized to initial dry hydrogel mass) of nanofibers (1M HCl, 37°C).

The swelling and degradation properties of the POH/POA+PEO nanofibers were subsequently analysed via gravimetric analysis at 37 °C in 10 mM PBS, mimicking physiological conditions. Swelling of the dry nanofibrous hydrogel mat occurred rapidly, with the maximum water content of ~91 % achieved in less than one minute (Figure 4.3A) followed by minimal deswelling over the next 50 hours (Figure S4.4, likely attributable to diffusion of the PEO out of the matrix and the corresponding loss of osmotic driving force for gel swelling). In comparison, a (pre-dried) bulk hydrogel of the same POH/POA composition required ~2 hours to achieve equilibrium swelling and reached only ~73% water content (Figures 4.3A and S4.4). This rapid and higher-magnitude swelling facilitated by the nanofibrous network structure is of potential interest in barrier applications (e.g. following abdominal surgeries) given that the gel could be stored dry in a mat but quickly re-hydrated to prevent tissue adhesions. In addition, while the transition temperature of the current POEGMA hydrogels is > 90 °C such that it is not functionally thermoresponsive in water[30], we expect precursor polymers with lower LCST values would also exhibit faster and higher magnitude swelling/deswelling responses for the same reason. Incubation of the same dry electrospun network in 1M HCl (to acid-catalyze degradation of hydrazone cross-links under accelerated conditions) results in initial swelling of the gel over the course of ~24 hours (corresponding to a combination of

re-hydration plus swelling due to degradation of the hydrazone cross-links) followed by complete dissolution of the network within ~100 hours (Figures 4.3B and 4.3C). SEM indicates a loss of fibrous morphology over this same time period (Figure S4.5), consistent with degradation. Similar experiments in PBS indicated complete dissolution of the network over 8-10 weeks. Based on our previous work[31], the degradation kinetics could be further adjusted if desired by changing the number of reactive functional groups on POH and/or POA or the concentration of POEGMA used to prepare the nanofibers.

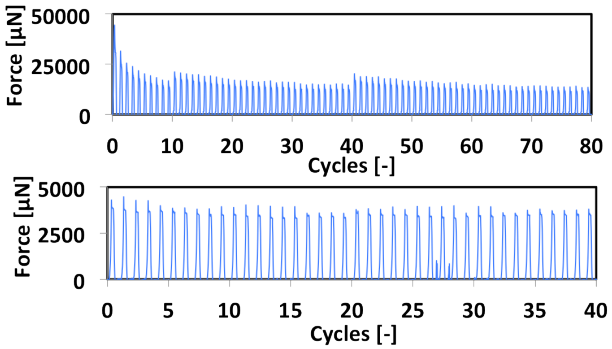

Figure 4.4. Mechanical properties of POH/POA+PEO nanofibers: (A) tensile cycling of dry nanofiber mat (80 cycles, 20% elongation/cycle, top); (B) compressive cycling of swollen nanofiber network (PBS, 40 cycles, 50% compression/cycle, bottom).

The resulting nanofiber hydrogels are mechanically strong and coherent in both the wet and dry states, at least relative to other hydrogel-based systems, and could be physically handled with ease. Tensile cycling of the dry POH/POA+PEO scaffold was performed using a MicroSquisher (CellScale Biomaterials Testing) by mounting the scaffold via 5 puncture pins and performing cyclic 20% stretching experiments in tensile mode. While significant plastic deformation was observed over the first 6 cycles (reducing the peak force observed by roughly one half), the dry matrix remained intact after 80 cycles, with full elastic recovery of the matrix observed each cycle following the initial deformation period (Figures 4.4A and S4.6a). Tensile testing of the 10 mM PBS-swollen POH/POA+PEO gel (10% elongation) over >300 cycles yielded a tensile modulus of ~0.3 kPa (Table S4.2, Figure S4.7), while

compression testing (50% compression) yielded an elastic modulus of 2.1 kPa maintained over at least 40 cycles with minimal hysteresis (Figures 4.4B and S4.4b). Note that a bulk hydrogel with the same overall composition has a compressive modulus of 4.8 kPa under the same testing conditions (Table S4.3); furthermore, the compressive modulus of the bulk hydrogel is constant as a function of the compressive strain while nanofibrous hydrogels show higher moduli at higher % compressions as the space between the nanofibers is compressed (Table S4.3). Thus, nanofibrous gels have mechanics relevant for use in both the wet and dry states. Finally, direct encapsulation of alkaline phosphatase (AP) or β-galactosidase (β-gal) by mixing the enzyme in the POH solution prior to electrospinning indicated that the scaffolds can maintain >80% (AP) or ~60% (β-gal) activity in the released enzyme fraction over multiple days. (Figure S4.8). This activity retention is significantly higher than achieved with conventional electrospinning[39] and is this suggestive of the relative inertness of this method to biomolecules.

4.4 Conclusions

In summary, a single-step, all-aqueous reactive electrospinning process is demonstrated to successfully produce synthetic degradable nanofibrous hydrogels based on poly(oligoethylene glycol methacrylate) without the need for solvents or external cross-linkers. The POEGMA/PEO electrospun nanofibers swell rapidly (reaching equilibrium within one minute, compared to ~2 hours for a bulk hydrogel of the same composition), degrade over the period of ~2 days in acidic conditions and ~8 weeks in physiological buffer (with the potential to tune this degradation rate by polymer modification), and exhibit relevant mechanical properties for biomedical use. We anticipate possible applications of these nanofibrous hydrogel scaffolds in both the dry state (wound dressings, barrier materials) and the wet state (tissue engineering matrices, drug delivery).

4.5 Acknowledgements

Funding from the Natural Sciences and Engineering Research Council of Canada and the NSERC CREATE-IDEM (Integrated Development of Extracellular Matrices) training program is gratefully acknowledged. José Moran-Mirabal is thanked for use of his electrospinning equipment and helpful advice.

4.6 Reference

(1) Stevens, M. M.; George, J. H. Exploring and Engineering the Cell Surface Interface. *Science* **2005**, *310* (November), 1135–1138.

(2) O'Leary, L. E. R.; Fallas, J. a.; Bakota, E. L.; Kang, M. K.; Hartgerink, J. D. Multi-Hierarchical Self-Assembly of a Collagen Mimetic Peptide from Triple Helix to Nanofibre and Hydrogel. *Nature Chemistry*. Nature Publishing Group 2011, pp 821–828.

(3) Luo, J.; Tong, Y. W. Self-Assembly of Collagen-Mimetic Peptide Amphiphiles into Biofunctional Nanofiber. *ACS Nano* **2011**, *5* (10), 7739–7747.

(4) Wu, E. C.; Zhang, S.; Hauser, C. a E. Self-Assembling Peptides as Cell-Interactive Scaffolds. *Adv. Funct. Mater.* **2012**, *22* (3), 456–468.

(5) Vemula, P. K.; Kohler, J. E.; Blass, A.; Williams, M.; Xu, C.; Chen, L.; Jadhav, S. R.; John, G.; Soybel, D. I.; Karp, J. M. Self-Assembled Hydrogel Fibers for Sensing the Multi-Compartment Intracellular Milieu. *Sci. Rep.* **2014**, *4*, 4466.

(6) Jayawarna, V.; Ali, M.; Jowitt, T. a.; Miller, A. F.; Saiani, A.; Gough, J. E.; Ulijn, R. V. Nanostructured Hydrogels for Three-Dimensional Cell Culture through Self-Assembly of Fluorenylmethoxycarbonyl-Dipeptides. *Adv. Mater.* **2006**, *18* (5), 611–614.

(7) Blanazs, A.; Verber, R.; Mykhaylyk, O. O.; Ryan, A. J.; Heath, J. Z.; Douglas, C. W. I.; Armes, S. P. Sterilizable Gels from Thermoresponsive Block Copolymer Worms. *J. Am. Chem. Soc.* **2012**, *134* (23), 9741–9748.

(8) Greiner, A.; Wendorff, J. H. Electrospinning: A Fascinating Method for the Preparation of Ultrathin Fibers. *Angew. Chemie - Int. Ed.* **2007**, *46* (30), 5670–5703.

(9) Doshi, J.; Reneker, D. H. Electrospinning Process and Applications of Electrospun Fibers. *Conf. Rec. 1993 IEEE Ind. Appl. Conf. Twenty-Eighth IAS Annu. Meet.* **1993**, *35*, 151–160.

(10) Yang, Y.; Jia, Z.; Li, Q.; Guan, Z. Experimental Investigation of the Governing Parameters in the Electrospinning of Polyethylene Oxide Solution. *IEEE Trans. Dielectr. Electr. Insul.* **2006**, *13* (3), 580–584.

(11) Yao, L.; Haas, T. W.; Guiseppi-Elie, A.; Bowlin, G. L.; Simpson, D. G.; Wnek, G. E. Electrospinning and Stabilization of Fully Hydrolyzed Poly(Vinyl Alcohol) Fibers. *Chem. Mater.* **2003**, *15* (9), 1860–1864.

(12) Schiffman, J. D.; Schauer, C. L. Cross-Linking Chitosan Nanofibers. *Biomacromolecules* **2007**, *8* (2), 594–601.

(13) Rho, K. S.; Jeong, L.; Lee, G.; Seo, B.-M.; Park, Y. J.; Hong, S.-D.; Roh, S.; Cho, J. J.; Park, W. H.; Min, B.-M. Electrospinning of Collagen Nanofibers: Effects on the Behavior of Normal Human Keratinocytes and Early-Stage Wound Healing. *Biomaterials* **2006**, *27* (8), 1452–1461.

(14) Frohbergh, M. E.; Katsman, A.; Botta, G. P.; Lazarovici, P.; Schauer, C. L.; Wegst, U. G. K.; Lelkes, P. I. Electrospun Hydroxyapatite-Containing Chitosan Nanofibers Crosslinked with Genipin for Bone Tissue Engineering. *Biomaterials* **2012**, *33* (36), 9167–9178.

(15) Tang, C.; Saquing, C. D.; Harding, J. R.; Khan, S. a. In Situ Cross-Linking of Electrospun Poly(Vinyl Alcohol) Nanofibers. *Macromolecules* **2010**, *43* (2), 630–637.

(16) Qin, X.-H.; Wang, S.-Y. Electrospun Nanofibers from Crosslinked Poly(Vinyl Alcohol) and Its Filtration Efficiency. *J. Appl. Polym. Sci.* **2008**, *109* (2), 951–956.

(17) Kim, S. H.; Kim, S. H.; Nair, S.; Moore, E. Reactive Electrospinning of Cross-Linked Poly(2-Hydroxyethyl Methacrylate) Nanofibers and Elastic Properties of Individual Hydrogel Nanofibers in Aqueous Solutions. *Macromolecules* **2005**, *38* (9), 3719–3723.

(18) Wang, Y.; Cheng, C.; Ye, Y.; Yen, Y.; Chang, F. Bioinspired Photo-Cross-Linked Nanofibers from Uracil- Functionalized Polymers. **2012**, 8–11.

(19) Baştürk, E.; Oktay, B.; Kahraman, M. V. Dual-Crosslinked Thiol-Ene/Sol Gel Hybrid Electrospun Nanowires: Preparation and Characterization. *J. Polym. Res.* **2015**, *22* (7), 133.

(20) Lee, S. J.; Lee, S. G.; Kim, H.; Lyoo, W. S. Improvement of the Water Resistance of Atactic Poly(Vinyl Alcohol) Nanowebs by a Heat Treatment. *J. Appl. Polym. Sci.* **2007**, *106* (5), 3430–3434.

(21) Ji, Y.; Ghosh, K.; Li, B.; Sokolov, J. C.; Clark, R. A. F.; Rafailovich, M. H. Dual-Syringe Reactive Electrospinning of Cross-Linked Hyaluronic Acid Hydrogel Nanofibers for Tissue Engineering Applications. *Macromol. Biosci.* **2006**, *6* (10), 811–817.

(22) Ji, Y.; Ghosh, K.; Shu, X. Z.; Li, B.; Sokolov, J. C.; Prestwich, G. D.; Clark, R. A. F.; Rafailovich, M. H. Electrospun Three-Dimensional Hyaluronic Acid Nanofibrous Scaffolds. *Biomaterials* **2006**, *27* (20), 3782–3792.

(23) Price, M. E.; Cornelius, R. M.; Brash, J. L. Protein Adsorption to Polyethylene Glycol Modified Liposomes from Fibrinogen Solution and from Plasma. *Biochim. Biophys. Acta - Biomembr.* **2001**, *1512* (2), 191–205.

(24) Feng, W.; Zhu, S.; Ishihara, K.; Brash, J. L. Protein Resistant Surfaces: Comparison of Acrylate Graft Polymers Bearing Oligo-Ethylene Oxide and Phosphorylcholine Side Chains. *Biointerphases* **2006**, *1* (1), 50.

(25) Alibeik, S.; Zhu, S.; Brash, J. L. Surface Modification with PEG and Hirudin for Protein Resistance and Thrombin Neutralization in Blood Contact. *Colloids Surfaces B Biointerfaces* **2010**, *81* (2), 389–396.

(26) Peppas, N. a.; Hilt, J. Z.; Khademhosseini, A.; Langer, R. Hydrogels in Biology and Medicine: From Molecular Principles to Bionanotechnology. *Adv. Mater.* **2006**, *18* (11), 1345–1360.

(27) Lin, C. C.; Anseth, K. S. PEG Hydrogels for the Controlled Release of Biomolecules in Regenerative Medicine. *Pharm. Res.* **2009**, *26* (3), 631–643.

(28) Lutz, J. F. Polymerization of Oligo(Ethylene Glycol) (Meth)Acrylates: Toward New Generations of Smart Biocompatible Materials. *J. Polym. Sci. Part A Polym. Chem.* **2008**, *46* (11), 3459–3470.

(29) Lutz, J.-F.; Hoth, A. Preparation of Ideal PEG Analogues with a Tunable Thermosensitivity by Controlled Radical Copolymerization of 2-(2-Methoxyethoxy)Ethyl Methacrylate and Oligo(Ethylene Glycol) Methacrylate. *Macromolecules* **2006**, *39* (2), 893–896.

(30) Smeets, N. M. B.; Bakaic, E.; Patenaude, M.; Hoare, T. Injectable and Tunable Poly(Ethylene Glycol) Analogue Hydrogels Based on Poly(Oligoethylene Glycol Methacrylate). *Chem. Commun.* **2014**, *50* (25), 3306–3309.

(31) Smeets, N. M. B.; Bakaic, E.; Patenaude, M.; Hoare, T. Injectable Poly(Oligoethylene Glycol Methacrylate)-Based Hydrogels with Tunable Phase Transition Behaviours: Physicochemical and Biological Responses. *Acta Biomater.* **2014**, *10* (10), 4143–4155.

(32) Bakaic, E.; Smeets, N. M. B.; Dorrington, H.; Hoare, T. "Off-the-Shelf" Thermoresponsive Hydrogel Design: Tuning Hydrogel Properties by Mixing Precursor Polymers with Different Lower-Critical Solution Temperatures. *RSC Adv.* **2015**, *5* (42), 33364–33376.

(33) Cai, W.; Gupta, R. B. Fast-Responding Bulk Hydrogels with Microstructure. *J. Appl. Polym. Sci.* **2002**, *83* (1), 169–178.

(34) Ramakrishna, S.; Fujihara, K.; Teo, W.-E.; Lim, T.-C.; Ma, Z. *An Introduction to Electrospinning and Nanofibers*; 2005.

(35) Shenoy, S. L.; Bates, W. D.; Frisch, H. L.; Wnek, G. E. Role of Chain Entanglements on Fiber Formation during Electrospinning of Polymer Solutions: Good Solvent, Non-Specific Polymer-Polymer Interaction Limit. *Polymer (Guildf).* **2005**, *46* (10), 3372–3384.

(36) Gupta, P.; Elkins, C.; Long, T. E.; Wilkes, G. L. Electrospinning of Linear Homopolymers of Poly(Methyl Methacrylate): Exploring Relationships between Fiber Formation, Viscosity, Molecular Weight and Concentration in a Good Solvent. *Polymer (Guildf).* **2005**, *46* (13), 4799–4810.

(37) Fong, H.; Chun, I.; Reneker, D. H. Beaded Nanofibers Formed during Electrospinning. *Polymer (Guildf).* **1999**, *40* (16), 4585–4592.

(38) Jaeger, R.; Bergshoef, M. M.; Batlle, C. M. I.; Schönherr, H.; Julius Vancso, G.

Electrospinning of Ultra-Thin Polymer Fibers. *Macromol. Symp.* **1998**, *127* (1), 141–150.

4.7 Support information

Table S4.1 Molecular weight and degree of functionalization of precursor polymers used for nanofibrous hydrogel preparation.

Polymer	Functional Group [-]	Theoretical Functional Monomer [mol%]	Actual Functional Monomer [mol%]	M_n [kDa]	PDI [-]	Average # of Functional Groups/Chain
POH	$NHNH_2$	30.0	28.9	33.4	3.3	18
POA	CHO	30.0	27.8	22.8	3.0	13

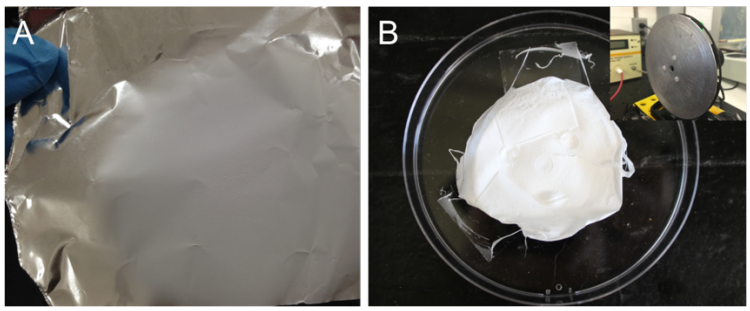

Figure S4.1. Electrospinning nanofiber mat on (A) aluminum foil and (B) rotating aluminum disk.

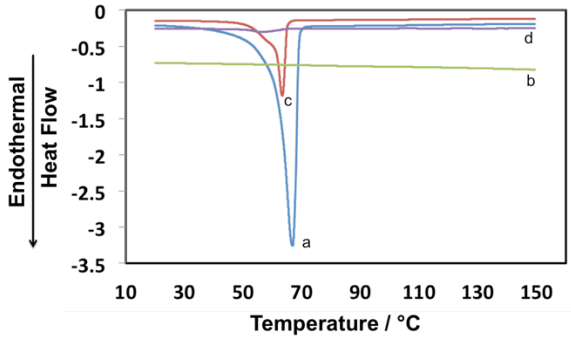

Figure S4.2 DSC thermograms of a) PEO-only electrospun nanofibers (blue), b) POH/POA bulk hydrogel after lyophilization (green), c) POH/POA+PEO electrospun nanofibers prior to soaking (red), and d) POH/POA+PEO electrospun nanofibers after immersion in DIW overnight (purple)

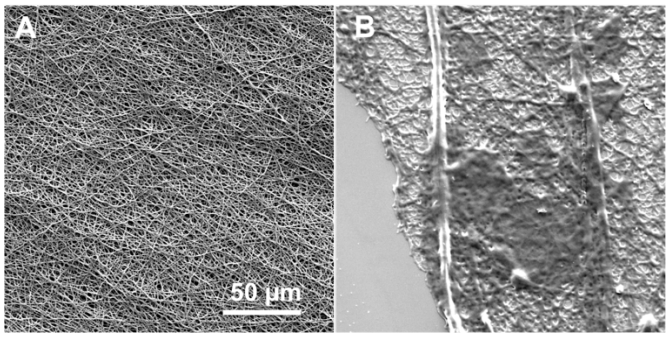

Figure S4.3 SEM images of POH/POA+PEO electrospun fibers before and after soaking (24 h) in DIW water.

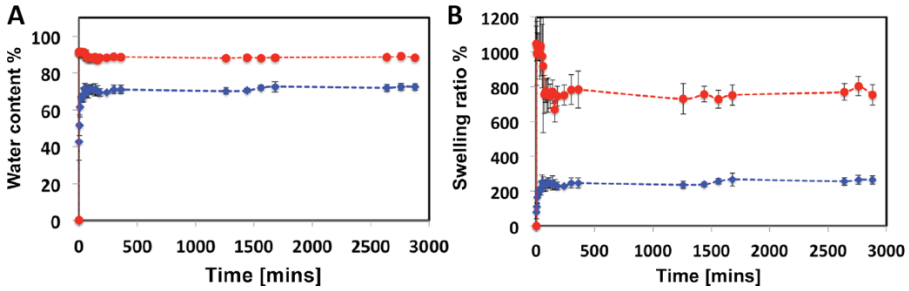

Figure S4.4 Swelling kinetics of electrospun hydrogel relative to a bulk hydrogel with the same composition and similar dimensions: (A) water content as a function of time; (B) swelling ratio as a function of time.

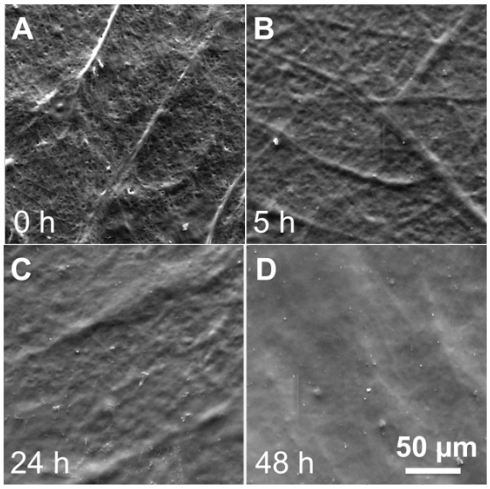

Figure S4.5 SEM images tracking degradation of nanofibers in 1M HCl at 37 °C after (A) 0 h; (B) 5 h; (C) 24 h; (D) 48 h

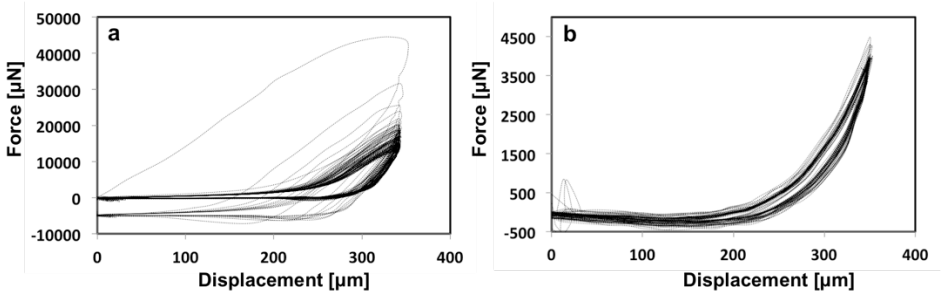

Figure S4.6. Mechanical properties of POH/POA+PEO nanofibers: (a) tensile cycling of dry nanofiber mat (80 cycles, 20% elongation/cycle); (b) compressive cycling of swollen nanofiber network (PBS, 40 cycles, 50% compression/cycle).

Table S4.2. Tensile modulus at different % elongation; the thickness of nanofibrous hydrogels was 0.4 ± 0.1 mm (n=5)

Tensile (%)	Modulus (kPa)
10%	0.26 ± 0.05
20%	1.45 ± 0.80

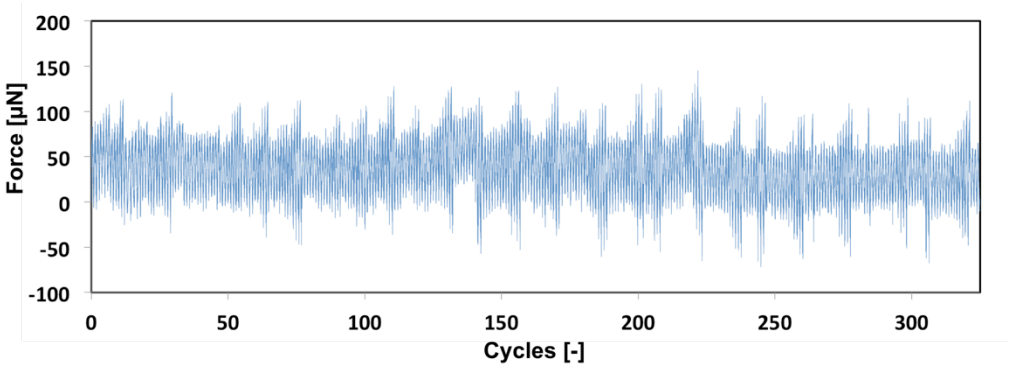

Figure S4.7. Mechanical properties of POH/POA+PEO nanofibers: tensile cycling of swollen nanofiber mat in 10 mM PBS (325 cycles, 10% elongation/cycle).

Table S4.3. Compressive testing at different % compression values for both the POH/POA+PEO nanofibrous hydrogels and a bulk hydrogel with the same overall composition as POH/POA+PEO nanofibrous hydrogels. The thickness of bulk hydrogel and nanofibrous hydrogels were 1.7 ± 0.2 mm and 0.4 ± 0.1 mm, respectively. (n=3)

Compression (%)	Compressive Modulus (kPa)	
	Fibrous hydrogel	Bulk hydrogel
20%	0.9 ± 0.3	3.8 ± 1.6
30%	1.7 ± 0.6	4.1 ±1.8
40%	1.8 ± 0.6	4.6 ± 1.0
50%	2.1 ±0.1	4.8 ± 1.2

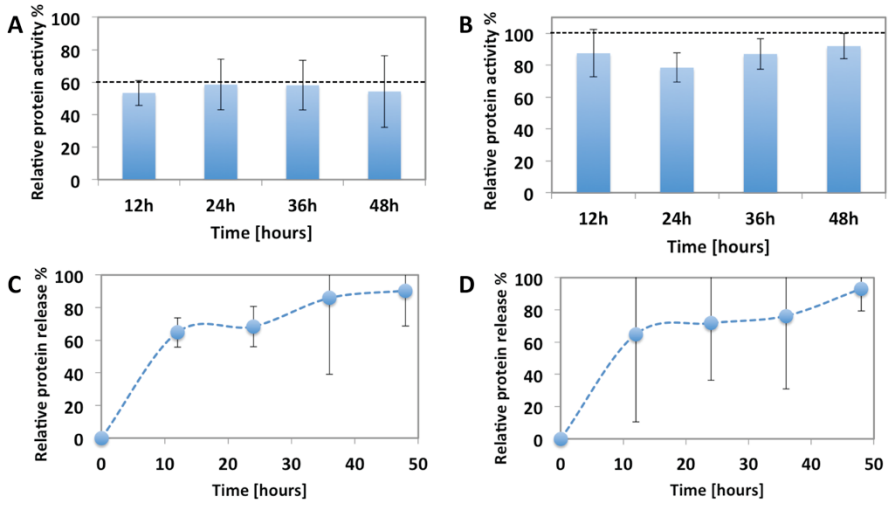

Figure S4.8. Encapsulation of β-gal and AP in electrospun nanofibrous hydrogel: (A,B) percentage activity of (A) β-gal and (B) AP in electrospun samples relative to the same concentration of enzyme freshly dissolved in the PBS release medium; (C,D) percentage of (C) β-gal and (D) AP release at each time point relative to the total loaded enzyme concentration. (n=4)

AP retains at least 80% of its fresh solution activity while β-gal retains ~60% of its activity in fresh solution following electrospinning after at least 48 hours of incubation in PBS (Fig. S8A-B), demonstrating that the electrospinning method is sufficiently mild to maintain the majority of enzyme activity even after drying during electrospinning and in the presence of hydrazone cross-linking chemistry. Note that electrospinning the same enzymes into a hollow polycaprolactone nanofiber results in only ~30% enzyme activity for AP (ref. 39 in main manuscript), suggesting the inertness of this reactive electrospinning process to biomolecules. In addition, the electrospun fibers release the majority of the encapsulated enzyme within the first few hours of soaking and facilitate nearly 100% release after 2 days, further confirming that the enzymes are not grafted or otherwise bound to the fibers and thus more likely to retain their activity.

Chapter 5

Fast thermo-responsive POEGMA-based nanofibrous hydrogel for controlling cell interactions

Abstract

Reactive electrospinning is demonstrated as a viable method to create fast-responsive and degradable macroporous thermoresponsive hydrogels based on poly(oligoethylene glycol methacrylate) (POEGMA). Hydrazide and aldehyde-functionalized POEGMA precursor polymers were co-electrospun to create hydrazone crosslinked nanofibrous hydrogels in a single processing step that removes the need for porogens or phase separation-driving additives. The resulting nanofibrous hydrogels can respond reversibly and repeatedly to changes in external temperature within seconds, in contrast to the minutes-to-hours response times observed with bulk hydrogels. Furthermore, nearly quantitative cell delamination can be achieved within two minutes of incubation at 4 °C, resulting in the recovery of more (as well as more proliferatively active) cells from the substrate relative to a conventional trypsinization protocol. The combined macroporosity, nanoscale feature size, and interfacial switching potential of these nanofibrous hydrogels thus offer promise for manipulating cell-hydrogel interactions as well as other applications in which rapid responses to external stimuli are desirable.

Keywords: thermoresponsive hydrogels, electrospinning, nanofibers, cell delamination

5.1 Introduction

Thermoresponsive hydrogels that can spontaneously gel and/or undergo swelling/deswelling transitions upon heating have attracted considerable recent attention.[1,2] Lower critical solution temperature (LCST) polymer-based hydrogels that exhibit discontinuous volume phase transitions at which hydrogels shrink upon heating are by far

the most commonly investigated type of thermoresponsive hydrogel[1,3,4], although upper critical solution temperature hydrogels that swell upon heating have also been reported[5–7]. The dynamic properties of such hydrogels have been widely exploited for drug delivery[8,9], tunable cell adhesion[10,11], switchable biosensors with on/off potential[12,13], reversible biomolecule scavenging[14,15] microfluidic gates[16,17], and other applications.

Poly(N-isopropylacrylamide) (PNIPAM) is the most widely investigated thermoresponsive polymer given its convenient near-physiological volume phase transition temperature (VPTT) of ~32 °C and its highly discontinuous phase transition. In the context of cell engineering, PNIPAM graft and hydrogel-based interfaces have shown particular promise for thermoreversible cell adhesion and recovery, with Okano's lab (using PNIPAM-grafted glass surfaces fabricated by surface-initiated reversible addition-fragmentation chain transfer (SI-RAFT) polymerization[18–20]) and Takezawa's lab (using PNIPAM/collagen coatings on polystyrene) both reporting such functionality in 1990. Cells grown into coherent cell sheets could adhere to the substrate at 37 °C but delaminated from the substrate at 20 °C for 1 h.[19] Compared to traditional enzymatic cell detachment (e.g. using trypsin), thermal delamination has been demonstrated to substantially better maintain the native extracellular matrix and thus the functionality of recovered cell sheet.[19,21] Similar thermal switching of cell adhesion has been demonstrated from PNIPAM-based hydrogels[22,23] using the same basic mechanism.

More recently, other emerging thermoresponsive polymers have shown similar properties while avoiding some of the potentially concerning toxicity of the NIPAM monomer. Of particular interest, poly(oligoethylene glycol methacrylate) (POEGMA) polymers and hydrogels can be prepared to be thermoresponsive over a physiologically-relevant temperature range by mixing longer chain (n=8-9 ethylene oxide repeat units) oligo(ethylene glycol) methacrylate (OEGMA) monomer with di(ethylene glycol) methyl ether methacrylate ($M(EO)_2MA$)[24–26]. Hydrogels and interfaces prepared with higher contents of the short chain $M(EO)_2MA$ monomer (80-90 mol%) have been demonstrated to facilitate analogous cell detachment behavior to PNIPAM interfaces.[27,28] Extending this work, we have recently prepared injectable and degradable analogues of these POEGMA-based materials by functionalizing copolymers with hydrazide and aldehyde functional groups respectively, enabling *in situ* gelation via hydrazone chemistry upon mixing[29,30] and effective cell detachment upon cooling.[31]

However, for any of the reported 3D hydrogel-based systems, the relatively slow kinetics of thermal transitions of bulk hydrogels remains a challenge in the context of translating such surfaces to practical applications, in particular avoiding longer delaminating cooling cycles that may impact cell behavior. Four general approaches have been investigated to accelerate thermal transitions within thermoresponsive hydrogels while retaining the overall bulk properties of the material, all of which aim to manipulate one or both of two key properties: (1) exploiting the known inverse relationship between the swelling/shrinking rate of a hydrogel and the square of its linear dimension to accelerate transition kinetics by reducing the dimensions of the collapsing sub-units; and/or (2) increasing the penetrability of water in and out of the hydrogel to provide hydrophilic pathways for water transport and avoid the formation of a collapsed "skin layer" at the interface that inhibits water transport[32].

First, macroporous thermoresponsive hydrogels have been produced by polymerizing hydrogels around porogens such as salt or poly(ethylene glycol)[33] (which can dissolve and diffuse out of the network following cooling) or dissolvable particles like polystyrene[34] or silica (which can be etched out of the network using organic solvents or HF respectively)[35]. This approach creates easier pathways for water transport as well as reduces the average dimension of the collapsing gel units to drive faster responses to thermal stimuli, although a broad range of domain sizes typically still results due to the random nature of the pore distributions generated. Alternately, to avoid the subsequent need to remove the porogen, methods such as freeze drying, manipulating hydrogen bonding interactions (e.g. polymerization in the presence of phenol[36]), or driving *in situ* phase separation during polymerization (e.g. polymerization in the presence of sucrose[37]) have also been demonstrated, although these methods provide substantially less control over both pore size and feature size. Second, hydrophilic nanodomains can be engineered into thermoresponsive hydrogels to provide pathways for water penetration into bulk hydrogels. Such domains have been introduced via the use of hydrophilic nanoscale crosslinkers[37], the copolymerization of hydrophilic macromonomers or dendrimers[38,39], or the formation of a hydrophilic interpenetrating polymer network[40], among other approaches. However, the inclusion of hydrophilic domains tends to at least in part suppress the overall phase transition, limiting the degree of hydrophilic-hydrophobic switching and the magnitude of deswelling achievable. Third, bulk hydrogels can be constructed using nanogels as

building blocks, exploiting the smaller size of the thermoresponsive unit to accelerate transitions. Nanogels can be applied as reactive crosslinkers for conventional gel synthesis, embedded phases that can enhance the rate of thermal collapse of the surrounding hydrogel phase[41,42], or as the building blocks of the gels themselves.[43] While generally promising, such systems typically require multiple polymerization steps to prepare (i.e. fabrication/functionalization of the nanogel followed by fabrication of the hydrogel). Fourth, nanofibrous thermoresponsive hydrogels have been prepared. For example, Jing et al. electrospun PNIPAM with epoxide-bearing polyhedral oligomeric silsesquioxane (POSS) crosslinker to form hydrogel nanofibers following heat treatment,[44] while Kim et al. performed simultaneous electrospinning and UV-induced crosslinking NIPAM with a UV-reactive benzophenone (BP) conjugated co-monomer to fabricate responsive nanofibrous hydrogels. In our view, this approach is of particular interest in that it exploits both the feature size and porosity/water penetrability mechanisms of accelerating hydrogel transitions and offers the potential for the fabrication of a fast-responsive hydrogel in a single processing step without requiring additional additives. However, neither of these nanofiber forming approaches, nor the previously described methods to fabricate macroporous thermoresponsive hydrogels using other strategies, result in degradable hydrogel structures. Introducing the potential for degradation of the scaffold would be highly advantageous in the context of potentially translating thermoresponsive cell signalling into an *in vivo* tissue engineering context.

We have recently reported a reactive electrospinning method in which hydrazide and aldehyde-functionalized non-thermoresponsive POEGMA oligomers are co-extruded in the presence of an electric field to spontaneously form hydrazone-crosslinked nanofibrous hydrogels without any post treatment.[45] Herein, we demonstrate the reactive electrospinning of thermoresponsive POEGMA-based hydrogels to fabricate fast-swelling nanofibrous and degradable thermoresponsive hydrogels in a single processing step. The nanofibrous structured hydrogel showed both extremely fast responses to temperature change (within seconds, as fast or faster than previously reported materials) in addition to the capacity for highly efficient single cell delamination upon a temperature stimulus.

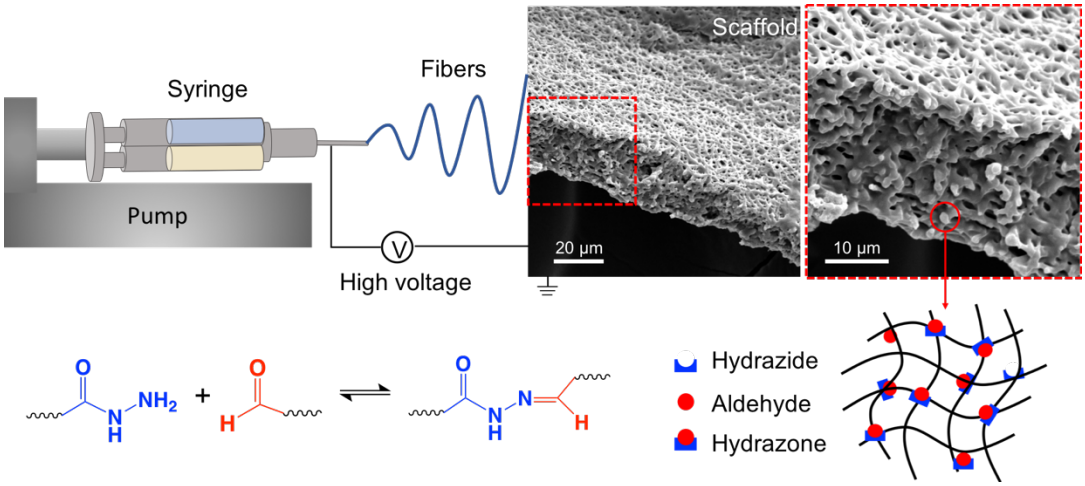

Figure 5.1 Electrospinning setup to prepare crosslinked hydrogel nanofibers.

5.2 Materials and methods

5.2.1 Materials

Oligo(ethylene glycol) methyl ether methacrylate ($OEGMA_{475}$, M_n = 475 g/mol, Sigma Aldrich, 95%) and di(ethylene glycol) methyl ether methacrylate ($M(EO)_2MA$, Sigma Aldrich, 95 %) were purified by passing through a column of basic aluminum oxide (Sigma Aldrich, type CG-20) to remove the methyl ether hydroquinone (MEHQ) and butylated hydroxytoluene (BHT) inhibitors before use. Poly (ethylene oxide) (PEO, M_w = 600,000 g/mol, Sigma-Aldrich), acrylic acid (AA, Sigma Aldrich, 99%), 2,2-azo-bis-isobutryic acid dimethyl ester (AIBMe, Wako Chemicals, 98.5%), dioxane (Caledon Labs, 99%), adipic acid dihydrazide (ADH, Alfa Aesar, 98%), N'-ethyl-N-(3-dimethylaminopropyl)-carbodiimide (EDC, Carbosynth, Compton CA, commercial grade), thioglycolic acid (TGA, Sigma Aldrich, 98%) were all used as received. N-(2,2-dimethoxyethyl) methacrylamide (DMEMAm) was synthesized as previously reported.[46] Milli-Q grade distilled deionized water (DIW) was used for all experiments. NIH 3T3 mouse fibroblast cells were purchased from ATCC (Cedarlane Laboratories, Burlington, ON). Dulbecco's Modified Eagle's Medium (DMEM, ThermoFisher), bovine calf serum (BCS, Sigma Aldrich), penicillin-streptomycin (ThermoFisher), PrestoBlue cell viability reagent (ThermoFisher), trypsin-EDTA solution (Sigma Aldrich) and phosphate buffered saline (PBS, pH = 7.4, ThermoFisher) were used as received.

5.2.2 Synthesis of hydrazide-functionalized POEGMA (POH)

Hydrazide-functionalized POEGMA precursors were synthesized as previously described.[47] In brief, AIBMe, AA, and a combination of $OEGMA_{475}$ and $M(EO)_2MA$ depending on the targeted phase transition temperature of the thermoresponsive hydrogels (see Table 1) were dissolved in 20 mL dioxane and purged with nitrogen for 30 mins prior to polymerization. Subsequently, the solution was placed in an oil bath at 75 °C for 4 hours under magnetic stirring to allow for polymerization to occur. The resulting poly(OEGMA-*co*-AA) polymer was then purified by dialysis (6+ hours for 6 cycles) and lyophilized. The purified copolymer was then re-dissolved in 100 mL DIW and functionalized with hydrazide groups by adding a 5-fold molar excess of ADH and a 2.5-fold molar excess of EDC relative to the measured -COOH content of the pre-polymer and maintaining the reaction pH at 4.75 using 0.1 M HCl until the pH stabilized (~4 hours). The solution was kept stirring overnight and then purified by dialysis (6+ hours for 6 cycles). The final polymer was obtained after lyophilization and was stored as a 15 w/w% solution in DIW at 4 °C. All hydrazide-functionalized POEGMA (POH) precursors are labeled as PO_xH_y, which x represents the mole ratio of $OEGMA_{475}$ in copolymer and y is mol% of monomer residues functionalized with a hydrazide group according to the reaction stoichiometry. For example, $PO_{10}H_{10}$ denotes that the molar ratio of $OEGMA_{475}$: $M(EO)_2MA$ is 10 : 90 and that 10 mol% of monomer residues in the pre-polymer are functionalized with a hydrazide group.

5.2.3 Synthesis of aldehyde-functionalized POEGMA (POA)

Aldehyde-functionalized POEGMA precursors were synthesized as previously reported.[47] AIBMe, DMEMAm, and a combination of $OEGMA_{475}$ and $M(EO)_2MA$ depending on the targeted phase transition temperature (see Table 5.1) were dissolved in 20 mL dioxane and purged with nitrogen for 30 mins. Polymerization proceeded by placing the mixture in an oil bath at 75 °C for 4 hours under magnetic stirring. Subsequently, to cleave the acetal group on DMEMAm monomer residues, the poly(OEGMA-*co*-DMEMAm) pre-polymer was dissolved in 100 mL of 0.25 M HCl and stirred overnight. The final polymer was purified by dialysis (6+ hours for 6 cycles), lyophilized, and stored as a 15 w/w% solution in DIW at 4 °C. All aldehyde-functionalized POEGMA (POA) precursors are labeled as PO_xA_y, where x represents the mole ratio of $OEGMA_{475}$ in copolymer (relative to M(EO)-

$_2$MA) and y is mol% of monomer residues functionalized with an aldehyde group according to reaction stoichiometry.

5.2.4 Characterization of polymer precursors

Polymer molecular weight was measured via gel permeation chromatography (GPC, Waters, Mississauga, ON) using a Waters 515 HPLC pump, Waters 717 plus Autosampler and three columns (Waters Ultrahydrogel-120, -250, -500; 7.8 × 300 mm; 6 μm particles). Samples were run at 30 °C in an aqueous buffer consisting of 0.5 M sodium nitrate and 25 mM 2-(cyclohexylamino) ethane sulfonic acid maintained at pH 10.0. The degree of hydrazide functionalization in POH was determined using conductometric base-into-acid titration (Mantech) by calculating the number of -COOH groups in the polymer before and after the EDC/ADH reaction; the difference in the titratable -COOH fraction corresponds to the fraction of acrylic acid residues converted to hydrazide groups. The degree of aldehyde functionalization in POA was determined by ^{1}H-NMR (600 MHz, Bruker) by taking the ratio of aldehyde proton signal at 9.52 ppm to the methyl proton signal at 0.81 ppm.

5.2.5 Preparation of electrospun nanofibrous hydrogels

PEO (2.5 wt%, M_w = 600,000g/mol) and either PO_xH_{10} or PO_xA_{10} (both at 7.5 wt%) were co-dissolved in DIW. The resulting PEO/POH and PEO/POA solutions were then separately loaded into a double barrel syringe fitted a static mixer and capped with a blunt-tip 18G needle. Electrospinning was performed under ambient conditions by applying a voltage of 10 kV between the blunt needle and the aluminum disk collector, using a falling distance of 10 cm and a double barrel syringe compression rate of 10 μm/min using a syringe pump (Harvard Appartus). All scaffolds were prepared at humidity values < 30% RH to ensure adequate drying of the aqueous precursor solutions upon electrospinning to form well-defined nanofibers. For comparisons of nanofibrous versus bulk hydrogel properties, bulk hydrogels with the same chemical composition were prepared by extruding the same precursor polymers from the double-barrel syringe into a 1 cm rubber mold. Humidity was controlled as described in Chapter 4.

5.2.6 Microscopy

The nanostructure of the electrospun scaffolds was determined by scanning electron microscopy (SEM, Vega II LSU instrument) using an operating voltage of 10 kV. Samples were sputter-coated with a ~30 nm gold layer prior to imaging to prevent charging. Confocal laser scanning microscopy (CLSM, Nikon) was used to assess cell morphology. Optical microscopy of cells was conducted using a Nikon Eclipse LV100N POL epifluorescence microscope (Nikon Instruments, Mississauga, Ontario) using a 10× objective lens.

5.2.7 Swelling and degradation kinetics

Swelling kinetics were measured at both 25 °C and 37 °C in 10 mM PBS. In brief, electrospun or bulk hydrogel scaffolds of comparable dimensions were placed into cell culture inserts (ThermoFisher) that were subsequently placed into 4 mL PBS per well of a 24-well plate. At predetermined time intervals, the inserts were dried and weighted. The swelling ratio as a function of time was calculated gravimetrically according to Equation 1:

$$Swelling\ ratio\ \% = \frac{W_{swollen} - W_{initial}}{W_{initial}} \times 100\%$$

Degradation kinetics were determined using the same gravimetric method but using 1M HCl instead of PBS as the incubation medium. Note that these experiments were designed to compare the degradation rates of the different scaffolds rather than to mimic a specific physiological condition.

5.2.8 Phase transition behavior

The lower critical solution temperatures (LCST) of the precursor polymers was determined using a Variant Cary 100 UV-visible spectrophotometer. Polymer precursors were dissolved in 10 mM PBS at a concentration of 10 mg/mL and then transferred into a quartz cuvette. The transmittance of the samples were measured at 500 nm at temperatures ranging from 20 to 80 °C by a ramping the temperature at a rate of 1 °C/min. The volume phase transition temperatures (VPTT) of nanofibrous electrospun hydrogels were determined by visual inspection against a 1x1 cm^2 grid as the temperature was ramped from 20 to 40 °C.

5.2.9 Cell culture

NIH 3T3 mouse fibroblast cells were cultured in DMEM medium with 10 % BCS and 1 % penicillin-streptomycin, with both cells cultured to ~ 80% confluency at 37 °C and 5% CO_2 before subsequent use.

5.2.10 Cytotoxicity assay

The cytotoxicity of polymer precursors for electrospinning was assessed using the PrestoBlue assay. Both 3T3 and Psi2 12S6 cells were seeded in 96 well-plates with a density of 10,000 cell per well and incubated in 100 μL DMEM at 37 °C and 5% CO_2 for 24 hours. Subsequently, the plates were washed with PBS and polymer precursors at concentrations from 2 mg/mL to 10 mg/mL (dissolved in 100 μL of fresh DMEM) was added to each well and incubated for an additional 24 hours. Following, the media (including the polymers) was replaced with 90 μL of fresh DMEM and 10 μL of PrestoBlue reagent and incubated for one hour prior to measurement. Cell viabilities were assessed using a fluorescence plate reader (Infinite M200 Pro, Tecan, 560 nm excitation/ 590 nm emission), with the result normalized to a cell-only (non-treated) well as control and a medium-only well as a blank. Four replicates were conducted per condition tested, with the error bar representing the standard deviation of these measurements.

5.2.11 Cell adhesion assay

All polymer precursors were filtered using a 0.20 μm filter and electrospun within a biosafety cabinet; subsequently, all swollen scaffolds were placed under UV light for 1h to ensure sterility. POEGMA electrospun scaffolds were placed in a non-treated 24 well-plate (VWR) and immersed in 800 μL PBS/well for swelling. A stainless-steel nut was used to weigh down each scaffold to the bottom of well. After x hours of equilibration, the PBS was removed, and the wells were washed with 800 μL of fresh DMEM (24 hour incubation time). Subsequently, 800 μL of DMEM containing 20,000 cells per well was incubated at 37 °C and 5% CO_2 for 24 hours. To label cells for tracking, carboxyfluorescein diacetate succinimidyl ester (CFSE) and 4′,6-diamidino-2-phenylindole (DAPI) were used to label cells by staining cytoplasmic protein and nuclei respectively. Cell adhesion was observed by tracking the co-localization of these cell dyes using confocal microscopy. Cells with

same density were also cultured in treated 24 well-plate without any scaffold present using the same protocol as a control (n=4 per condition tested).

5.2.12 Cell delamination assay

POEGMA electrospun scaffolds were placed in a non-treated 48 well-plate as above description. Subsequently, 600 μL of DMEM containing 10,000 cells per well was added to each well and incubated at 37 °C and 5% CO_2 for 48 hours. Afterwards, the media was removed and cells were treated by one of three protocols: (1) 400 μL of fresh DMEM pre-heated at 37 °C was added and the plate was incubated at 37 °C for 2 mins (media change but no temperature stimulus); (2) 400 μL of fresh DMEM from the refrigerator (4 °C) was added and the plate was incubated at 4 °C for 2 mins (media change with temperature stimulus); (3) 100 μL of TrypLE express enzyme (1X, no phenol red, ThermoFisher) was added and incubated for 2 mins at 37 °C, followed by neutralization via the addition of 300 μL of DMEM, also pre-heated to 37 °C (conventional enzymatic cell delamination control). Following the 2 min incubation period in each case, the upper layer of media from each well was transferred to a new 48 well-plate and incubated for 24 hours to allow any cells in the media to adhere to and/or grow on the new 48-well plate. Cell delamination was determined by fluorescence imaging of the cells on the scaffolds (using the same CFSE and DAPI and confocal microscopy protocols outlined previously) and observing the replated cells in the fresh 48-well plates using optical microscopy.

Table 5.1 Chemical characterization of the synthesized POEGMA polymer precursors.

Polymer	$OEGMA_{475}$ mmol	$M(EO)_2MA$ mmol	Functional groups [-]	Functional monomer [mol %]	M_n $\times 10^3$ g/mol	PDI
$PO_{10}H_{10}$	1.9	16.5	$NHNH_2$	10.2 %	17.4	2.2
$PO_{100}H_{10}$	8.4	0	$NHNH_2$	10.1 %	27.0	3.5
$PO_{10}A_{10}$	1.9	16.5	CHO	10. 6 %	19.8	2.2
$PO_{100}A_{10}$	8.4	0	CHO	10.4 %	23.8	2.9

5.3 Results and discussion

5.3.1 Physiochemical properties of polymer precursors

The chemical properties of the prepared POEGMA-hydrazide (POH) and POEGMA-aldehyde (POA) polymers with different phase transition temperatures are shown in Table 5.1. Compared to our earlier work on bulk hydrogels, substantially lower hydrazide and aldehyde contents are incorporated into the precursor polymers used for this work to substantially slow gelation prior to electrospinning but exploit water evaporation during the spinning process to *in situ* concentrate the precursor polymers and thus drive gelation following ejection of the precursor solution from the electrospinning needle. Here, gelation time was controlled to be >20 mins to match the electrospinning feed rate and ensure continuous processing.[45] The molecular weight (M_n) of all polymer precursors was maintained at <40 kDa to promote renal clearance of the precursor polymers upon hydrogel degradation.[48]

Two different sets of POEGMA precursors - PO_{10} and PO_{100} - were prepared by changing the ratio of copolymer between $OEGMA_{475}$ to $M(EO)_2MA$ (Table 5.1). The transmittance of each polymer precursor solution as a function of temperature was measured by UV-vis spectrophotometry to determine the precursor polymer LCSTs. $PO_{10}H$ and $PO_{10}A$ exhibited LCST transitions at 52 °C and 44 °C respectively, while $PO_{100}H$ and $PO_{100}A$ showed no functional LCST (> 80 °C) (Figure 5.2). This result is consistent with the incorporation of the short-chain $M(EO)_2MA$ monomer in the PO_{10} precursor polymers, the polymer of which has a known lower LCST value.

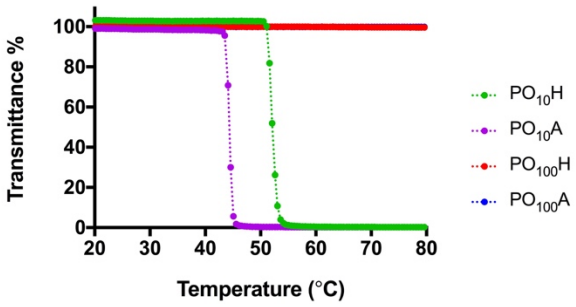

Figure 5.2 LCST transitions of polymer precursors measured via UV/vis spectrophotometry at a polymer concentration of 10 mg/mL in 10 mM PBS.

5.3.2 Morphologies of thermoresponsive scaffolds

The morphologies of the electrospun nanofibers based on both PO_{10} and PO_{100} precursor polymers are shown in Figure 5.3. Both sets of precursor polymers yielded nanofibrous networks under the electrospinning conditions used (Fig. 5.3A, B), although the inclusion of the 2.5 wt% PEO (600 kDa) electrospinning aid was required in order to generate nanofibrous networks in both cases. The diameter of the PO_{10} hydrogel nanofibers (0.68 ± 0.18 μm) was slightly higher and has a slightly broader distribution than that observed for the PO_{100} nanofibers (0.49 ± 0.11 μm) (Fig. 5.3C). We attribute this result to the faster crosslinking kinetics of the PO_{10} precursor polymers due to the lower steric bulk of the shorter ethylene oxide side chains[31], resulting in more gelation (or at least viscosity build-up) prior to ejection of the precursor polymer solution from the needle and thus less stretching of the precursor polymer solution upon electrospinning.

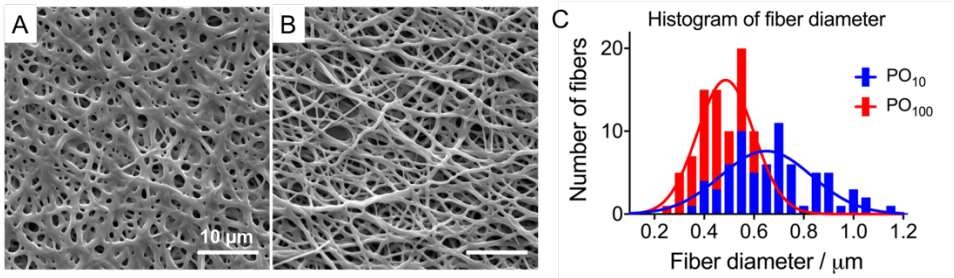

Figure 5.3 (A-B) SEM images of electrospun hydrogel nanofibers based on PO_{10} (A) and PO_{100} (B). (C) Distribution of fiber diameter for each nanofibrous hydrogel (n=x fibers analyzed per sample).

5.3.3 Physiochemical properties of electrospun scaffolds

The gravimetric swelling ratios and swelling kinetics of PO_{10} and PO_{100} scaffolds (from the dry state following electrospinning) at both 22 °C and 37 °C are shown in Figure 5.4A. PO_{100} swelled to a water content of ~88% independent of temperature, while PO_{10} swelled to a water content of ~78%, again consistent with the lower LCST of the PO_{10} precursor polymers and thus the lower water affinity of the PO_{10}-based hydrogels. In both cases, the swelling was extremely fast, with equilibrium water contents achieved within 1 minute from the dry state owing to the macroporous nature and nanoscale dimensions of the nanofibrous gel scaffolds. Macroscopic swelling measurements on pre-hydrated gel nanofibrous mats show the expected thermal response of the PO_{10} scaffolds (Figure 5.5A),

with both the bulk dimensions and the transparency of the scaffolds substantially decreasing upon heating to 37°C (above the VPTT of the PO_{10}-based hydrogels[31]). Again, the response of nanofibrous hydrogel to temperature change occurred within seconds while bulk gels of similar dimensions required several minutes to respond; for example, although the nanofibrous gels had long achieved the equilibrium swelling observed in Fig. 5.4A, there was no obvious volume change in the corresponding bulk hydrogels one minute following a temperature change from 25 °C to 37 °C (Figure 5.5B). Furthermore, the scaffold showed quick responses (in seconds) after 4 heating-cooling cycles (Figure 5.5C), demonstrating the stability and reversible thermoresponsiveness of the hydrogel nanofibers. The degradation kinetics of the PO_{10} hydrogel reflects this temperature responsiveness, with complete degradation observed in 90 hours in acid-accelerated conditions at 25 °C while only around half of scaffold mass degraded away over the same time period at 37 °C. This result is consistent with the more collapsed structure of the PO_{10} scaffold reducing the diffusibility of the hydrolyzing H^+ ions into the gel nanofibers, reducing the rate of hydrolysis at 37 °C versus that observed at room temperature.

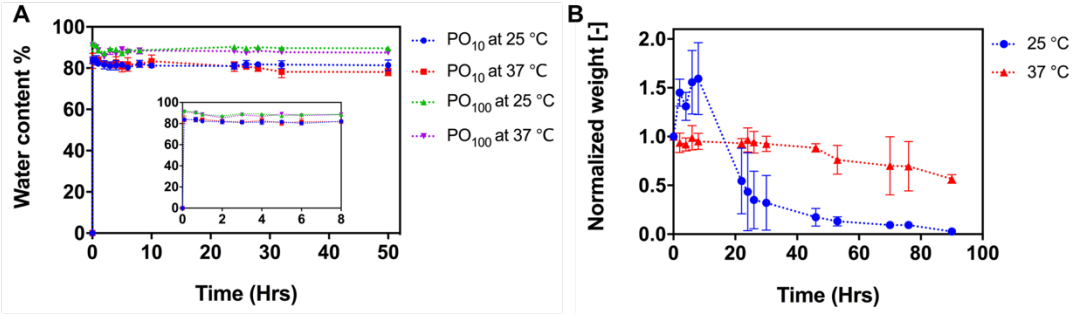

Figure 5.4 (A) Swelling measurements of PO_{10} nanofibrous hydrogel in 10 mM PBS at 25 °C and 37 °C. (B) Degradation kinetics of PO_{10} nanofibrous hydrogel in 1M HCl at 25 °C and 37 °C.

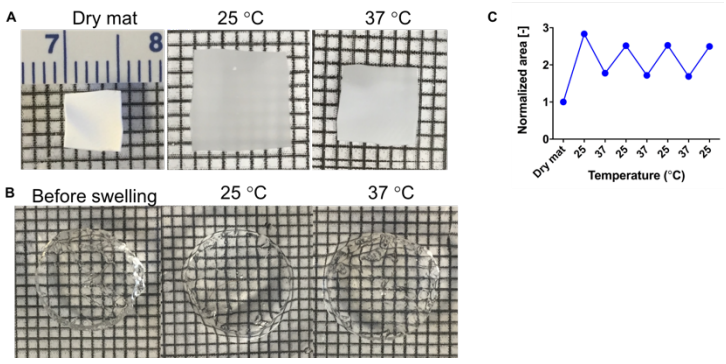

Figure 5.5 (A) Optical images of PO_{10} nanofibrous hydrogel scaffold before and after swelling in 10 mM PBS at 25 °C and 37 °C (1 minute of equilibrium at each new condition). (B) Corresponding optical images of PO_{10} bulk hydrogel before and after swelling in 10 mM PBS at 25 °C and 37 °C (1 minute of equilibration at each new condition). (C) Normalized projected area changes of PO_{10} nanofibrous scaffold before and after swelling with repeats of cooling (25 °C) and heating (37 °C) (x minutes of equilibration at each new condition).

5.3.4 Cell toxicity of polymer precursors

Prior to assessing the potential for the PO_{10} thermoresponsive hydrogels for reversible cell delamination, the cytotoxicity of the polymer precursors was tested using a PrestoBlue assay on NIH 3T3 mouse fibroblast cells (Figure 5.6). High cytocompatibility was observed for all polymers and gel precursors used in the electrospinning fabrication process at concentrations up to 5 mg/mL, with all polymers except for $PO_{100}A$ maintaining this high cytocompatibility up to 10 mg/mL (a high concentration for a closed *in vitro* cell toxicity assay). The moderate cytotoxicity of the $PO_{100}A_{10}$ precursor is attributed to the presence of aldehyde functionalized groups, although it should be noted that the relatively slow degradation of the nanofibrous networks (even in accelerated acid conditions) would result in functional concentrations of this precursor polymer significantly lower than this tested concentration in any practical usage scenario.

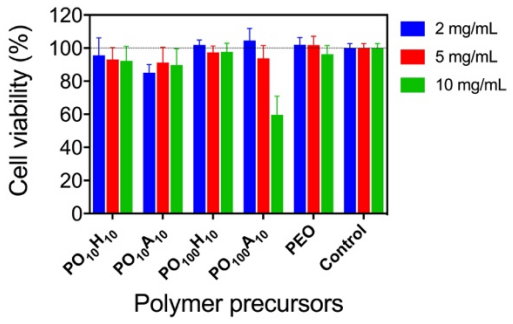

Figure 5.6 Cell viabilities of 3T3 mouse fibroblast cells with polymer precursors used for electrospinning as a function of concentration using the PrestoBlue assay (n=4 per test)

5.3.5 Cell adhesion

The adhesion of 3T3 fibroblasts on both thermoresponsive (PO_{10}) and non-thermoresponsive (PO_{100}) electrospun scaffolds relative to that observed on a control plasma treated well-plate is shown in Figure 5.7. Substantially more cells adhered to the PO_{10} hydrogel scaffold compared to the PO_{100} hydrogel scaffold, consistent with the increased interfacial hydrophobicity of the PO_{10} scaffold at 37 °C (above its VPTT). It is also notable that substantially higher cell adhesion was observed to both scaffolds relative to that observed for the corresponding bulk hydrogels[31], suggesting that the increased interfacial roughness of the nanofibrous hydrogel substantially increases the adhesivity of cells to what even for PO_{10} remains a highly hydrated gel scaffold. Indeed, the cell density on the PO_{10} nanofibrous hydrogel nearly matches that of the tissue culture polystyrene control, indicative of the high potential of the thermoresponsive PO_{10} scaffold to support cell adhesion under normal physiological conditions.

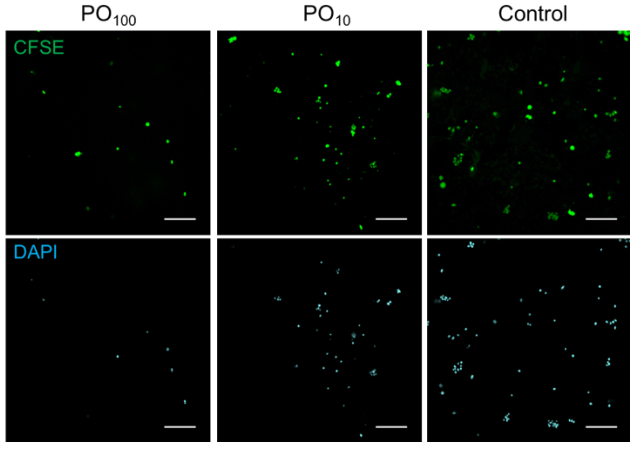

Figure 5.7 Confocal images of 3T3 mouse fibroblast cell adhesion on PO100 nanofibrous scaffolds (left), PO10 nanofibrous scaffolds (middle), and a tissue culture polystyrene control (right). Cells were stained using CFSE (488 nm, green – top row) and DAPI (405 nm, blue – bottom row). Scale bars = 200 μm.

5.3.6 Cell detachment

The potential for thermal delamination from the fast thermoresponsive PO_{10} nanofibrous scaffolds was studied by plating 3T3 cells on top of swollen electrospun PO_{10} scaffolds (Figure 5.8A). Following 48 hours of incubation of the cells on the scaffolds, the media was removed and the scaffolds were treated by incubating the scaffolds for two minutes in (1) 37 °C DMEM (no thermal or enzymatic treatment - left column, Fig. 5.8B); (2) 4 °C DMEM (thermal but no enzymatic treatment – right column, Fig. 5.8B); or (3) a standard trypsin solution (enzymatic but no thermal treatment – middle column, Fig. 5.8B). Temperature-induced delamination from the PO_{10} nanofibrous scaffolds is shown to be at least as effective as the conventional trypsin treatment, with cells successfully delaminated via trypsinization and thermal treatment relative to the 37 °C control (as determined via image analysis of Fig. 5.8B and corresponding replicate images, n=4). Analogously, when the recovered cells from the overhead media were re-plated on a fresh 48-well plate, Figure 5.9 shows that the recovered cells following thermal delamination maintain both their morphology and as well as their capacity proliferate to cover the plate following 24 hours of incubation, higher than the cell densities observed after trypsinization over the same time period. Given the similar degrees of delamination observed for thermal and trypsin treatments (Fig. 5.8B), this result suggests that the impact of the thermal delamination process on the proliferative cycle of the cells is significantly lower than that associated with trypsinization. This result is also consistent with previous reports that indicate the increased maintenance of the ECM around cells following thermal delamination versus enzymatic delamination is beneficial to promote and maintain cell viability and behavior following delamination.[11,22] Collectively these results suggest that the thermoresponsive nanofibrous scaffolds facilitate fast (<2 min), nearly quantitative, and highly functional cell delamination.

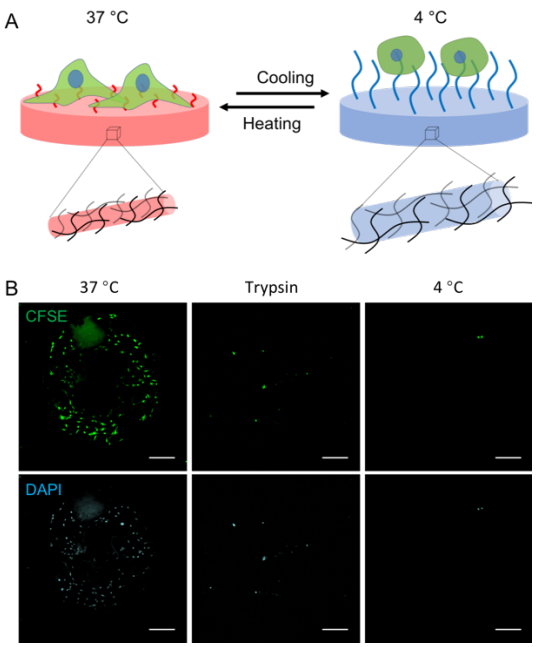

Figure 5.8 (A) Schematic of the mechanism of cell adhesion and thermally-induced delamination by thermoresponsive hydrogel nanofibers. (B) Confocal images of 3T3 fibroblast cells still adhered to PO_{10} scaffolds after 2 minutes of incubation in fresh 37 °C DMEM media (left column), fresh 4 °C DMEM media (middle column), and standard trypsinization media (right column). Cells were stained using CFSE (488 nm, green) and DAPI (405 nm, blue) for visualization. Scale bars = 200 μm.

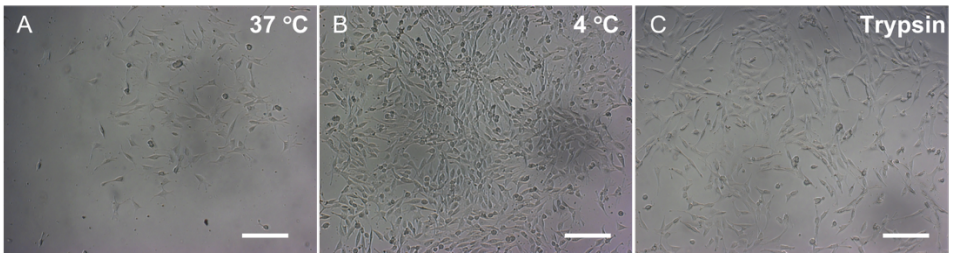

Figure 5.9 Optical images of recovered cells following delamination by treatment with fresh 37 °C DMEM media (A), fresh 4 °C DMEM media (B), and standard trypsinization media (C). Scale bars = 200 μm.

5.4 Conclusions

Thermoresponsive and degradable hydrogel nanofibers can be prepared via reactive electrospinning of thermoresponsive hydrazide and aldehyde-functionalized precursor polymers in a single and rapid processing step. Lowering the LCST of the precursor polymers led to the fabrication of nanofibrous and macroporous hydrogels that exhibited

fast temperature-responsive swelling (within seconds) over multiple thermal cycles as well as substantially enhanced cell adhesion relative to both more hydrophilic and corresponding bulk hydrogels. Furthermore, fast (<2 minutes) and nearly quantitative cell delamination was observed from the nanofibrous hydrogels, resulting in the recovery of both a higher fraction of cells as well as more highly proliferative cells than achieved using a standard trypsinization protocol. Overall, these results suggest the potential of thermoresponsive POEGMA-based nanofibrous hydrogels used as scaffolds for various cell engineering applications in both 2D and 3D in which the dynamic manipulation of cell-scaffold interactions is desirable.

5.5 Acknowledgement

Funding from the Natural Sciences and Engineering Research Council of Canada and the NSERC CREATE-IDEM (Integrated Development of Extracellular Matrices) training program is gratefully acknowledged. José Moran-Mirabal is thanked for use of his electrospinning equipment and helpful advice.

5.6 References

(1) Klouda, L.; Mikos, A. G. Thermoresponsive Hydrogels in Biomedical Applications. *Eur. J. Pharm. Biopharm.* **2008**, *68* (1), 34–45.

(2) Klouda, L. Thermoresponsive Hydrogels in Biomedical Applications A Seven-Year Update. *Eur. J. Pharm. Biopharm.* **2015**, *97*, 338–349.

(3) Jeong, B.; Kim, S. W.; Bae, Y. H. Thermosensitive Sol–Gel Reversible Hydrogels. *Adv. Drug Deliv. Rev.* **2012**, *64*, 154–162.

(4) Schmaljohann, D. Thermo- and PH-Responsive Polymers in Drug Delivery. *Adv. Drug Deliv. Rev.* **2006**, *58* (15), 1655–1670.

(5) Asadujjaman, A.; Espinosa de Oliveira, T.; Mukherji, D.; Bertin, A. Polyacrylamide “Revisited”: UCST-Type Reversible Thermoresponsive Properties in Aqueous Alcoholic Solutions. *Soft Matter* **2018**, *14* (8), 1336–1343.

(6) Ye, H.; Owh, C.; Loh, X. J. A Thixotropic Polyglycerol Sebacate-Based Supramolecular Hydrogel Showing UCST Behavior. *RSC Adv.* **2015**, *5* (60), 48720–48728.

(7) Boustta, M.; Colombo, P.-E.; Lenglet, S.; Poujol, S.; Vert, M. Versatile UCST-Based Thermoresponsive Hydrogels for Loco-Regional Sustained Drug Delivery. *J. Control. Release* **2014**, *174*, 1–6.

(8) Dinarvand, R.; D'Emanuele, A. The Use of Thermoresponsive Hydrogels for On-off Release of Molecules. *J. Control. Release* **1995**, *36* (3), 221–227.

(9) Sivakumaran, D.; Bakaic, E.; Campbell, S. B.; Xu, F.; Mueller, E.; Hoare, T. Fabricating Degradable Thermoresponsive Hydrogels on Multiple Length Scales via Reactive Extrusion, Microfluidics, Self-Assembly, and Electrospinning. *J. Vis. Exp.* **2018**, *2018* (134), 1–12.

(10) Schmaljohann, D.; Oswald, J.; Jørgensen, B.; Nitschke, M.; Beyerlein, D.; Werner, C. Thermo-Responsive PNiPAAm-g-PEG Films for Controlled Cell Detachment. *Biomacromolecules* **2003**, *4* (6), 1733–1739.

(11) Cooperstein, M. A.; Canavan, H. E. Biological Cell Detachment from Poly(N-Isopropyl Acrylamide) and Its Applications. *Langmuir* **2010**, *26* (11), 7695–7707.

(12) Comminges, C.; Frasca, S.; Sütterlin, M.; Wischerhoff, E.; Laschewsky, A.; Wollenberger, U. Surface Modification with Thermoresponsive Polymer Brushes for a Switchable Electrochemical Sensor. *RSC Adv.* **2014**, *4* (81), 43092–43097.

(13) Toma, M.; Jonas, U.; Mateescu, A.; Knoll, W.; Dostalek, J. Active Control of SPR by Thermoresponsive Hydrogels for Biosensor Applications. *J. Phys. Chem. C* **2013**, *117* (22), 11705–11712.

(14) Zhou, G.; Harruna, I. I.; Zhou, W. L.; Aicher, W. K.; Geckeler, K. E. Nanostructured Thermosensitive Polymers with Radical Scavenging Ability. *Chem. – A Eur. J.* **2006**, *13* (2), 569–573.

(15) Gant, R. M.; Abraham, A. A.; Hou, Y.; Cummins, B. M.; Grunlan, M. A.; Coté, G. L. Design of a Self-Cleaning Thermoresponsive Nanocomposite Hydrogel Membrane for Implantable Biosensors. *Acta Biomater.* **2010**, *6* (8), 2903–2910.

(16) Pernia Leal, M.; Torti, A.; Riedinger, A.; La Fleur, R.; Petti, D.; Cingolani, R.; Bertacco, R.; Pellegrino, T. Controlled Release of Doxorubicin Loaded within Magnetic Thermo-Responsive Nanocarriers under Magnetic and Thermal Actuation in a Microfluidic Channel. *ACS Nano* **2012**, *6* (12), 10535–10545.

(17) Ryu, S.; Yoo, I.; Song, S.; Yoon, B.; Kim, J.-M. A Thermoresponsive Fluorogenic Conjugated Polymer for a Temperature Sensor in Microfluidic Devices. *J. Am. Chem. Soc.* **2009**, *131* (11), 3800–3801.

(18) Nagase, K.; Okano, T. Thermoresponsive-Polymer-Based Materials for

Temperature-Modulated Bioanalysis and Bioseparations. *J. Mater. Chem. B* **2016**, *4* (39), 6381–6397.

(19) Fukumori, K.; Akiyama, Y.; Kumashiro, Y.; Kobayashi, J.; Yamato, M.; Sakai, K.; Okano, T. Characterization of Ultra-Thin Temperature-Responsive Polymer Layer and Its Polymer Thickness Dependency on Cell Attachment/Detachment Properties. *Macromol. Biosci.* **2010**, *10* (10), 1117–1129.

(20) Matsuzaka, N.; Nakayama, M.; Takahashi, H.; Yamato, M.; Kikuchi, A.; Okano, T. Terminal-Functionality Effect of Poly(N-Isopropylacrylamide) Brush Surfaces on Temperature-Controlled Cell Adhesion/Detachment. *Biomacromolecules* **2013**, *14* (9), 3164–3171.

(21) Nagase, K.; Yamato, M.; Kanazawa, H.; Okano, T. Poly(N-Isopropylacrylamide)-Based Thermoresponsive Surfaces Provide New Types of Biomedical Applications. *Biomaterials* **2018**, *153*, 27–48.

(22) Haraguchi, K.; Takehisa, T.; Ebato, M. Control of Cell Cultivation and Cell Sheet Detachment on the Surface of Polymer/Clay Nanocomposite Hydrogels. *Biomacromolecules* **2006**, *7* (11), 3267–3275.

(23) Wang, T.; Liu, D.; Lian, C.; Zheng, S.; Liu, X.; Wang, C.; Tong, Z. Rapid Cell Sheet Detachment from Alginate Semi-Interpenetrating Nanocomposite Hydrogels of PNIPAm and Hectorite Clay. *React. Funct. Polym.* **2011**, *71* (4), 447–454.

(24) Lutz, J. F. Polymerization of Oligo(Ethylene Glycol) (Meth)Acrylates: Toward New Generations of Smart Biocompatible Materials. *J. Polym. Sci. Part A Polym. Chem.* **2008**, *46* (11), 3459–3470.

(25) Lutz, J.-F.; Akdemir, Ö.; Hoth, A. Point by Point Comparison of Two Thermosensitive Polymers Exhibiting a Similar LCST: Is the Age of Poly(NIPAM) Over? *J. Am. Chem. Soc.* **2006**, *128* (40), 13046–13047.

(26) Lutz, J.-F.; Hoth, A. Preparation of Ideal PEG Analogues with a Tunable Thermosensitivity by Controlled Radical Copolymerization of 2-(2-Methoxyethoxy)Ethyl Methacrylate and Oligo(Ethylene Glycol) Methacrylate. *Macromolecules* **2006**, *39* (2), 893–896.

(27) Erik, W.; Katja, U.; Andreas, L.; Hans G., B.; André, L.; Claus, D.; Jean-François, L. Controlled Cell Adhesion on PEG-Based Switchable Surfaces. *Angew. Chemie Int. Ed.* **2008**, *47* (30), 5666–5668.

(28) Uhlig, K.; Wischerhoff, E.; Lutz, J.-F.; Laschewsky, A.; Jaeger, M. S.; Lankenau, A.; Duschl, C. Monitoring Cell Detachment on PEG-Based Thermoresponsive

Surfaces Using TIRF Microscopy. *Soft Matter* **2010**, *6* (17), 4262–4267.

(29) Smeets, N. M. B.; Bakaic, E.; Patenaude, M.; Hoare, T. Injectable and Tunable Poly(Ethylene Glycol) Analogue Hydrogels Based on Poly(Oligoethylene Glycol Methacrylate). *Chem. Commun.* **2014**, *50* (25), 3306–3309.

(30) Bakaic, E.; Smeets, N. M. B.; Dorrington, H.; Hoare, T. "Off-the-Shelf" Thermoresponsive Hydrogel Design: Tuning Hydrogel Properties by Mixing Precursor Polymers with Different Lower-Critical Solution Temperatures. *RSC Adv.* **2015**, *5* (42), 33364–33376.

(31) Smeets, N. M. B.; Bakaic, E.; Patenaude, M.; Hoare, T. Injectable Poly(Oligoethylene Glycol Methacrylate)-Based Hydrogels with Tunable Phase Transition Behaviours: Physicochemical and Biological Responses. *Acta Biomater.* **2014**, *10* (10), 4143–4155.

(32) Kaneko, Y.; Yoshida, R.; Sakai, K.; Sakurai, Y.; Okano, T. Temperature-Responsive Shrinking Kinetics of Poly (N-Isopropylacrylamide) Copolymer Gels with Hydrophilic and Hydrophobic Comonomers. *J. Memb. Sci.* **1995**, *101* (1), 13–22.

(33) Zhang, X.-Z.; Yang, Y.-Y.; Chung, T.-S.; Ma, K.-X. Preparation and Characterization of Fast Response Macroporous Poly(N-Isopropylacrylamide) Hydrogels. *Langmuir* **2001**, *17* (20), 6094–6099.

(34) Chu, L.-Y.; Kim, J.-W.; Shah, R. K.; Weitz, D. A. Monodisperse Thermoresponsive Microgels with Tunable Volume-Phase Transition Kinetics. *Adv. Funct. Mater.* **2007**, *17* (17), 3499–3504.

(35) Serizawa, T.; Wakita, K.; Akashi, M. Rapid Deswelling of Porous Poly(N-Isopropylacrylamide) Hydrogels Prepared by Incorporation of Silica Particles. *Macromolecules* **2002**, *35* (1), 10–12.

(36) Li, X.; Zhang, X.-Z.; Chu, Y.-F.; Xu, X.-D.; Cheng, S.-X.; Zhuo, R.-X.; Wang, Q.-R. Fast Responsive Poly(N-Isopropylacrylamide) Hydrogels Prepared in Phenol Aqueous Solutions. *Eur. Polym. J.* **2006**, *42* (10), 2458–2463.

(37) Zhang, J.-T.; Cheng, S.-X.; Huang, S.-W.; Zhuo, R.-X. Temperature-Sensitive Poly(N-Isopropylacrylamide) Hydrogels with Macroporous Structure and Fast Response Rate. *Macromol. Rapid Commun.* **2003**, *24* (7), 447–451.

(38) Liu, F.; Tao, G.; Zhuo, R. Synthesis of Thermal Phase Separating Reactive Polymers and Their Applications in Immobilized Enzymes. *Polym. J.* **1993**, *25*, 561.

(39) Kurisawa, M.; Yokoyama, M.; Okano, T. Gene Expression Control by Temperature with Thermo-Responsive Polymeric Gene Carriers. *J. Control. Release* **2000**, *69* (1), 127–137.

(40) Shibayama, M.; Nagai, K. Shrinking Kinetics of Poly(N-Isopropylacrylamide) Gels T-Jumped across Their Volume Phase Transition Temperatures. *Macromolecules* **1999**, *32* (22), 7461–7468.

(41) Xia, L.-W.; Xie, R.; Ju, X.-J.; Wang, W.; Chen, Q.; Chu, L.-Y. Nano-Structured Smart Hydrogels with Rapid Response and High Elasticity. *Nat. Commun.* **2013**, *4*, 2226.

(42) Yue, L.-L.; Xie, R.; Wei, J.; Ju, X.-J.; Wang, W.; Chu, L.-Y. Nano-Gel Containing Thermo-Responsive Microspheres with Fast Response Rate Owing to Hierarchical Phase-Transition Mechanism. *J. Colloid Interface Sci.* **2012**, *377* (1), 137–144.

(43) Antoniuk, I.; Kaczmarek, D.; Kardos, A.; Varga, I.; Amiel, C. Supramolecular Hydrogel Based on PNIPAm Microgels Connected via Host-Guest Interactions. *Polymers (Basel).* **2018**, *10* (6), 1–17.

(44) Wang, J.; Sutti, A.; Wang, X.; Lin, T. Fast Responsive and Morphologically Robust Thermo-Responsive Hydrogel Nanofibres from Poly(N-Isopropylacrylamide) and POSS Crosslinker. *Soft Matter* **2011**, *7* (9), 4364–4369.

(45) Xu, F.; Sheardown, H.; Hoare, T. Reactive Electrospinning of Degradable Poly(Oligoethylene Glycol Methacrylate)-Based Nanofibrous Hydrogel Networks. *Chem. Commun.* **2016**, *52* (7), 1451–1454.

(46) Smeets, N. M. B.; Bakaic, E.; Patenaude, M.; Hoare, T. Injectable and Tunable Poly(Ethylene Glycol) Analogue Hydrogels Based on Poly(Oligoethylene Glycol Methacrylate). *Chem. Commun.* **2014**, *50* (25), 3306–3309.

(47) Smeets, N. M. B.; Bakaic, E.; Yavitt, F. M.; Yang, F.-C.; Rheinstädter, M. C.; Hoare, T. Probing the Internal Morphology of Injectable Poly(Oligoethylene Glycol Methacrylate) Hydrogels by Light and Small-Angle Neutron Scattering. *Macromolecules* **2014**, *47* (17), 6017–6027.

(48) Patenaude, M.; Smeets, N. M. B.; Hoare, T. Designing Injectable, Covalently Cross-Linked Hydrogels for Biomedical Applications. *Macromol. Rapid Commun.* **2014**, *35* (6), 598–617.

Chapter 6

Single-Step Reactive Electrospinning of Cell-Loaded Nanofibrous Scaffolds as Ready-to-Use Tissue Patches

Abstract

A reactive electrospinning strategy is used to fabricate viable and proliferative cell-loaded nanofibrous hydrogel scaffolds in a single step using an all-aqueous approach. In situ-gelling and degradable hydrazone-crosslinked poly (oligo ethylene glycol methacrylate)-based hydrogel nanofibrous networks can be produced directly in the presence of cells to support long-term cell viability, adhesion, and proliferation, in contrast to bulk hydrogels of the same composition. Furthermore, the capacity of the gel nanofibers to retain bound water maintains this high cell viability and proliferative capacity following a freeze/thaw cycle without requiring any cryoprotectant additives, ideal properties for ready-to-use functional tissue patches.

Keywords: Cell electrospinning; Hydrogel; Nanofibers; Cell encapsulation; Tissue scaffolds

6.1 Introduction

Tissue engineering approaches typically aim to mimic the chemical, mechanical, interfacial (i.e. hydrophilicity), and structural properties of native extracellular matrix (ECM) that are known to direct cell responses *in vivo*.[1–4] Hydrogels have attracted significant interest in

this context given their low non-specific protein adsorption, cytocompatibility, ease of functionalization, and biomimetic mechanics relative to soft tissues.[5] Multiple types of both bulk[6] and injectable[7] hydrogels have been explored for this purpose with some notable successes, including a range of structured hydrogels with well-defined porosities targeted to support cell spreading and/or growth within the matrix[8–10].

However, significant challenges remain that limit the utility of hydrogel scaffolds for tissue engineering. First, cells tend not to adhere strongly to hydrogels, requiring the incorporation of functional tags such as RGD peptides[11–13] or other cell signalling molecules[10,14] to promote cell interactions with the scaffold. The enhanced substrate-cell contact area achieved in 3D relative to 2D can facilitate sufficient cell adhesion to maintain cell viability even with cell-repellent hydrogel compositions; however, cells encapsulated in such scaffolds typically do not spread or grow, as desired for functional tissue engineering. Second, native ECM contains multiple types of fibrous structures, primarily based on collagen and elastin, on length scales ranging from a few to hundreds of nanometers that provide essential topographical support for cell adhesion and migration[15,16]. While electrospun nanofibrous scaffolds based on water-insoluble polymers have demonstrated promise due to their capacity to provide such topographical signaling[1,13,17–19], these types of nanofibrous structures are difficult to reproduce in synthetic hydrogel scaffolds more appropriate for engineering soft tissues[2,6,11,15,16]. Third, existing methods to create structured hydrogels (e.g. porogen templating[20], gas foaming[21], emulsification[22], freeze drying[23], stereolithography[24], and conventional electrospinning[25]) require additives, energy inputs, and/or organic solvents, making these methods either partially or fully incompatible with cells. Consequently, cells must be loaded into such scaffolds post-fabrication, generally via simple diffusion (although other techniques such as microfluidic loading and vacuum filtration have also been used to accelerate the process[26–28]). Although some of these studies have reported uniformly-seeded scaffolds using such techniques, such post-seeding strategies have a much higher probability of presenting non-uniform cell distributions, challenges in terms of precise spatial patterning of cells, and/or reasonably long fabrication times to allow time for cells to diffuse into and adhere to the matrix. While 3D bioprinting can in part address these challenges, the resolution of existing 3D bioprinting approaches is insufficient to create the nanoscale topologies particularly useful for cell signaling.[29]

Given that electrospinning has the capacity to create the types of nanofibrous but microporous networks particularly suitable for cell growth, significant effort has been invested in adapting conventional electrospinning processes to include cells, albeit with mixed success. Simply electrospinning polymer fibers on top of plated cells is suitable to create 2D cell scaffolds but cannot create scaffolds in which cells are distributed in 3D.[30] Alternately, coaxial needles in which the cell medium was contained within the core and a polymer solution was extruded as a shell have been reported to encapsulate both mammalian[31] and bacterial cells[32,33] within polymeric microfibers. However, the polymer used for the outer shell must be either water-soluble (in which case the scaffold dissolves when placed in media) or water-insoluble and dissolved in an organic solvent (inducing cytotoxicity during processing and leaving behind a water-insoluble polymer shell that encapsulates the cells and presents challenges with nutrient transport). Side-by-side simultaneous cell electrospraying and nanofiber electrospinning[34] offers another option for creating 3D cell-loaded scaffolds but requires organic solvents and a fairly complex electrospinning geometry.

Recently, we reported an alternative approach to fabricate hydrogel-based nanofibers via an all-aqueous process based on the concept of reactive electrospinning.[35] Oligomers based on poly(oligoethylene glycol methacrylate) (POEGMA), a poly(ethylene glycol)-mimetic polymer with significantly enhanced chemical and mechanical tunability[36], were functionalized with hydrazide and aldehyde groups and electrospun from a double barrel syringe. Mixing of the functional oligomers results in rapid *in situ* hydrazone crosslinking to covalently stabilize well-defined nanofibers without requiring any post-crosslinking, organic solvents, or additives. The hydrazone bond is also hydrolytically labile, enabling slow (~12 week) degradation of the scaffold over time[35]. Relative to previously reported electrospun hydrogels based on either ECM components like collagen or gelatin or synthetic polymers[13,37], our approach is unique in that it can be done using only water as a solvent and/or does not require external energy inputs (e.g. UV irradiation or heating) or any type of templating fiber.

Herein, we apply these unique advantages to directly fabricate uniform cell-loaded nanofibrous scaffolds capable of supporting cell adhesion and growth in 3D in a single step by co-electrospinning cells with our functional oligomer solutions. The topography and hygroscopicity of the resulting nanofibrous hydrogel network facilitate cell responses not

observed in conventional (i.e. non-fibrous) hydrogel networks and stabilize cells upon freezing, preserving the capacity of cells to remain viable and proliferate within the scaffolds following cold storage without the need for added cryoprotectants.

6.2 Experimental Section

6.2.1 Synthesis of POEGMA polymers

Hydrazide-functionalized POEGMA (POH) and aldehyde-functionalized POEGMA (POA) were synthesized by free radical polymerization as previously described.[35] In brief, POH was prepared by adding 2,2-azo-bis-isobutryic acid dimethyl ester (AIBMe, 37 mg, 0.16 mmol, Wako Chemicals), oligo (ethylene glycol) methyl ether methacrylate (OEGMA, 4.0 g, 8.4 mmol, Sigma-Aldrich), acrylic acid (AA, 0.25 g, 3.5 mmol, Sigma-Aldrich) and dioxane (20 mL, Caledon Labs) to a flask and polymerizing at 75 °C for 4 hours under magnetic stirring to form poly(OEGMA-*co*-AA). Following purification via dialysis (6x6 hr cycles against distilled deionized water), poly(OEGMA-*co*-AA) was functionalized with hydrazide groups via the addition of adipic acid dihydrazide (ADH, 2.65 g, 15.2 mmol, Alfa Aesar) and N'-ethyl-N-(3-dimethylaminopropyl)-carbodiimide (EDC, 1.18 g, 6.2 mmol, Carbosynth, Compton CA) to obtain POH. POA was prepared by adding AIBMe (50 mg, 0.22 mmol), OEGMA (4.0 g, 8.4 mmol), N-(2,2-dimethoxyethyl) methacrylamide (DMEMAm, 0.60 g, 3.5 mmol, synthesized in-house as previously described[36]) and dioxane (20 mL) to a flask and polymerizing at 75 °C for 4 hours under magnetic stirring to form poly(OEGMA-co-DMEMAm). Following purification via dialysis (6x6 hr cycles against distilled deionized water), the poly(OEGMA-co-DMEMAm) polymer was dissolved in 100 mL of 0.25 M HCl to hydrolyze the acetal groups to aldehydes. Both final polymers were purified by dialysis (6x6 hr cycles against distilled deionized water), lyophilized, and stored in sterile 1× PBS at a concentration of 15 wt% at 4 °C for further use. The molar concentrations of functional groups on POH and POA were calculated by ^{1}H-NMR (600 MHz, Bruker) and titration (ManTech automatic titrator, 0.1 M NaOH titrant, 1 mg/mL polymer solution), while the molecular weights of POH and POA were

determined by aqueous gel permeation chromatography. See Support Information Table S1 for full characterization data and methodologies for the precursor polymers.

6.2.2 Cell culture

NIH 3T3 fibroblasts (ATCC) and C2C12 myoblasts (ATCC) were cultured in Dulbecco's Modified Eagle's Medium (DMEM, Life Technologies) with 10% fetal bovine serum (FBS, ThermoFisher) and 1% penicillin-streptomycin (ThermoFisher) in a gas plasma-treated polystyrene petri dish (VWR). Both 3T3 fibroblasts and C2C12 myoblasts were cultured to ~80% confluency before use. Non-treated petri dishes (Fisher Scientific) were used to culture both bulk and nanofibrous hydrogel-encapsulated cells to ensure that no driving force was present for cells to migrate from the scaffolds to adhere on the petri dishes. All cells were incubated at 37°C and 5% CO_2.

6.2.3 Preparation of cell-loaded electrospun nanofibrous hydrogels

Poly (ethylene oxide) (PEO, M_w = 600,000 g/mol, Sigma-Aldrich) was dissolved in sterile DMEM at a concentration of 5 wt%. Subsequently, 0.25 mL of PEO solution was added to 0.25 mL POH or POA solution (both at 15 wt%) to form the POH+PEO and POH+POA precursor electrospinning solutions with a net concentration of 7.5 wt% POH or POA and 2.5 wt% PEO. All precursor solutions were filtered through a 0.2 mm syringe filter to ensure sterility. Cells were added to the POH+PEO precursor solution by centrifuging a 1 mL cell suspension (1×10^6 cells/mL) and suspending the resulting cell pellet in the POH+PEO precursor solution. Subsequently, 0.5 mL of the POH+PEO+cells suspension and 0.5 mL of POA+PEO solution were loaded into separate barrels of a double-barrel syringe equipped with a static mixer (MedMix L series, 2.5 mL capacity). An 18 G blunt needle was connected to the end of the static mixer, and a 10 kV potential difference was applied between the needle and a patterned collector consisting of multiple wires separated by a 1 cm air gap (Glassman High Voltage, 0 to 20kV, input 700 μA, 115 V 1PH AC input). A syringe pump was used to pump the precursor solutions at a rate of 10 μL/min for one hour for electrospinning, after which the (dry) scaffold was immediately transferred into

the DMEM growth media. Cell-free controls were performed using the same parameters but excluding cells from the POH+PEO precursor solution. The entire protocol was conducted inside a biosafety cabinet to maintain sterility, with the humidity for all experiments maintained between 23-26% RH. The resulting cell densities for 3T3 and C2C12-loaded electrospun hydrogels were 4600 ± 2500 cell/cm^2 and 4200 ± 1300 cells/cm^2 respectively (20 images analyzed per sample).

6.2.4 Preparation of cell-loaded bulk hydrogels

The precursor solutions were prepared as described above for the electrospun scaffolds but omitting the PEO electrospinning aid, resulting in POH and POA concentrations of 15 wt% in the pre-gel solutions; note that the 7.5 wt% solutions as used for electrospinning cannot form bulk gels; gelation is possible with the lower concentrations in electrospinning only because of solvent evaporation during the spinning process to increase the polymer concentration. The same double barrel syringe used for electrospinning experiments was used to extrude hydrogels into a rubber mold of diameter 9 mm and thickness 2 mm, with macroscopic gelation apparent after ~30 minutes. Hydrogels were maintained at room temperature for one hour (to be consistent with the electrospinning protocol) and then transferred into DMEM media and cultured using the same techniques as the electrospun scaffolds.

6.2.5 Mechanical properties of scaffolds

The Microsquisher (CellScale Biomaterials Testing, Waterloo, Canada) was used to measure the elastic properties of electrospun cell-loaded scaffolds. Samples were loaded on the instrument by puncturing them with forks consisting of 5 pins (diameter 254 μm) spaced 7 mm apart. The forks were then attached to a 559 μm gauge cantilever to allow for high-resolution mechanical measurements. Samples were stretched to 10% elongation over at least 15 cycles, using with loading and recovery durations of 20 seconds each and relaxation times of 5 seconds. The thickness of tested samples was ~50 μm. See Support Information Video S1 for a visual description of the testing method.

6.2.6 Microscopic analysis of cell-loaded scaffolds

Scanning electron microscopy (SEM, Tecan Vega II LSU instrument) was used to observe both scaffold and cell morphologies after electrospinning. All SEM images were collected at a voltage of 10 kV using a working distance of 6 mm. SEM samples were prepared by mounting the electrospun scaffolds on a SEM stub and subsequently sputter coating the scaffolds with gold to prevent charging. Confocal laser scanning microscopy (CLSM, Nikon) and fluorescence microscopy (FL, Axiovert 200, Carl Zeiss) were used to track cell live/dead responses, the proliferation of cells within the scaffolds, and cell morphologies after fluorescence staining using excitation wavelengths described in the following sections relevant to each assay conducted. Bright field (BF) images were also collected to correlate the cell location with the fibrous network. Confocal z-stack images (3D view) were collected by scanning planes at 10 μm intervals (the approximate diameter of the cells used) from the bottom to the top of the electrospun scaffold, using the same imaging parameters as used to collect the 2D images for each plane. For cell proliferation tracking, all parameters such as the voltage, offset, and gain were kept the same from day 1 to day 18, allowing for accurate tracking of the fluorescence emitted per cell in the CFSE assay.

6.2.7 CFSE staining for cell tracking

Carboxyfluorescein diacetate succinimidyl ester (CellTrace™ CFSE, ThermoFisher) was used to label cells to track proliferation and assess morphology. For proliferation assays from fresh samples and to assess the distribution of cells within the electrospun scaffolds, 3T3 or C2C12 cells were pre-stained with CFSE stock as per the manufacturer's protocol and then electrospun as described previously. For freeze-thaw proliferation assays, pre-encapsulated 3T3 cells were stained one day following the thawing of the scaffold, again using the same protocol but adding 4 x 3 mL washes in PBS to ensure any stain not taken up by cells is removed from the hydrogel scaffold. For cell morphology assays, pre-loaded 3T3 or C2C12 were stained with CFSE (using the recommended protocol with the additional washes) on the day the morphology assessment was conducted (i.e. following

either 1, 5, 7 and 18 days of cell culture). In this latter assay, paraformaldehyde stock (PFA, Sigma-Aldrich, 3 wt%) was used to fix the cells prior to imaging.

6.2.8 Far Red staining for cell tracking

In addition to CFSE, Far red (CellTrace^{TM} CFSE, ThermoFisher) was used to label cells to track proliferation within the freeze-thawed cell-loaded scaffolds. Cells were stained with Far Red stock solution following the manufacturer's protocol at the first day after thawing, after which the same imaging procedure as outlined for CFSE tracking was conducted.

6.2.9 Rhodamine 123 labeling of POA

Rhodamine 123 (Sigma Aldrich) was used to label the POA precursor polymer to enable imaging of the polymer distribution within the nanofibrous electrospun hydrogels in the dry and swollen states. Rhodamine 123 (5 mg) was mixed with POA precursor solution (1 g, 15 wt% in deionized water) for 24 hours under magnetic stirring to form a Schiff base that was subsequently reduced to a stable secondary amine linkage via the addition of sodium cyanoborohydride (8.25 mg, 10 mol eq. to rhodamine 123, 48 hours under stirring). The resulting labeled polymer was purified via dialysis (6x6 hr cycles against distilled deionized water), with the final rhodamine 123-labeled POA product lyophilized and stored in a 15 wt% solution in 1x PBS at 4 °C.

6.2.10 Cell viability assays

Cytotoxicity of polymer precursors For assessing the cytotoxicity of the polymer precursors, 3T3 fibroblasts or C2C12 myoblasts were seeded in a 96 well plate at a density of 10,000 cells per well and incubated in 100 μL DMEM at 37°C and 5% CO_2 for 24 hours. The plate was then washed with PBS and the growth medium replaced with 100 μL of DMEM containing POH, POA, and/or PEO, at concentrations ranging from 1 to 2 mg /mL, with cells then incubated for an additional 24 hours. Subsequently, the medium (with the materials) was removed and replaced with 90 μL of fresh DMEM and 10 μL of PrestoBlue reagent (ThermoFisher), followed by an additional one hour incubation step at 37°C. Cell

viabilities were estimated using a plate reader (Infinite M200 Pro, Tecan) to measure fluorescence (560 nm excitation/ 590 nm emission), with the result normalized to a cell-only (non-treated) control. Cell viabilities in the polymer precursor solutions used for electrospinning (7.5 wt% of POH/POA, 2.5 wt% of PEO) following the same method.

Cell viabilities during electrospinning For assessing cell viability as a function of applied voltage during electrospinning, a cell suspension of 100,000 cells/mL in DMEM media was processed at voltages of 0, 5, 10 and 15 kV using the same setup used for hydrogel scaffolds but increasing the feed rate to 200 μL/min (1 cm falling distance) and using a 60 mm × 15 mm petri dish petri dish as the collector to ensure all cells were collected. Following, the cells were aliquoted into separate wells of a 96 well plate, with each well containing 10,000 cells in 100 μL DMEM. Cells were cultured at 37°C for 24 hours before assessing viability using the same PrestoBlue protocol outlined above. For assessing cell viability as a function of dehydration time, cells were seeded in a 96 well plate at a density of 10,000 cells per well in 100 μL DMEM at 37°C for 24 hours. Following, the DMEM was removed and the plate was left in the incubator for defined times. Cell viability following different media-free exposure times was then assessed using the same PrestoBlue protocol outlined previously. For assessing cell viability as a function of cell stress during electrospinning, a cell suspension of 1,000,000 cells/mL was centrifuged and the cell media was replaced PEO (600 kDa) dissolved in PBS at different concentrations (1 wt%, 2 wt% and 3 wt%). The cell suspension in PEO was then loaded in a 3 mL syringe and electrospun into a 60 mm × 15 mm petri dish at voltages of 0, 5, 10, and 15 kV using feed rate of 200 μL/min and a 1 cm falling distance. The (liquid) product was then transferred into a 96 well plate at a concentration of 10,000 cells/well in 100 μL of DMEM+PEO solution. Cells were cultured at 37°C for 24 hours before assessing viability using the same PrestoBlue protocol outlined above.

Live/dead assay For assessing cell viability within the electrospun nanofibrous hydrogels and the conventional bulk hydrogels, a calcein AM/ethidium homodimer-1 (Et-D)

LIVE/DEAD assay (ThermoFisher) was used following the manufacturer's protocol except using longer incubation time (~1.5 h) at room temperature to allow the dyes to fully penetrate into the gel phase and an additional 4 x 3 mL PBS washes to ensure any non-bound dye was fully removed from the gel.

Frozen cell-matrix preparation 3T3 cell-loaded nanofibrous hydrogels were produced via electrospinning as previously described. After 1 h of electrospinning, the electrospun matrix was immediately immersed in liquid nitrogen (-195°C) without adding any additional cryoprotectants and left frozen in liquid nitrogen for 3 weeks. Following, the frozen scaffold was placed in pre-heated 37°C DMEM growth media (with 10 % FBS and 1% PS) to thaw and then, without any further purification steps, placed in an incubator and cultured over times ranging from 1 to 18 days. Cell viability (LIVE/DEAD assay) and proliferation (CFSE assay) were assessed as previously described for the fresh scaffolds.

6.3 Results and Discussion

6.3.1 Cell viability following electrospinning

POEGMA-hydrazide (POH) and POEGMA-aldehyde (POA) were synthesized by free radical polymerization as previously described[35] (Supporting Information Table S6.1), with neither precursor polymers exhibiting significant cytotoxicity to either 3T3 mouse fibroblasts or C2C12 mouse myoblast cells used herein as proof-of-concept cells (Supporting Information Figure S1a-b). Nanofiber precursor solutions were then prepared consisting of 7.5 wt% POH/POA and 2.5 wt% poly(ethylene oxide) (PEO, M_w=600,000 g/mol) in a sterile mixture of 1:1 phosphate buffered saline (PBS) and DMEM cell medium; PEO was added as an electrospinning aid to ensure sufficient chain entanglement to create nanofibers[35]. 3T3 or C2C12 cells (10^6 cells/mL) were suspended in the POH+PEO precursor solution, after which both precursor solutions were loaded into a double barrel syringe equipped with a static mixer (to ensure intimate mixing between the precursor polymers) and electrospun onto a stationary parallel electrode collector (Figure 6.1). Note

that the high viscosity of the PEO electrospinning aid prevents cell settling in the syringe (Supporting Information, Figure S6.2), maintaining a uniform cell density throughout the scaffold electrospinning process. Both 3T3 and C2C12 cells also maintained high viabilities when exposed to the nanofiber precursor solutions (Supporting Information Figure S6.1c). Electrospinning 3T3 and C2C12 cells alone under high voltage resulted in very high cell viability (91 ± 5 % for 3T3 and 98 ± 4 % for C2C12 at 15 kV, Supporting Information Figure S6.1d), consistent with previous reports that indicated minimal cell death due to the low (~700 mA) current used for electrospinning[38]. Furthermore, despite the fact that scaffolds were collected "dry", cells electrospun without any scaffolding materials maintained high viabilities after 1 h in dehydrated conditions at 37 °C (91± 7% for 3T3 and 83 ± 1 % for C2C12 cells relative to the same cells plated at the same concentration without electrospinning processing, Supporting Information Figure S6.1e). The high hygroscopicity of the gel scaffold would significantly prolong this viability when cells are co-electrospun with the scaffolding materials, although all scaffolds were still collected after 1 h of electrospinning since this time is sufficient to allow for the fabrication of a uniform self-supported cell-loaded patch. This processing time is orders of magnitude faster than typical approaches reported, which commonly require hours/days long solvent extraction/porogen removal and diffusive post-loading of cells. Similarly, when cells were electrospun in PEO-only solutions, the viscosity of which (Supporting Information Table S6.2) can induce additional shear stresses on the cells during the fiber stretching process[39], high cell viabilities were again achieved provided voltages did not exceed 10 kV (Supporting Information Figure S6.1f-g). As such, neither the polymer precursors nor the electrospinning process significantly impacted cell viability.

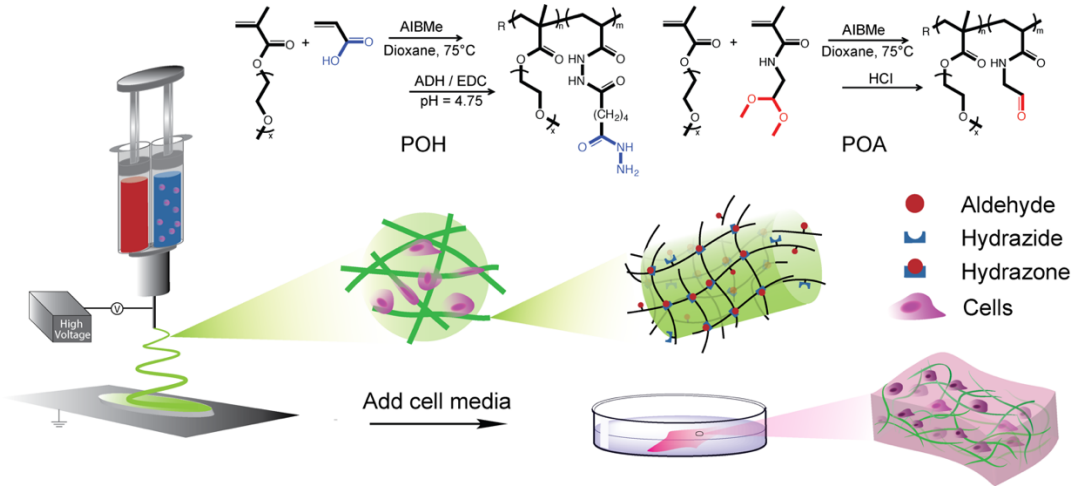

Figure 6.1 Schematic diagram demonstrating the reactive cell electrospinning process for cell encapsulation in nanofibrous hydrogels in a single, all-aqueous step.

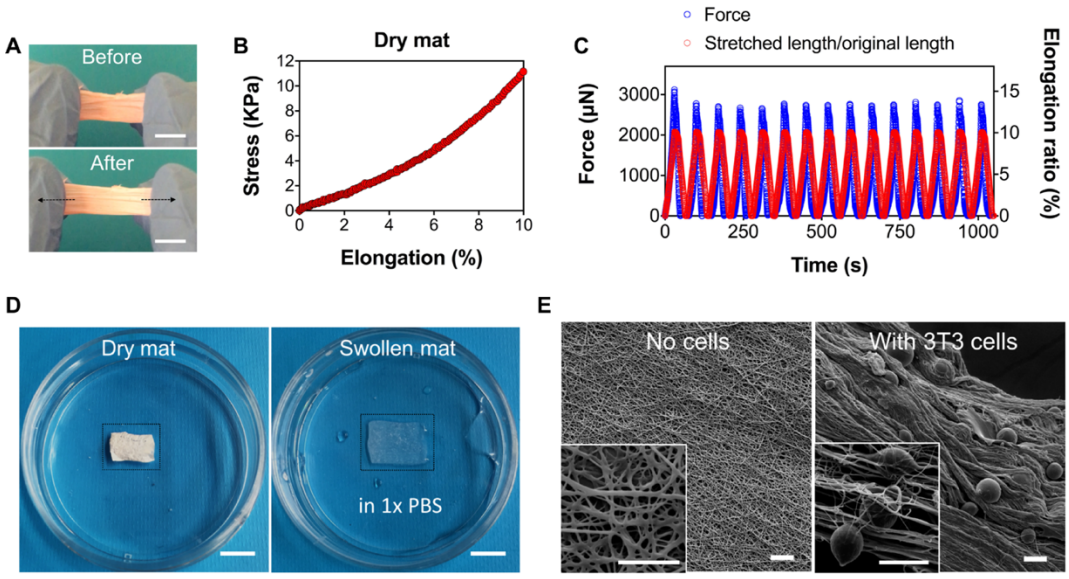

Figure 6.2 (A) Cell-loaded POEGMA electrospun scaffolds before and after manual stretch. Scale bars = 1 cm. (B) Stress-strain curve of a dry cell-loaded electrospun mat. (C) Cyclic tensile test of dry cell-loaded scaffold (10% elongation, 15 cycles) demonstrating the elasticity of the dry scaffolds. (D) Electrospun scaffold containing cells before and after swelling in 1× PBS. Scale bars = 1 cm. (E) SEM images of POEGMA nanofibers electrospun with and without 3T3 cells. Scale bars = 20 μm.

6.3.2 Mechanical and morphological properties of cell-loaded scaffolds

The electrospun cell-loaded scaffold was easy to handle and could be physically stretched without breaking (Figure 6.2A and Supporting Information Video S6.1), with a dry tensile modulus of ~100 kPa. (Figure 6.2B). Repeated tensile cycling at 10% elongation indicated the highly elastic properties of the scaffold in the dry state (Figure 6.2C and Supporting Information Video S6.1). The hydrogel nanofibers reswelled within one minute when immersed back into DMEM or PBS to form a nearly transparent matrix that maintained stability and shape over ~30 days of incubation time (Figure 6.2D and Supporting Information Video S6.1); in contrast, PEO-only electrospun scaffolds without the gelling POEGMA component dissolved fully within seconds.[35] The presence of cells during the electrospinning process slightly increased the average nanofiber diameter from 0.4 ± 0.1 μm in the absence of cells to 0.8 ± 0.2 μm (with 3T3 cells) or 0.7 ± 0.3 μm (with C2C12 cells) (Figure 6.2E and Supporting Information Table S6.3); this corresponds to a water content of ~95 % inside the gel nanofibers upon rehydration . This result is consistent with the applied voltage being less effective at stretching the nanofibers during the electrospinning process in the presence of large and elastic cells, although the nanoscale fiber dimensions are maintained. The nanofibrous scaffold structure was maintained following swelling (Figure 6.3A-B), with the swollen fiber diameter of 2.2 ± 0.2 μm significantly smaller than achieved by even the best existing 3D printing processes (Supporting Information Figure S6.3).

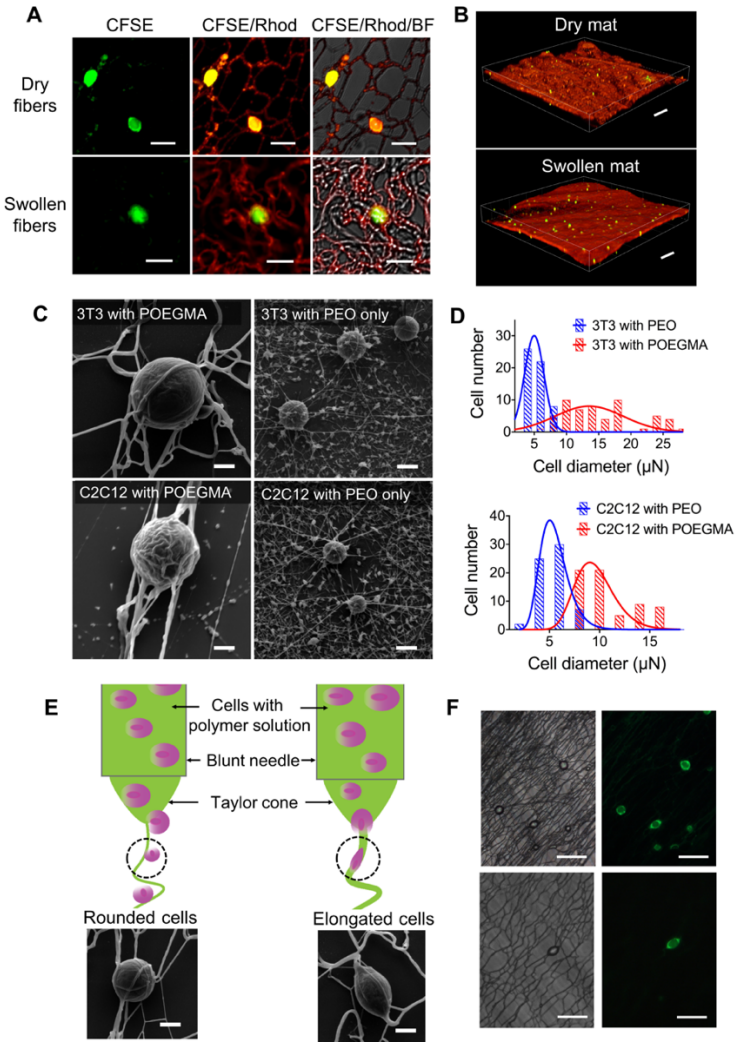

Figure 6.3 Electrospun cells can remain hydrated and assume different morphologies within nanofibrous hydrogel scaffolds. (A) Confocal images of 3T3 cells pre-stained with CFDA-SE (CFSE, green) and POEGMA electrospun nanofibers pre-stained with Rhodamine 123 (Rhod, red) imaged in fluorescence mode (488 nm and 563 nm excitation) and bright field (BF) mode in the dry and swollen states. Scale bar = 20 μm. (B) 3D confocal reconstructions of the nanofiber and cell distributions of dry (top) and swollen (bottom) scaffolds. Scale bars = 200 μm. (C) SEM images of 3T3 fibroblasts and C2C12 myoblasts electrospun within POEGMA hydrogel nanofibers and PEO fibers. Scale bars = 5 μm. (D) Cell diameter distributions of 3T3 fibroblasts (n=56) and C2C12 myoblasts (n=64) electrospun within POEGMA hydrogel nanofibers and PEO fibers. (E) Proposed mechanism for the formation of rounded and elongated cells depending on the position of the cells relative to the Taylor cone during electrospinning. Scale bars = 5 μm. (F) Bright field and fluorescence microscope images of 3T3 cells pre-stained with CFDA-SE show cells with both rounded (entrapped) and elongated (encapsulated) morphologies; the correspondence of the cell positioning between the light field images and the CFSE-stained fluorescence images confirm the identity of the cells in each image. Scale bars = 50 μm. All electrospun POEGMA nanofibers were prepared using 7.5 wt% POH/POA mixed with 2.5 wt% PEO; PEO-only fibers were prepared with 2.5 wt% PEO only (10 kV, 1 h).

6.3.3 Morphologies of encapsulated cells

SEM images of cells within the nanofibrous scaffolds (i.e. dried and under vacuum) exhibited cell average diameters of 15 ± 6 μm for 3T3 and 10 ± 3 μm for C2C12, identical to the diameters of fresh cells in DMEM suspension (14 ± 2 μm for 3T3 and 12 ± 2 μm for C2C12); in contrast, cells electrospun in a PEO-only matrix were significantly smaller (5 ± 2 μm for 3T3 and 6 ± 2 μm for C2C12) (Figure 6.3C-D and Supporting Information Table S6.3). This result demonstrates the unique capacity of the hydrogel scaffold to bind water and thus supporting a hydrated environment around the cells even when the scaffold is macroscopically dry, allowing cells to maintain their morphology even in a vacuum.

Two clearly distinct cell morphologies are evident for both 3T3 and C2C12 electrospun cell scaffolds (Figure 6.3E-F and Supporting Information Figure S6.4). The majority of cells (~90% in both scaffold types, as per image analysis) were rounded and appear to be physically entrapped *between* a web of nanofibers (Figure 6.3E) and/or surrounded by sheaths of nanofibers when thicker scaffolds were prepared (Supporting Information Figure S6.4a-b). However, a significant sub-population of cells (~10% in both scaffold types) appeared significantly elongated and encapsulated *within* nanofibers (Figure 6.3E), with both the position of the cells and direction of elongation corresponding directly to that of a single or a few aligned nanofibers (Supporting Information Figure S6.4c-d). This result is consistent with the probabilities of cells streaming *beside* the Taylor cone (i.e. nanofibers form independently to entrap cells *between* fibers) or *within* the Taylor cone (i.e. a gel sheath forms directly *around* cells) during electrospinning.

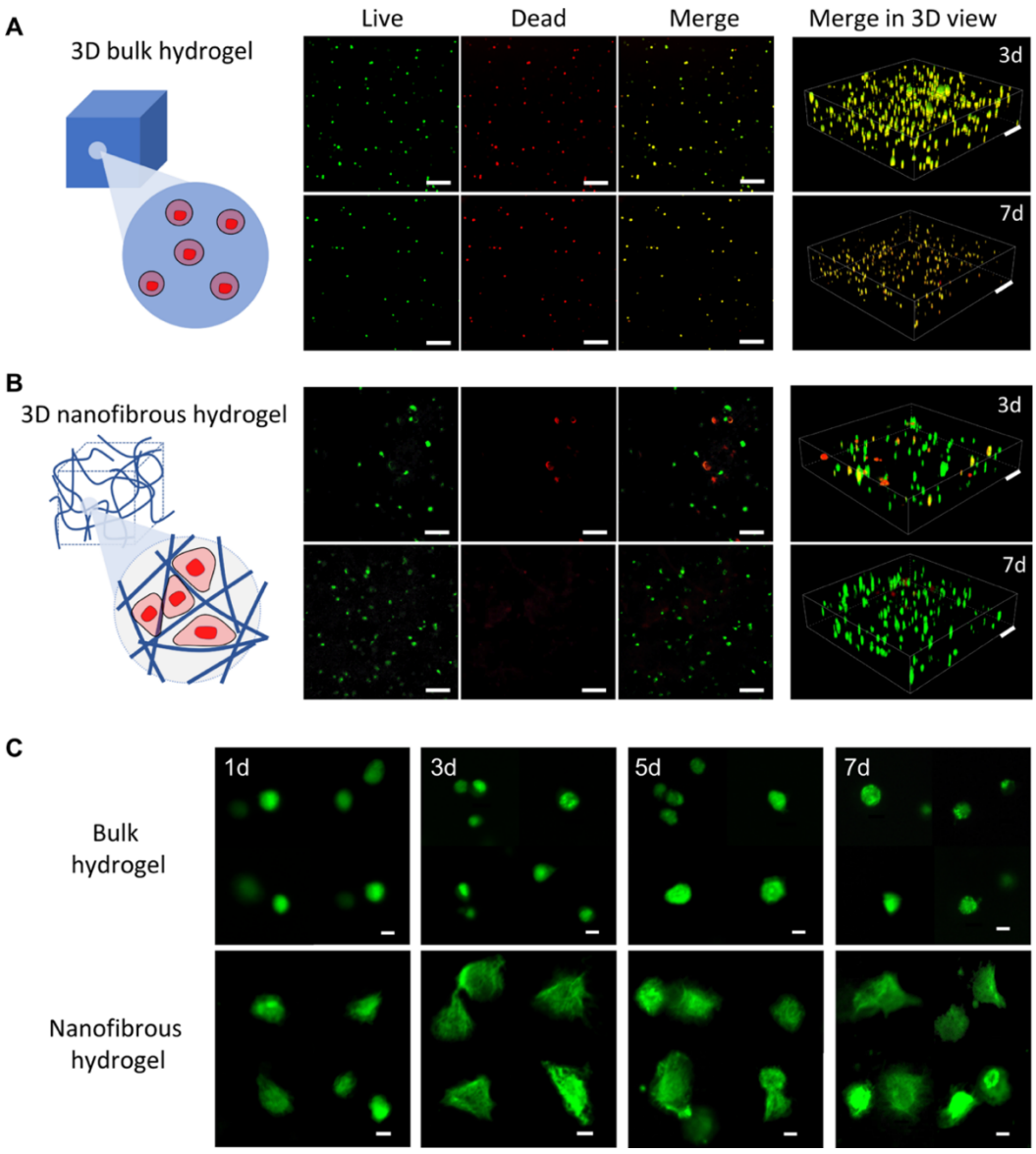

Figure 6.4 Electrospun nanofibrous hydrogels can maintain significantly higher cell viabilities and uniquely support cell-matrix interactions relative to bulk hydrogels of the same composition. (A-B) Confocal images of 3T3 cells encapsulated in (A) bulk hydrogels or (B) electrospun nanofibrous hydrogels of the same chemical composition after 3 days and 7 days of incubation showing live cells (green, 488 nm), dead cells (red, 561 nm), the overlay between the green and red channels, and 3D images showing the distribution of cells throughout the scaffold volume. Scale bars = 200 μm. (C) Comparison of cell morphology of 3T3 cells within bulk and nanofibrous hydrogels of the same chemical composition following 1, 3, 5, and 7 days of incubation (n=4). Scale bars = 10 μm. Cell density = 1×10^6 cells/mL in all cases. 3T3 cells were post-stained using CFDA-SE and fixed using PFA prior to imaging.

6.3.4 Cell viability in nanofibrous hydrogel scaffolds

To investigate the viability of cells within the electrospun scaffolds, a calcein AM/ethidium homodimer-1 LIVE/DEAD stain was used to characterize cells within the scaffolds 3 and 7 days post-electrospinning (Figure 6.4A-B; see Supporting Information Figure S6.5 for C2C12 results). Significantly more live cells (green) and fewer dead cells (red) were observed after 3 days of incubation in the electrospun hydrogel scaffolds compared to bulk hydrogels of an identical chemical composition. Furthermore, in the bulk hydrogels, cells staining as green (alive) tended also to stain red, indicative of apoptotic cells[40] (yellow in the composite image, Figure 6.4A); such cells are not evident in the electrospun nanofibrous gel (Figure 6.4B). This difference becomes even more distinct after 7 days, with 3D confocal microscopy images demonstrating that an increasing percentage of the cells in the nanofibrous hydrogels remained viable (suggestive of proliferation of live cells inside the matrix) while only apoptotic or dead cells were found in the bulk hydrogels (Figure 6.4 and Supporting Information Figure S6.5). Interestingly, this viability difference is observed even though the bulk hydrogels were never dried (i.e. they were extruded and *in situ*-gelled all in the hydrated state) while the electrospun scaffolds were macroscopically dry during the fabrication process, a processing difference that would in most cases result in significantly lower cell viability in the dried (electrospun) scaffolds but here shows the opposite. This difference in cell viability is matched by a clear difference in cell shape, with cells entrapped within the bulk hydrogel remaining spherical and small over the full seven-day assay while cells in the electrospun nanofibrous hydrogel appearing both larger and more asymmetric in shape, the latter consistent with the formation of adhesions with the cell scaffold (Figure 6.4C). Note that plating cells on top of the same POEGMA hydrogel in 2D results in almost complete suppression of cell adhesion[41], consistent with the high hydrophilicity of POEGMA-based hydrogels previously reported[42]. As such, the nanofibrous morphology significantly enhances the capacity of cells to interact with the matrix and thus remain viable over extended periods. We hypothesize this result is attributable to the nanofibers providing increased internal surface area and topological cues consistent with those in native ECM. Interestingly, performing the same experiment within a Geltrex ECM-based matrix results in similar cell viability compared to the electrospun

scaffold after 3 days but substantially higher cell death after 7 days (Supporting Information Figure S6.6). The improved performance of the electrospun POEGMA scaffolds is attributed to the higher persistence of the POEGMA scaffold (providing adhesion sites for cells over a longer period of time) and/or the role of the nanofibrous scaffold in enhancing for nutrient/waste transport in and out of the scaffold.

6.3.5 Cell proliferation in nanofibrous hydrogel scaffolds

Cell proliferation within the nanofibrous hydrogel scaffolds was subsequently tracked via long-term (18 day) incubation of the cell-loaded scaffolds in growth media. Both 3T3 and C2C12 cells proliferate within the electrospun hydrogel scaffolds in all three dimensions, with 3D confocal microscopy images indicating that cells uniformly fill the full volume of the nanofibrous hydrogel scaffold (Figure 6.5A-D, Supporting Information Figure S6.7a-b). Image analysis of the 3D confocal microscopy images suggest a ~4-fold increase in cell density for C2C12 cells and a ~3-fold increase in cell density for 3T3 cells between day 1 and day 18 of cell culture (Figure 6.5E). A simultaneous increase in cell number and decrease in fluorescence intensity per cell were also observed for each cell type using the CFSE assay tracking 2D sections of the scaffolds as a function of time (Figure 6.5F-G and Supporting Information Figure S6.7c), confirming that the increase in cell number is a result of the proliferation of live encapsulated cells as a parent cell splits its fluorescence between two daughter cells. Proliferation was not observed when either 3T3 or C2C12 cells were plated on a non-treated petri dish (i.e. no cell adhesion), while a similar degree of cell proliferation was observed between the 3D nanofibrous hydrogel and cells plated directly on a treated (i.e. adhesive) 2D petri dish assay (Supporting Information Figure S6.8). Coupled with the clear asymmetrical cell morphologies observed at incubation times of 5 days and later within the nanofibrous hydrogel networks (Figure 6.5), these results confirm that electrospun gel scaffolds can support cell-scaffold interactions and subsequent proliferation within the scaffold.

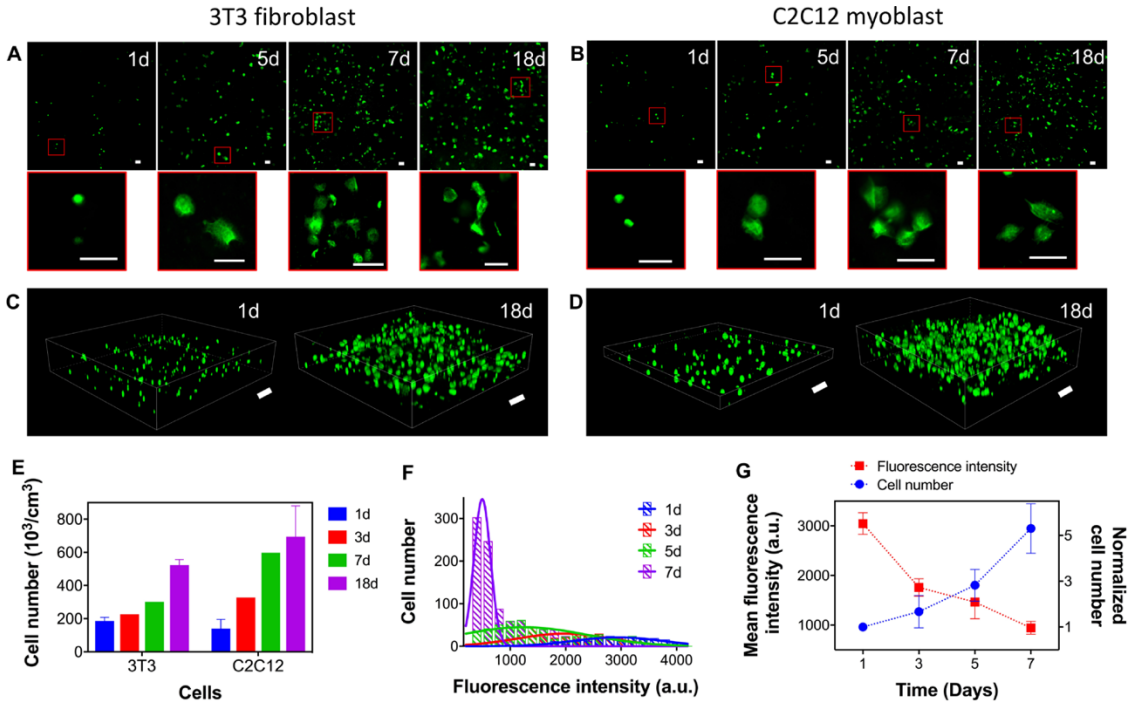

Figure 6.5 Cells can proliferate and spread within electrospun nanofibrous hydrogels. (A-B) Confocal fluorescence microscopy images of 3T3 (A) and C2C12 (B) cells after 1, 5, 7 and 18 days of cell culture demonstrating increasing cell number over time; subset images show the concurrent changes in cell morphology as a function of culture time. Scale bars = 50 μm. (C-D) 3D confocal microscopy images of 3T3 (C) and C2C12 (D) cells encapsulated in POEGMA hydrogel nanofibers after 1 day and 18 days. Scale bars = 200 μm. All cells were post-stained using CFDA-SE (488 nm, green) and fixed using 3 wt% PFA prior to imaging. (E) Volumetric 3T3 and C2C12 cell densities measured via ImageJ analysis of 3D confocal microscopy images in Figure 4C-D as a function of culture time, confirming cell proliferation within the electrospun scaffolds. All cells were post-stained using CFDA-SE and fixed using PFA prior to imaging (n=3 images per sample). (F) Histogram of 3T3 cell number versus fluorescence intensity per cell of 3T3 cells at 1, 3, 5 and 7 days calculated via CFDA-SE staining and the 2D confocal microscopy images in Supporting Information Figure S5c (n=4, 2 images per sample for analysis). (G) Mean fluorescence intensities and normalized 3T3 cell numbers at 1, 3, 5 and 7 days culture times from (e) (n=4, 4 images per sample for calculation). Cell density = 1×10^6 cells/mL.

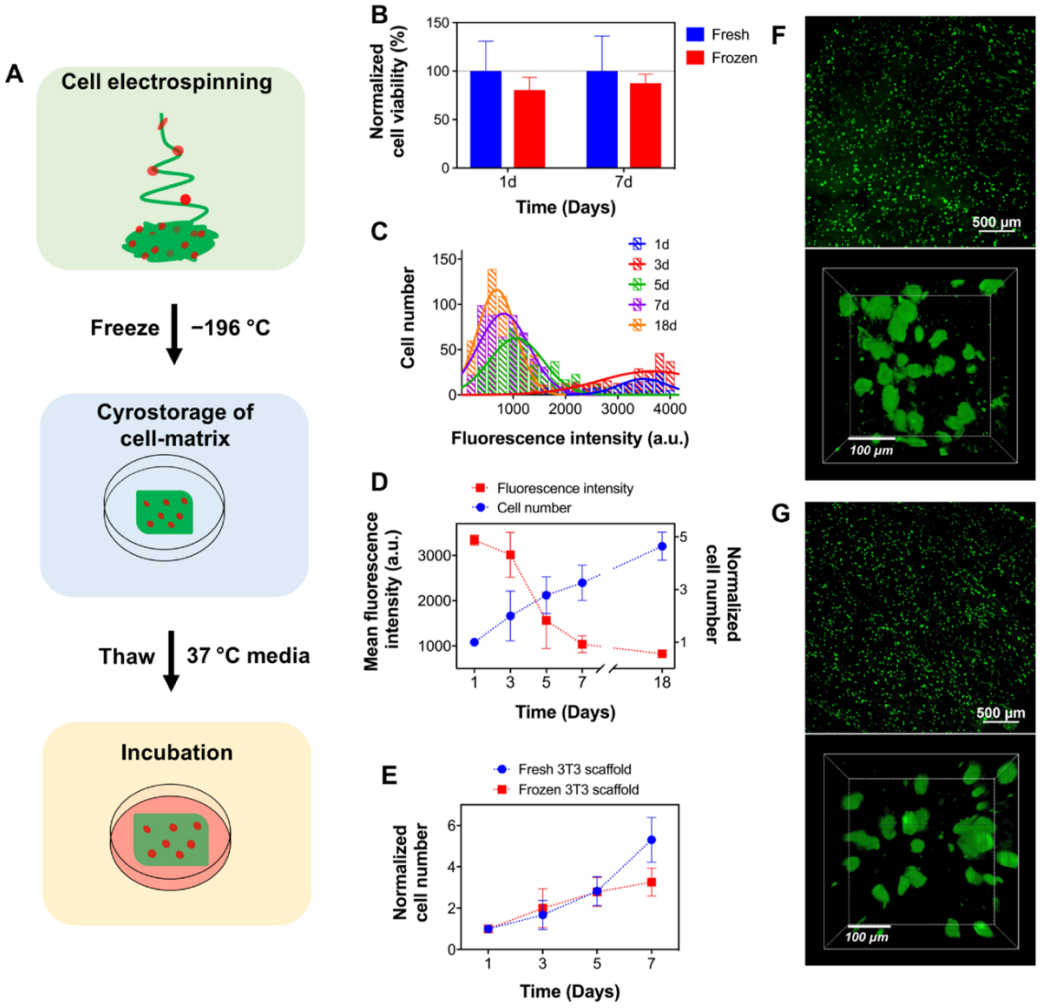

Figure 6.6 Electrospun nanofibrous hydrogels can maintain cell viability and cell proliferative ability after a freeze/thaw cycle without additional cryoprotectants. (A) Schematic of the process to prepare, freeze, and thaw an electrospun tissue patch. (B) Comparison of normalized cell viabilities of fresh and frozen 3T3 cells loaded in POEGMA electrospun scaffolds confirming that the nanofibrous scaffolds could protect cells during freezing. (n=4, calculated from 3D confocal images). (C) Histogram of 3T3 cell number versus fluorescence intensity per cell of 3T3 cells following a freeze/thaw cycle after 1,3, 5, 7 and 18 day culture times, calculated from confocal images (Supporting Information Figure S8a) using CFDA-SE staining (n=4, 2 images per sample for analysis). (D) Mean fluorescence intensities and normalized 3T3 cell number following a freeze/thaw cycle after 1, 3, 5, 7, and 18 day culture times (n=4, 3 images per sample for calculation). (n=4, 4 images per sample for calculation). (E) Comparison of proliferation of 3T3 cells with and without freezing at 1, 3, 5 and 7 days calculated from 2D confocal images using CFDA-SE staining. (F-G) Confocal microscopy of 3T3 cells within fresh (F) and frozen (G) POEGMA nanofibrous scaffolds captured by 2D (top) and 3D (bottom) images after 18 day culture. Cell density = 1×10^6 cells/mL in all cases. 3T3 cells were post-stained using CFDA-SE and fixed using PFA prior to imaging.

6.3.6 Storage-stable tissue patches following a freeze/thaw cycle

Given the capacity of the scaffold to bind water and promote cell adhesion/proliferation, the potential of reactive cell electrospinning to create ready-to-use tissue patches that could be frozen, thawed, and used as needed by a patient was next assessed. Electrospun 3T3 cell scaffolds were quick frozen in liquid nitrogen immediately after the 1 hour electrospinning experiment, stored frozen for 14 days in liquid nitrogen, thawed in pre-warmed DMEM at 37 °C, and then cultured identically to the fresh scaffolds (Figure 6.6A). High cell viability was maintained within the scaffold after the freeze/thaw process despite the fact that no cryoprotectants were used, with 80% viability after 1 day and 87% after 7 days compared to a fresh scaffold (Figure 6.6B). In contrast, if cells are frozen alone (outside a scaffold) in the absence of a cryoprotectant such as DMSO, almost complete cell death is observed in the same time frame (Supporting Information, Figure S6.9). A similar clear increase in the number and percentage of viable cells was observed via live/dead assay results (Supporting Information Figure S6.10a). Cell shape changed from rounded immediately after thawing to irregular at day 18 (Supporting Information Figure S6.10b), consistent with the capacity of cells to adhere to the matrix (as observed with fresh scaffolds, Figure 6.4C). Furthermore, the proliferative capacity of 3T3 cells within the 3D electrospun matrix was maintained even after freezing and cryostorage (Supporting Information Figure S6.10c), with both CFSE (Figure 6.6C-D) and Far Red (Supporting Information Figure S6.11) assays indicating the same concurrent increase in cell density and decrease in fluorescence intensity per cell between day 1 and day 18 consistent with cell division events. Indeed, very similar rates of cell proliferation were observed within the fresh and frozen/thawed scaffolds without any apparent lag period in cell proliferation as is often observed following conventional cryostorage (Figure 6.6E, F-G and Supporting Information Video S6.2), suggesting minimal if any cell stress as a result of the freeze/thaw process; we expect that the absence of a required cryoprotectant eliminates the induction period. Together, these observations suggest that the electrospun scaffolds can themselves serve as a cryoprotectant for cells without the need for the additives or step-wise freezing protocols.[43–45] We attribute this result to the combination of the macroscopic drying of the scaffold during electrospinning (leaving minimal non-bound water to freeze) and the

capacity of the hydrogel nanofibers to bind water and thus prevent large-scale ice crystal formation[46,47]. In this manner, reactive hydrogel cell electrospinning allows for one-step fabrication of a functional cell-loaded tissue patch that can be stored between fabrication and use, a significant potential benefit in terms of translating cellularized scaffolds to the clinic.

6.4 Conclusions

In summary, we have demonstrated that reactive electrospinning of hydrazone-crosslinkable POEGMA polymer precursors can create cellularized nanofibrous hydrogel scaffolds in a single and rapid all-aqueous processing step by simply adding cells to one of the precursor polymer solutions. Cells maintain both high viability as well as proliferative capacity following fabrication, in contrast to conventional bulk hydrogels of the same composition. In addition, the capacity of the hydrogel nanofibers to retain bound water both prevents dehydration (and thus cell death) during electrospinning and maintains cell viability and proliferative capacity following a freeze/store/thaw cycle. Together, these properties offering the possibility of creating ready-to-use cellularized tissue patches that can be stored and used immediately as required in therapeutic applications without requiring any purification or additional scaffold preparation steps at the point of care, in contrast to other existing cellularized scaffolds.

6.5 Acknowledgments

Funding from the Natural Sciences and Engineering Research Council of Canada (NSERC, Discovery Grant RGPIN 356609 and Strategic Project Grant SPG-447372-13) is gratefully acknowledged. The authors would like to thank Dr. Harald Stöver for access to a confocal microscope.

6.6 References

(1) Dvir, T.; Timko, B. P.; Kohane, D. S.; Langer, R. Nanotechnological Strategies for Engineering Complex Tissues. *Nat. Nanotechnol.* **2011**, *6* (1), 13–22.

(2) Stevens, M. M.; George, J. H. Exploring and Engineering the Cell Surface Interface. *Science* **2005**, *310* (November), 1135–1138.

(3) Watt, F. M.; Huck, W. T. S. Role of the Extracellular Matrix in Regulating Stem Cell Fate. *Nat. Rev. Mol. Cell Biol.* **2013**, *14* (8), 467–473.

(4) Place, E. S.; Evans, N. D.; Stevens, M. M. Complexity in Biomaterials for Tissue Engineering. *Nat. Mater.* **2009**, *8* (6), 457–470.

(5) Drury, J. L.; Mooney, D. J. Hydrogels for Tissue Engineering: Scaffold Design Variables and Applications. *Biomaterials* **2003**, *24* (24), 4337–4351.

(6) Benoit, D. S. W.; Schwartz, M. P.; Durney, A. R.; Anseth, K. S. Small Functional Groups for Controlled Differentiation of Hydrogel-Encapsulated Human Mesenchymal Stem Cells. *Nat. Mater.* **2008**, *7* (10), 816–823.

(7) Zhang, J.; Muirhead, B.; Dodd, M.; Liu, L.; Xu, F.; Mangiacotte, N.; Hoare, T.; Sheardown, H. An Injectable Hydrogel Prepared Using a PEG/Vitamin E Copolymer Facilitating Aqueous-Driven Gelation. *Biomacromolecules* **2016**, *17* (11), 3648–3658.

(8) Hwang, C. M.; Sant, S.; Masaeli, M.; Kachouie, N. N.; Zamanian, B.; Lee, S.-H.; Khademhosseini, A. Fabrication of Three-Dimensional Porous Cell-Laden Hydrogel for Tissue Engineering. *Biofabrication* **2010**, *2* (3), 035003.

(9) Lee, T. T.; García, J. R.; Paez, J. I.; Singh, A.; Phelps, E. A.; Weis, S.; Shafiq, Z.; Shekaran, A.; del Campo, A.; García, A. J. Light-Triggered in Vivo Activation of Adhesive Peptides Regulates Cell Adhesion, Inflammation and Vascularization of Biomaterials. *Nat Mater* **2015**, *14* (3), 352–360.

(10) Khalili, A. A.; Ahmad, M. R. A Review of Cell Adhesion Studies for Biomedical and Biological Applications. *Int. J. Mol. Sci.* **2015**, *16* (8), 18149–18184.

(11) Baker, B. M.; Chen, C. S. Deconstructing the Third Dimension - How 3D Culture Microenvironments Alter Cellular Cues. *J. Cell Sci.* **2012**, *125* (13), 3015–3024.

(12) Burdick, J. A.; Anseth, K. S. Photoencapsulation of Osteoblasts in Injectable RGD-Modified PEG Hydrogels for Bone Tissue Engineering. *Biomaterials* **2002**, *23* (22), 4315–4323.

(13) Baker, B. M.; Trappmann, B.; Wang, W. Y.; Sakar, M. S.; Kim, I. L.; Shenoy, V. B.; Burdick, J. a.; Chen, C. S. Cell-Mediated Fibre Recruitment Drives Extracellular Matrix Mechanosensing in Engineered Fibrillar Microenvironments. *Nat. Mater.* **2015**, *14* (12), 1262–1268.

(14) Vega, S. L.; Kwon, M.; Mauck, R. L.; Burdick, J. A. Single Cell Imaging to Probe Mesenchymal Stem Cell N-Cadherin Mediated Signaling within Hydrogels. *Ann. Biomed. Eng.* **2016**, *44* (6), 1921–1930.

(15) Blow, N. Cell Culture: Building a Better Matrix. *Nat. Methods* **2009**, *6* (8), 619–622.

(16) Watt, F. M.; Huck, W. T. S. Role of the Extracellular Matrix in Regulating Stem Cell Fate. *Nat Rev Mol Cell Biol* **2013**, *14* (8), 467–473.

(17) Feiner, R.; Engel, L.; Fleischer, S.; Malki, M.; Gal, I.; Shapira, A.; Shacham-Diamand, Y.; Dvir, T. Engineered Hybrid Cardiac Patches with Multifunctional Electronics for Online Monitoring and Regulation of Tissue Function. *Nat. Mater.* **2016**, *15* (March), 1–8.

(18) Greiner, A.; Wendorff, J. H. Electrospinning: A Fascinating Method for the Preparation of Ultrathin Fibers. *Angew. Chemie - Int. Ed.* **2007**, *46* (30), 5670–5703.

(19) Sill, T. J.; von Recum, H. A. Electrospinning: Applications in Drug Delivery and Tissue Engineering. *Biomaterials*. 2008, pp 1989–2006.

(20) Delaney, J. T.; Liberski, A. R.; Perelaer, J.; Schubert, U. S. Reactive Inkjet Printing of Calcium Alginate Hydrogel Porogens—a New Strategy to Open-Pore Structured Matrices with Controlled Geometry. *Soft Matter* **2010**, *6* (5), 866.

(21) Annabi, N.; Mithieux, S. M.; Weiss, A. S.; Dehghani, F. The Fabrication of Elastin-Based Hydrogels Using High Pressure CO2. *Biomaterials* **2009**, *30* (1), 1–7.

(22) Liu, S.; Jin, M.; Chen, Y.; Gao, H.; Shi, X.; Cheng, W.; Ren, L.; Wang, Y. High Internal Phase Emulsions Stabilised by Supramolecular Cellulose Nanocrystals and Their Application as Cell-Adhesive Macroporous Hydrogel Monoliths. *J. Mater. Chem. B* **2017**, *5* (14), 2671–2678.

(23) Kumar, A.; Mishra, R.; Reinwald, Y.; Bhat, S. Cryogels: Freezing Unveiled by Thawing. *Mater. Today* **2010**, *13* (11), 42–44.

(24) Chan, V.; Zorlutuna, P.; Jeong, J. H.; Kong, H.; Bashir, R. Three-Dimensional

Photopatterning of Hydrogels Using Stereolithography for Long-Term Cell Encapsulation. *Lab Chip* **2010**, *10* (16), 2062–2070.

(25) Pham, Q. P.; Sharma, U.; Mikos, A. G. Electrospinning of Polymeric Nanofibers for Tissue Engineering Applications: A Review. *Tissue Eng.* **2006**, *12* (5), 1197–1211.

(26) Wanasekara, N. D.; Ghosh, S.; Chen, M.; Chalivendra, V. B.; Bhowmick, S. Effect of Stiffness of Micron/Sub-Micron Electrospun Fibers in Cell Seeding. *J. Biomed. Mater. Res. Part A* **2014**, *103* (7), 2289–2299.

(27) Onoe, H.; Takeuchi, S. Cell-Laden Microfibers for Bottom-up Tissue Engineering. *Drug Discov. Today* **2015**, *20* (2), 236–246.

(28) Takei, T.; Kitazono, Z.; Ozuno, Y.; Yoshinaga, T.; Nishimata, H.; Yoshida, M. Vascular-like Network Prepared Using Hollow Hydrogel Microfibers. *J. Biosci. Bioeng.* **2016**, *121* (3), 336–340.

(29) Atala, S. V. M. & A. 3D Bioprinting of Tissues and Organs. *Nat. Biotechnol.* **2014**, *32* (8), 773–785.

(30) Dalton, P. D.; Klinkhammer, K.; Salber, J.; Klee, D.; Möller, M. Direct in Vitro Electrospinning with Polymer Melts. *Biomacromolecules* **2006**, *7* (3), 686–690.

(31) Townsend-Nicholson, A.; Jayasinghe, S. N. Cell Electrospinning: A Unique Biotechnique for Encapsulating Living Organisms for Generating Active Biological Microthreads/Scaffolds. *Biomacromolecules* **2006**, *7* (12), 3364–3369.

(32) Gensheimer, M.; Becker, M.; Brandis-Heep, A.; Wendorff, J. H.; Thauer, R. K.; Greiner, A. Novel Biohybrid Materials by Electrospinning: Nanofibers of Poly(Ethylene Oxide) and Living Bacteria. *Adv. Mater.* **2007**, *19* (18), 2480–2482.

(33) Klein, S.; Kuhn, J.; Avrahami, R.; Tarre, S.; Beliavski, M.; Green, M.; Zussman, E. Encapsulation of Bacterial Cells in Electrospun Microtubes. *Biomacromolecules* **2009**, *10* (7), 1751–1756.

(34) Stankus, J. J.; Guan, J.; Fujimoto, K.; Wagner, W. R. Microintegrating Smooth Muscle Cells into a Biodegradable, Elastomeric Fiber Matrix. *Biomaterials* **2006**, *27*, 735–744.

(35) Xu, F.; Sheardown, H.; Hoare, T. Reactive Electrospinning of Degradable Poly(Oligoethylene Glycol Methacrylate)-Based Nanofibrous Hydrogel Networks. *Chem. Commun.* **2015**, *52*, 23–25.

(36) Smeets, N. M. B.; Bakaic, E.; Patenaude, M.; Hoare, T. Injectable and Tunable

Poly(Ethylene Glycol) Analogue Hydrogels Based on Poly(Oligoethylene Glycol Methacrylate). *Chem. Commun.* **2014**, *50* (25), 3306–3309.

(37) Celebioglu, A.; Yildiz, Z. I.; Uyar, T. Electrospun Crosslinked Poly-Cyclodextrin Nanofibers: Highly Efficient Molecular Filtration Thru Host-Guest Inclusion Complexation. *Sci. Rep.* **2017**, *7* (1), 7369.

(38) Jayasinghe, S. N. Cell Electrospinning: A Novel Tool for Functionalising Fibres{,} Scaffolds and Membranes with Living Cells and Other Advanced Materials for Regenerative Biology and Medicine. *Analyst* **2013**, *138* (8), 2215–2223.

(39) Fatih Canbolat, M.; Tang, C.; Bernacki, S. H.; Pourdeyhimi, B.; Khan, S. Mammalian Cell Viability in Electrospun Composite Nanofiber Structures. *Macromol. Biosci.* **2011**, *11* (10), 1346–1356.

(40) Youn, H.-Y.; McCanna, D. J.; Sivak, J. G.; Jones, L. W. In Vitro Ultraviolet-Induced Damage in Human Corneal, Lens, and Retinal Pigment Epithelial Cells. *Mol. Vis.* **2011**, *17* (January), 237–246.

(41) Smeets, N. M. B.; Bakaic, E.; Patenaude, M.; Hoare, T. Injectable and Tunable Poly(Ethylene Glycol) Analogue Hydrogels Based on Poly(Oligoethylene Glycol Methacrylate). *Chem. Commun.* **2014**, *50* (25), 3306–3309.

(42) Lutz, J.-F.; Andrieu, J.; Üzgün, S.; Rudolph, C.; Agarwal, S. Biocompatible, Thermoresponsive, and Biodegradable: Simple Preparation of "All-in-One" Biorelevant Polymers. *Macromolecules* **2007**, *40* (24), 8540–8543.

(43) Deller, R. C.; Vatish, M.; Mitchell, D. A.; Gibson, M. I. Synthetic Polymers Enable Non-Vitreous Cellular Cryopreservation by Reducing Ice Crystal Growth during Thawing. *Nat. Commun.* **2014**, *5*, 3244.

(44) Huang, H.; Zhao, G.; Zhang, Y.; Xu, J.; Toth, T. L.; He, X. Predehydration and Ice Seeding in the Presence of Trehalose Enable Cell Cryopreservation. *ACS Biomater. Sci. Eng.* **2017**, *3* (8), 1758–1768.

(45) Pegg, D. E. Principles of Cryopreservation. *Methods Mol. Biol.* **2007**, *368*, 39–57.

(46) Müller-Plathe, F. Different States of Water in Hydrogels? *Macromolecules* **1998**, *31* (19), 6721–6723.

(47) Tanaka, M.; Hayashi, T.; Morita, S. The Roles of Water Molecules at the Biointerface of Medical Polymers. *Polym J* **2013**, *45* (7), 701–710.

6.7 Support Information

Table S6.1 Molecular weight and degree of functionalization of precursor polymers

Polymer	Functional Group [-]	Theoretical Functional Monomer [mol%]	Actual Functional Monomer [mol%]	M_n [kDa]	PDI [-]
POH	$NHNH_2$	33.1	32.2	29.0	3.2
POA	CHO	29.2	28.2	25.2	3.4

Notes: Actual functional monomer mol% for POH was measured using conductometric titration by comparing the number of -COOH groups before and after adipic acid dihydrazide conjugation to poly(OEGMA-co-AA). Actual functional monomer mol% for POA was measured via ^{1}H NMR by comparing the signal of the aldehyde proton at ~ 9.5 ppm to that of methyl proton signal at ~0.81 ppm from the acetal protecting group. M_n and PDI were measured via aqueous gel permeation chromatography using a Waters 515 HPLC pump, a Waters 717 plus Autosampler and three columns (Waters Ultrahydrogel-120, -250, -500; 7.8 × 300 mm; 6 μm particles). Samples were run in an aqueous buffer consisting of 0.5 M sodium nitrate and 25 mM 2-(cyclohexylamino)ethanesulfonic acid maintained at pH 10.0 at 30 °C.

Table S6.2 Viscosity of PEO at different concentrations

PEO conc. (wt %)	1 %	2%	3%	4%	5%	6%
Viscosity (cP)	23.1	94.4	305.3	804	2024	4719

Notes: Viscosity measurements were conducted using a Brookfield viscometer.

Table S6.3 Diameters of electrospun fibers and cells

	Fiber Diameter (μm)			Cell Diameter (μm)		
	Scaffold	Surrounding rounded cells	Surrounding elongated cells	Hydrogel nanofibers	PEO nanofibers	In suspension
No cells	0.4 ± 0.1	-	-	-	-	-
3T3	0.8 ± 0.2	0.6 ± 0.1	1.2 ± 0.4	15 ± 6	5 ± 1	14 ± 2
C2C12	0.7 ± 0.3	0.6 ± 0.2	1.2 ± 0.3	10 ± 3	6 ± 2	12 ± 2

Notes: Fiber diameters were calculated based on ImageJ analysis of SEM images (n = ~130 fibers for the bulk scaffold, ~50 fibers surrounding rounded cells, and ~20 fibers surrounding elongated cells). Cell diameters were calculated based on ImageJ analysis of SEM images (n = ~60 cells per sample).

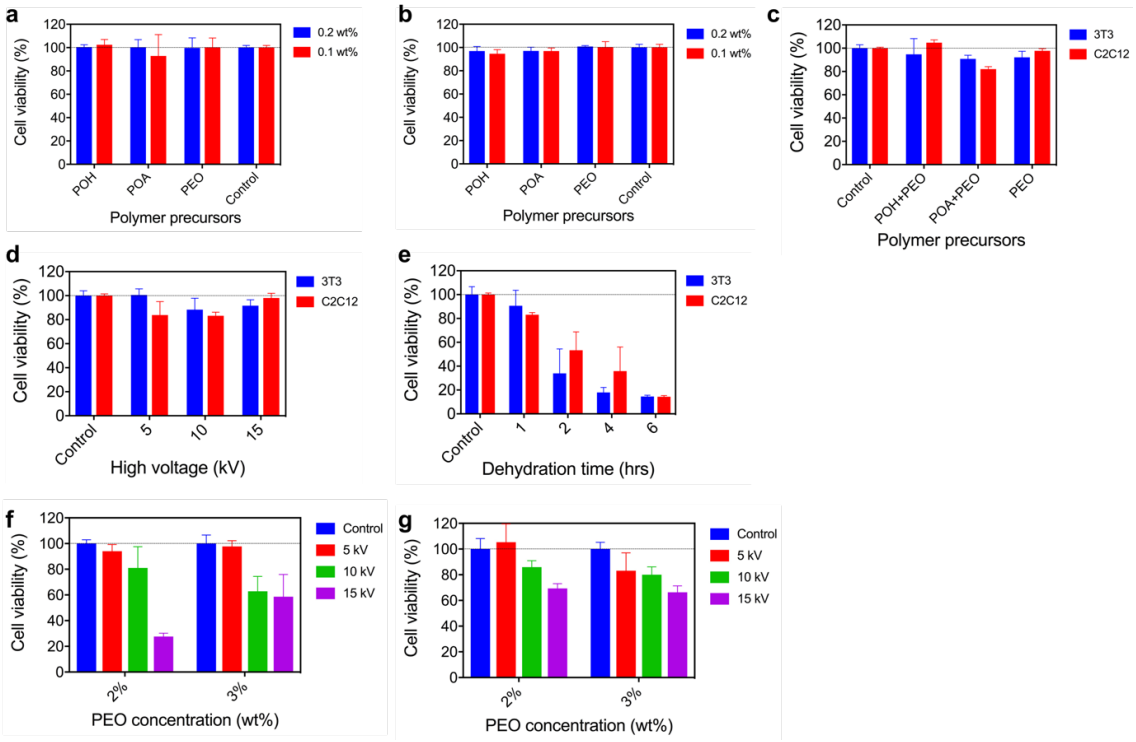

Figure S6.1. (a,b) Cell viabilities of 3T3 (a) and C2C12 (b) cells in the presence of precursor polymers for cell electrospinning (POH, POA and PEO). Cell density is 10,000 cells per well. (c) Cell viabilities of 3T3 and C2C12 cells in polymer precursors consisting of (i) 7.5 wt% POH/POA + 2.5 wt% PEO and (ii) 2.5 wt% PEO only during the one hour exposure time used in the electrospinning process (average ± s.d., n=4). (d,e) Cell viabilities of 3T3 and C2C12 cells when electrospun alone (in DMEM media) under different voltages (c) and dehydrated over different times following removal of media (d) at 37 °C in an incubator (average ± s.d., n=4). (f,g) Cell viabilities of 3T3 (f) and C2C12 (g) cells suspended in different PEO solution concentrations when processed at different high voltages (average ± s.d., n=4). Cell density is 10,000 cells per well.

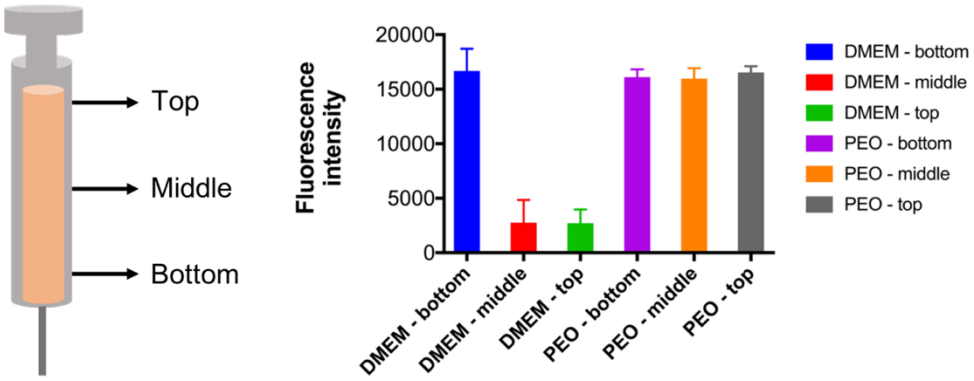

Figure S6.2 Cells remain suspended in the pre-electrospinning solution: 3T3 cells (10^6 cells/mL) were placed in DMEM medium or 2.5 wt% PEO dissolved in DMEM (as used for the core electrospinning work) in a 1mL syringe. The syringes were mounted vertically for 1.5 h, after which cell media was extruded by needle from different layers (bottom from top) into a 96 well-plate. After 24 h to allow the cells in each layer to adhere, cell viability and number were determined using PrestoBlue assay. Cells settle in the DMEM medium alone but remain suspended uniformly in the DMEM/PEO solution, avoiding any issues with cell settling during electrospinning.

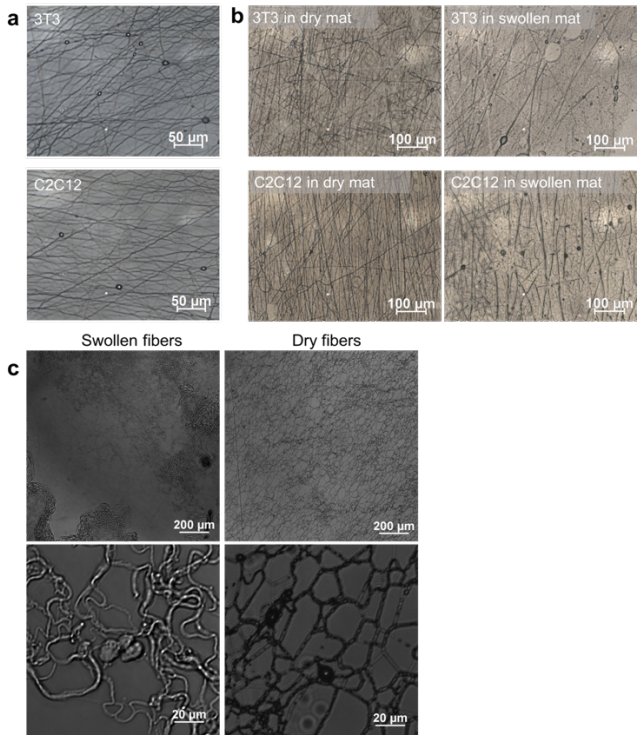

Figure S6.3 (a) Optical microscopy images of 3T3 (top) and C2C12 (bottom) cells entrapped between POEGMA electrospun nanofibers. (b) Microscopy images of 3T3 (top) and C2C12 (bottom) cells encapsulated in thick scaffolds before and after swelling at same spot. (c) low resolution (top) and high resolution (bottom) optical (bright-field) confocal images of swollen (left) versus dry (right) nanofibrous scaffolds in the presence of 3T3 cells.

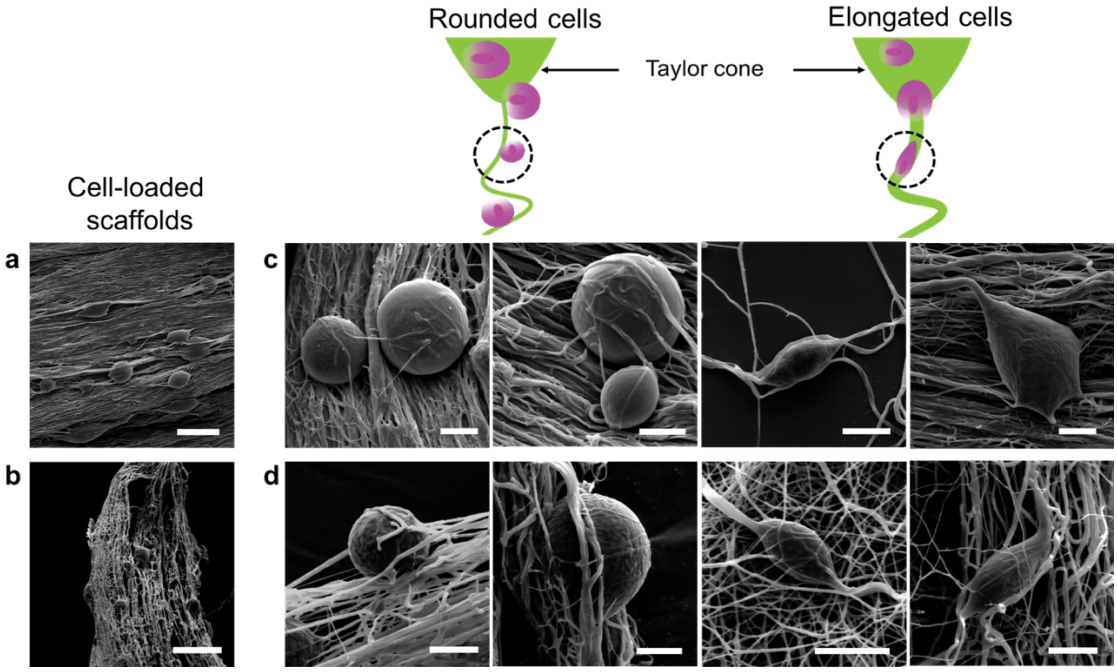

Figure S6.4 (a,b) SEM images of 3T3 (a) and C2C12 (b) cells within thick POEGMA electrospun scaffolds. Scale bars = 50 μm. (c,d) SEM images of 3T3 (c) and C2C12 (d) showing both rounded and elongated cells loaded in POEGMA nanofibrous scaffolds. Scale bars = 10 μm.

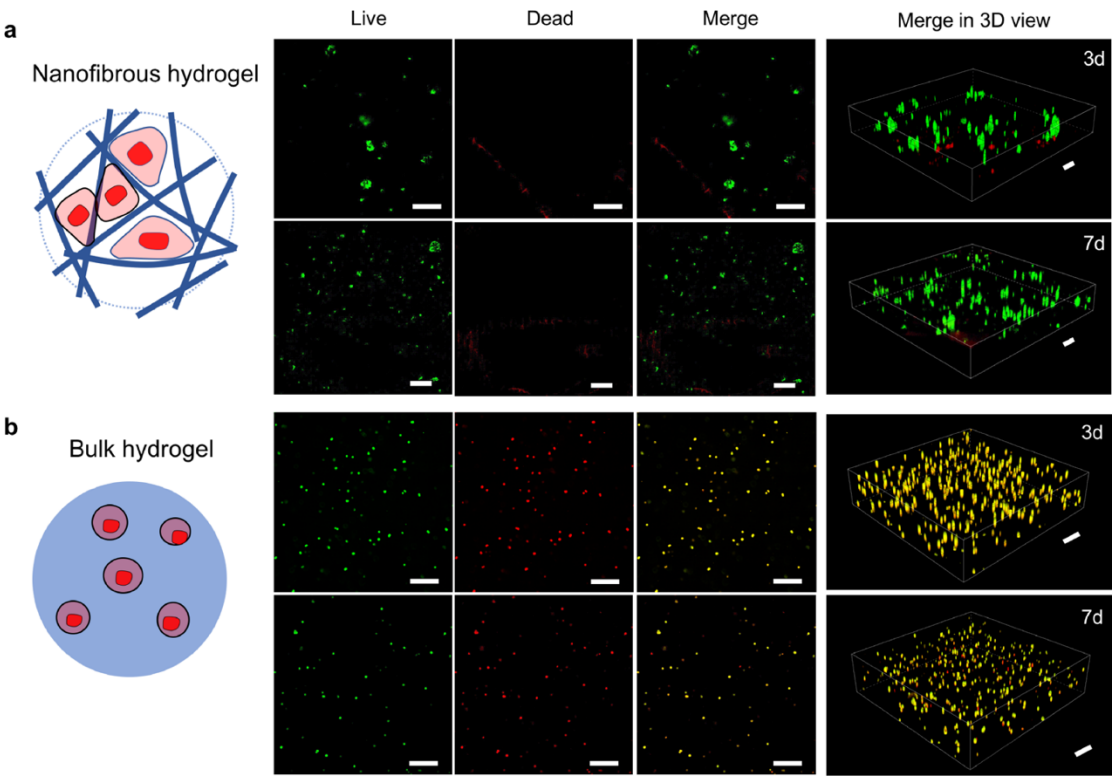

Figure S6.5 (a) LIVE/DEAD assay of C2C12 cells entrapped within nanofibrous POEGMA hydrogels after 3 days and 7 days of incubation showing live cells (488 nm, green), dead cells (561 nm, red), the overlay between the green and red channels, and 3D images acquired via confocal microscopy. Scale bars, 200 μm. (b) LIVE/DEAD assay of C2C12 cells entrapped within bulk hydrogels of the same chemical composition after 3 days and 7 days of incubation showing live cells (488 nm, green), dead cells (561nm, red), the overlay between the green and red channels, and 3D images acquired via confocal microscopy acquired via confocal microscopy. Scale bars = 200 μm. Electrospun nanofibrous hydrogels exhibit significantly higher cell viabilities with more green (live) cells and fewer red (dead cells); conventional hydrogels exhibit primarily yellow (red+green stain overlaid) cells indicative of apoptosis. Note that different gains were used to achieve optimized live/dead imaging between days 3 and 7, such that the total cell number apparent between images is not directly comparable.

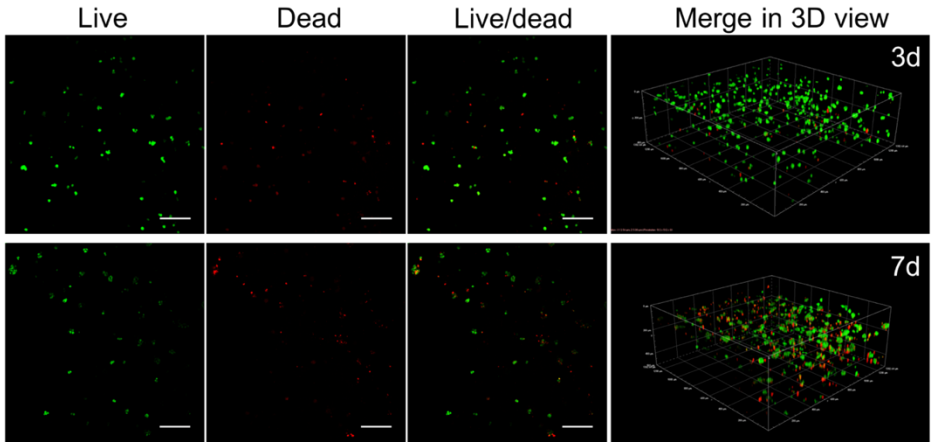

Figure S6.6 Cell viability and expansion in Geltrex ECM-based hydrogels: Confocal images of 3T3 cells encapsulated in Geltrex ECM-based matrix after 3 days (top row) and 7 days (bottom row) of incubation showing live cells (green, 488 nm), dead cells (red, 561 nm), the overlay between the green and red channels, and 3D images showing the distribution of cells throughout the scaffold volume. Scale bars = 200 μm. To prepare the scaffolds, Geltrex matrix was thawed in a refrigerator at 4 °C overnight before use. Cells ($1x10^6$ cells/mL) were mixed with the Geltrex solution at 4 °C, after which the cell-laden matrix was incubated at 37 °C for 10 mins to form the gel. The cells were incubated in media as for the electrospinning trials.

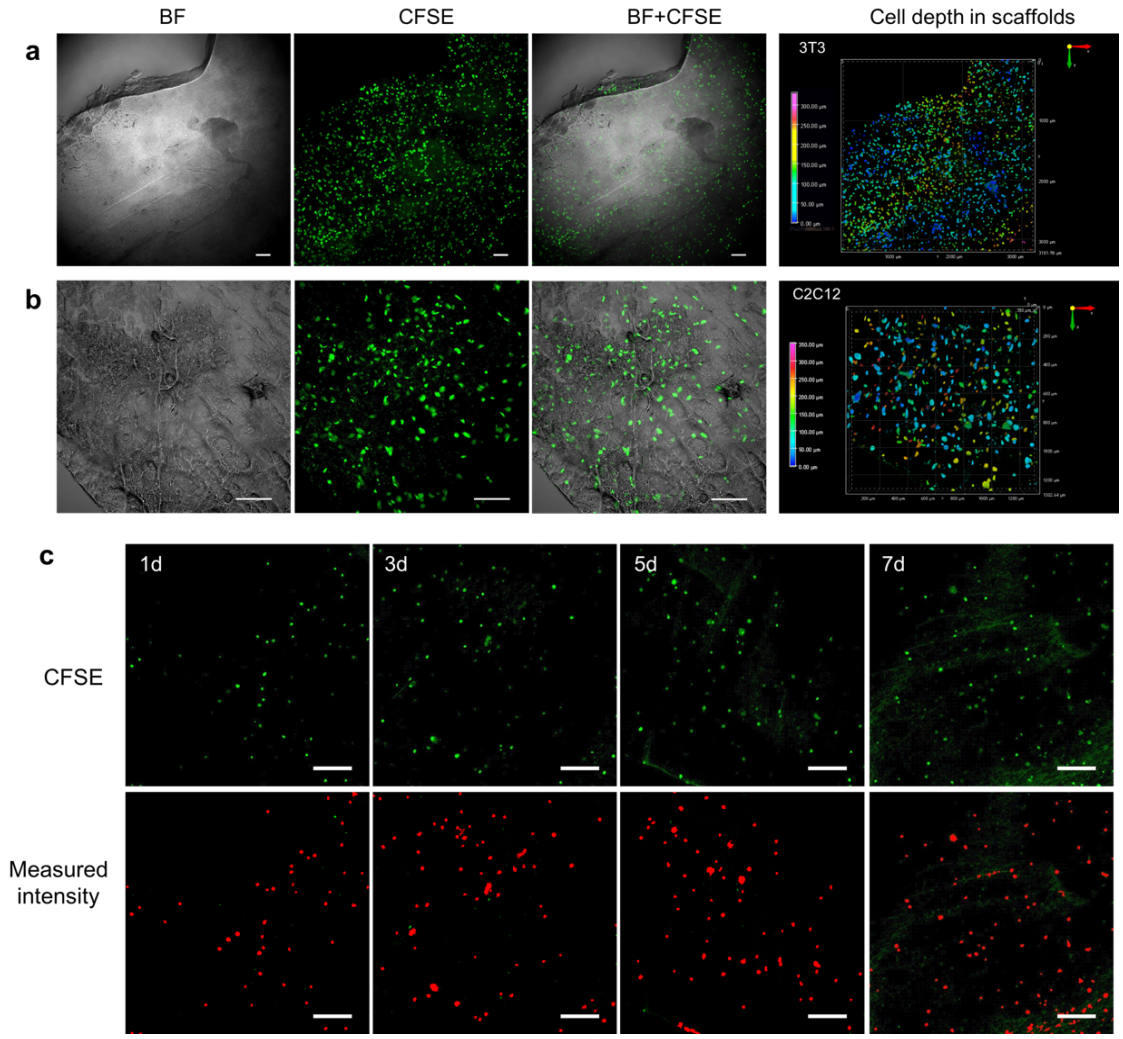

Figure S6.7 (a,b) Confocal images of 3T3 (a) and C2C12 (b) cells (post-stained with CFSE, 488 nm excitation wavelength) encapsulated in POEGMA nanofibrous scaffolds (bright field, BF) (fresh). (c) Confocal microscopy images (top) and measured fluorescence intensity of each cell (bottom) of 3T3 cells stained with CFDA-SE (488 nm, green) within a nanofibrous hydrogel scaffold at 1, 3, 5 and 7 day culture times (fresh). Scale bars = 200 μm. Cell density = $1x10^6$ 3T3 cells/mL.

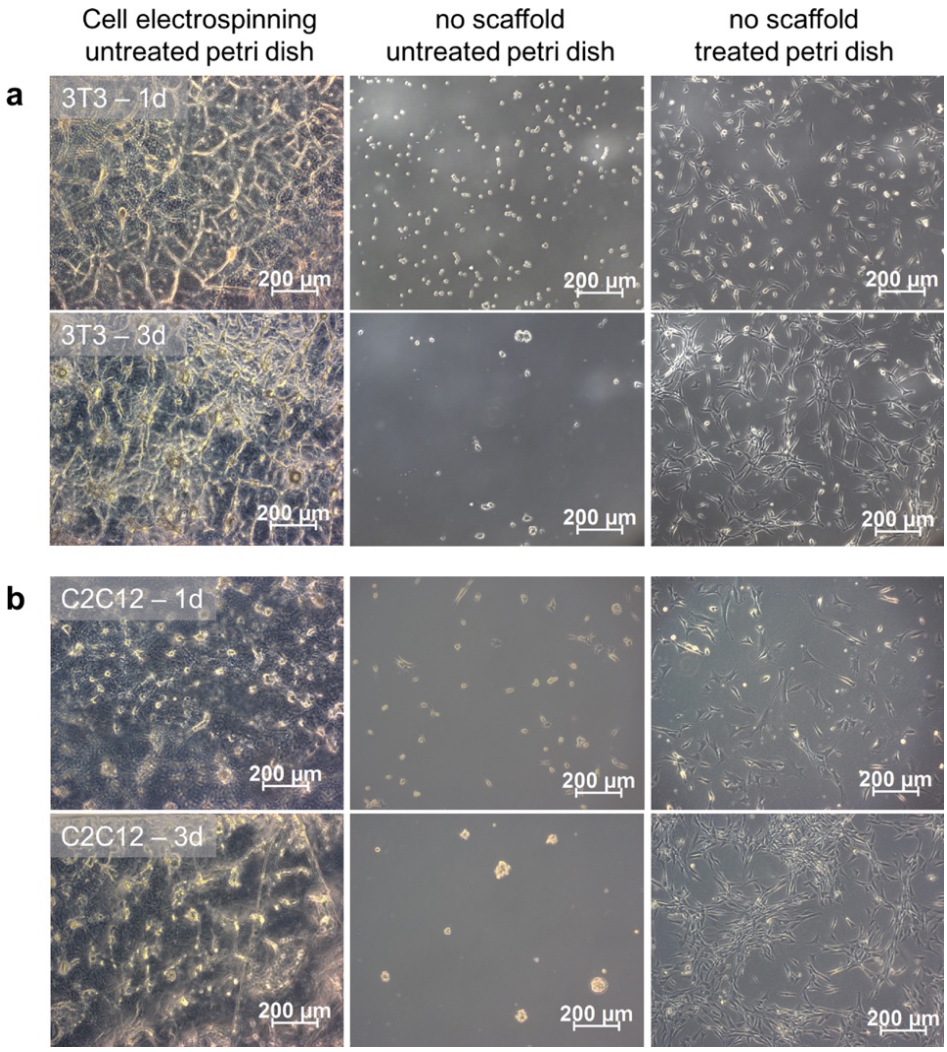

Figure S6.8 Optical microscopy images of (a) 3T3 and (b) C2C12 cells entrapped within cell-loaded nanofibrous scaffolds (column 1), plated on untreated (non-adherent) petri dishes without a scaffold (column 2), and plated on treated (adherent) petri dishes without a scaffold (column 3) after 1 and 3 days. The initial cell density used for the 2D experiments (columns 2 and 3) was 5,000 cells/cm^2, selected to match the 2D projected cell densities of 4600 ± 2500 cells/cm^2 (3T3) and 4200 ± 1300 cells/cm^2 (C2C12) in the electrospun scaffolds (column 1). Cells can adhere and proliferate inside the 3D nanofibrous scaffold in a manner similar to that observed on 2D treated petri dish, but cells plated on an untreated petri dish do not adhere and thus do not proliferate.

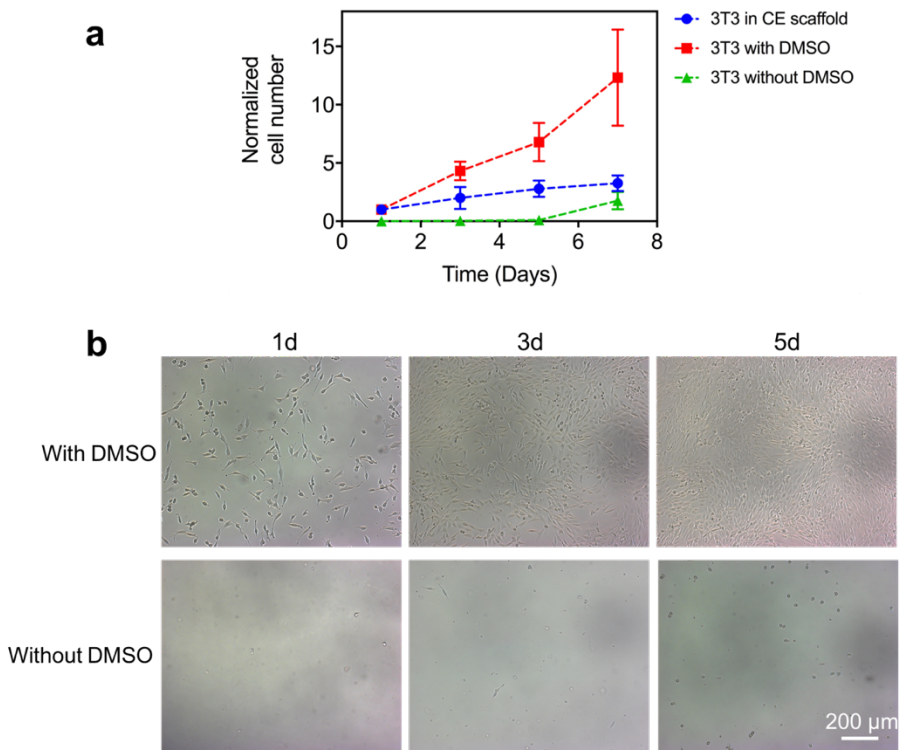

Figure S6.9 (a) Normalized cell number of 3T3 cells following freezing in the electrospun scaffold (blue), inside a 5 % DMSO/DMEM solution (red) and inside DMEM solution alone (green), normalized relative to cell density after 1 day of cells stored in the standard 5% DMSO/DMEM storage solution using the conventional freeze/thaw technique. The cryoprotective potential of the scaffold is evidenced by the high maintenance of cell viability inside the scaffold relative to the conventional cryostorage protocol; (b) 3T3 cell morphology and number following freezing and re-thawing in 5 % DMSO/DMEM (top) relative to DMEM alone (bottom).

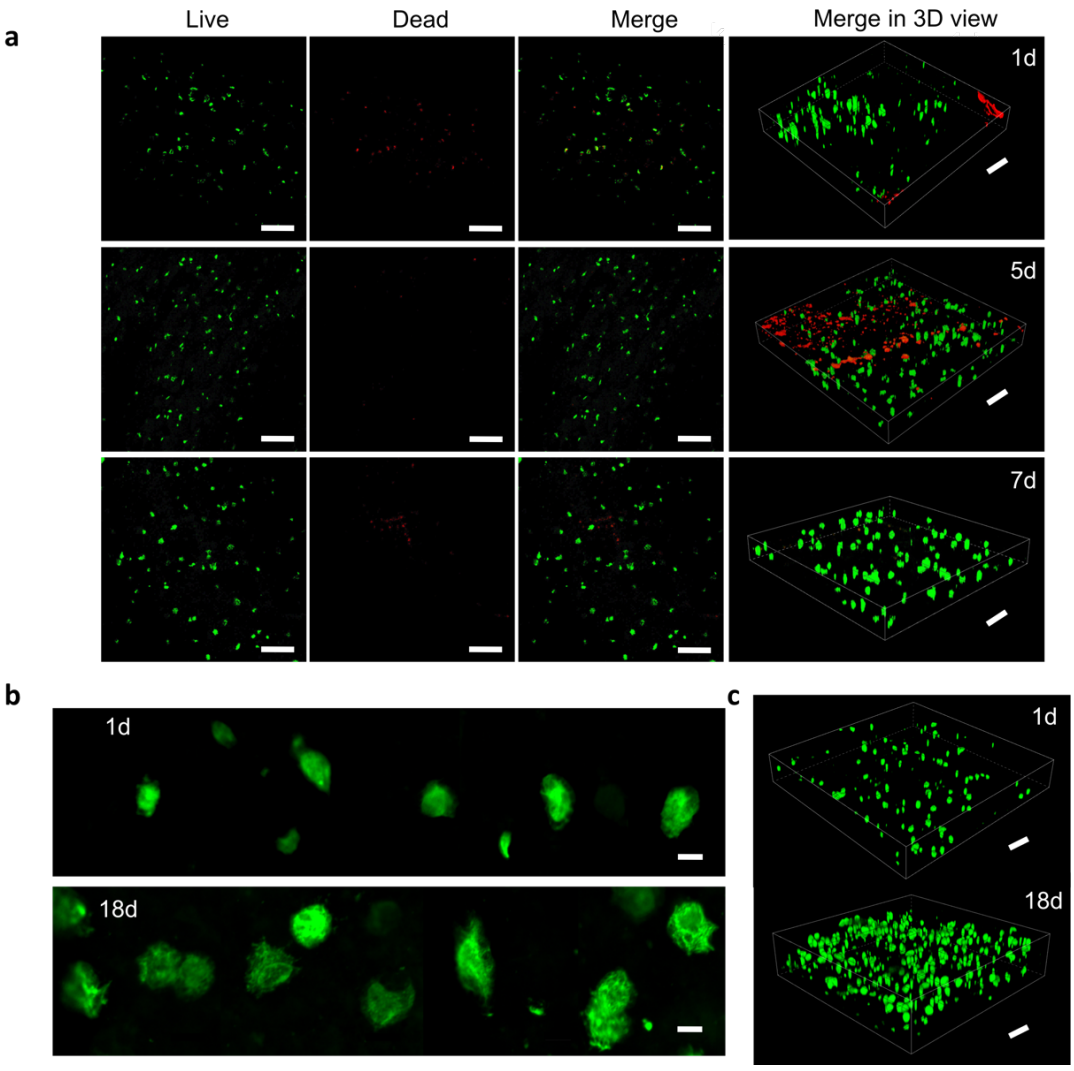

Figure S6.10 (a) Live/dead assay results of 3T3-loaded electrospun hydrogel scaffolds following a freeze/thaw cycle showing both live (green, 488 nm) and dead (red, 561 nm) cells after 1, 5, and 7 days of cell culture. Scale bars = 200 μm. (b) Comparison of 3T3 cell morphology within an electrospun nanofibrous hydrogel scaffold following a freeze/thaw cycle after 1 day and 18 days of culturing. Cells were stained with CFDA-SE at the time of processing and fixed using 3 wt% PFA prior to imaging. Scale bars = 20 μm. (c) 3D images of 3T3 cells encapsulated in POEGMA hydrogel nanofibers following a freeze/thaw cycle after 1 day and 18 days of culturing (same process as c). Scale bars = 200 μm.

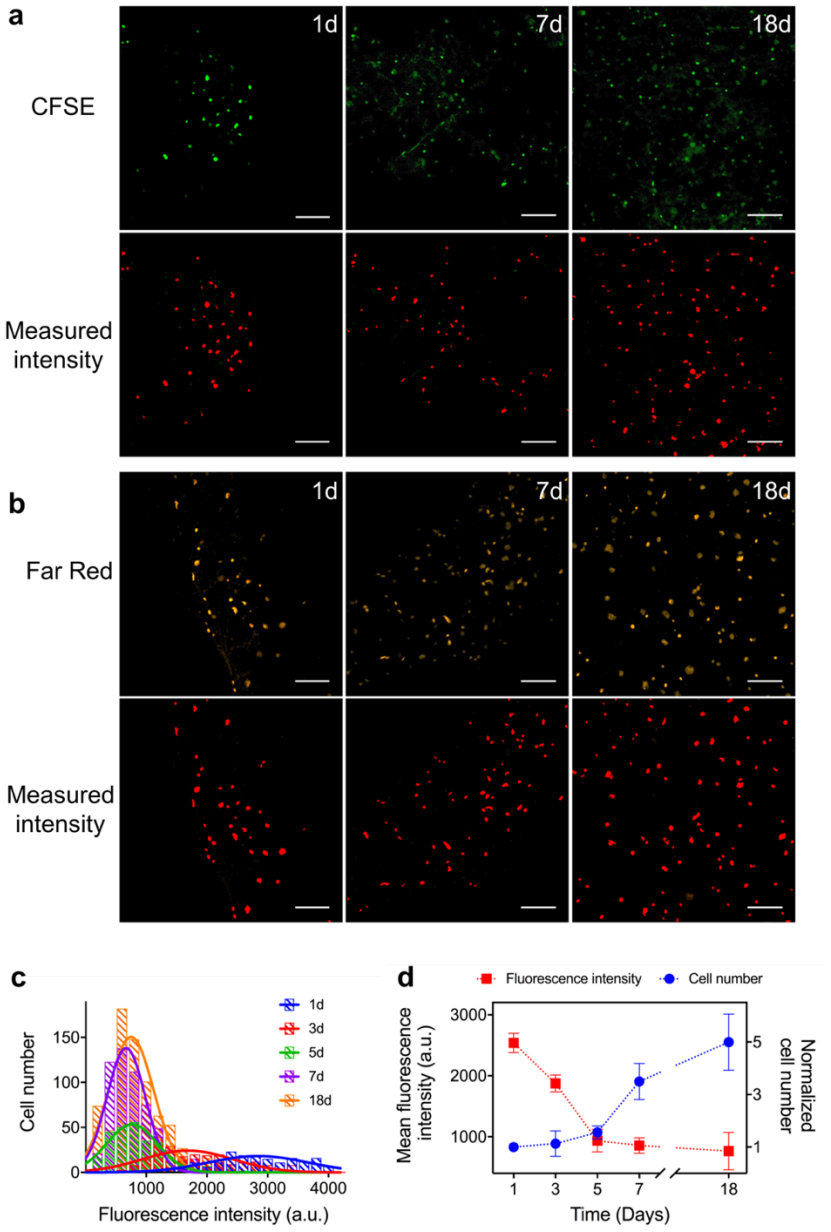

Figure S6.11 (a-b) Confocal microscopy images (top) and measured intensity of each cell (bottom, using the confocal imaging software to isolate cells from any background signals) of 3T3 cells stained with CFDA-SE (488 nm, green, a) and Far Red (640 nm, orange) within a nanofibrous hydrogel scaffold after a freeze/thaw cycle at 1, 7 and 18 days culture times. Scale bars = 200 µm. (c) Histogram of 3T3 cell number versus fluorescence intensity per cell of 3T3 cells following a freeze/thaw cycle at 1, 3, 5, 7 and 18 day culture times using the Far Red assay (calculated from (b), n=4, 2 images/sample for analysis). (d) Mean fluorescence intensities and normalized 3T3 cell number following a freeze/thaw cycle at 1, 3, 5, 7 and 18 day culture times using the Far Red assay (n=4, 3 images.sample for analysis). Cell density = 1×10^6 cells/mL.

Chapter 7

Single Step, All-Aqueous Electrospinning of Nanostructured Degradable Macroporous Hydrogel Networks with Controllable Internal Morphologies

Abstract

A single-step method that avoids the use of non-aqueous solvents is reported to prepare hydrogel networks with controlled morphologies on both the nanoscale and the microscale via electrospinning. Hydrazide and aldehyde-functionalized poly(oligo ethylene glycol methacrylate) (POEGMA) are co-spun from a double barrel syringe together with poly(ethylene oxide) (PEO) as an electrospinning aid. By varying the concentrations and molecular weights PEO and/or POEGMA, different morphologies from pure fibers to "beaded network" morphologies with tunable bead sizes can be fabricated, all of which remain stable as a monolithic structure once swollen in water due to the covalent crosslinks formed within the gel structure following mixing of the precursor polymers at the electrospinning tip. The rates and magnitudes of swelling, degradation times, and mechanics of the resulting scaffolds can all be tuned based on a combination of nanoscale (i.e. crosslink density within the gel, based on the precursor polymer concentration) and microscale (i.e. the macroscale network structure formed) control, with an atypical independence of swelling relative to mechanics and degradation rates observed. Furthermore, the internal morphology of the networks is demonstrated to alter both the cell responses within the scaffolds. We anticipate such networks to have significant potential

benefits as biological scaffolding materials, providing networks with tunable mechanics and highly controllable nano- and microstructures in a single, all-aqueous processing step.

Keywords: Hydrogel; Scaffold; Nanostructure; Electrospinning; Chain entanglement

7.1 Introduction

Electrospinning technology has received significant attention in recent decades as a simple and versatile method to prepare nano- and microfibers.[1,2] Creating fibrous networks of materials can result in significantly different materials properties (e.g. mechanics, diffusivity, etc.) and thus unique applications for those materials in varied fields such as tissue engineering,[3,4] drug delivery,[5,6] catalysis,[7–9] and sensors.[10,11] Electrospinning produces fibrous networks based on the balance between the surface tension of the polymer solution and charge repulsion between induced charges on the polymers under a high voltage, inducing ejection of a stretched jet from the spinneret tip. Entanglement within the polymer solutions used for electrospinning is essential for the formation of fibers, counterbalancing the role of surface tension in driving the formation of droplets.[12,13] Rapid solvent evaporation between the needle and the grounded collector results in the conversion of the jet to (typically solid) fibers.[2,14] Based on this mechanism, a variety of properties affect the structure of an electrospun fiber, including factors influencing polymer chain entanglement (e.g. molecular weight,[15,16] solution concentration,[17] and viscosity[18]], the capacity of the electrospinning process to stretch the jet to create smaller fibers (e.g. electric field,[14] voltage,[19] and solution feed rate[20]), and the capacity for effective solvent removal before the jet hits the collector (e.g. solvent boiling point[21] and humidity[22]). Rational choice of polymer concentration and molecular weight (both of which are directly correlated to the number of chain entanglements formed) has been identified as particularly important to determine whether fibers (high entanglement) or beads (low entanglement) are formed under a specific set of processing conditions.[12,13,23]

While the majority of previous electrospinning work has focused on creating networks of water-insoluble polymer scaffolds [24,25] or rapidly dissolving scaffolds of water-soluble polymers[26,27], our interest lies in the use of electrospinning to create *hydrogel* networks. Such networks would have controlled porosities on both the macroscale (based on the electrospinning parameters used) and the nanoscale (based on the crosslinking density

within each gel fiber). Porosity control on both these length scales is anticipated to have potential benefits particularly in terms of tissue engineering applications, in which the nanoscale crosslink density can be used to tune the mechanics of the cell substrate (shown to significantly influence the behavior of cells, particularly stem cells[28]) while the macroscale porosity can be used to promote cell signaling and spreading throughout the scaffold. In addition, many native soft extracellular matrices have an inherently fibrous microstructure[29,30], allowing a gel-based nanofiber network to better mimic both the mechanics/chemistry as well as the underyling morphology of native ECMs. Typical approaches to fabricate hydrogel-based electrospun networks require the use of post-crosslinking methods such as glutaraldehyde treatment[31,32] or UV irradiation[25,33] to effectively crosslink the electrospun polymer into gel fibers. However, both these approaches can induce cytotoxicity to co-electrospun cells in addition to adding an extra processing step.

Recently, we have reported an alternate method to fabricate nanofibrous hydrogel scaffolds based on *reactive electrospinning*, in which water-soluble hydrazide and aldehyde-functionalized pre-polymers (based on poly(oligoethylene glycol methacrylate, a PEG-mimetic polymer that is significantly easier to chemically functionalize[34,35]) are co-spun from a double-barrel syringe.[36] Gelation via hydrazone bond formation occurs upon mixing and is greatly accelerated as water rapidly evaporates following jetting of the polymer solution out of the needle, facilitating rapid mixing-induced gelation in most cases prior to collection. Relative to other methods to create nanofibrous gel networks, this strategy offers the distinct advantages of not requiring any external crosslinkers or initiators, using only water as a solvent, and resulting in a degradable network (via hydrazone bond hydrolysis back into the precursor polymers) even when synthetic polymers are used as the basis of the network. While poly(ethylene oxide) (PEO) is used as an electrospinning aid to achieve sufficient entanglements to allow electrospinning of the low molecular weight and highly branched POEGMA precursor polymers, PEO can be rapidly dissolved out of the network following processing to leave behind a pure POEGMA gel network.[37]

In typical scaffolding applications, 100% fibers are desired as the product of electrospinning, with the formation of beads (which leads to a complete loss of scaffold integrity) and the intermediate "beaded fiber" structures (which decrease the regularity and in most cases the mechanics of the network[38–40]) typically considered a negative outcome.

However, in the context of gel electrospinning, the covalent crosslinks that form both *between* and *within* the fibers/beads during the process can permit the maintenance of mechanically strong and stable macrostructures even in the presence of a large bead fraction; this is atypical in most electrospinning applications. Given the clear links between cell behavior and the nanoscale roughness of a cell substrate[41,42], such structures (coupled with control over the underlying mechanics of the gel itself, easily achievable in our system by changing the concentration or the density of hydrazide/aldehyde functional groups in the precursor polymers[43]) are of potential interest for cell scaffolding applications. Alternately, even if individual beads are formed (i.e. electrospraying instead of electrospinning resulted from the process conditions), the *in situ*-gelation and all-aqueous properties of our reactive electrospinning/spray process would offer a potentially attractive alternative for single or few cell encapsulation applications, currently pursued largely via either air jetting of polymer solution droplets into a gelation bath (typically resulting in bead diameters of >100 μm containing multiple cells[44,45]) or microfluidics (typically requiring the use of an oil-based dispersing phase and still limited in terms of minimum size[46,47]).

Herein, we investigate the use of reactive electrospinning to create nanostructured hydrogels with varying morphologies ranging from purely fibrous structures to beaded fibres (with controlled nanoscale dimensions) to bead networks. Dimensionally stable and mechanically strong gel scaffolds can be created even at very low fiber:bead ratios, owing to the covalent crosslinking between the nanoscale features upon drying that effectively binds the scaffolds together. We anticipate that such control, mediated simply by changing the molecular weight of the PEO electrospinning aid and the concentration of the POEGMA precursor polymers, may have significant implications in biomedical applications in which the potential to create macroporous scaffolds with well-defined internal morphologies on multiple length scales can have clear benefits.

7.2 Materials and methods

7.2.1 Materials

Poly(ethylene oxide) (PEO, M_w = 600,000 g/mol and M_w = 1,000,000 g/mol) was purchased from Sigma-Aldrich. Oligo(ethylene glycol) methyl ether methacrylate (OEGMA, M_n = 500 g/mol) was purchased from Sigma-Aldrich and purified using a

column of basic aluminum oxide to remove the methyl ether hydroquinone (MEHQ) and butylated hydroxytoluene (BHT) inhibitors. Acrylic acid (AA, Sigma Aldrich, 99%), 2,2-azobisisobutryic acid dimethyl ester (AIBMe, Wako Chemicals, 98.5%), dioxane (Caledon Labs, 99%), adipic acid dihydrazide (ADH, Alfa Aesar, 98%), and N'-ethyl-N-(3-dimethylaminopropyl)-carbodiimide (EDC, Carbosynth, Compton CA, commercial grade), were all used as received. For all experiments, Milli-Q grade deionized water (DIW) or sterile phosphate buffered saline (1× PBS) was used. N-(2,2-dimethoxyethyl)methacrylamide (DMEMAm) was synthesized as previously reported.[48]

7.2.2. Synthesis of hydrazide and aldehyde-functionalized POEGMA polymers

Both functionalized POEGMA hydrogel precursor polymers were synthesized as previously reported.[48] Hydrazide-functionalized POEGMA (POH) was prepared by dissolving AIBMe (37 mg, 0.16 mmol), OEGMA (4.0 g, 8.4 mmol), and AA (0.25 g, 3.5 mmol) in 20 mL of dioxane inside a 50 mL Schlenk three-neck flask. After 30 minutes of nitrogen purging, the solution was placed in an oil bath at 75 °C for 4 hours under magnetic stirring. Following removal of the dioxane by rotary evaporation, the residual poly(OEGMA-*co*-AA) polymer was purified by dialysis (6+ hours for 6 cycles) and lyophilized. Following, ~4 g of poly(OEGMA-*co*-AA) was dissolved in 100 mL DIW, after which ADH (2.65 g, 15.2 mmol) and EDC (1.18 g, 7.6 mmol) were added to the solution. The pH of the solution was adjusted to pH = 4.75 using 0.1 M HCl continually over the reaction period until the pH stabilized (~ 4 hours). The solution was stirred overnight and then purified by dialysis (6+ hours for 6 cycles). The final polymer was obtained by lyophilization and was stored as a 15 w/w% solution in DIW at 4 °C. Aldehyde-functionalized POEGMA (POA) was prepared using a similar protocol, starting with a solution of AIBMe (50 mg, 0.22 mmol), OEGMA (4.0 g, 8.4 mmol), and DMEMAm (0.60 g, 3.5 mmol) in 20 mL of dioxane. After evaporation of the dioxane following the end of the polymerization period, the polymer was dissolved in 100 mL of 0.25 M HCl and stirred for 24 hours to hydrolyze the acetal groups to aldehyde groups. The final polymer was

subsequently purified by dialysis (6+ hours for 6 cycles) and lyophilized. Both polymers were stored as 15 w/w% solutions in DIW or 1× PBS at 4 °C.

7.2.3. Preparation of electrospun hydrogels

PEO (M_w = 600,000 g/mol (600PEO) or M_w = 1,000,000 g/mol (1000PEO), dissolved at concentrations of x = 0.67-3 wt% as indicated by the code PEO_x) and either POH or POA (dissolved at concentrations of y = 7.5-10 wt%, as indicated by the code PO_y) were co-dissolved in DIW; ratios used for specific electrospinning experiments are shown in Tables 1-2. The subsequent PEO+POH and PEO+POA solutions were loaded into separate barrels of a double barrel syringe equipped with a static mixer capped by a blunt-tip 18 G needle (Fig. 7.1). A voltage of 10 kV was applied to the tip of the blunt needle, while the distance between the needle and the grounded collector (a x10 cm diameter aluminum disk) was maintained at 10 cm for all experiments. All samples were prepared at room temperature with a relative humidity of 26-30% and a polymer solution overall flow rate of ~10 μL/min. PEO-only scaffolds excluding the POH/POA components (PO_0) were prepared as controls at the same total PEO concentrations.

For creating cell-loaded scaffolds, the same procedures and materials were used aside from dissolving 10^6 cells/mL in the PEO+POH precursor solution. Electrospinning was conducted for a maximum of one hour (previously shown to facilitate the maintenance of high cell viability within the scaffold even under dry collection conditions), after which the cell scaffolds were immediately transferred to the appropriate culture media.

Table 7.1 Electrospinning recipes and feature sizes associated with reactive electrospinning of PEO + POH/POA or PEO alone.

Scaffold Category	Sample Name	PEO (wt %)	POH/POA (wt %)	Morphology	Diameter (μm)
POH/POA + 600PEO	$600PEO_{2.5}PO_{7.5}$	2.5	7.5	Fibers only	0.42 ± 0.14
	$600PEO_{2}PO_{7.5}$	2	7.5	Beaded fibers	N/A[a]
	$600PEO_{1.5}PO_{7.5}$	1.5	7.5	Beads	1.4 ± 0.25
600PEO only	$600PEO_{3}PO_{0}$	3	0	Fibers only	0.20 ± 0.02
	$600PEO_{2.5}PO_{0}$	2.5	0	Beaded fibers	N/A[a]
	$600PEO_{2}PO_{0}$	2	0	Beaded fibers	N/A[a]
	$600PEO_{1.5}PO_{0}$	1.5	0	Beaded fibers	N/A[a]
	$600PEO_{1}PO_{0}$	1	0	Beads	0.56 ± 0.06
POH/POA + 1000PEO	$1000PEO_{2}PO_{7.5}$	2	7.5	Fibers only	0.36 ± 0.06
	$1000PEO_{1.5}PO_{7.5}$	1.5	7.5	Beaded fibers	N/A[a]
	$1000PEO_{1}PO_{7.5}$	1	7.5	Beads	1.81 ± 0.28
	$1000PEO_{0.5}PO_{7.5}$	0.5	7.5	Beads	2.61 ± 0.24
1000PEO only	$1000PEO_{2}PO_{0}$	2	0	Fibers only	0.2 ± 0.02
	$1000PEO_{1.5}PO_{0}$	1.5	0	Beaded fibers	N/A[a]
	$1000PEO_{1}PO_{0}$	1	0	Beaded fibers	N/A[a]
	$1000PEO_{0.5}PO_{0}$	0.5	0	Beads	0.40 ± 0.06

[a] Due to the heterogeneity of the beaded fiber networks, no characteristic size was reported for these networks

7.2.4. Characterization

Scanning electron microscopy (SEM, Tecan Vega II LSU) was used to observe the morphologies of electrospun hydrogel scaffolds using an operating voltage of 10 kV. Aqueous gel permeation chromatography (GPC, using a Waters 717 plus Autosampler and columns including ultrahydrogel-120, -250, -500; 7.8 × 300 mm; 6 μm particles) was used to measure molecular weight and PDI by dissolving samples in a buffer of 0.5 M sodium nitrate and 25 mM 2- (cyclohexylamino)ethanesulfonic acid maintained at pH 10.0 at 30 °C. Attenuated total reflectance Fourier transform infrared spectroscopy (ATR-FTIR) was used to confirm the presence of PEO and POEGMA within the scaffolds. The tensile and

compressive properties of electrospun scaffolds were tested using a MicroSquisher (CellScale Biomaterials Testing, Waterloo, Canada). Differential scanning calorimetry (DSC, Auto Q20, TA instruments) was used to detect the PEO removal after immersing in water. Swelling kinetics were measured at 37°C in 10 mM PBS (pH 7.4) by loading the electrospun scaffolds into cell culture inserts that were subsequently placed inside a 24-well plate and submerged in 4 mL PBS. At predetermined time intervals, the inserts were removed, excess PBS was wicked off the surface of the scaffolds using a Kimwipe, and the inserts were weighed. The water content was calculated gravimetrically using equation (1):

$$Water\ content\% = \frac{W_{swollen} - W_{dry}}{W_{swollen}} \times 100\% \qquad (1)$$

Acid-accelerated degradation (allowing facile comparison of the relative degradability of different morphologies under a short experimental time frame[48]) was performed using the same method but instead immersing the samples in 0.1M HCl at 37 °C.

7.2.5. Cell culture

NIH 3T3 fibroblasts (ATCC) were cultured in Dulbecco's Modified Eagle's Medium (DMEM, Life Technologies) with 10% fetal bovine serum (FBS, ThermoFisher) and 1% penicillin-streptomycin (ThermoFisher) in a gas plasma-treated polystyrene flask (VWR) to ~80% confluency before use. Non-treated petri dishes (Fisher Scientific) were used to culture cell-loaded scaffolds. All cells were incubated at 37°C and 5% CO_2.

7.2.6. Cytotoxicity and Live/Dead assay

3T3 fibroblasts were placed in a 96 well plate (10,000 cells in 100 μL DMEM per well) and incubated overnight at 37°C and 5% CO_2 before use. Each well were then washed with PBS and media were replaced with polymer precursors including POH, POA and PEO at the same concentrations as using in the electrospinning trials for 1 hour. Subsequently, the polymer solutions were aspirated, the cells were washed with PBS, and 90 μL of fresh DMEM and 10 μL of PrestoBlue reagent (ThermoFisher) were added. After one additional

hour of incubation at 37°C, the fluorescence intensity of each well was measured (560 nm excitation/ 590 nm emission) using a plate reader (Infinite M200 Pro, Tecan). A calcein AM/ethidium homodimer-1 LIVE/DEAD assay kit (ThermoFisher) was used to assess cell viabilities within electrospun scaffolds using the recommended protocol, using PBS to wash out unbound dye from the scaffold before imaging. Confocal laser scanning microscopy (CLSM, Nikon) and fluorescence microscopy (FL, Axiovert 200, Carl Zeiss) were used to observe cell viabilities and morphologies inside the scaffolds.

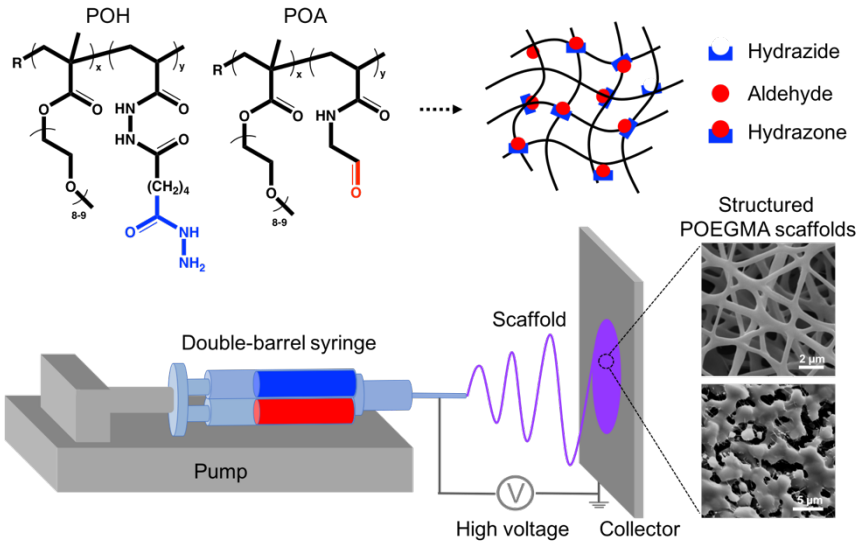

Figure 7.1 Scheme of reactive electrospinning setup to prepare structured POEGMA hydrogel scaffolds.

7.3 Results and discussion

7.3.1 Effect of PEO concentration on fiber structure

A double-barrel syringe assembly in which POH and POA aqueous solutions (both containing PEO as an electrospinning aid) were loaded into each of the two barrels was used for reactive electrospinning (Figure 7.1). Both precursor polymers had molecular weights of <30 kDa (28.1 kDa for POH, 23.8 kDa for POA, as per GPC analysis), facilitating kidney clearance following hydrazone crosslink hydrolysis. The degree of functionalization of each polymer was also similar (~30 mol% hydrazides for POH, ~29

mol% aldehydes for POA), resulting in minimal residual functional group contents in the hydrogel following electrospinning. The high molecular weight of the PEO electrospinning aid used (600 kDa or 1 MDa) is necessary to enable electrospinning of the low molecular weight and comb-like POEGMA polymer. DSC measurements confirm that a 24-hour soaking step can effectively remove all of the PEO electrospinning aid from every scaffold morphology tested (Fig. 7.2A, B), leaving a POEGMA gel scaffold after the washing step. AT-FTIR spectroscopy on one scaffold representing each morphology observed (fibers, beaded fibers, and beaded networks, see Table 7.1) also confirms the predominant presence of POEGMA in each of these scaffolds based on the appearance of the ester C=O stretch at ~1700 cm^{-1} in the washed scaffolds (Fig. 7.2C).

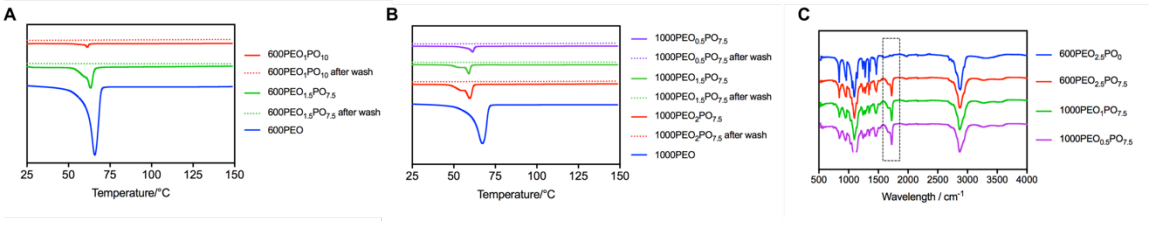

Figure 7.2 (A-B) Differential scanning calorimetry (DSC) of POH/POA+PEO electrospun scaffolds before and after washing PEO. (C) Characterization of ATR-FTIR to prove the presence of POEGMA in electrospun scaffolds.

Figure 7.3 shows the macroscopic properties and internal morphologies of reactive electrospun POEGMA hydrogel scaffolds prepared using different concentrations of 600PEO and a fixed 7.5 wt% concentration of the POH/POA reactive precursor polymers before and after washing with DIW to hydrate the gel network and remove the PEO electrospinning aid (see Table 7.1 for the full compositions in each barrel). Macroscopically, dry fibrous mats were produced as a result of the electrospinning process that remained fully intact following hydration (Figs. 7.3A,B) Microscopically, as anticipated based on other electrospinning work[23], a clear transition from fibers only to beads was observed as the 600PEO concentration was reduced, consistent with the reduced total number of entanglements as the PEO content was lowered. A pure nanofiber network (with fibers ~400 nm in diameter) is observed for $600PEO_{2.5}PO_{7.5}$ (Fig. 7.3C), a network

that is maintained (albeit significantly swollen) when immersed in water (Fig. 7.3D). When the PEO content was reduced to 2 wt% ($600PEO_2PO_{7.5}$, Fig. 7.3E), fibers were observed connecting beads, hypothesized to correlate to PEO-rich fibres connecting POEGMA-rich beads; subsequent soaking of this scaffold resulted in elimination of these connecting fibers but maintenance (and swelling) of the beaded structures (Fig. 7.3F), consistent with this hypothesis. However, unlike most electrospun materials, the beaded morphology in Fig. 7.3E remained macroscopically intact as a coherent mat even following elimination of the connecting PEO fibers, owing to hydrazone crosslink formation between the beads that can uniquely occur via our reactive electrospinning process. A further reduction in the PEO content (Fig. 7.3G) results in a nearly pure bead-like morphology, although the persistence and swelling of the beads upon soaking is again indicative of covalent crosslinking within each bead (Fig. 7.3H). Interestingly, as the prevalence of beads within the scaffold increased, a closer correlation was observed between the collected (dry) and post-swollen (re-dried) morphologies. We hypothesize that this observation is attributable to the higher PEO contents in these samples which, upon removal by soaking, would result in larger voids within a less crosslinked POEGMA gel network (i.e. in which the higher PEO concentration sterically interferes with covalent crosslinking between adjacent POEGMA polymers) and thus more swelling in the POEGMA scaffold left behind.

To decouple the impacts of the POEGMA precursor polymers and the 600PEO electrospinning aid on the morphologies produced, 600PEO was individually electrospun to determine the morphologies it alone would produce at the same concentrations (Fig. 7.3I-M). While an all-fibrous structure was evident for $600PEO_3PO_0$ (Fig. 7.3I, higher than any tested concentration in the presence of POEGMA), elongated beads started to form at $600PEO_{2.5}PO_0$ (Fig. 7.3J), a concentration that in the presence of POEGMA gave an all-fibrous structure (Fig. 7.2C). More rounded beads appeared at lower 600PEO concentrations until only beads were observed for $600PEO_1PO_0$ (Fig. 7.3M), the lowest PEO concentration tested. Not surprisingly, without the addition of the POH/POA crosslinking pair, all of the PEO-only electrospun matrices quickly dissolved once re-exposed to water, consistent with the lack of crosslinking within these PEO-only fibers.

The diameters of fibers (Fig. 7.3I) and beads (Fig. 7.3M) produced were 0.20 ± 0.02 μm and 0.56 ± 0.06 μm respectively, both significantly smaller than those observed when POEGMA was co-spun (0.42 ± 0.14 μm and 1.40 ± 0.25 μm respectively). Thus, the inclusion of POH/POA resulted in the maintenance of a fibrous morphology at lower PEO concentrations while at the same time resulting in higher feature sizes, confirming the key role of the POH/POA precursor polymers in controlling the fiber morphology despite its significantly lower viscosity and capacity for chain entanglement.

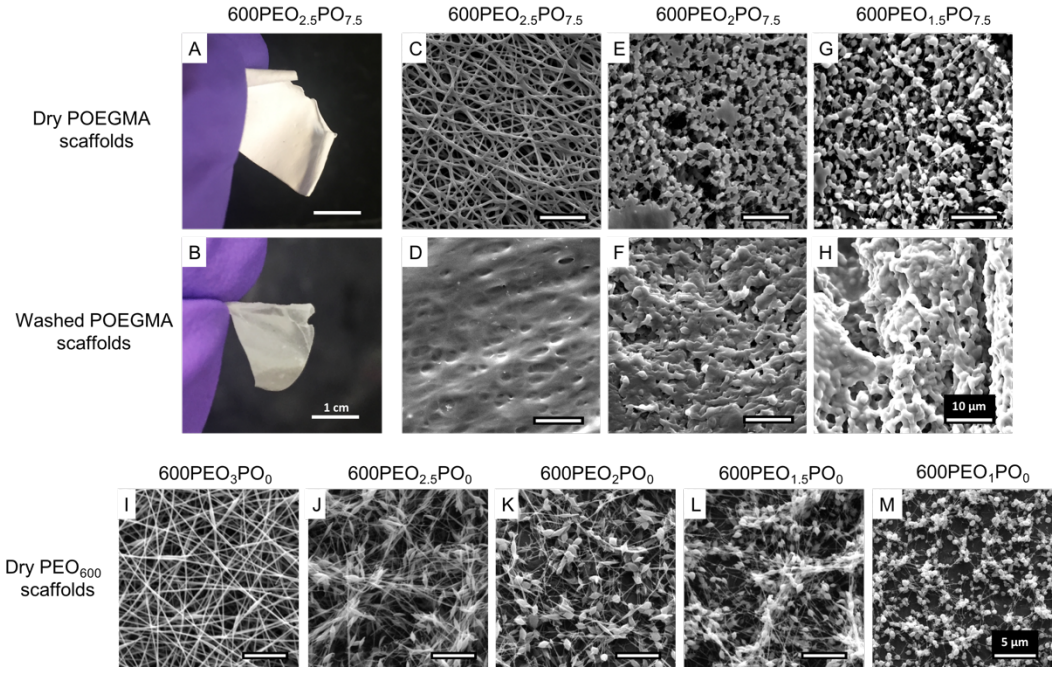

Figure 7.3 (A-B) Optical images of 7.5 wt% POH/POA+ 2.5 wt% 600PEO scaffolds ($600PEO_{2.5}PO_{7.5}$) before (A) and after (E) washing with DIW. (C-H) SEM images of POH/POA+ 600PEO prepared with different concentrations of polymer precursors before (C, E, G) and after (D, F, H) washing with DIW (24 h our soaking). (I-M) SEM images of electrospinning 600PEO only (without POH/POA) at the same electrospinning conditions but at different PEO concentrations. All samples were prepared using a 10 kV potential difference and a 10 cm of falling distance at room temperature (dry collection).

7.3.2 Effect of PEO molecular weight on fiber structure

To investigate the effect of PEO molecular weight on the morphologies of gel scaffolds formed via reactive electrospinning, 1000PEO (M_w = 1000,000 g/mol) at concentrations

ranging from 0.5 wt% to 2 wt% was used as the electrospinning aid. Figure 7.3 shows the resulting morphologies produced, while Table 7.1 summarizes the recipes and the feature sizes produced in each electrospinning experiment. Electrospinning 1000PEO alone (no POH/POA) resulted in a fiber/beaded fiber transition at ~1.5 wt% PEO ($1000PEO_{1.5}PO_{7.5}$ in Fig. 7.4F) and the production of a bead-only morphology at 0.5 wt% ($1000PEO_{0.5}PO_{7.5}$ in Fig. 7.5D); these concentrations are lower than those observed for 600PEO (Fig. 7.3), consistent with the higher degree of chain entanglement expected with the higher molecular weight PEO polymer. As with 600PEO, all of these 1000PEO-only structures rapidly dissolved when immersed with water, consistent with the lack of crosslinking in these scaffolds. In contrast to the 600PEO results, the threshold for the fiber : beaded fiber transition with 1000PEO was not significantly different in the presence of POH/POA; for example, at a 1000PEO concentration of 1.5 wt%, both POH/POA+ 1000PEO (Fig. 7.4F) and 1000PEO-only (Fig. 7.4B) scaffolds exhibited similar beaded fiber structures, while neither sample showed significant fiber formation at 1 wt% 1000PEO or less (Figs. 7.4C-D and 4G-H). This result is consistent with the higher inherent viscosity and degree of chain entanglement facilitated by 1000PEO alone, which makes the additional minimal changes in viscosity and entanglement as a result of adding the same 7.5 wt% concentration of POH/POA less influential toward the overall electrospinning properties than it was with 600PEO. However, a very large difference in feature size is observed between the POH/POA+1000PEO and 1000PEO only samples; for example, the diameter of beads in $1000PEO_{0.5}PO_{7.5}$ was 2.61 ± 0.24 μm (Fig. 7.4H) while that of the $1000PEO_{0.5}PO_{0}$ was only 0.40 ± 0.06 μm (Fig. 7.4D). Similarly, decreasing the 1000PEO concentration from 1 wt% to 0.5 wt% resulted in minimal changes in scaffold morphology whether or not POH/POA was added (Figs. 7.4C-D) but resulted in a large change in feature size from 1.81 ± 0.28 μm to 2.61 ± 0.24 μm only in the presence of the POH/POA gelling pair (Figs. 7.4G-H). Thus, by simply varying the concentration of the electrospinning aid, the size of gel microbeads produced can be controlled. As with the POH/POA + 600PEO scaffolds, immersion of the POH/POA + 1000PEO scaffolds in water resulted in the fiber (Fig. 7.4I), beaded-fiber (Fig. 7.4J) and bead (Figs. 7.4K-L) morphologies being maintained, albeit obviously expanded (even after re-drying) following swelling; this is also consistent with the 600PEO results. However, it is notable that the capacity to still form network structures at extremely low (0.5 wt%) 1000PEO concentrations results in even better maintenance of the dry scaffold dimensions following swelling when 1000PEO is used as the electrospinning aid (e.g. comparing Figs. 7.4H and 7.4L). Again, all these scaffolds could

be picked up as intact samples both before and after re-hydration, even scaffolds exhibiting the all-bead morphologies achieved at lower PEO contents.

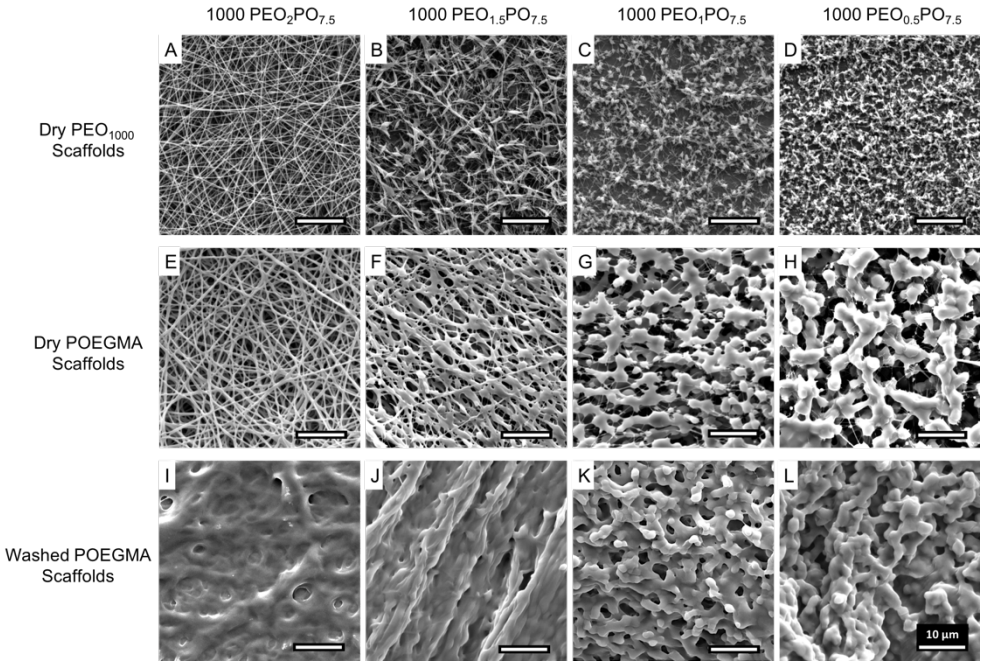

Figure 7.4 SEM images of electrospun 1000PEO only (A-D) and POH/POA+ 1000PEO (E-H) scaffolds with different 1000PEO concentrations. (I-L) SEM images of electrospun POH/POA+1000PEO scaffolds (scaffolds E-H) after washing with DIW.

7.3.3 Effect of POH/POA concentration

Changing the concentration of the gel precursor polymers further expands the scope of morphologies that can be achieved. Figure 7.5 shows the scaffold morphologies produced at low PEO concentrations (0.67 or 1 wt%) but at POH/POA concentrations of 10 wt%; the recipes and characterization of the feature sizes for these scaffolds are shown in Table 2. A beaded fiber morphology was observed for $1000PEO_1PO_{10}$ (Fig. 7.5B); in contrast, for $1000PEO_1PO_{7.5}$ (same PEO content but lower POH/POA content) only beads are generated (Fig. 7.4G). This result is again consistent with a higher precursor concentration inducing more entanglement in the polymer solution, promoting the formation of at least some fibers. Bead-only morphologies are still produced when lower PEO molecular weight

(600PEO$_1$PO$_{10}$, Fig. 7.5A) or lower 1000PEO concentrations (1000PEO$_{0.67}$PO$_{10}$, Fig. 7.5C) are used. Following soaking, there are further differences observed depending on the POH/POA concentration used. While bead-rich morphologies prepared with 7.5 wt% POH/POA were maintained but minimally altered following swelling and subsequent drying, similar dry-state morphologies prepared at 10 wt% POH/POA maintained a much more networked and apparently swollen structure following the swelling/drying cycle. This result is likely attributable to the increased effective crosslink density both within and between each of the nanoscale features at the higher 10 wt% POH/POA concentration, resulting in a more networked final microstructure that is better maintained upon re-hydration.

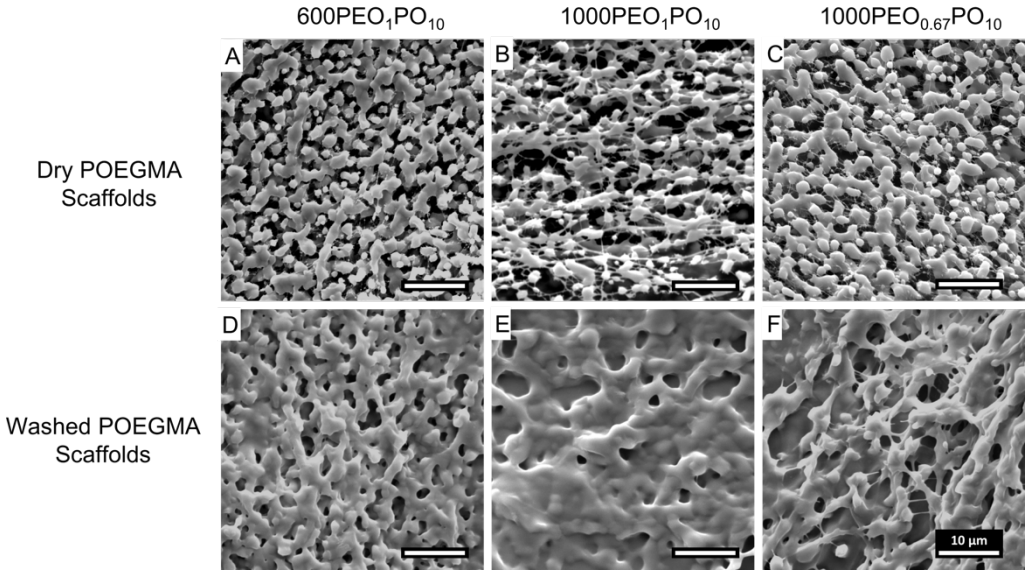

Figure 7.5 SEM images of electrospun hydrogels prepared with POH/POA concentrations of 10 wt% before (A-C) and after (D-F) soaking in DIW. (A, D) POH/POA + 600PEO (1 wt%); (B, E) POH/POA + 1000PEO (1 wt%); (C, F) POH/POA + 1000PEO (0.67 wt%).

Table 7.2 Electrospinning recipes and feature sizes associated with reactive electrospinning POH/POA at a concentration of 10 wt%

Sample name	PEO (wt %)	POH/POA (wt %)	Morphology	Diameter (μm)
$600PEO_1PO_{10}$	1	10	Bead	1.77 ± 0.30
$1000PEO_1PO_{10}$	1	10	Beaded fiber	N/A[a]
$1000PEO_{0.67}PO_{10}$	0.67	10	Bead	1.83 ± 0.33

[a] Due to the heterogeneity of the beaded fiber networks, no characteristic size was reported for these networks

7.3.4 Mechanism of different morphologies formed during reactive electrospinning

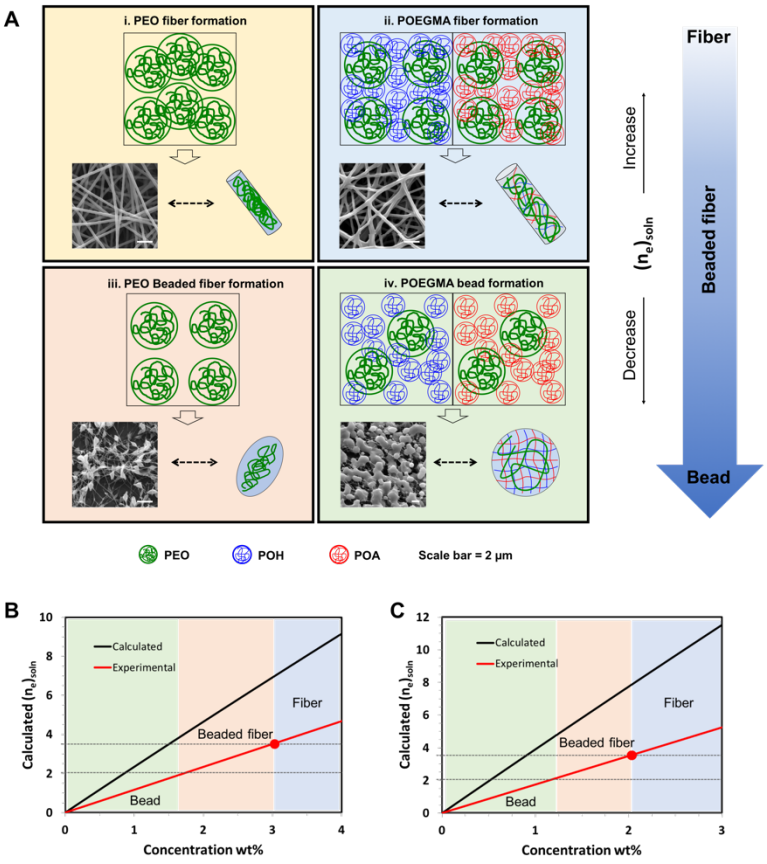

Figure 7.6 (A) Schematic of chain entanglements that determine fiber or bead formation. (B-C) Plot of entanglement numbers as function of calculated (black) and experimental (red) concentrations of 600PEO (B) and 1000PEO (C).

Although the *in situ* crosslinking in the POEGMA/PEO reactive electrospinning system is significantly different than most prior electrospinning work, the general transition from

fibers to beaded fibers and beads appears to mirror conventional, non-reactive electrospinning. Gupta et al[17] reported a physical representation to predict the fiber or bead formation using the critical chain overlap concentration c^* (below which, in the dilute regime, only beads are formed) and the critical entanglement concentration c_e. In general, when $c^* < c < c_e$ (the "semidilute untangled" regime), chain overlap exists but is insufficient to provide enough chain entanglements to enable fiber formation, resulting in bead-rich morphologies (generally beaded fibers) forming during electrospinning; conversely, when $c > c_e$ (the "semidilute entangled" regime), sufficient chain entanglements are present to enable fiber formation.[12,13,49] For 600PEO electrospun alone, c_e lies between 2.5-3 wt% PEO, consistent with the switch between a fiber and beaded fiber morphology. However, adding the POH/POA gelling pair resulted in pure fiber formation at 2.5 wt% (Fig. 7.3C), suggesting an effective lowering of c_e in the presence of POH/POA that, although short and highly branched, can add enough to chain entanglement to enable fiber formation. Fig. 7.6A shows this correlation schematically for 600PEO; a similar diagram could be drawn for 1000PEO at lower c^* and c_e values consistent with the higher degree of inherent entanglement with the higher molecular weight 1000PEO. Void spaces in the semidilute unentangled regime ($c^* < c < c_e$, Fig. 6A-iii) are filled by adding POH/POA (Fig. 7.6A-ii), introducing sufficient additional chain entanglements to enter the semidilute entangled regime.[50,51] Alternately, if the PEO concentration is lowered, chain overlap significantly decreases even if the free volume is largely filled by the short and highly branched POH/POA polymers (Fig. 7.6A-iv), increasing the required c_e value for entanglements and thus resulting in bead formation.

Shenoy et al. [12,52] reported an alternate semi-empirical methodology to determine the "electrospinnability" of a polymer solution by predicting the transition from electrospinning (fibers) to electrospraying (fibers + beads) using the solution entanglement number $(n_e)_{soln}$, defined by equation (2):

$$(n_e)_{soln} = \frac{M_w}{(M_e)_{soln}} = \frac{(\emptyset_p M_w)}{M_e} \qquad (2)$$

Here, M_e is the entanglement molecular weight in the melt (related to the average molecular weight between entanglements), ϕ is the volume fraction of polymer chains in solution, and M_w is polymer molecular weight. Entanglement numbers > 3.5 will lead to pure fibers, while bead-on-fiber morphologies are observed at entanglement numbers 2-3.5 and only

beads formed (i.e. electrospray) at entanglement numbers < 2.[12,23] Using a PEO entanglement molecular weight of 2.1×10^3 g/mol,[12,51] the calculated $(n_e)_{soln}$ is plotted as a function of the concentrations of 600PEO (Fig. 7.6B) and 1000PEO (Fig. 7.6C). The black line was calculated based on equation (2), while the red line was obtained from the experimental fiber/beaded fiber transition concentrations (i.e. the concentration at which $(n_e)_{soln} = 3.5$) at 3 wt% for 600PEO and 2 wt% for 1000PEO (Table 7.1). The theoretical entanglement concentration (black) is lower than that observed in the experimental data (red) for both PEO molecular weights; this is consistent with the strong hydrogen bonding observed in the DIW solvent used for these experiments which is not fully accounted for in this model.[1214] However, this model correctly predicts the general trend of lower critical PEO contents required for fiber formation with higher molecular weight PEO observed in the experimental data. It should be emphasized that, although there is some degree of gelation of POH/POA in the static mixer between the contact between the streams and the electrospinning needle, the relatively small apparent impact of the POEGMA precursor polymers on the overlap/entanglement concentrations suggest that gelation by the time the polymers reach the tip is minimal.

7.3.5. Hydrogel properties of scaffolds as a function of scaffold morphology

The water binding capacity of dry scaffolds of different morphologies was assessed by immersing each scaffold in 10 mM PBS at 37 °C. Figs. 7.7A-B show the kinetics of swelling between the scaffolds while Fig. 7.7C shows the equilibrium swelling ratio (relative to the initial dry scaffold weight) for each scaffold produced. All scaffolds, regardless of morphology, absorbed water rapidly and reached their equilibrium water content in ~1 min., 1-2 orders of magnitude faster than a conventional bulk gel made of the same polymer composition. Clear trends were noted in the equilibrium swelling degree as a function of both scaffold concentration and morphology. For a given POH/POA concentration, equilibrium water contents vary with morphology, with small bead (1.4 -1.8 μm) or beaded fiber morphologies swelling substantially more than either larger bead (≥ 2 μm) or fibrous morphologies independent of the molecular weight of the PEO electrospinning aid (Fig. 7.7A-B). We hypothesize this result is attributable to the intermediate morphology possessing both higher specific surface areas than the larger bead structures as well as the lower PEO contents (and consequently the higher POEGMA volume fractions) relative to the fibrous structures.

To assess the relative impacts of the different feature sizes and scaffold chemistries on the degradation rates of the scaffolds, three beaded network samples were exposed to accelerated acid-catalyzed degradation conditions (0.1 M HCl at 37 °C) (Fig. 7.7D). Reducing the PEO content without changing the POEGMA concentration (i.e. comparing $1000PEO_1PO_{7.5}$ to $1000PEO_{0.5}PO_{7.5}$) results in more swelling and slightly faster degradation, consistent with the higher initial volume fraction of POEGMA gel in the low-PEO scaffold; increasing the POEGMA content without significantly changing the bead size (i.e. comparing $600PEO_1PO_{10}$ to $1000PEO_1PO_{7.5}$) resulted in reduced swelling and slower degradation consistent with the higher expected crosslink density within the POEGMA hydrogel phase. All degradation kinetics tested were significantly slower than the corresponding bulk hydrogel prepared at the same concentrations, consistent with water evaporation during the electrospinning process effectively concentrating the polymers during the gelation process and thus increasing the crosslinking density achieved.[43]

Compressive moduli of electrospun scaffolds, measured at 30 %, 40 % and 50 % compression in 10 mM PBS, are shown in Table 3. In general, all compressive moduli increase as the degree of compression increases, as anticipated[37]. Significant modulus increases were also observed regardless of the PEO content when the POH/POA concentrations were increased from 7.5 wt% to 10 wt%; for example, the modulus of a 1 wt% 1000PEO scaffold increased from 13.2 ± 1.0 kPa to 22.4 ± 0.8 kPa upon increasing the wt% of POEGMA precursor polymers used (Table 7.3). This result is consistent with the higher crosslink density expected when scaffolds are prepared with higher gel precursor polymer concentrations. However, the molecular weight of the PEO electrospinning aid had no significant impact on the compressive modulus; for example, modulus values of $600PEO_{1.5}PO_{7.5}$ and $1000PEO_{1.5}PO_{7.5}$ are very similar at each % compression tested, while the 30% compression moduli of $600PEO_1PO_{10}$ and $1000PEO_1PO_{10}$ were 21.1 ± 1.5 kPa and 22.4 ± 0.8 kPa respectively, even though both the PEO molecular weight and the morphology (from bead to beaded fiber) both change between these samples. This result is consistent with the PEO being fully washed out of each of the scaffolds (i.e. the properties of the PEO itself do not significantly impact the mechanical properties of the scaffolds). In addition, scaffolds with beaded fiber or small beaded network morphologies ($600PEO_{1.5}PO_{7.5}$ and $1000PEO_{1.5}PO_{7.5}$) showed consistently lower moduli values than fibers or larger beaded networks, particularly at lower compression. These intermediate

morphology scaffolds also exhibit the highest degree of swelling (Figs. 7.7A-B), both consistent with lower effective crosslink densities (at least between the fibers/beads) in these scaffolds.

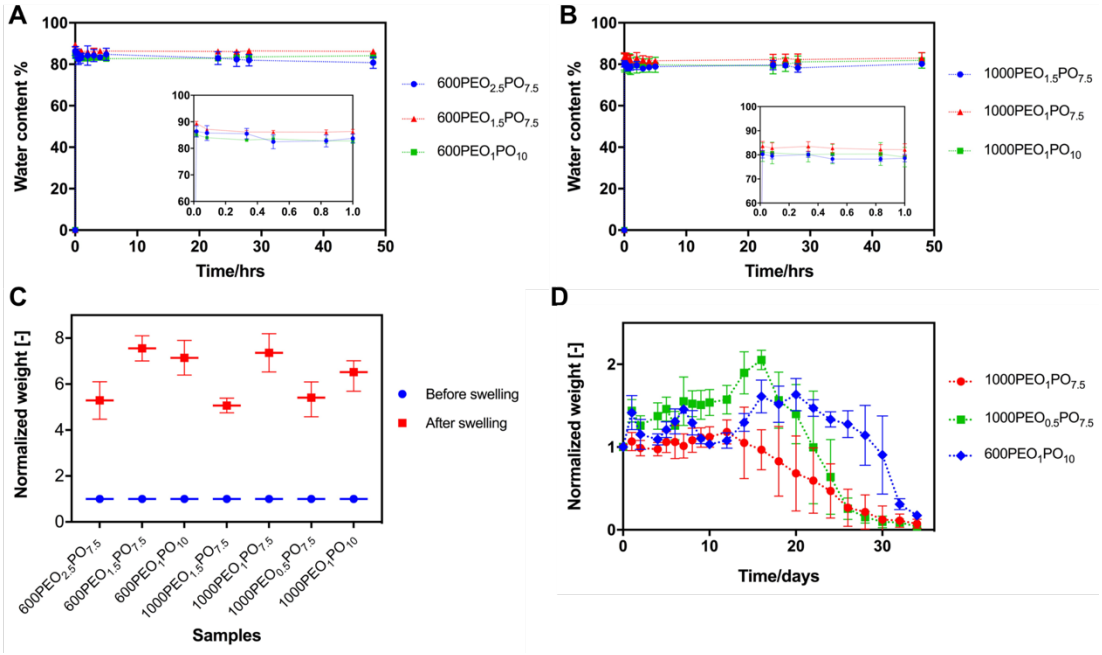

Figure 7.7 (A-B) Swelling of POH/POA + PEO electrospun scaffolds prepared with 600PEG (A) and 1000PEG (B) in 10 mM PBS at 37°C. (C) Normalized weights of scaffolds with different morphologies before and after swelling in 10 mM PBS. (D) Accelerated degradation kinetics of beaded network POH/POA + PEO electrospun scaffolds with different POEGMA concentrations and bead sizes measured in 0.1M HCl at 37°C.

Table 7.3 Compression mechanical properties of electrospun POH/POA + PEO scaffolds

Compression	$600PEO_{1.5}PO_{7.5}$	$600PEO_1PO_{10}$	$1000PEO_{1.5}PO_{7.5}$	$1000PEO_1PO_{7.5}$	$1000PEO_1PO_{10}$	$1000PEO_{0.67}PO_{10}$
%	kPa	kPa	kPa	kPa	kPa	kPa
30%	5.7 ± 0.1	21.1 ± 1.5	4.4 ± 0.1	13.2 ± 1.0	22.4 ± 0.8	13.7 ± 1.2
40%	7.8 ± 0.3	22.0 ± 0.4	7.0 ± 0.2	N/A	30.2 ± 1.6	24.7 ± 1.2
50%	18.3 ± 0.8	N/A	22.7 ± 2.8	N/A	N/A	N/A

7.3.6. Cell encapsulation within scaffolds

Given that clear differences in internal hydrogel morphology are observed on a length scale highly relevant to cells (0.4-2.6 microns), the effects of the different morphologies developed on the potential for cell growth within the scaffolds was assessed by suspending 3T3 mouse fibroblast cells in the POH+PEO loaded barrel of the double barrel syringe and conducting reactive cell electrospinning using our previously reported strategy (Fig. 7.8A, Chapter 6). Both the POEGMA polymers and PEO were shown to be non-cytotoxic at the concentration and timescales used for cell electrospinning (Fig.7.8B), suggesting the promise of this strategy.

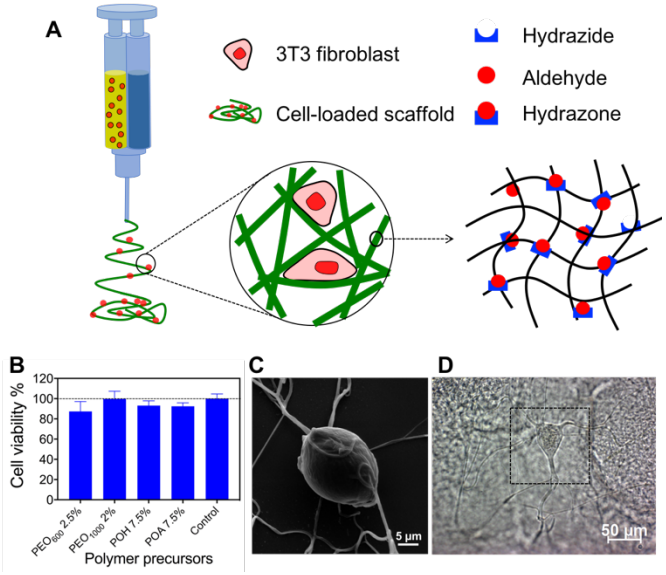

Figure 7.8 (A) Scheme of cell electrospinning to encapsulate 3T3 fibroblasts in POEGMA based hydrogels. (B) Cell viabilities of 3T3 fibroblasts with electrospun polymer precursors. (C) SEM images of 3T3 cell loaded in $600PEO_{2.5}PO_{7.5}$ electrospun nanofibers. (D) Bright field microscopic image of cell-loaded scaffold ($1000PEO_2PO_{7.5}$) in PBS.

Four different scaffold compositions that yield fibers ($600PEO_{2.5}PO_{7.5}$ and $1000PEO_2PO_{7.5}$) and beads ($600PEO_{1.5}PO_{7.5}$ and $1000PEO_{0.5}PO_{7.5}$) were selected for compositions demonstrated to show fibrous morphologies in the absence of cells, cells were observed to

be surrounded by POEGMA fibers. (Fig. 7.8C-D). Applying the LIVE/DEAD assay to the cells encapsulated inside the different scaffolds indicates that the vast majority of cells remain viable independent of morphology, although more dead cells were found in the $1000PEO_2PO_{7.5}$ scaffold due to the higher concentration/molecular weight of PEO resulting more shear stress applied to the cells as the more viscous pre-polymer solution was stretched into fibers. Both fibrous structures ($600PEO_{2.5}PO_{7.5}$ and $1000PEO_2PO_{7.5}$) showed increasing cell numbers between 3 days and 7 days of culture, suggesting the fibrous morphologies can effectively support cell proliferation. In comparison, while the cells remain highly viable, no significant increase of cell number was found in the beaded network samples over the same period of time independent of the different bead sizes (1.40 ± 0.25 μm for $600PEO_{1.5}PO_{7.5}$, 2.61 ± 0.02 μm for $1000PEO_{0.5}PO_{7.5}$, Table 7.1). This result is consistent with the increased specific surface area of nanofibers providing more cell binding sites and thus a higher capacity to support cell proliferation.[41] Overall, this result suggests that by using the exact same basic scaffold chemistry but changing the scaffold morphology we can either promote or suppress cell proliferation within the scaffolds without compromising cell viability inside the scaffolds. This result may be relevant to using these scaffolds for cell delivery (in which slow release of independent viable cells may be beneficial for regenerating native tissues) or tissue engineering (in which cell proliferation and communication is essential to form a tissue within the scaffold itself). [29,53]

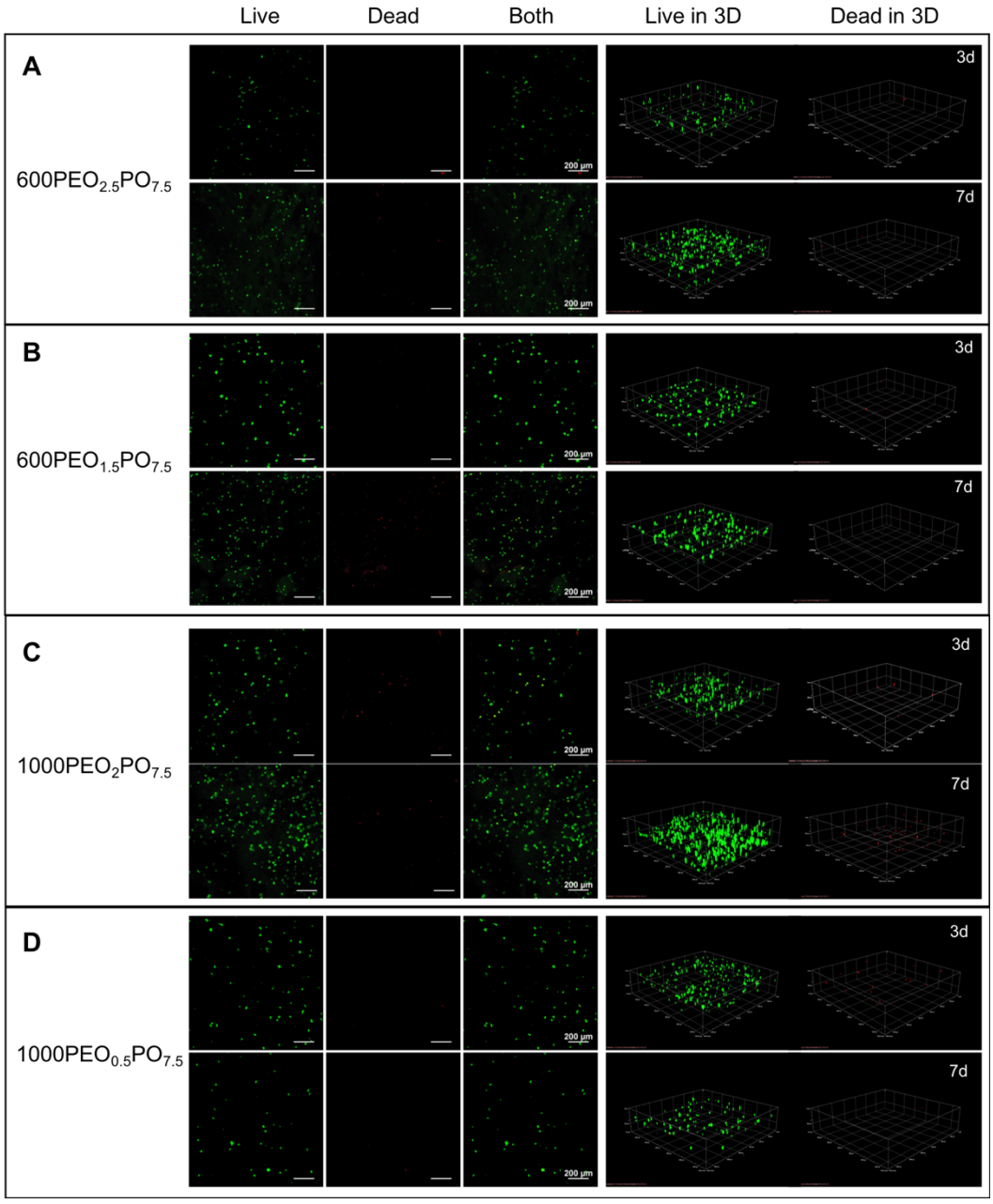

Figure 7.9 Confocal microscopy images of 3T3 fibroblasts co-electrospun into POEGMA scaffolds with different morphologies: (A-B) fibrous microstructure; (C-D) beaded network microstructure. Live cells were stained by calcein AM (488 nm, green) and dead cells were stained by ethidium homodimer-1 (546 nm, red).

7.4 Conclusion

A simple, single-step reactive electrospinning method has been demonstrated to enable the fabrication of nanostructured hydrogel scaffolds with well-defined morphologies consisting of all fibers, beaded fibers or beaded networks with tunable bead sizes. The *in situ* covalent hydrazone gelation chemistry effectively crosslinks these features together to form a monolithic scaffold even in cases where the internal structures produced are beads, allowing for the production of novel hydrogel morphologies. Adjusting the molecular weight of the PEO electrospinning aid and/or the concentrations of the PEO electrospinning aid or the POH/POA gel precursor polymers (all of which adjust the critical overlap and entanglement concentrations associated with electrospinning) can control both the type of morphology produced as well as the feature size of that morphology, enabling the production of hydrogel fibers or beads with defined dimensions. These morphologies, coupled with the concentration of the POEGMA gel component in the scaffold, result in systematic changes in scaffold water content, mechanics, and degradation, with beaded fibers or smaller beaded network morphologies generally showing higher swelling and weaker mechanics relative to pure fiber or larger beaded networks. Co-electrospinning cells into the scaffolds allow for maintenance of these different morphologies, presenting differential structural cues to cells that promote proliferation in fibrous scaffolds but no significant proliferation in beaded network scaffolds. Furthermore, the dry scaffolds produced by electrospinning are flexible, easy to handle, and easy to store. The capacity to introduce controlled nanostructuring in degradable macroporous hydrogel networks has significant potential applications in tissue engineering and drug delivery applications in which the nanostructuring can instruct cell responses to their substrate and/or control the release rate of a targeted therapeutic by controlling the diffusional path length, both of which are acute biomedical technology needs.

7.5 Acknowledgements:

The Natural Sciences and Engineering Research Council of Canada (NSERC, Discovery Grant RGPIN-356609 and Strategic Project Grant STGTP-447372-13) is acknowledged for funding this work.

7.6 References

(1) Bhardwaj, N.; Kundu, S. C. Electrospinning: A Fascinating Fiber Fabrication Technique. *Biotechnol. Adv.* **2010**, *28* (3), 325–347.

(2) Greiner, A.; Wendorff, J. H. Electrospinning: A Fascinating Method for the Preparation of Ultrathin Fibers. *Angew. Chemie - Int. Ed.* **2007**, *46* (30), 5670–5703.

(3) Sill, T. J.; von Recum, H. A. Electrospinning: Applications in Drug Delivery and Tissue Engineering. *Biomaterials*. 2008, pp 1989–2006.

(4) Frohbergh, M. E.; Katsman, A.; Botta, G. P.; Lazarovici, P.; Schauer, C. L.; Wegst, U. G. K.; Lelkes, P. I. Biomaterials Electrospun Hydroxyapatite-Containing Chitosan Nano Fi Bers Crosslinked with Genipin for Bone Tissue Engineering. *Biomaterials* **2012**, *33* (36), 9167–9178.

(5) Sridhar, R.; Lakshminarayanan, R.; Madhaiyan, K.; Amutha Barathi, V.; Lim, K. H. C.; Ramakrishna, S. Electrosprayed Nanoparticles and Electrospun Nanofibers Based on Natural Materials: Applications in Tissue Regeneration, Drug Delivery and Pharmaceuticals. *Chem. Soc. Rev.* **2015**, *44*, 790–814.

(6) Zeng, J.; Xu, X.; Chen, X.; Liang, Q.; Bian, X.; Yang, L.; Jing, X. Biodegradable Electrospun Fibers for Drug Delivery. *J. Control. Release* **2003**, *92* (3), 227–231.

(7) Formo, E.; Lee, E.; Campbell, D.; Xia, Y. Functionalization of Electrospun TiO 2 Nanofibers with Pt Nanoparticles and Nanowires for Catalytic Applications. *Nano Lett.* **2008**, *8* (2), 668–672.

(8) Patel, A. C.; Li, S.; Wang, C.; Zhang, W.; Wei, Y. Electrospinning of Porous Silica

Nanofibers Containing Silver Nanoparticles for Catalytic Applications. *Chem. Mater.* **2007**, *19* (6), 1231–1238.

(9) Wen, S.; Liang, M.; Zou, R.; Wang, Z.; Yue, D.; Liu, L. Electrospinning of Palladium/Silica Nanofibers for Catalyst Applications. *RSC Adv.* **2015**, *5* (52), 41513–41519.

(10) Lang, C.; Fang, J.; Shao, H.; Ding, X.; Lin, T. High-Sensitivity Acoustic Sensors from Nanofibre Webs. *Nat. Commun.* **2016**, *7*, 11108.

(11) Wang, X.; Drew, C.; Lee, S. H.; Senecal, K. J.; Kumar, J.; Samuelson, L. A. Electrospun Nanofibrous Membranes for Highly Sensitive Optical Sensors. *Nano Lett.* **2002**, *2* (11), 1273–1275.

(12) Shenoy, S. L.; Bates, W. D.; Frisch, H. L.; Wnek, G. E. Role of Chain Entanglements on Fiber Formation during Electrospinning of Polymer Solutions: Good Solvent, Non-Specific Polymer-Polymer Interaction Limit. *Polymer (Guildf).* **2005**, *46* (10), 3372–3384.

(13) Nie, H.; He, A.; Zheng, J.; Xu, S.; Li, J.; Han, C. C. Effects of Chain Conformation and Entanglement on the Electrospinning of Pure Alginate. *Biomacromolecules* **2008**, *9* (5), 1362–1365.

(14) Shin, Y. M.; Hohman, M. M.; Brenner, M. P.; Rutledge, G. C. Experimental Characterization of Electrospinning: The Electrically Forced Jet and Instabilities. *Polymer (Guildf).* **2001**, *42* (25), 09955–09967.

(15) Koski, A.; Yim, K.; Shivkumar, S. Effect of Molecular Weight on Fibrous PVA Produced by Electrospinning. *Mater. Lett.* **2004**, *58* (3–4), 493–497.

(16) Casper, C. L.; Stephens, J. S. Controlling Surface Morphology of Electrospun Polysterene Fibers: Effect of Humidity and Molecular Weight in Electrospinning Process. *Macromolecules* **2004**, *37*, 573–578.

(17) Gupta, P.; Elkins, C.; Long, T. E.; Wilkes, G. L. Electrospinning of Linear Homopolymers of Poly(Methyl Methacrylate): Exploring Relationships between

Fiber Formation, Viscosity, Molecular Weight and Concentration in a Good Solvent. *Polymer (Guildf).* **2005**, *46* (13), 4799–4810.

(18) McKee, M. G.; Wilkes, G. L.; Colby, R. H.; Long, T. E. Correlations of Solution Rheology with Electrospun Fiber Formation of Linear and Branched Polyesters. *Macromolecules* **2004**, *37* (5), 1760–1767.

(19) Deitzel, J. .; Kleinmeyer, J.; Harris, D.; Beck Tan, N. . The Effect of Processing Variables on the Morphology of Electrospun Nanofibers and Textiles. *Polymer (Guildf).* **2001**, *42* (1), 261–272.

(20) Beachley, V.; Wen, X. Effect of Electrospinning Parameters on the Nanofiber Diameter and Length. *Mater. Sci. Eng. C* **2009**, *29* (3), 663–668.

(21) Luo, C. J.; Nangrejo, M.; Edirisinghe, M. A Novel Method of Selecting Solvents for Polymer Electrospinning. *Polymer (Guildf).* **2010**, *51* (7), 1654–1662.

(22) De Vrieze, S.; Van Camp, T.; Nelvig, A.; Hagstr??m, B.; Westbroek, P.; De Clerck, K. The Effect of Temperature and Humidity on Electrospinning. *J. Mater. Sci.* **2009**, *44* (5), 1357–1362.

(23) Munir, M. M.; Suryamas, A. B.; Iskandar, F.; Okuyama, K. Scaling Law on Particle-to-Fiber Formation during Electrospinning. *Polymer (Guildf).* **2009**, *50* (20), 4935–4943.

(24) Yao, Q.; Cosme, J. G. L.; Xu, T.; Miszuk, J. M.; Picciani, P. H. S.; Fong, H.; Sun, H. Three Dimensional Electrospun PCL/PLA Blend Nanofibrous Scaffolds with Significantly Improved Stem Cells Osteogenic Differentiation and Cranial Bone Formation. *Biomaterials* **2017**, *115*, 115–127.

(25) Wade, R. J.; Bassin, E. J.; Rodell, C. B.; Burdick, J. a. Protease-Degradable Electrospun Fibrous Hydrogels. *Nat. Commun.* **2015**, *6*, 6639.

(26) Dalton, P. D.; Klinkhammer, K.; Salber, J.; Klee, D.; Möller, M. Direct in Vitro Electrospinning with Polymer Melts. *Biomacromolecules* **2006**, *7* (3), 686–690.

(27) Zhang, J.-F.; Yang, D.-Z.; Xu, F.; Zhang, Z.-P.; Yin, R.-X.; Nie, J. Electrospun

Core−Shell Structure Nanofibers from Homogeneous Solution of Poly(Ethylene Oxide)/Chitosan. *Macromolecules* **2009**, *42* (14), 5278–5284.

(28) Lim, S. H.; Mao, H.-Q. Electrospun Scaffolds for Stem Cell Engineering. *Adv. Drug Deliv. Rev.* **2009**, *61* (12), 1084–1096.

(29) Place, E. S.; Evans, N. D.; Stevens, M. M. Complexity in Biomaterials for Tissue Engineering. *Nat. Mater.* **2009**, *8* (6), 457–470.

(30) Watt, F. M.; Huck, W. T. S. Role of the Extracellular Matrix in Regulating Stem Cell Fate. *Nat. Rev. Mol. Cell Biol.* **2013**, *14* (8), 467–473.

(31) Heydarkhan-Hagvall, S.; Schenke-Layland, K.; Dhanasopon, A. P.; Rofail, F.; Smith, H.; Wu, B. M.; Shemin, R.; Beygui, R. E.; MacLellan, W. R. Three-Dimensional Electrospun ECM-Based Hybrid Scaffolds for Cardiovascular Tissue Engineering. *Biomaterials* **2008**, *29* (19), 2907–2914.

(32) Annabi, N.; Mithieux, S. M.; Weiss, A. S.; Dehghani, F. Cross-Linked Open-Pore Elastic Hydrogels Based on Tropoelastin, Elastin and High Pressure CO2. *Biomaterials* **2010**, *31* (7), 1655–1665.

(33) Stephens-Altus, J. S.; Sundelacruz, P.; Rowland, M. L.; West, J. L. Development of Bioactive Photocrosslinkable Fibrous Hydrogels. *J. Biomed. Mater. Res. Part A* **2011**, *98A* (2), 167–176.

(34) Lutz, J. F. Polymerization of Oligo(Ethylene Glycol) (Meth)Acrylates: Toward New Generations of Smart Biocompatible Materials. *J. Polym. Sci. Part A Polym. Chem.* **2008**, *46* (11), 3459–3470.

(35) Lutz, J.-F.; Hoth, A. Preparation of Ideal PEG Analogues with a Tunable Thermosensitivity by Controlled Radical Copolymerization of 2-(2-Methoxyethoxy)Ethyl Methacrylate and Oligo(Ethylene Glycol) Methacrylate. *Macromolecules* **2006**, *39* (2), 893–896.

(36) Xu, F.; Sheardown, H.; Hoare, T. Reactive Electrospinning of Degradable Poly(Oligoethylene Glycol Methacrylate)-Based Nanofibrous Hydrogel Networks.

Chem. Commun. **2015**, *52*, 23–25.

(37) Xu, F.; Sheardown, H.; Hoare, T. Reactive Electrospinning of Degradable Poly(Oligoethylene Glycol Methacrylate)-Based Nanofibrous Hydrogel Networks. *Chem. Commun.* **2015**, *52*, 23–25.

(38) Zheng, J.; He, A.; Li, J.; Xu, J.; Han, C. C. Studies on the Controlled Morphology and Wettability of Polystyrene Surfaces by Electrospinning or Electrospraying. *Polymer (Guildf).* **2006**, *47* (20), 7095–7102.

(39) Lee, K. H.; Kim, H. Y.; Bang, H. J.; Jung, Y. H.; Lee, S. G. The Change of Bead Morphology Formed on Electrospun Polystyrene Fibers. *Polymer (Guildf).* **2003**, *44* (14), 4029–4034.

(40) Wang, L.; Topham, P. D.; Mykhaylyk, O. O.; Yu, H.; Ryan, A. J.; Fairclough, J. P. A.; Bras, W. Self-Assembly-Driven Electrospinning: The Transition from Fibers to Intact Beaded Morphologies. *Macromol. Rapid Commun.* **2015**, *36* (15), 1437–1443.

(41) Stevens, M. M.; George, J. H. Exploring and Engineering the Cell Surface Interface. *Science* **2005**, *310* (November), 1135–1138.

(42) J., F. K.; Fei, X.; Todd, H. Structured Macroporous Hydrogels: Progress, Challenges, and Opportunities. *Adv. Healthc. Mater.* **2017**, *7* (1), 1700927.

(43) Smeets, N. M. B.; Bakaic, E.; Patenaude, M.; Hoare, T. Injectable and Tunable Poly(Ethylene Glycol) Analogue Hydrogels Based on Poly(Oligoethylene Glycol Methacrylate). *Chem. Commun.* **2014**, *50* (25), 3306–3309.

(44) Zhang, W.; He, X. Encapsulation of Living Cells in Small (~100 Mm) Alginate Microcapsules by Electrostatic Spraying: A Parametric Study. *J. Biomech. Eng.* **2009**, *131* (7), 74515–74516.

(45) Tan, W.-H.; Takeuchi, S. Monodisperse Alginate Hydrogel Microbeads for Cell Encapsulation. *Adv. Mater.* **2007**, *19* (18), 2696–2701.

(46) Jovanović, Ž.; Stojkovska, J.; Obradović, B.; Mišković-Stanković, V. Alginate

Hydrogel Microbeads Incorporated with Ag Nanoparticles Obtained by Electrochemical Method. *Mater. Chem. Phys.* **2012**, *133* (1), 182–189.

(47) Shibata, H.; Heo, Y. J.; Okitsu, T.; Matsunaga, Y.; Kawanishi, T.; Takeuchi, S. Injectable Hydrogel Microbeads for Fluorescence-Based in Vivo Continuous Glucose Monitoring. *Proc. Natl. Acad. Sci.* **2010**, *107* (42), 17894–17898.

(48) Smeets, N. M. B.; Bakaic, E.; Patenaude, M.; Hoare, T. Injectable and Tunable Poly(Ethylene Glycol) Analogue Hydrogels Based on Poly(Oligoethylene Glycol Methacrylate). *Chem. Commun.* **2014**, *50* (25), 3306–3309.

(49) Dobrynin, A. V; Colby, R. H.; Rubinstein, M. Scaling Theory of Polyelectrolyte Solutions. *Macromolecules* **1995**, *28* (6), 1859–1871.

(50) Polymer, I.; Huggins, F. 4. Polymer Solutions and Blends. *J. Phys. Chem. C* **1942**, *51*, 1–23.

(51) Fetters, L. J.; Lohse, D. J.; Colby, R. H. CHAPTER 25 Chain Dimensions and Entanglement Spacings. *Phys. Prop. Polym. Handb.* **2006**, 445–452.

(52) Shenoy, S. L.; Bates, W. D.; Wnek, G. Correlations between Electrospinnability and Physical Gelation. *Polymer (Guildf).* **2005**, *46* (21), 8990–9004.

(53) Masuda, S.; Shimizu, T. Three-Dimensional Cardiac Tissue Fabrication Based on Cell Sheet Technology. *Adv. Drug Deliv. Rev.* **2016**, *96*, 103–109.

Chapter 8

Conclusions

8.1 Significance and summary

The work presented in this thesis explored the applications of injectable hydrogels in applications ranging from drug delivery to tissue engineering, on length scales ranging from the macroscale to the nanoscale, and using structures ranging from microbeads to nanofibers.

Chapter 2 reviews recent publications on the preparation of structured hydrogels using different techniques and described the opportunities for applying such hydrogels in tissue engineering. Among the examples given in this review is the approach I explored throughout all my PhD projects in terms of fabricating poly(oligoethylene glycol methacrylate) (POEGMA)-based polymer precursors functionalized with hydrazide and aldehyde groups that can crosslink *in situ* at room temperature to form hydrazone bond without any post-treatment, a chemistry previously developed in our lab. These hydrazone crosslinkable hydrogels can be degraded over ~1 month in PBS buffer or over a few days in acidic conditions. The ease of fabrication and non-toxicity of polymer precursors suggest promising applications in the fields of drug delivery and tissue engineering, which are further explored in the remainder of the thesis.

For drug delivery applications, ***Chapter 3*** focus on the use of injectable bulk hydrogels to deliver protein *in vitro*. In this chapter, we used a high-throughput method to accelerate the fabrication of multiple hydrogels based on both the POEGMA precursor polymers previously described as well as a range of other natural and synthetic polymer precursors

also functionalized with hydrazide or aldehyde groups. Specifically, a broad range of polymer precursors including thermoresponsive polymers, non-thermoresponsive polymers, charged polymers, neutral polymers, natural polymers and synthetic polymers were mixed in different combinations and different ratios using high-throughput robotics to create a library of 126 hydrogels in 30 minutes. Subsequently, high-throughput characterization methods were developed and then applied to measure the physiochemical and *in vitro* pharmacological properties of the hydrogel library, including mechanics, transparency, swelling ratio, degradation, and drug release kinetics. This work shows the potential of high-throughput screening to fabricate and test hydrogels with targeted properties, in particular demonstrating design rules for hydrogels that can facilitate both prolonged and high efficiency release of protein cargoes essential for many next-generation therapeutics.

Given the similarities between the properties of hydrogels and soft tissues, hydrogels have been widely used as scaffolds for tissue engineering and cell encapsulation. However, most hydrogels cannot reproduce the internal nanofibrous structures in native ECM. ***Chapter 4*** describes a simple and one-step electrospinning process based on reactive electrospinning from a double-barrel syringe enabling co-delivery of a hydrazide polymer precursor ($PO_{100}H_{30}$) and an aldehyde polymer precursor ($PO_{100}A_{30}$) at the electrospinning needle. Upon mixing, the precursor polymers start crosslinking as the same time as the extruded jet is stretched by the applied electric field, resulting in continuous production of well-defined hydrazone crosslinked gel nanofibers. These POEGMA hydrogel nanofibers exhibited stable mechanical properties both in dry and wet state as well as very fast swelling responses owing to the nanoscale gel structure.

Chapter 5 extends the functionality of such scaffolds by using the same reactive electrospinning technique to prepare thermoresponsive macroporous nanofibrous hydrogel from thermoresponsive POEGMA-based polymer precursors ($PO_{10}H_{10}$ and $PO_{10}A_{10}$). The existence of short side-chain ($M(EO)_2MA$) in POEGMA hydrogel induced a phase transition just below ~37 °C, resulting in a nanofibrous hydrogel scaffold that reversibly

swelled and deswelled within seconds to thermal stimuli, exploiting both the potential for water penetration (macroporosity) and the nanoscale dimensions to achieve among the fastest reported bulk thermoresponsive hydrogel transitions while introducing degradability into the scaffold. The hydrophilic-to-hydrophobic thermal transition was then applied to enable nearly quantitative cell delamination from the nanofibrous scaffolds within two minutes of cooling while preserving the function and proliferative capacity of the cells. Such performance is highly beneficial for culturing highly sensitive cells in which the ECM degradation caused by the typical trypsinization protocols may significantly change cell properties.

Though stable and effective nanofibrous hydrogel have been prepared to mimic ECM, it is still a challenge to encapsulate cells inside the matrix to obtain uniformly cell-loaded scaffolds. To address this problem, ***Chapter 6*** introduced a creative method to fabricate a "ready-to-use" cellularized nanofibrous hydrogel scaffolds prepared by the all-aqueous reactive electrospinning of POEGMA polymers directly in the presence of cells. High voltage was proven to be safe for processing cells, particularly when cells were co-electrospun with hydrogel nanofibers that reduced both the effective shear stress and dehydration that are typically problematic with cell electrospinning. Both 3T3 fibroblasts and C2C12 myoblasts exhibited significantly higher viabilities and proliferative capacities in the electrospun matrices compared to injectable bulk hydrogels, given that the nanostructure provided more physical support for cell adhesion and more free space for nutrient transport and cell motility; 4-5 fold increases in cell density were observed after 18 days culturing. Remarkably, this cell-loaded scaffold can also be stored in liquid nitrogen directly following the electrospinning process without any added cryoprotectant and maintain high cell viability and proliferative potential following thawing, to our knowledge a unique set of properties. This simple technique thus represents a new and attractive option to prepare storable, transportable, and functional "on-demand" tissue patches for potential use in clinic.

Finally, ***Chapter 7*** explored how the reactive electrospinning technique can be used to develop hydrogel scaffolds with different morphologies. By increasing the concentration of POEGMA in mixed electrospun precursors, the structure of scaffold can be adjusted from "pure beads" to "bead-on-fiber" to "pure fibers", with these morphological transitions explored from fundamental electrospinning theory. Moreover, based on the results from Chapter 6, 3T3 fibroblast cells were successfully encapsulated in these nano-/macrostructured hydrogel scaffolds to provide cells with different morphological cues for adhesion and proliferation, introducing more opportunities for using such scaffolds in the context of tissue engineering.

Collectively, this thesis describes new ways to fabricate bulk, nanofibrous, and microbead hydrogel morphologies using the new approaches of high-throughput synthesis and reactive electrospinning technique to create functional biomedical devices useful for both protein delivery and tissue/cell engineering applications.

8.2 Future directions

This thesis has developed two key enabling technologies: high-throughput synthesis and characterization of *in situ*-gelling hydrogels and reactive electrospinning to create degradable nanofibrous hydrogel networks. In future work, we will both apply and extend these developments in multiple ways:

(1) We will apply a latent variable analysis to fit the high-volume data in Chapter 3 to a multivariate statistical model and subsequently use that model to predict new compositions of optimized hydrogels with specific target properties. For example, we can minimize protein release rate while maximizing total protein release to enable the delivery of higher doses of therapeutic proteins for longer periods of time. Coupled with the "training data" from the high-throughput screening, this model will enable the rapid design of custom hydrogels with specific applications using mixtures of "off-the-shelf" components, using either the pre-polymers already tested or new pre-polymers.

(2) Cell adhesion and cell delamination of PO_0 electrospun scaffolds (prepared entirely with $M(EO)_2MA$ monomer) will also be studied to assess the impact of the volume phase transition temperature of the nanofibers on both cell adhesion as well as the degree and functionality of cell delamination. It is expected that optimizing the phase transition temperature of the scaffold will lead to even faster and/or more effective cell recovery upon thermally-induced delamination. The mechanics of the various thermoresponsive scaffolds will also be measured using a MicroSquisher (Cell Scale Biomaterials Testing) to correlate the structure and mechanics of the scaffolds with the observed delamination behavior.

(3) Cell reactive electrospinning will be applied to fabricate scaffolds containing stratified mixtures of two cell types. As a preliminary experiment, we will use skin fibroblasts and skin epithelial cells electrospun in layers to assess the relative viability of the two cell types as well as how the scaffold allows the two cell types to proliferate, spread into each other, and signal the different cell types. The advantage of this approach is that a single electrospun fibrous network can be produced that contains multiple types of cells with at least stratified spatial organization, offering interesting potential to form more complex tissue patches using a simple processing strategy.

(4) Protein release will be measured from the structured nanofibrous network hydrogels described in Chapter 7. It is anticipated that the beaded fiber or beaded network morphologies may facilitate significantly prolonged protein release relative to the nanofibrous networks given the larger dimensions and likely higher internal degree of crosslinking within the beaded domains. Such a result, given the cell proliferation results already reported in this thesis, may offer interesting opportunities to load growth factors into the gel scaffolds and facilitate their controlled release over time to direct cell responses.